A Decomposition Strategy Based on Thermoeconomic Isolation Applied to the Optimal Synthesis/Design and Operation of an Advanced Fighter Aircraft System

Diego Fernando Rancruel Arce

Thesis submitted to the Faculty of the
Virginia Polytechnic Institute and State University
in partial fulfillment of the requirements for the degree of

Master of Science
in
Mechanical Engineering

Dr. Michael von Spakovsky, Chair
Dr. Walter O'Brien
Dr. Michael Ellis
Dr. Peter King
Dr. Ricardo Muñoz

February 7, 2002
Blacksburg, Virginia

Keywords: optimization, decomposition, thermoeconomics, exergy, MDO

A Decomposition Strategy Based on Thermoeconomic Isolation Applied to the Optimal Synthesis/Design and Operation of an Advanced Fighter Aircraft System

by Diego Fernando Rancruel Arce

Abstract

A decomposition methodology based on the concept of "thermoeconomic isolation" applied to the synthesis/design and operational optimization of an advanced tactical fighter aircraft is the focus of this research. Conceptual, time, and physical decomposition were used to solve the system-level as well as unit-level optimization problems. The total system was decomposed into five sub-systems as follows: propulsion sub-system (PS), environmental control sub-system (ECS), fuel loop sub-system (FLS), vapor compressor and PAO loops sub-system (VC/PAOS), and airframe sub-system (AFS) of which the AFS is a non-energy based sub-system.

Configurational optimization was applied. Thus, a number of different configurations for each sub-system were considered. The most promising set of candidate configurations, based on both an energy integration analysis and aerodynamic performance, were developed and detailed thermodynamic, geometric, physical, and aerodynamic models at both design and off-design were formulated and implemented. A decomposition strategy called Iterative Local-Global Optimization (ILGO) developed by Muñoz and von Spakovsky was then applied to the synthesis/design and operational optimization of the advanced tactical fighter aircraft. This decomposition strategy is the first to successfully closely approach the theoretical condition of "thermoeconomic isolation" when applied to highly complex, highly dynamic non-linear systems. This contrasts with past attempts to approach this condition, all of which were applied to very simple systems under very special and restricted conditions such as those requiring linearity in the models and strictly local decision variables. This is a major advance in decomposition and has now been successfully applied to a number of highly complex and dynamic transportation and stationary systems. This thesis work presents the detailed results from one such application, which additionally considers a non-energy based sub-system (AFS).

Acknowledgements

This work would not have been possible without the help of numerous people. Firstly, I would like to thank my advisor, Dr. Michael von Spakovsky, for providing me the opportunity to come to Virginia Tech and conduct this research. Dr. von Spakovsky's trust and faith in my capabilities were invaluable. Many thanks to Drs. Walter O'Brien, Michael Ellis, Ricardo Muñoz, and Peter King for serving in my committee and for the valuable input they have given me over the course of this research. I am very grateful to Dr. King for the support, suggestions, and important information which were used to develop the Aerodynamic and Propulsion system models.

Special thanks to Dr. Ricardo Muñoz for his invaluable help during this project, his comments and advice were fundamental through all stages of this work. Most of all, I would like to thank Dr. Muñoz for his honest and selfless friendship.

The comments and suggestions made by Jim Louviere of LMTAS are greatly appreciated. I would also like to thank Honeywell Engines and Systems for allowing us to use their excellent FAST software.

This work was conducted under the sponsorship of the U.S. Air Force Office of Scientific Research.

The list of people in my family and friends who have helped me throughout the years is just too long to write in detail. I have been blessed with good people who have been with me in good and bad times. They should share the pride I feel because they are a big part of what I have been able to accomplish. I would like to thank as well my friends in Blacksburg, Borja, Cristina, David, Ivan, Nathan, and Todd. They have always been an important source of support.

This work is especially dedicated to my parents, Idalia and Carlos, thanks to whom I became the person I am. Through life they have given me support, freedom, example, and most importantly the love I need to reach my goals.

Diego Fernando Rancruel Arce

Table of Contents

List of Figures

List of Tables

Nomenclature

A, a	Speed of sound	*d*	Number of design variables
A	Area	*D*	Drag, fuselage depth
AAF	Air-to-Air Fighter	*E*	Exergy, energy
AFS	Air Frame Sub-system	$E_{vc/paos}$	Power extraction from the PS to the VC/PAOS
AR	Aspect ratio	*ECS*	Environmental Control Sub-System
BCA	Best cruise altitude	*EPAY*	Expendable payload
BCM	Best cruise Mach number	*esc*	Escape dash
bleed	ECS bleed	*f*	Objective function, coupling function vector
BP	Bleed port	*F*	"Uninstalled" thrust
B_h	Horizontal tail span	*F*	Fuselage lift factor
C	Objective function, cost	*FLS*	Fuel Loop Sub-system
C	Specific fuel consumption	F_w	Fuselage width at horizontal tail interception
$\dot{C}$	Cost rate	*g*	Acceleration of gravity
cac	Combat acceleration	*G, g*	Vector of inequality constraints
C_L	Lift coefficient	*h*	Altitude
$C_{L\alpha}$	Slope of the lift curve	*H,h*	Vector of inequality constraints
C_D	Drag coefficient	*HX*	Heat exchanger
C_{D0}	Drag coefficient at zero lift	*HPC*	High pressure compressor
ct_1	Combat turn 1	*HPT*	High pressure turbine
ct_2	Combat turn 2	*HX*	Heat exchanger

ILGO	Iterative Local-Global Optimization	*MINLP*	Mixed integer non-linear programming problem
K	Constant	*MILP*	Mixed integer linear programming problem
K	Induced drag factor	*N*	Number of turns
K_{dw}	Delta wing factor	N_z	Ultimate load factor
K_{vs}	Sweep wing factor	*n*	Load factor
K_{tpg}	Landing gear tripod factor	*o*	Number of operational variables
K_{cb}	Landing gear cross beam factor	*ORS*	Optimum response surface
K_{dwf}	Delta wing factor	*P*	Product
L	Fuselage length	$\dot{p}$	Product rate
LCC	Life cycle cost	$\vec{p}$	Coupling function, coupling function vector
loi	Loiter	*PPAY*	Permanent payload
LPT	Low pressure turbine	*PR*	Pressure ratio
$\dot{m}$	Mass flow rate	*PRvv*	Pressure setting for the ECS regulating valve
M	Mach number	$PR_{v\text{-}comp}$	Vapor compressor pressure ratio
M_0	Fuel tank initial mass	*PS*	Propulsion Sub-system
m_{creg}	ECS cold air flow rate	*Ps*	Weight specific excess power
m_{byp}	ECS bypass air flow rate	$S_{exposed}$	Exposed wing planform
m_{hot}	ECS hot air flow rate	*q*	Load factor
m_{vap}	VC/PAOS vapor refrigerant flow rate	$\dot{Q}$	Heat transfer rate
m_{Hpao}	VC/PAOS hot PAO flow rate	$\dot{Q}_{ecs\text{-}vcpaos}$	Heat rejection rate from the ECS to the VC/PAOS
mil	Military	$\dot{Q}_{vc\text{-}paos\text{-}fls}$	Heat rejection rate from the VC/PAOS to the FLS
mmn	Maximum Mach number	*R*	External input, resource

r	Intermediate resource	*T_t/c*	Tail thickness ratio
R	Additional or "parasitic" drag	*T_λ*	Tail taper ratio
Re	Reynolds number	*TSFC*	Thrust specific fuel consumption
RFP	Request for proposal	*t/c*	Wing thickness to chord ratio
S	Wing planform area	*V*	Velocity
SL	Sea level	*VC/PAOS*	Vapor Compressor and PAO Loops Sub-system
SFC	Engine specific fuel consumption	*u*	Coupling function
Sp	Vehicle speed in kiloknots	*W*	Weight, fuselage width
S_w	Trapezoidal wing area	W_E	Empty weight
S_{csw}	Control surface area	W_{TO}	Take-off gross weight
S_{ht}	Horizontal tail area	*WATE*	Weight Analysis of Turbine Engines
S_{exposed}	Exposed wing planform	*v*	Vector of flow and thermodynamic variables
t	Time	*w*	Vector of geometric variables
T	"Installed" thrust, total time for the set of load/environmental conditions	*x*	Vector of design variables
T_{it}	High pressure turbine inlet temperature	*y, Y*	Vector of operational variables
T_{tank}	Fuel tank temperature	*Z*	Capital function (weight, cost)
T_AR	Tail aspect ratio	*Z*	Capital function (weight, cost)

Greek

α	Step-size, thrust fraction, engine bypass ratio
β	Weight fraction
δ	Design point
ε	Small number
ϕ	Inlet and nozzle drag coefficients
θ	Thermodynamic cycle improvement
γ	Specific heat ratio, input function
Γ	Vector or inequality constraints for dynamic energy systems
H	Vector or equality constraints (analysis system of equations) for dynamic systems
φ	Stall margin (%)
λ, Λ	Shadow price, vector of shadow prices
λ	Wing taper ratio
$\Lambda_{\max t}$	Sweep of the wing at the chord location where the airfoil is thickest
Λ_{LE}	Wing sweep leading edge angle
Λ	Wing sweep angle
π	Leg weight ratio
τ	Number of time segments into which the set of load/environmental conditions is divided
ε	Heat exchanger effectiveness
ξ	Value of a coupling function
ψ	Value of a coupling function
ζ	Cost function

Superscripts

o	Reference, initial value
**	Optimum
p	Capital
*	Restricted optimum
◊	Feasible and "promising" solution

Subscripts

decs	ECS drag
f	Fuel, final
ref	Reference
i	Initial
it	Inlet temperature
o	Reference, initial value
wecs	ECS weight
0	Ambient
**0*	Optimum

Chapter 1

Introduction

As the level of interaction between the various sub-systems of energy systems has increasingly become complex, the more important the need has become to carry out the synthesis/design[1] of the system in a completely integrated fashion in order that the demands imposed by all the sub-systems be accommodated in the best way possible. Unfortunately, when developing new systems or operating existing ones, the lack of comprehensive synthesis/design tools forces today's engineer to rely heavily on rules-of-thumb, individual experience, and a fairly non-integrated, non-interdisciplinary approach of basic calculations, i.e. simple *trade-off analysis.* Powerful software tool are accessible. However, these are designed for single point analysis or not integrated . In cases where optimization is considered, partially due to the fact that new and more potent computers have become available and optimization tools more popular, it is seen as a straightforward mathematical problem, which for large-scale, highly non-linear optimization problems can be very limiting to say the least. Even significant increases in computational power are not sufficient to offset the ever increasing complexity of energy systems and the ensuing synthesis/design problem. Therefore, the need for methods that permit effective solutions of large-scale optimization problems is still an area of research, which generates great interest.

The need for more complex, efficient, and cost effective systems makes it imperative not only to analyze a greater number of possible configurations and technologies but also to synthesize / design systems in a way which optimizes these systems taking into account load and environmental variations over time. This contrasts with the common practice of designing a system for a single design point (typically chosen to be close to the most demanding operating point) followed by a verification of proper operation at off-design.

[1] Note that *synthesis* refers to changes in system configuration while *design* here refers exclusively to, for example, the nominal (full load or design point) capacity and performance of a given component or technology.

In formulating the entire synthesis/design problem (i.e. identifying all the interacting sub-systems, choosing the possible configurations and decision variables, and defining the physical constraints), it may turn out that solving the entire problem as a single problem (as opposed to solving a set of multiple problems) is simply impractical. The reasons are multiple:

- The number of decision variables involved may simply be too large for an efficient solution. In fact, given the current state of mathematical optimization, a solution may not be obtainable at all in the most complex cases.
- A single group of engineers may not possess all the expertise required for dealing with the technologies, sub-systems, and components involved in the problem.
- The integration of different computer codes, which simulate different aspects of the system, may be difficult. This is even more the case if such codes are written on entirely different platforms. In addition, these codes may not be available for use to all the members of the entire team (i.e. not all sub-teams may have access).
- Even in cases when code integration is possible, the overhead is simply too great to make the optimization viable. This is especially the case if the simulation tools are computationally expensive to use (e.g., as is often the case with CFD codes).
- The synthesis/design of the different sub-systems may, in many cases, be done at different stages and times, crossing company lines. Furthermore, it is not uncommon to have design teams that are not located entirely at one facility, which added to cultural differences, complicates the task at hand even further.

The overall problem being addressed is very complex and difficult to solve. In its entirety it represents a mixed integer, non-linear programming (MINLP) problem for which no general solution has been found. This is further complicated by the need to examine the largest number and most complete set of alternative syntheses and designs at each level of the problem in the shortest amount of time possible. Fundamental issues, which need to be examined, include the following:

1. the effects of decomposition on convergence to a global optimum[2] or a set of near-global optima for the system as a whole; the system itself may consist of a number of sub-systems, a single sub-system, or a single component;

[2] It should be noted that reference to a "global optimum" here is not meant to be taken in a strictly mathematical sense, i.e. the concern here is not in proving that decomposition necessarily leads to a Kuhn-Tucker point, but instead that in using decomposition coupled to mathematical optimization that the synthesis/design of the system

2. the justification for decomposition and its relationship to the global optima found without decomposition;
3. the effects on decomposition and the search for global optima that a mixed discrete and continuous decision variable space will have; this relates to the complete MINLP problem and will be examined here but not fully implemented;
4. the effects of material and geometric changes at the component or sub-component level on the thermodynamic and heat and mass transfer phenomena occurring within individual components or sub-components (e.g., heat exchangers, turbo-machinery, ram-air nozzles, zones within specific components, etc.);
5. the coupling between the physical phenomena at the component and sub-component levels and the thermodynamic, heat and mass transfer and even aerodynamic phenomena (e.g., ram-air inlet) found elsewhere in the system;
6. the coupling between the dynamics of the overall system and the dynamic or transient responses of individual sub-systems and components and the effects these have on component geometry and material selections as well as component and sub-system integration;
7. the effect, which changes in the physical phenomena at the component or sub-system level under off-design conditions, have on overall system synthesis/design;
8. the coupling between the non-energy-based subsystem phenomena (e.g., aerodynamic) and those for the aircraft's energy-based sub-systems/ components;
9. the relevance of using the 1st and 2nd Law of thermodynamics as a measure of the relative importance of the physical phenomena taking place in the system and as a guide to component and system level changes which alter these phenomena in ways consistent with the global optima sought for synthesis/design;

---

as a whole can be improved even for very complex, highly dynamic problems involving a large number of degrees of freedom. If this "global" or "system-level" optimum (improvement) happens to coincide with a Kuhn-Tucker point, that is all to the better. However, the impracticality of proving this for very large and complex problems of practical interest is simply a waste of time since we are concerned here with system-level (global) and component-level (local) improvements in synthesis/design and not mathematical proofs.

10. the significance of using 2nd Law as opposed to 1st Law of thermodynamics based quantities on decomposition and convergence to global synthesis/design optima;
11. the limits on decomposition imposed by thermodynamic as well as cost-based considerations;

Fundamental issues 1 to 3 above deal with the mathematical foundations of decomposition and the nature of the design spaces created by modeling and optimizing the system as well as its subsystems and components. Establishing and understanding the basis for decomposition and the characteristics of the design spaces involved is essential for being able to deal effectively with this highly complex problem of interrelated physical phenomena.

A clearer understanding of these physical phenomena and their interrelationships is also essential. The next four issues (4 to 7) deal with these, i.e. the fundamental aspects of how and why these occur at the component and sub-component levels as well as at the sub-system and system levels and how they are effected by other phenomena occurring locally, upstream / downstream, or in some place not directly linked to the phenomenon or phenomena in question. Obviously, the dynamic and off-design aspects of these phenomena are also of importance and need to be examined in order to deduce their impact on the overall problem. Studying these phenomena and their interrelationships could be enhanced by the use of CFD as well as experimental models (particularly as they relate to heat exchangers and their interactions within an overall system) coupled to the type of lumped-parameter models used at the sub-system and system levels for optimization.

The next issue, issue 8, needs to be studied in order to gain a better understanding of the fundamental basis for decomposition as applied to non-energy based aircraft sub-systems. It can also lead to an understanding of the coupling, which exists, between the physical phenomena occurring in these sub-systems and those occurring in an aircraft's energy-based sub-systems.

The remaining three issues (9 to 11) are essential for establishing and understanding the fundamental basis for using the 1st and 2nd Laws of thermodynamics in modeling the physical phenomena present. The impact this has on approaches (e.g. trade-off analysis versus mathematical optimization) for effectively

synthesizing and designing components/sub-components and sub-systems can and should be clearly delimited.

In conclusion, the research plan outlined here represents a unique opportunity to study the fundamental nature of the couplings which exist between the basic physical phenomena occurring within a given component / sub-component and those occurring elsewhere in the sub-system / sub-systems with which the component / sub-component interacts. Understanding the impact of these couplings is, in fact, as important as understanding the individual phenomena, which occur locally. Thus, the work carried on over the last three years at Virginia Tech under the sponsorship of the AFOSR has to one extent or another addressed all the issues. Although the use of CFD experimental approaches as suggested to help addressing issues 4 to 7 was excluded due to limitations in time and money, nonetheless the high fidelity, lumped parameters models used for analysis and optimization were sufficient for addressing these issues. The results are published in two reports (Muñoz and von Spakovsky, 1999; Rancruel, von Spakovsky, and Muñoz, 2001), one Ph.D. dissertation (Muñoz, 2000), four conference papers (Muñoz and von Spakovsky 1999, 2000a,b,c), and three journals papers (Muñoz and von Spakovsky 2001a,b, 2002). It is furthermore expected that the results presented in this M.S. thesis will results in a couple of conference papers and a like number of journal papers.

1.1 System Synthesis/Design Process

Those involved in system synthesis/design can never quite agree as to just where exactly the process begins. The designer thinks it starts with a new system concept. The sub-system specialist thinks that nothing can begin until initial sub-system capabilities are estimated. The customer feels that the process starts with his/her requirements. They are all correct, since system synthesis/design is an integrated effort as shown in Figure 1.1. Requirements are set by customer needs, while concepts are developed to meet those needs. Synthesis/design points toward new concepts, technologies and requirements, which in turn can initiate a whole new system synthesis/design effort. The synthesis/design process can be broken into three major phases, as depicted in Figure 1.2.

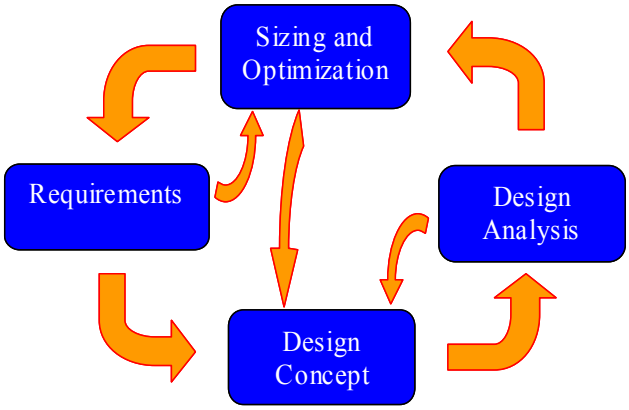

Figure 1.1 The design wheel.

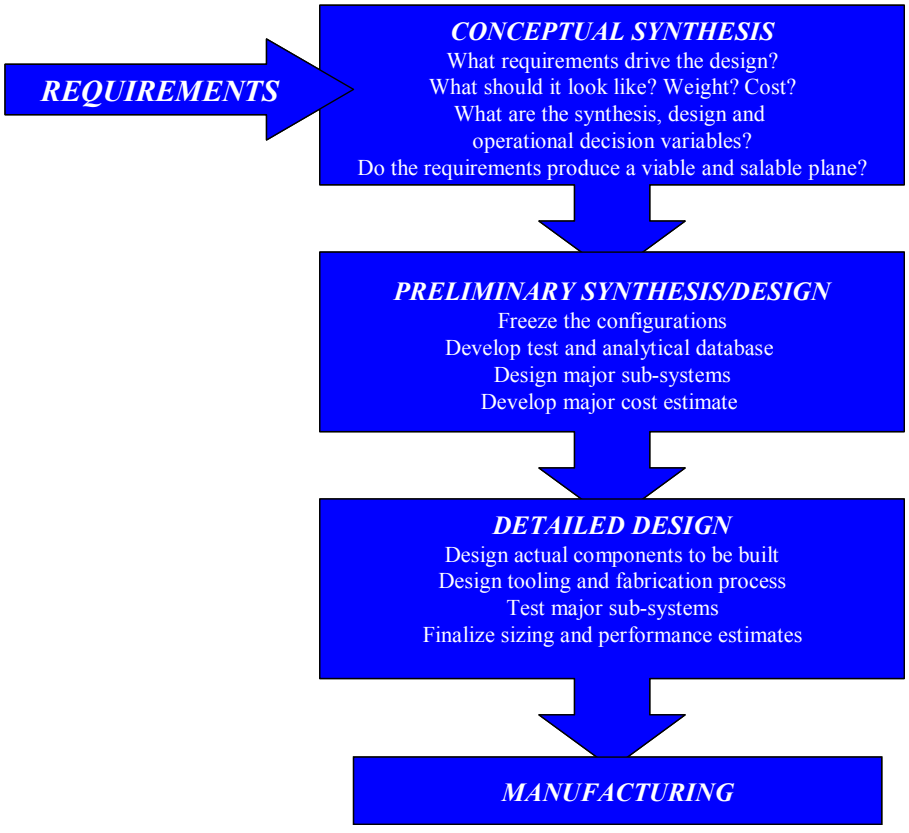

Figure 1.2 Three phases of aircraft synthesis/design.

1.1.1 Conceptual System Synthesis Stage

It is in the conceptual system synthesis stage that many of the basic questions of configuration arrangement are answered. Conceptual synthesis is characterized by a large number of configuration alternatives and trade studies and a continuous,

evolutionary change to the system concept under consideration. The first questions are asked and then explored, e.g., given a set of energy and performance needs:

- What types of sub-systems are available to meet these needs?
- Can any affordable system be built that meets the requirements?

If the answer to the latter is no, the customer may wish to review or relax the requirements. In the conceptual synthesis stage the requirements are used to guide and evaluate the development of the overall system configuration. The level of detail in conceptual synthesis is not very deep. However, the constraints, limits and interactions among all the different components and sub-systems is so crucial that it requires years of expertise to be able to create good conceptual configurations at this point in the development process.

A key aspect of the conceptual synthesis stage is that it is a very fluid process. The configuration must be adaptable and is always changing both to incorporate new things learned during the process and to evaluate potential improvements. During the conceptual synthesis stage a number of alternative configurations are studied to determine which best meet the established requirements. The final result is a set of likely configurations or a super-configuration to evaluate in more detail during the preliminary system synthesis/design stage. As one goes through conceptual, preliminary, and detail synthesis/design, the level of detail of the system, sub-systems, and components both in terms of modeling and analysis increases steadily.

1.1.2 Preliminary System Synthesis/Design Stage

The preliminary system synthesis/design can be said to begin when the major conceptual configurational changes are over. The big questions to be addressed are:

- What is the best system configuration (components and their inter-connections)?
- What are the best technical characteristics of each component (dimensions, material, capacity, performance, etc.)?
- What are the best flow rates, pressures, and temperatures of the various working fluids?
- What is the best operating point of the system at each instant of time?

During this stage, specialists in different areas design and analyze their respective sub-systems or components. This stage is the one on which this research work is focused, offering a new approach for solving the integrated system synthesis/design optimization problem. The ultimate objective during the synthesis/design stage is to determine which single configuration and design is to be considered during the detailed system design stage.

1.1.3 Detailed System Design Stage

Assuming a favorable decision for entering full-scale development, the detailed system design stage seeks to define what are the actual pieces of equipment to be fabricated and assemble. This stage starts by identifying which phenomena must be modeled in greater detail; which analytical, numerical, and experimental high fidelity tools will be used; and what detailed costs are involved. This last and most expensive part of the system synthesis/design development process is characterized by a large number of designers, preparing detailed drawings or CAD/CAM files with actual fabrication geometries and dimensions. While, for instance, during an aircraft conceptual synthesis stage, the designers are concerned about such top-level issues as the number of engines required or the sweep of the wing, during the detailed system design stage, the designers concern themselves more with, for example, the exact radius of the corner of a pocket cutout on a flap track. Another important part of the detailed system design stage is what is called production design. Specialists determine how the system will be fabricated starting with the simplest subassemblies and building up to the final assembly process. Production designers often wish to modify the design for easy manufacture, modifications which can have a major impact on important figures of merit such as performance, weight, etc. At this point issues such as reliability/availability, material substitutions, and manufacturing and assembly criteria are addressed. Compromises are inevitable. However, the system must still meet the original requirements and constraints.

1.2 Synthesis/Design Stages: Tools

There are a number of tools and methodologies available to the engineer today. Of these, probably the most common and the least sophisticated is the system/component simulation package which aids the engineer in the synthesis and design process but forces the engineer, nonetheless, to rely heavily on rules-of-thumb

and experience. Some exceptions to these tools are those based on pinch technology, exergy analysis, and expert systems[3]. A brief description of these is given in Chapter 2. There are, however, significant limitations as to what can be done with all of the above. Approaches for overcoming these limitations are mathematically based. They simultaneously model the physical and/or economic aspects of a system and its components. This permits the use in a *single-level* approach of optimization algorithms whether deterministic (gradient-based) or heuristic (non-gradient based) which search the solution space of all possible solutions (see Fig. 1.3) for the optimum synthesis, design and/or operation of a system and its sub-systems and components. Furthermore, when such a single-level approach is unable to solve the synthesis/design optimization problem due to its complexity (both mathematical and cultural: see Muñoz and von Spakovsky, 2002), a *multi-level* approach using *decomposition* may be used to formulate the optimization problem in such a way as to permit the use of a gradient or non-gradient based algorithm which can then successfully solve the problem. A discussion of these *optimization algorithms* and of *decomposition* is given in Chapter 2.

1.3 Thesis Objectives

Based on the discussion presented above, it is clear that there exists a need for a general methodology that will permit the integrated synthesis/design optimization of energy and non-energy systems. The required method should not only allow for the solution of the overall synthesis/design problem by dividing it into smaller sub-problems but facilitate as well the difficult task of sub-system integration. The general objective of this research is to show how application of the decomposition optimization strategy for system synthesis/design called Iterative Local-Global Optimization (ILGO) developed earlier (Muñoz, 2000; Muñoz and von Spakovsky, 200a,b, 2002) meets this need by satisfying the following requirements:

- is capable of using dissimilar modeling codes, possibly written on different platforms;

[3] Note that all of the methodologies and tools described here are those which can in some way enhance an *integrated synthesis/design environment.* Such an environment facilitates *communication* between a set of synthesis / design tools as well as across platforms in order that the development process for new technologies be improved. However, as any such environment, its effectiveness depends very much on the tools of which it is comprised.

- effectively deals with the synthesis problem (i.e. deals with the presence of integer and binary variables) so that advanced optimization algorithms to solve the complex mixed-integer problem (typically non-linear) are supported;
- is modular so that analyses and optimizations can be divided to the greatest extent possible into clearly separated tasks assigned to specialty organizations;
- permits geographically dispersed organizations to carry out optimization tasks aimed at optimizing the entire system; thus, the method must allow for each organization to influence the other organizations' tasks while retaining responsibility for its own objectives;
- requires the minimum possible number of repetitions (i.e. re-optimizations);
- supports concurrent and parallel tasks;
- integrates as many parameters as possible within each sub-problem but not so many that it cannot be adequately defined and solved;
- is sufficiently general to handle systems in both stationary or aircraft/aerospace applications;
- supports multiple design points (i.e. can be used in dynamic systems);
- guarantees, in the event of a premature halt in the process, a solution which is an improvement over the initial synthesis / design.

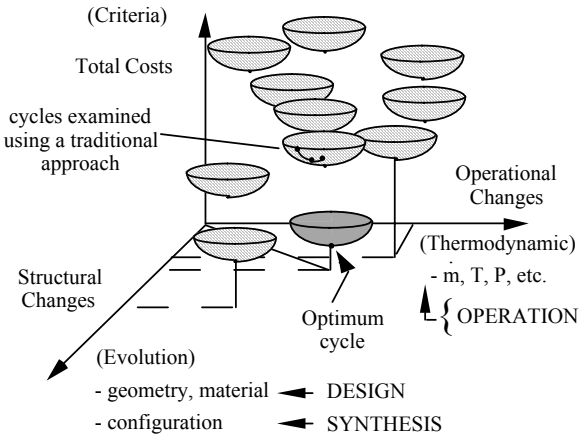

Figure 1.3 The synthesis, design and operational solution space of energy systems[4] (Olsommer, von Spakovsky, and Favrat, 1997).

[4] Note that the smooth surfaces are a simplification introduced for illustration purposes only of this non-continuous, non-contiguous, highly non-linear space.

In addition to the above set of requirements, the proposed methodology should shed some light on the usefulness of 1st and 2nd Law quantities for optimization purposes (e.g., Newberry, 2000; Bejan, 2000; Paulus and Gaggioli, 2000).

It is assumed in what follows that system modeling requires a high level of detail (and is, therefore, expensive to simulate and optimize) and involves large numbers of independent, continuous, and discrete variables. In this research work, the synthesis/design problem is set up in a general way so that streams and couplings may be represented by energy (or exergy) or by any other relevant quantity, depending on which better facilitates the interface between the energy as well as non-energy sub-systems.

The specific goal of the work proposed for this thesis research is demonstrating the feasibility of using ILGO for the preliminary synthesis/design optimization of an Advanced Tactical Fighter Aircraft (ATFA). Sub-systems for this ATFA include a propulsion sub-system (PS), a fuel loop sub-system (FLS), a vapor compressor/PAO loops sub-system (VC/PAOS), an environmental control sub-system (ECS), an airframe sub-system (AFS), and expendable and permanent payloads sub-systems (EPAYS and PPAYS). This requires the development of a general, high fidelity, flight performance model for the aircraft system, which itself is based on high performance aircraft technology. ILGO must be used for dynamically optimizing in an integrated fashion each of the sub-systems' syntheses/designs, taking into account the optimal behavior of each sub-system at off-design as well as at its synthesis/design point. Such a tool will enhance any integrated synthesis/design environment through a systematic and efficient selection of the best set of configurations (syntheses) and designs which comprise a system's synthesis/design space. The following is a list of the major objectives envisioned:

- Gain a fundamental understanding of how a high performance aircraft system and its sub-systems operate and a general comprehension of the fundamental phenomena present in each part of the process.
- Create the physical and thermodynamic models for components and sub-systems and in turn describe their connectivities. Include models for off-design behavior, which lead to the full modeling and optimization of the system over an entire mission profile.

- Develop appropriate component weight, fuel consumption, and cost functions, which relate cost to appropriate decision (synthesis/design and operational) variables.
- Apply a decomposition strategy, which permits both local/unit (i.e. component and sub-system) and global/system optimizations and provides for an on-going communication between these levels of optimization.
- Define the computational tools necessary for solving the set of mathematical optimization problems created.
- Use the models and computational tools for both optimizing the system locally (i.e. at the component and sub-system levels) and globally (i.e. at the system level).
- Document and analyze the results for the optimal synthesis/design of a high performance aircraft system.

As to the ILGO decomposition technique, which in fact consists of two versions (ILGO-A and ILGO-B), this is a completely original development by Muñoz (2000;) and Muñoz and von Spakovsky (2001a,b, 2002). In particular, they have developed a general methodology for the decomposed synthesis/design optimization of highly coupled, highly dynamic energy systems. Their work shows that the ILGO decomposition technique is an extremely useful tool that not only permits the solution of the overall synthesis/design optimization problem for highly complex systems by dividing the problem into smaller sub-problems but also facilitates the difficult task of sub-system integration. A detailed description of the different decomposition approaches for the optimization of a system's synthesis/design is given in Chapter 3.

Chapter 2

State-of-the-Art of Energy Systems Synthesis/Design Analysis and Optimization

A current trend is to incorporate aspects of process control, energy utilization, and environmental impact early in the synthesis/design process. This is because we are no longer just interested in a narrowly defined optimal process. The process must be energy efficient, flexible, environmentally friendly, and easy to control. It has been shown that one way to accomplish this difficult task is to consider some aspects of the various sub-problems simultaneously and as early as possible. A number of algorithms involving general mathematical formulations and hybrid techniques have been proposed. The question of optimal solutions needs to be further analyzed as parametric objective functions are usually encountered. Thus, the optimal solution involves an optimal trade-off between the various terms (for example, between process design, energy utilization, control design, and environmental impact). In parallel with these integrated algorithms, integrated tools also need to be developed.

The synthesis/design of complex energy systems requires that sophisticated methodologies and tools be developed and applied. In fact, a number of these with varying degrees of sophistication have been the subject of research since the 1950s. Of these, probably the most common and the least sophisticated is the system/component simulation package which aids the engineer in the synthesis/design process but forces the engineer, nonetheless, to rely heavily on rules-of-thumb and experience. However, more structured tools exist. One can broadly classify the latter depending on the fundamental purpose for which they are used. Analysis methodologies and tools are typically used to gain a fundamental understanding of a process or system. The information is then used to rationally define a set of possible configurations, designs, or modes of operation. Optimization methodologies and tools

are used to determine a system's synthesis/design/operation so that a figure of merit is maximized or minimized. A description of two types of methodologies/tools is given in the sections below. However, some fundamentals about system modeling and optimization are given first.

2.1 Energy System Synthesis/Design Modeling and Optimization Fundamentals

2.1.1 Modeling of an Energy System

The modeling of an engineering system typically begins with the selection of a number of degrees of freedom represented by parameters which can be varied at will within acceptable limits. These independent parameters or variables, hereby represented by a vector $\vec{x}$, are then used to create two systems of equations to represent the model of the system, i.e.

$$\vec{H} = \begin{Bmatrix} \vec{h}_1(\vec{x}) \\ \vec{h}_2(\vec{x}) \\ \vec{h}_3(\vec{x}) \\ \vdots \\ \vec{h}_n(\vec{x}) \end{Bmatrix} = \vec{0} \quad ; \text{and } \vec{G} = \begin{Bmatrix} \vec{g}_1(\vec{x}) \\ \vec{g}_2(\vec{x}) \\ \vec{g}_3(\vec{x}) \\ \vdots \\ \vec{g}_n(\vec{x}) \end{Bmatrix} \le \vec{0} \tag{2.1}$$

The vector of equality constraints $\vec{H}$ is composed of sub-vectors $\vec{h}_i$ each of which mathematically describes a phenomenon usually within the realm of a particular discipline. The elements of the sub-vectors $\vec{h}_i$ are known as the *state* equations. For energy systems, a number of different disciplines are represented by $\vec{H}$, the most common being the thermal sciences, materials, controls, and economics[5]. The vector of inequality constraints $\vec{G}$ represents natural or artificial limitations imposed upon the system.

Any arbitrary vector $\vec{x}$ may not satisfy the constraints imposed by equations (2.1). In this case, equations (2.1) act as system *evaluators*. A feasible solution is one that has a vector of independent variables that satisfies equations (2.1). The process of finding a vector that leads to a feasible solution is typically iterative. The speed of this

[5] In this work, the thermal sciences and economics are used directly. Controls are implicitly involved in the synthesis/design whenever there is a need for adjusting certain parameters over time. Physical limitations on the components or materials used are incorporated in the models by constraints.

process is oftentimes slow because in practical systems the size of $\vec{x}$ is large and the systems of equations (2.1) are highly non-linear. A system evaluator coupled to the iterative scheme just described is called a system *analyzer*.

The representation of the relevant phenomena is accomplished by means of the software implementation of the mathematical models of the system. For obvious practical reasons, different "codes" are developed with each representing a particular aspect of the system. Thus, it is common to talk about thermodynamic, sizing, CFD, or costing codes, although some exceptions exist. Examples of the latter are codes that are capable of blending in a single analysis fluid mechanics, heat transfer, and stress analysis. In addition, for reasons having to do with company organization, codes for different types of technologies, multi-disciplinary or not, are disaggregated. It is, therefore, common to have an engine code, a structures code, and so on.

2.1.2 Nonlinear Constrained Optimization

Once a model or a set of models of the engineering system exist, the option to optimize subject to a set of constraints exists. It is the model or set of models of the system described in the previous section that form the set of nonlinear constraints used in the formulation of the optimization problem. This problem is expressed in general terms by

$$\text{Minimize } f(\vec{x}) \tag{2.2}$$

with respect to $\vec{x}$ and subject to the following equality and inequality constraints:

$$\vec{H}(\vec{x}) = \vec{0} \tag{2.2.1}$$

$$\vec{G}(\vec{x}) \le \vec{0} \tag{2.2.3}$$

Note that an inequality constraint $g_j \le 0$ is active if $g_j = 0$. By definition all equality constraints are active. The first order necessary and sufficiency conditions for a point to be a local and a global minimum, respectively, are called the Karush-Kuhn-Tucker or Kuhn-Tucker conditions. The conditions are stated in the following theorem:

The Lagrange Multiplier Theorem

Let $\vec{x}^*$ be a local minimizer for problem (2.2). Then there exist vectors $\vec{\lambda}^*$ and $\vec{\mu}^*$ such that

$$\vec{\mu}^* \geq \vec{0} \tag{2.3}$$

$$\nabla f(\vec{x}^*) + \vec{\lambda}^{*T} \nabla \vec{H}(\vec{x}^*) + \vec{\mu}^{*T} \nabla \vec{G}(\vec{x}) = \vec{0} \tag{2.4}$$

$$\vec{\mu}^{*T} \vec{G}(\vec{x}) = \vec{0} \tag{2.5}$$

One normally refers to $\vec{\lambda}^*$ and $\vec{\mu}^*$ as the Lagrange multiplier vectors of equality and inequality constraints. In the literature, $\vec{\mu}^*$ is sometimes called the Karush-Kuhn-Tucker multipliers.

In addition to these first order necessary conditions for a local minimum, first order sufficiency conditions, which guarantee that the local minimizer $\vec{x}^*$ is a global minimizer, also exist. These additional conditions place certain restrictions of convexity or concavity on the objective function $f(\vec{x})$ and the equality and inequality functions $\vec{H}(\vec{x})$ and $\vec{G}(\vec{x})$, respectively. For a detailed discussion of these conditions and others, the reader is referred to Floudas (1995). All of the conditions briefly outlined above lay the foundations of optimality for the nonlinear optimization (programming) problem, problem (2.2). In practice, these conditions, especially those for sufficiency, are oftentimes difficult if not *impossible* to meet. Thus, an effective search of the space of all possible solutions is fraught with the uncertainties of knowing where the global optimum or a set of near-global optimums lie.

2.1.3 Basic Formulations for Energy System Analysis and Optimization[6]

Consider the energy system of Figure 2.1, which is composed of two units[7] or two disciplines. In the above figure, the $\vec{g}_i$ (i=1,2) are the vectors representing the limits or constraints imposed upon the units or disciplines; and the r_i's are the residuals in

[6] In this section some of the terminology compiled by Balling and Sobieszczanski-Sobieski (1996) is used.
[7] A unit refers to either a component or a sub-system.

the state equations. The vectors $\vec{u}_{12}$ and $\vec{u}_{21}$ are the coupling functions. The two unit or discipline analyzers may be executed in parallel if values are set for the coupling functions, say $\vec{u}_{12}^{o}$ and $\vec{u}_{21}^{o}$.

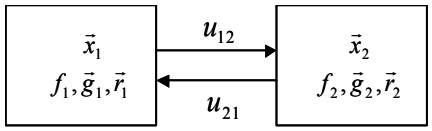

Figure 2.1 A simple energy system.

If one were now to optimize this system, it might be possible in some cases to define multiple objective functions which need be optimized simultaneously. The optimization is then carried out by assigning weights to each of them in order to obtain a unique objective. An area of mathematical optimization specializes in this type of multi-objective problems. In energy systems, one is oftentimes concerned with a single objective function (e.g., costs[8], thermodynamic efficiency, fuel consumption, specific fuel consumption, etc.). In this thesis work, the optimization problems are defined using a single objective function. The scalars f_1 and f_2 are the contributions of units or disciplines 1 and 2 to the overall objective function f. Other objectives (e.g., range, acceleration, etc.) are then cast as constraints. The optimization problem is, therefore, stated as minimizing $f = f_1 + f_2$.

A number of solution approaches to the above posed problem are possible depending on whether or not an analysis or a single- or multi-level optimization technique is applied. Before proceeding with a discussion of these, some additional observations are made.

2.1.4 Additional Comments

In mathematical optimization, the best system is the one that minimizes (or maximizes) an objective function. Let us assume that minimization of the total cost is

[8] For aircraft systems, these costs include those traditionally associated with the manufacture and performance of each component as well as those associated with the impact of a component's size (weight and volume) on aircraft performance. In fact, an important fraction of total fuel usage is due to drag which in turn is a function of weight, volume, and aero-surface shape, resulting in an indirect cost for each sub-system/component. Therefore, the goal of synthesis/design is not only one of minimizing the energy usage and capital costs of each sub-system/component but even more importantly, the indirect energy sub-system/component costs associated with the performance levels of the aircraft itself.

the objective and that the optimization problem has a solution, i.e. a system has been determined that satisfies the objective. Is this indeed the solution sought or must one also compare the performance of this system with the performance of other (non-optimal) systems based on other points of view, e.g., maintainability or environmental effects? There may be cases when such a comparison shows that the 'optimal' with respect to the cost of the system is not at all good when these other points of view are considered (attempts to translate other aspects into cost are made but there may still be aspects that cannot be handled in this way). Multi-objective optimization is an attempt to correct such deficiencies. However, the solution then depends on subjective weighting factors or additional criteria. The point of all this is that the optimal solution may not be unique and is 'optimal' only in the strict mathematical sense. Thus, even if the synthesis/design procedure can be automated, expert human intervention is needed to evaluate the results and reach a final decision.

Another issue is the following. In the usual synthesis/design process of an energy system, the designer uses his knowledge and experience to select the type, configuration, and technical characteristics of a workable system (i.e. a system that is technically feasible and satisfies a given set of needs), which he then evaluates for its technical and economic performance and for ways of improving it. If the system synthesis (type and configuration) is given, the decisions to be taken are of a rather quantitative nature. If, however, the synthesis is not given, in addition to quantitative decisions, there is need for many qualitative decisions, which may be non-deterministic. In such a case, innovation and creativity play a vital role. Given the multitude of energy system types and the variations in each type, one may question whether it is ever possible to replace the experienced designer's mental process with an algorithm consisting of a set of formulae and rules. On the other hand, in today's complex world, this same multitude of types and variations makes it rather impossible even for an experienced designer to evaluate all possible alternatives. Consequently, an automated procedure, if properly used, can be of invaluable help to the designer.

Finally, the next section deals with the mathematical, algorithmic, and computational tools that are required to transform a set of synthesis/design requirements into a workable and eventually "best" or optimum energy system.

2.2 Energy System Synthesis/Design Analysis and Optimization Tools

2.2.1 Energy System Synthesis/Design Analysis Techniques

In Chapter 1, some well-known energy system analysis methodologies/tools were mentioned (e.g., pinch technology, exergy analysis, and expert systems). An explanation of each of these is given in the following sections.

2.2.1.1 Pinch Technology

The term "Pinch Technology" was introduced by Linnhoff and Vredeveld (1982) to represent a new set of thermodynamically based methods that guarantee minimum energy levels in the design of heat exchanger networks. Over the last two decades, it has emerged as an unconventional development in process design and energy conservation. The term 'Pinch Analysis' is often used to represent the application of the tools and algorithms of Pinch Technology for studying industrial processes.

Pinch technology presents a simple methodology for systematically analyzing heat exchanger networks and the surrounding utility systems with the help of the 1^{st} Law of Thermodynamics. This law provides the energy equation for calculating the enthalpy changes (ΔH) in the streams passing through a heat exchanger. In addition, since heat energy may only flow in the direction of hot to cold, 'temperature crossovers' of the hot and cold stream profiles through the heat exchanger unit are prohibited. In practice, the hot stream can only be cooled to a temperature defined by the 'temperature approach' of the heat exchanger. The temperature approach is the minimum allowable temperature difference (ΔT_{min}) in the stream temperature profiles for the heat exchanger unit. The temperature level at which ΔT_{min} is observed in the process is referred to as "pinch point" or "pinch condition". The pinch defines the minimum driving force allowed in the exchanger unit.

A set of simple rules can be applied to guide the selection of a near optimum heat exchanger network. These rules simply stated are: do not transfer heat across the pinch, use a hot stream above the pinch and use a cold stream below the pinch. It has been claimed that pinch technology is a tool that can be used for process design (Linhoff, 1989), which indeed it can. However, based on the results of a challenge problem solved in the early 1990s (Linhoff and Alanis, 1991; Gaggioli et al., 1991), it would appear that exergy analysis as applied by an expert may be superior for that

purpose, a fact which is not surprising since exergy analysis is based on both the 1st and 2nd Laws and more complete as an overall analysis tool. An interesting (and spirited) comparison between pinch technology and exergy analysis is given by Sama (1995)

2.2.1.2 Exergy Analysis

Like pinch technology, exergy[9] analysis (e.g., Gaggioli et al., 1991) is a systematic but less structured way of analyzing alternative synthesis/design options for energy systems and components. Though less structured than pinch technology or other 1st Law approaches, it does provide a more complete picture and a greater number of insights into the overall synthesis, design, and operational problem since it accounts both for the quantity and quality of all energy conversions present in a process. Furthermore, it is not primarily centered on heat exchange or mass exchange networks. It uses a set of common sense guidelines (e.g., Sama, 1995; Sama, Qian and Gaggioli, 1989) to detect and avoid or remove the so-called 2nd Law errors[10] in synthesis, design and operation in order to guarantee a more cost-effective and/or better performing system. The objective of this type of analysis is the judicious expenditure of exergy (availability)[11] to reduce not just fuel costs but total costs. An incomplete list of "common sense guidelines", which would be used in an exergy analysis along with exergy balances of the system and each of its components and sub-systems, is the following:

- Do not use excessively large or excessively small thermodynamic driving forces in process operations.
- Minimize the mixing of streams with differences in temperature, pressure, or chemical composition.
- Do not discard energy at high temperatures to the ambient or to cooling water.
- Do not heat refrigerated streams with hot streams or with cooling water.

[9] Exergy is defined as the maximum theoretical useful work that could be obtained if a system were allowed to interact with a second idealized system called the *reference environment* (or *"dead state"*). Exergy is in fact a measure of the departure of the state of the system from that of the reference environment, i.e. it is the maximum potential for change or "departure from equilibrium" with the reference environment ("dead state").

[10] It is somewhat misleading to simply call these 2nd Law errors since in fact, exergy and the concept of irreversibility and exergy generation are based on both the 1st and 2nd Laws of thermodynamics.

[11] The terms *exergy* and *availability* are interchangeable. Either combines the notions of the *quantity* of energy resulting from the 1st Law and the *quality* of energy resulting from the 2nd Law into a single entity which can be used to assess the real thermodynamic losses which occur within, to, and from a system.

- When choosing streams for heat exchange, try to match streams where the final temperature of one is close to the initial temperature of the other.
- When exchanging heat between two streams, the exchange is more efficient if the flow heat capacities of the streams are similar. If there is a big difference between the two, consider splitting the stream with the larger heat capacity.
- Minimize the use of intermediate heat transfer fluids when exchanging heat between two streams.
- Heating (or refrigeration) is more valuable the further its temperature is from the ambient.
- The economic optimum ΔT of a heat exchanger decreases as the temperature decreases and vice versa.
- Minimize the throttling of steam or other gases.
- The larger the mass flow, the larger the opportunity to save (or to waste) energy.
- Use simplified exergy (or availability) consumption calculations as a guide to process modifications.
- Some exergy inefficiencies cannot be avoided. Others can. Concentrate on those which can.

2.2.1.3 Expert Systems

Unlike the two systematic approaches just described, expert systems are not a type of analysis but a form of artificial intelligence (AI) which organizes and efficiently and quickly makes available the knowledge and experience of more than one person (Sciubba and, 1999; Sciubba 1995).

Expert Systems (ES) are based on *relational languages* that use the symbolism of formal propositional logic. They draw inferences from a number of *facts* stored in a particular database, properly called a *knowledge-base.* These facts can be synthesis/design data, synthesis/design rules, physical or logical constraints, etc. Each ES manipulates this knowledge in its own way, according to a logical procedure contained in its *inference engine*. AI and ES techniques are described and application examples presented in Frangopoulos, von Spakovsky, and Sciubba, (2001).

Knowledge-based expert systems, or simply expert systems, use human knowledge to solve problems that normally would require human intelligence. These

expert systems represent the expertise knowledge as data or rules within the computer. These rules and data can be called upon when needed to solve problems. Conventional computer programs perform tasks using conventional decision-making logic containing little knowledge other than the basic algorithm for solving that specific problem and the necessary boundary conditions. This program knowledge is often embedded as part of the programming code, so that as the knowledge changes, the program has to be changed and then rebuilt. Knowledge-based systems collect the small fragments of human know-how into a knowledge-base which is used to reason through a problem, using the knowledge that is appropriate. A different problem, within the domain of the knowledge-base, can be solved using the same program without reprogramming. The ability of these systems to explain the reasoning process through back-traces and to handle levels of confidence and uncertainty provides an additional feature that conventional programming does not handle.

Most expert systems are developed via specialized software tools called shells. These shells come equipped with an inference mechanism (backward chaining, forward chaining, or both), and require knowledge to be entered according to a specified format. These shells qualify as languages, although certainly with a narrower range of application than most programming languages. For more detailed information on expert system shells, see the "Expert System Shells at Work" series by Schmuller (1991, 1992).

2.2.2 System Synthesis/Design Single-Level[12] Optimization Techniques

The single-level optimization techniques that can be employed to solve the problems posed above[13] depends on the type of optimization problem at hand. A general depiction of this problem for the synthesis/design optimization of energy systems is shown in Figure 2.2. Depending on its nature and level of complexity, such a problem can be classified in a number of ways (Rao, 1996), i.e.

[12] A "single-level" as opposed to "multi-level" technique refers to the fact that no *decomposition* is employed to break the optimization problem into a set of nearly equivalent smaller problems in order to facilitate the solution of the larger problem and overcome both the mathematical and cultural difficulties which exist with highly complex, highly dynamic problems (see *section 2.2.3*).

[13] This, of course, assumes that they are simple enough to be solved with a single-level approach which, in fact, they may not be (see Figure 2.2). If not, they could still be employed provided they were used in conjunction with a multi-level approach, i.e. with a *decomposition* technique (see *section 2.2.3*).

- Classification Based on the Existence of Constraints: any optimization problem may be classified as constrained or unconstrained, depending on whether or not constraints exist in the problem.
- Classification Based on the Nature of the Decision (Independent) Variables: if the decision variables can be treated as parameters, the problem is classified as a static or parametric optimization problem. If, on the other hand, the decision variables are represented by functions, the problem is called a trajectory optimization problem.

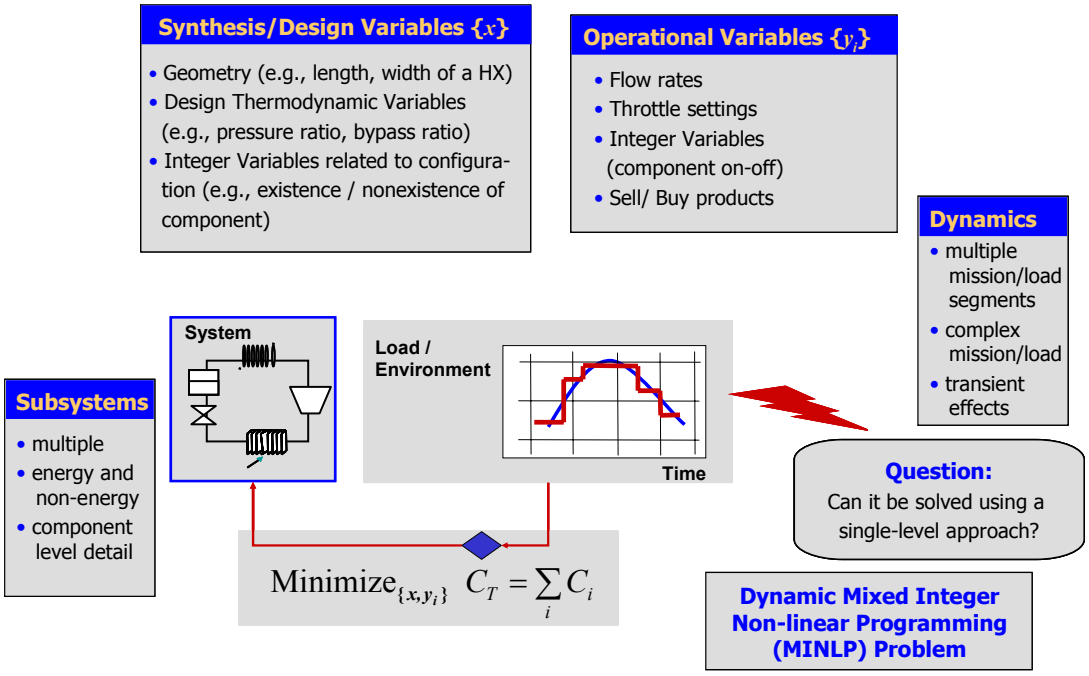

Figure 2.2 General depiction of the synthesis/design optimization problem for energy systems.

- Classification Based on the Nature of the Equations Involved: according to this classification, optimization problems can be linear, non-linear, geometric or quadratic programming problems. A problem is geometric if the objective function can be expressed as the sum of power terms (i.e. a polynomial). A quadratic problem is a non-linear programming problem with a quadratic objective function and linear constraints.
- Classification Based on the Permissible Values of the Independent Variables: depending on the values permitted for the decision variables, optimization

problems can be classified as integer, real valued, or mixed integer programming problems.

- Classification Based on the Deterministic Nature of the Independent Variables: optimization problems can be classified as stochastic or deterministic programming problems.
- Classification Based on the Separability of the Functions: optimization problems can be classified as separable or non-separable depending on whether the objective function or constraint functions can be written as the sum of n functions.
- Classification Based on the Number of Objective Functions: optimization problems can be classified as single and multi-objective programming problems.
- Classification Based on the synthesis/design stage: Optimization problems can be address in different ways according to the synthesis/design stage. For early stages (Synthesis) the following approaches are mostly used. First, heuristics and evolutionary search, which are rules based on engineering experience and on physical concepts (e.g., exergy) are applied to generate feasible configurations, which are subsequently improved by applying a set of evolutionary rules in a systematic way. These rules may come from special techniques, such as exergy analysis. Artificial Intelligence and Expert Systems have proven effective in generating appropriate configurations. Second, techniques used to find optimum configurations, which attempt to reach pre-determined targets that have been identified by application of physical rules. Principles from thermodynamics and other physical sciences are applied to obtain targets for the optimal system configuration. These targets can correspond to upper or lower bounds on the best possible configuration and provide vital information for improvement of existing configurations. Attempts have been made to introduce economics at a second level, but the whole approach is mathematically non-rigorous and, consequently, the configuration obtained may be non-optimal. Methods starting with a superstructure are used. The final objective is to reduce this superstructure to the optimal configuration. A superstructure is considered with all the possible (or necessary) components and interconnections. An objective function is specified and the optimization problem is formulated. The solution of the optimization problem gives the optimal system configuration, which, inevitably, depends on (and is restricted by) the initial superstructure.

Many of the most difficult energy system synthesis/design optimization problems are single-objective, mixed integer, non-linear, deterministic optimization problems. The focus here is on techniques which can be used to solve these types of problems directly or indirectly in conjunction with some *decompo8sition* technique (see footnotes 12 and 13 above and *section 2.2.3* below). These techniques will be broadly divided into two categories: gradient-based and non-gradient-based algorithms.

2.2.2.1 Gradient-Based Algorithms

The gradient-based algorithms of optimization are a class of search methods for real-valued functions. These methods use the gradient of a given function as well as function values. Although most energy system synthesis/design problems are constrained, it is useful to start with a general description of the methods for unconstrained problems. Thus, consider the unconstrained optimization problem

Minimize $f(\vec{x})$ (2.6)

w.r.t. $\vec{x}$

The resulting iterative algorithm is given by

$$\vec{x}^{k+1} = \vec{x}^{k} - \alpha^{k} \nabla f(\vec{x}^{k}) \tag{2.7}$$

where α is a sufficiently small step-size. The choice of the step-size α_k leads to a number of algorithms: the steepest descent method, Newton and quasi-Newton methods (e.g., the Fletcher and Powell and the BFGS methods), conjugate direction methods (e.g., the methods of Fletcher-Reeves, Polar-Ribiere, and Hestenes-Stiefel).

A number of gradient-based methods exist for solving non-linear programming problems such as the one given above. Optimization methods that handle the constraints explicitly are known as direct methods. Indirect methods attempt to find an optimum by solving a sequence of unconstrained problems. Examples of the latter are the Interior ands Exterior Penalty and the Augmented Lagrange Multiplier methods. Examples of direct methods are the Sequential Linear and Quadratic programming methods, the Method of Feasible Directions (MFD), the Generalized Reduced Gradient Method, and the Rosen Projection Method. Two of the most popular methods are briefly described below.

Method of Feasible Directions (MFD)

The iterative algorithm that results from this method begins by choosing a feasible starting point and moving to a better point according to the iterative formula

$$\vec{x}^{k+1} = \vec{x}^{k} + \alpha \cdot \vec{S}^{k} \tag{2.8}$$

where $\vec{x}^{k}$ is the starting point, $\vec{S}^{k}$ is the direction of movement, and α is the step length. The value of α is chosen so that $\vec{x}^{k+1}$ lies in the feasible region. The search direction $\vec{S}^{k}$ is found such that (1) a small move in that direction does not violate any constraint and (2) the value of the objective function decreases in that direction. A vector $\vec{S}$ is a usable feasible direction if (Chong and Zak, 1996)

$$\frac{d}{d\alpha} f(\vec{x}^{k} + \alpha \cdot \vec{S})\Big|_{\alpha=0} = \vec{S}^{T} \nabla f(\vec{x}^{k}) < 0 \tag{2.9}$$

$$\frac{d}{d\alpha} g_{j}(\vec{x}^{k} + \alpha \cdot \vec{S})\Big|_{\alpha=0} = \vec{S}^{T} \nabla g_{j}(\vec{x}^{k}) \leq 0 \tag{2.10}$$

In the Zoutendijk's implementation of the method, the usable feasible direction is taken as the negative of the gradient direction if the initial point of the iteration lies in the interior, i.e.

$$\vec{S}^{k} = \nabla f(\vec{x}^{k}) \tag{2.11}$$

Otherwise, equations (2.9) and (2.10) are used to find an adequate search direction.

Sequential Quadratic Programming (SQP)

The SQP method has a theoretical basis that is related to the solution of a set of nonlinear equations using Newton's method and the derivation of simultaneous nonlinear equations using the Kuhn-Tucker conditions, which form the Lagrangian of the constrained optimization problem. For a complete derivation of the method, see for example Rao (1996).

Algorithmically SQP is identical to equation (2.8) where the feasible search direction, $\vec{S}$, is found from solving the following quadratic problem, i.e. find the $\vec{S}$ which minimizes

$$Q(S) = \nabla f(x)^{T} S + \frac{1}{2} S^{T} [H] S \tag{2.12}$$

subject to

$$\beta_j g_j(\vec{x}) + \nabla g_j(\vec{x})^T \vec{S} \le 0 \tag{2.12.1}$$

$$\beta_j h_j(\vec{x}) + \nabla h_j(\vec{x})^T \vec{S} = 0 \tag{2.12.2}$$

where $\left[\vec{H}\right]$ is a positive definite matrix that is taken initially as the identity matrix and is updated in subsequent iterations so as to converge to the Hessian matrix of the Lagrangian of the original problem (2.6). The last two constraints are linearized by taking $\beta_j = 1$ if $g_j(\vec{x}) \le 0$ and $\beta_j = 0.9$ if $g_j(\vec{x}) > 0$. Problem (2.12) is then easily solved using a linear quadratic programming algorithm.

2.2.2.2 Non-gradient-Based Optimization Algorithms

Most practical energy system synthesis/design problems are characterized by mixed continuous,-discrete variables, and discontinuous and nonconvex synthesis/design surfaces. If standard nonlinear programming techniques such as the ones presented above are used exclusively for this type of problem, they will be insufficient and in most cases find a relative optimum that is closest to the starting point (i.e. a local minimum or maximum). In addition to this, gradient-based methods cannot use discrete variables since gradients with respect to integer numbers are not defined.

A number of methods circumvent the above problems by means of specialized search schemes. These types of algorithms specialize in performing a complete search of the entire synthesis/design space and as a consequence are often referred to as global search algorithms[14]. Among these are rule-based expert systems and their more advanced implementations such as Tabu search and Hybrid expert systems. The latter are heuristic methods and have received considerable attention lately. However, the most popular and most developed methods for global search are Neural Networks, Simulated Annealing and Genetic Algorithms. Here we briefly describe the last two methods.

[14] It should be noted that since such algorithms do not use Lagrange's method or some derivative thereof for finding a local or a global optimum, one cannot strictly speaking from a mathematical standpoint claim that one has found a Kuhn-Tucker point at the end of the search. On the other hand, practice shows that the point found is indeed typically close to a Kuhn-Tucker point although again as pointed out in footnote 2 above this is not our concern here since we are not interested in mathematical proofs but in improved syntheses/designs.

Simulated Annealing (SA)

Simulated annealing (SA) is a very smart variant of the connectivity matrix method (page 30) and, in spite of some limitations that are discussed below, is a very reliable process synthesizer. Though originally conceived as a multi-variable optimization tool, it was later adapted to function as a synthesis/design optimizer.

Simulated annealing was introduced by Metropolis et al. (1953) and is used to approximate the solution of very large combinatorial optimization problems (e.g., NP-hard problems). The technique originates from the theory of statistical mechanics and is based upon the analogy between the annealing of solids and solving optimization problems. Assuming the objective is to find the configuration that minimizes a certain cost function E, the algorithm can then be formulated as follows. Starting off at an initial configuration, a sequence of iterations is generated. Each iteration consists of the random selection of a configuration from the neighborhood of the current configuration and the calculation of the corresponding change in cost function ΔE. The neighborhood is defined by the choice of a generation mechanism, i.e. a ”prescription” to generate a transition from one configuration into another by a small perturbation. If the change in cost function is negative, the transition is unconditionally accepted; if the cost function increases, the transition is accepted with a probability based upon the Boltzmann distribution, namely,

$$P_{acc}(\Delta E) \approx \exp\left(-\frac{\Delta E}{kT}\right) \tag{2.13}$$

where k is a constant and the temperature T is a control parameter. This temperature is gradually lowered throughout the algorithm from a sufficiently high starting value (i.e. a temperature where almost every proposed transition, both positive and negative, is accepted) to a “freezing”" temperature, where no further changes occur. In practice, the temperature is decreased in stages, and at each stage the temperature is kept constant until thermal quasi-equilibrium is reached. All parameters which determine the temperature decrease (the initial temperature, stop criterion, temperature decrease between successive stages, number of transitions for each temperature value) factor into what is called the cooling schedule.

Consequently the four key “ingredients” for the implementation of simulated annealing are: the definition of configurations, a generation mechanism, i.e. the

definition of a neighborhood on the configuration space, the choice of a cost-function (i.e. objective function), and a cooling schedule.

Genetic Algorithms (GAs)

Genetic Algorithms (GAs) are based on the principles of genetics and Darwin's theory of natural selection. The basic elements of natural genetics - crossover, mutation, and selection - are used in the genetic search procedure. Genetic algorithms were formally introduced in the United States in the 1970s by John Holland at the University of Michigan. The continuing price/performance improvement of computational systems has made them attractive for some types of optimization. In particular, genetic algorithms work very well on mixed (continuous and discrete), combinatorial problems. They are less susceptible to getting 'stuck' at local optima than gradient search methods. But they tend to be computationally expensive.

The algorithm is started with a set of solutions (represented by chromosomes) called a population. Solutions from one population are taken and used to form a new population. This is motivated by a hope that the new population will be better than the old one. Solutions which are selected to form new solutions (offspring) are selected according to their fitness - the more suitable they are the more chances they have of reproducing.

In Holland's original algorithm, GAs are characterized by bit string representations (chromosomes) of possible solutions to a given problem and by transformations used to vary those coded solutions. The algorithm is based on an elitist reproduction strategy where the individuals considered most fit are allowed to reproduce, thus, strengthening the chromosomal makeup of the new generation. Although many schemes to represent syntheses / designs as chromosome-like strings are possible (Hajela, 1999), the most popular is the use of binary quantities[15]. Thus, each synthesis/design variable is represented as strings of 0s and 1s, with the string length defining the desired precision. A number of such strings constitute a population of syntheses / designs. The recommended number of individuals in a population is in

[15] Note, that depending on the application, other representations, e.g., floating point numbers, maybe more appropriate or useful than using a binary representation. An example of this is found in Olsommer, von Spakovsky, and Favrat (1999a).

the range 2n to 4n where n is the number of independent variables (Rao, 1996)[16]. Each has a corresponding fitness value, F_v. The fitness value could be the objective function in a maximization problem (or its inverse in a minimization problem).

Once a chromosomal representation of the synthesis/design variables for a given population is available, the evolutionary mechanisms of selection, crossover and mutation are applied. One simplistic approach to selecting members of a population is to eliminate the individuals whose fitness value is below the average for the entire population. The selection proceeds by making copies of the fittest individuals so that the size of the new generation is equal to the original. The crossover process allows for an exchange of synthesis/design characteristics among members of a population. From the many ways in which crossover can be done (Goldberg, 1989), the most widely used approach is to randomly select two mating parents followed by a swap of binary numbers at a random position. Mutation safeguards[17] the search from a premature loss of information during reproduction and crossover. The fundamental idea is to choose a few members of the population using a probabilistic scheme and then switch a 0 to a 1 or vice-versa at a random place on the string. The GA then proceeds from generation to generation until no further improvements in the fitness function are achieved.

The three most important aspects of using genetic algorithms are: (1) definition of the objective function, (2) definition and implementation of the genetic representation, and (3) definition and implementation of the genetic operators. Once these three have been defined, the generic genetic algorithm should work fairly well. Beyond that many different variations to improve performance can be implemented, including niching (i.e. the ability to find multiple optima), improved selection and reproduction schemes, non-binary chromosomal representations, and parallelization of the algorithm.

The Connectivity Matrix Method

This method is a direct application of Graph Theory to process design. It consists of the following steps:

[16] Note that this is not a hard and fast rule since in the work by Olsommer, von Spakovsky, and Favrat (1999a) and Muñoz and von Spakovsky (2001a,b), the authors have shown that even with a vary large number of degrees of freedom that the GA works best when the population is kept between 50 and 150 members.

[17] This is only true up to a point. Additional considerations such as the chromosomal representation as well as the methods of selection and crossover can have significant impacts on assuring that there is no significant loss of information too early in the search process (see Olsommer, von Spakovsky, and Favrat, 1999a).

1. Create a logical process scheme, which entails the selection of the chemical/physical sub-processes that constitute the main process.
2. Construct the Connectivity Matrix (CM) for the logical process scheme. The rows of CM represent fluxes of matter or of energy, while the columns represent "operations" to be performed on these fluxes.
3. "Translate" each operation listed in CM into a series of physical transformations and devise one elementary sub-process scheme for each transformation.
4. Substitute into each transformation in every sub-process the component that performs it. Notice that at this point technical and operational constraints may come into play and limit or deny altogether the feasibility of a certain solution.
5. The resulting matrix is the Connectivity Matrix of the real process P. A proper quantitative simulation of P must now be performed to obtain the optimal set of operational parameters.

It is apparent that this method is a direct translation of the "mental scheme" a process engineer applies to a synthesis/design task, and it is entirely deterministic. Unfortunately, it is also clear that the method is strongly biased by the choices made in steps 1 and 3. Choosing a process scheme in fact sets a major structural constraint on the resulting process configuration, and this step is entirely left to the "experience" of the designer.

Artificial Intelligence

In the preceding, it is tacitly assumed that *all* process synthesis/design calculations can be carried out by properly implemented automated routines. Process synthesis/design is a highly labor intensive and highly interdisciplinary task and is, therefore, by necessity performed by a team of specialists. As a consequence, it is also very expensive in monetary terms; and there is a strong incentive to reduce this labor intensity (measured in man-hours). The only task that has as of yet not been fully automated is the *conceptual* one: the choice of the type and of the characteristics of the process itself. This automation can be implemented by a direct application of Artificial Intelligence (AI) techniques, whose specific task is to allow the codification of procedures that somehow mimic the thinking patterns of the human mind. Artificial

Intelligence is defined as the part of computer science that investigates symbolic, non-algorithmic reasoning processes, and the representation of symbolic knowledge for use in machine inference (Sciubba and Melli, 19998). Currently, only a subset of these techniques, called Expert Systems (ES), has been successfully applied to system optimization. As discussed before, ESs can be used to reproduce the engineer's decisional path that proceeds from the synthesis/design data and constraints to possible process configurations.

Despite the fact that the mechanisms of brains are very different in detail from those in computers, nonetheless they may be doing similar sorts of things (storing, transforming, using information). This has led to the investigation of neural networks partly inspired by ideas about how brains work. Some artificial neural networks have developed entirely as practical solutions to engineering problems without much concern for accurate modeling of brain mechanisms. More recent work attempts to move towards more and more accurate models of real neurons, which are incredibly complex and varied.

Another recent development related to AI is the work on simulated evolution. Biological evolution managed to produce an enormous variety of living organisms closely suited to different sets of needs in different environments. By modeling those processes on computers, it turns out that it is possible to get the computers to evolve solutions to problems that we were previously unable to find. Genetic algorithms (GAs) are increasingly being used both as a research tool and as a means of getting computers to solve practical problems. Genetic Programming (GP) extends these ideas by using structures which are better suited to the problem than those used by GAs. For instance, a GP system may directly manipulate tree-like structures representing rules or computer programs. This work links up with studies in Artificial Life (Alife), which is concerned with simulated evolution of various kinds of artificial organisms, possibly competing or collaborating with one another. Evolutionary techniques may use AI in the systems they evolve. Similarly AI systems may use evolutionary techniques to help with some of the harder problem solving tasks.

2.2.3 System Synthesis/Design Multi-Level Optimization Techniques

The use of the gradient and non-gradient based optimization techniques outlined above to solve the synthesis/design optimization problem in a single-level approach

assumes that the problem is simple enough to be solved in this way. It may, in fact, not be. If not, these techniques can still be employed provided they are used in conjunction with a multi-level approach, i.e. with some *decomposition* technique(s) (see Frangopoulos, von Spakovsky, and Sciubba, 2002). *Decomposition* is employed to break the optimization problem into a set of nearly equivalent smaller problems in order to facilitate the solution of the larger problem and overcome both the mathematical and cultural difficulties, which exist with highly complex, highly dynamic systems. Thus, *decomposition* can make an intractable, highly complex, highly dynamic problem with a large number of degrees of freedom tractable. *Decomposition* may also be warranted when certain company and geographical boundaries (e.g., design teams located far from each other) do not permit solution of the original problem as a single problem.

Conceptually, decomposition can be viewed as an interface between a designer's models, simulators and/or analyzers and the optimization algorithms (i.e. gradient-and non-gradient based) to which they would be coupled (see Figure 2.3). This defines a multi-level approach which contrasts with the traditional single-level approach in which the interface is absent. Four principal types of decomposition define such a multi-level approach: *disciplinary*, *conceptual*, *time*, and *physical*. The first of these, *disciplinary decomposition*, decouples, for example, a problem's thermodynamics and

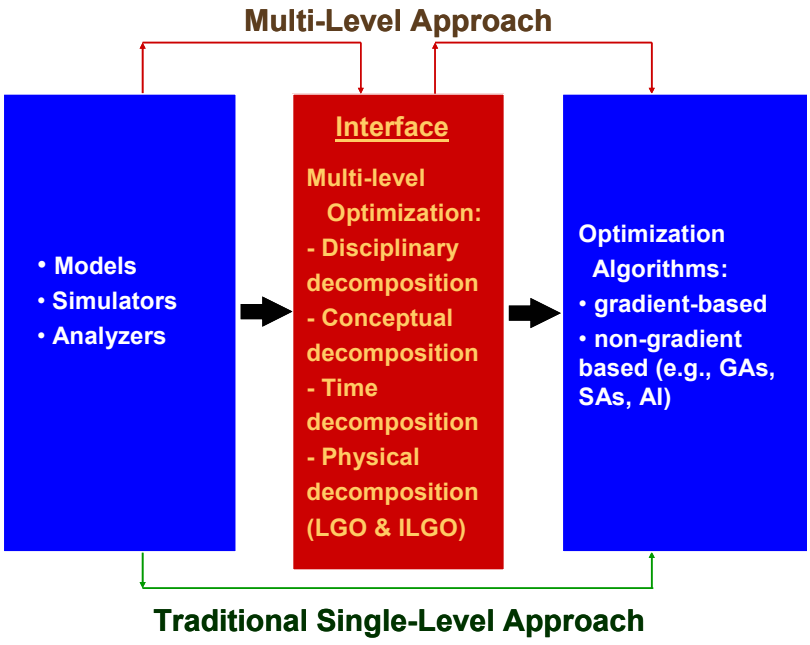

Figure 2.3 A conceptual view of decomposition.

economics (e.g., the costs associated with the manufacture, weight, and volume of components) and optimizes each discipline independently (e.g., El-Sayed, 1989; Zimering, Burnes, Rowe, 1999). *Physical decomposition* decomposes the system across unit (component or sub-system) boundaries (e.g., Muñoz and von Spakovsky, 2001a,b, 2002; Georgopoulos, von Spakovsky, and Muñoz 2002). For dynamic problems, it is also possible to divide the independent variables into *synthesis/design* variables (those which remain constant over time) and control or *operational* variables (those that can be varied in time). This breakdown is called *conceptual decomposition* (Frangopoulos, 1990; Olsommer, von Spakovsky, Favrat, 1999; Muñoz and von Spakovsky, 2001a,b, 2002; Georgopoulos, von Spakovsky, and Muñoz 2002). Finally, one additional form of decomposition, called *time decomposition* (e.g., Frangopoulos, 1990; Olsommer, von Spakovsky, Favrat, 1999; Muñoz and von Spakovsky, 2001a,b, 2002; Georgopoulos, von Spakovsky, and Muñoz 2002), decomposes or transforms a dynamic problem into a quasi-stationary one consisting of a series of stationary time segments.

In this work, only the latter three types of decomposition (conceptual, time, and physical) are used to solve the aircraft system synthesis/design optimization problem. A brief description of each of the four types of decomposition is given in the following sections.

2.2.3.1 Disciplinary Decomposition

The decision variables in energy system synthesis/design may be broken down into purely thermo-physical and transport variables (discipline: thermodynamics) and others which are purely geometrical (discipline: economics). Examples of the former are component adiabatic efficiencies, pressures, temperatures, and flow rates. Examples of the latter are the physical dimensions of a heat exchanger, the number of blades in a turbine, the technology level of the component (including the choice of material), etc.

With the above considerations in mind, it is possible to define a two-level optimization problem. At the highest level the problem would be one of minimizing the amount of fuel required to perform a given task. Typically the thermo-physical and transport variables are chosen by the high-level optimizer. These values are set as boundary parameters for each of the units in the system. The material (cost or weight)

used in each component is then minimized using the geometric parameters as the synthesis/design variables. The latter set of low-level problems uses geometry, technology, and material choices as decision variables.

2.2.3.2 Conceptual Decomposition

With conceptual decomposition the conceptual aspects of the optimization problem, i.e. synthesis, design, and operation, into two or three levels of optimization: i) *synthesis*, implying the set of components appearing in a system and their interconnections; ii) *design*, implying the technical specifications of the components and the properties of substances flowing throughout the system at the nominal load; and iii) *operation*, implying the operating properties of components and substances under specified conditions. An iterative procedure is used to move back and forth between the three levels of optimization, terminating once the global optimum[18] for the objective function has been found. This type of decomposition results in a set of nested optimization problems simpler than the original but much more computationally intensive (Olsommer, von Spakovsky, and Favrat, 1999a; Frangopoulos, 1990). To avoid this type of nesting, an approach used by Muñoz and von Spakovsky (2001a,b, 2002) completely separates the synthesis/design level(s) from the operational level, optimizing for the most stringent of the load/environmental conditions and a set of optimum and near-optimum feasible solutions determined for the given synthesis/design point. The overall computational burden is significantly reduced by the fact that only a limited number of feasible solutions need be optimally evaluated at off-design

2.2.3.3 Time Decomposition

The next type of decomposition is time decomposition, which decomposes the operational optimization problem into a series of quasi-stationary sub-problems each of which correspond to a given time interval. These can be optimized individually with respect to a set of unique operational/control variables and the results summed over all intervals. This form of decomposition complements the others.

[18] See footnotes 2 and 14 above.

2.2.3.4 Physical Decomposition

The final type of decomposition is physical decomposition, which looks at the system itself and breaks it down into a set of units (sub-systems, components, or sub-components), each of which forms a sub-problem within the context of the overall system optimization problem. All such approaches within the literature can be classified as Local-Global Optimization (LGO) other than the approach developed by Muñoz and von Spakovsky (2001a,b; 2002). This approach called Iterative Local-Global Optimization (ILGO) is the only one in the literature, which due to its unique features, successfully leads, for highly complex, highly dynamic systems, to what in the thermoeconomic literature is called a close approach to "thermoeconomic isolation" (Frangopoulos and Evans, 1984; von Spakovsky and Evans, 1993). The latter is defined as the ability to optimize independently each unit of a system and yet still arrive at the optimum for the system as a whole. The term "isolation" does not refer here to the individual optimization of a system component resulting from the optimization of the system as a whole. It is the opposite process of isolating components, optimizing their design, and then letting them interact in a system with the result that the system behaves optimally as well. A more complete discussion of "thermoeconomic isolation" is given in Chapter 3, Section 3.4.

In both LGO and ILGO, it is assumed that a number of disjoint sub-sets of the set of synthesis/design variables (one set for each unit and one, if needed in LGO, at the system level) can be established. Each set at the unit-level is used to optimize its respective sub-problem while the system-level set in LGO is used to optimize the overall problem at the system-level. For LGO, this results in a nested set of optimizations of unit-level problems within an overall system-level problem. In ILGO, there is no nesting due to the fact that these system level decision variables are replaced by coupling functions and a set of shadow prices (see the discussions in Chapter 3) which are then used to incorporate system-level information directly at the unit level, eliminating in the process the necessity of having to optimize explicitly at the system level.

Finally, the technique of physical decomposition (ILGO in particular) has the advantage of breaking the overall optimization problem into a set of much smaller, unit sub-problems, which can simplify a highly complex, non-linear problem of synthesis/design optimization and allow one to take into account a larger number of

decision variables (degrees of freedom) than would otherwise be possible. Physical decomposition makes it possible to simultaneously optimize not only at a system level, i.e. with respect to the system's performance and configuration, but also at a detailed component/sub-system level, i.e. with respect to the detailed geometry of the components themselves.

Chapter 3

Decomposition for the Large-Scale Optimization of Energy System Synthesis/Design

This chapter outlines three different decomposition strategies, i.e. *conceptual, time,* and *physical*, that address the need for large-scale, non-linear optimization. In the case of *physical decomposition*, two specific approaches are presented, namely, Local-Global Optimization (LGO) and Iterative Local-Global Optimization (ILGO). A number of versions of LGO can be found in the aerospace and thermoeconomics literature.

For a deeper understanding of the concepts presented in this chapter, the reader is referred to the work by Muñoz and von Spakovsky (2000a,b,c,d; 2001a,b). The case is made for the need of decomposition in the large-scale optimization of energy system synthesis/design. The problem in its full complexity is defined as a dynamic, non-linear, mixed integer programming problem. These presentations set the theoretical foundation for the work given in Chapters 4, 5 and 6.

3.1 The Dynamic, Nonlinear Mixed Integer Programming Problem

The synthesis/design optimization of an energy system in its most general form is a mixed integer non-linear programming (MINLP) problem with equality and inequality constraints. In general terms, this is expressed as

Minimize $f(\vec{x},\vec{y})$ (3.1)

w.r.t $\vec{x},\vec{y}$

subject to $\vec{H}(\vec{x},\vec{y}) = \vec{0}$ (3.2)

$\vec{G}(\vec{x},\vec{y}) \leq \vec{0}$ (3.3)

where $f(\vec{x},\vec{y})$ represents the figure of merit or objective of the optimization[19]; the vector $\vec{x}$ represents the set of independent synthesis/design variables of the system while $\vec{y}$ represents its set of operational or control variables. The synthesis/design variables typically correspond to geometric parameters (physical dimensions of components), design flow rates, design pressure ratios, and in a wider sense some discrete (e.g., material or technology choice) or binary (e.g., existence or nonexistence of a unit in the system configuration) parameters. Operational or control variables can be continuous variables (flow rates, valve settings) or binary variables (e.g., units on or off). The vector of equality constraints, $\vec{H}(\vec{x},\vec{y})=\vec{0}$, represents the mass and energy balances (or other balances such as, for example, those for exergy, momentum, etc.) as well as the performance constraints that the energy system must obey. The vector of inequality constraints, $\vec{G}(\vec{x},\vec{y})\le\vec{0}$, represents physical or artificial limitations imposed upon the system.

The modeling of an energy system typically begins with the selection of a number of degrees of freedom represented by parameters which can be varied at will within acceptable limits. These independent parameters or variables are then used to create two systems of equations to represent the energy system, i.e. equations (3.2) and (3.3).

The MINLP problem can be a highly complex problem which may not just be difficult to solve but may in fact be impossible to solve given the usual techniques of applied optimization. The complexity arises by virtue of the fact that a large number of degrees of freedom (both synthesis/design and operational variables) might be involved due to a desire to simultaneously optimize not only at a system level but at a detailed component/sub-system level. The complexity also arises because of detailed load profiles, of highly non-linear models, and of a mix of discrete and continuous variables. One option is to simplify the MINLP problem greatly by, for example, reducing the number of independent variables, considering only a single instant in time (i.e. only part of the load profile) or perhaps even linearizing certain or all of the aspects of the problem. The drawback, of course, to any of these measures is a loss of information, which may in fact not be necessary if the problem can be decomposed into a set of smaller problems, the solution to which closely approximates the solution to the combined problem.

[19] In the field of thermoeconomics, this is the total cost of the system.

3.2 Conceptual Decomposition

Two different types of conceptual decomposition were defined in *Chapter 2*, *section 2.2.3.2*: one which nests the operational-level optimizations within the synthesis/design level(s) of optimization and one which does not. The latter avoids this sort of nesting by completely separating the synthesis/design level(s) from the operational level. In this approach, the system's synthesis/design is optimized for the most stringent of the load/environmental conditions and a set of optimum and near-optimum feasible solutions determined for the given synthesis/design point. These feasible solutions are then optimized at all off-design conditions in order to determine the overall optimal solution. This type of decomposition (sometimes referred to as a form of time decomposition in the literature) reduces the computational burden seen with other approaches by assuming that only a limited number of feasible solutions need be optimally evaluated at off-design.

Most if not all energy systems must meet a set of loads (e.g., electricity, heat, and thrust) under a varying set of environmental conditions (e.g., ambient temperature and pressure). Thus, the synthesis/design optimization of the system must be done in such a way that the system is able to meet the most stringent load(s) and set of conditions as well as all other loads and conditions in the most efficient or cost effective manner. However, considering all load points simultaneously, especially for a very detailed load profile over a long period of time, further complicates an already complex problem. Conceptual decomposition surmounts this particular difficulty by decomposing the time variant features of synthesis/design into the synthesis/design at the most stringent load point, segment δ, followed by that at all other load points and conditions – i.e. a set, including the optimum and a number of near optimum syntheses/designs at the most stringent load point, are evaluated at all other load points in order to determine the optimal synthesis/design at all points[20]. The most stringent time segment (i.e. load point and set of environmental conditions) depends on the purpose of the system. In particular, for an advance tactical aircraft the most stringent time segment is defined by the mission envelope. The synthesis/design of the system is initially optimized with respect to this particular point that

[20] Obviously, conceptual decomposition makes the assumption that the global optimum found in this way approximates what would be found without conceptual decomposition. This is an assumption made on physical not mathematical reasoning, a discussion of which is beyond the scope of this thesis work. However, even if in certain cases this assumption is not true, the likelihood of a good solution is high (Muñoz and von Spakovsky, 2001a,b).

mathematically and on a thermoeconomic (thermodynamic and economic) basis is expressed in the following terms:

$$\textit{Minimize} \quad C_\delta = \left[\left(\sum_{r=1}^{R} c_r \dot{R}_r + \sum_{i=1}^{M} C_i^{operational} \right) \cdot \tau \right]_\delta + \sum_{i=1}^{M} C_i \tag{3.4}$$

$$\text{w.r.t.} \quad \widetilde{X}_\delta = \left\{ \vec{X}_1, \vec{X}_2, \cdots, \vec{X}_m \right\}_\delta \qquad \widetilde{Y}_\delta = \left\{ \vec{Y}_1, \vec{Y}_2, \cdots, \vec{Y}_m \right\}_\delta \tag{3.4.1}$$

subject to

$$\begin{aligned} \left[\vec{H} \right]_\delta &= \vec{0} \\ \left[\vec{G} \right]_\delta &\le \vec{0} \end{aligned} \tag{3.4.2}$$

where C_δ is the total cost of the energy system, C_i the capital cost of the i[th] unit (sub-system or component), M the number of units, τ the length of time considered for time segment i, $\dot{R}_r$ the rate of consumption of the r[th] resource, and c_r its unit cost. Finally, $C_i^{operational}$ represent other related operational cost of the i[th] unit such as maintenance. As is pointed out in Rancruel, von Spakovsky, and Muñoz (2001), the objective function, equation (3.4), deals with one time segment and can also be expressed in purely physical terms such as weight or fuel as was done in this research work.

The result obtained from solving equation (3.4) for a single synthesis / design is a set of feasible solutions (one optimal with respect to equation (3.4) and the others near-optimal) that satisfies the constraints given by equations (3.4.2). These solutions have a corresponding set of vectors $\widetilde{X}_\delta$ and $\widetilde{Y}_\delta$. The most promising of these feasible solutions are then used to minimize the total cost over the entire load/environmental profile for each of these feasible solutions. In order to obtain the synthesis/design that minimizes the total cost (or weight or fuel) of the energy system over the entire load/environmental profile, the following off-design optimization problem needs to be defined and solved for each time segment t where $t \neq \delta$

$$\textit{Minimize} \quad C_T^{operational} = \sum_{t=1}^{T-1} \left(\sum_{r=1}^{R} c_{rt} \dot{R}_r \right) \cdot \tau_t + \sum_{t=1}^{T-1} \left(\sum_{i=1}^{M} C_{it}^{operational} \right)_t \tag{3.5}$$

$$\text{w.r.t.} \quad \vec{Y}_t = \left\{ y_{1_t}, y_{2_t}, \ldots, y_{n_t} \right\} \tag{3.5.1}$$

$$\textit{subject to} \quad \left[\vec{H}\right]_{off-design} = \vec{0} \quad , \left[\vec{G}\right]_{off-design} \leq \vec{0} \tag{3.5.2}$$

$$\vec{X} - \vec{X}^{pf} = \vec{0} \tag{3.5.3}$$

where, $C_T^{operational}$ is the total operational cost of the system, $C_{it}^{operational}$ and c_{rt} represent other operational costs such as maintenance and resources unit cost respectively for the i[th] unit, which take into account the value of money in time and $\vec{Y}_t$ the set of system operational variables associated with the particular off-design time segment t of the load/environmental profile. Initially, the off-design optimization problem has to be solved for the T-1 off-design time segments with values of the synthesis/design independent (decision) variable vector $\vec{X}$ equal to $\vec{X}^{best}$, where $\vec{X}^{best}$ is the vector of the independent synthesis/design variables corresponding to the best (from the standpoint of the system-level cost objective) solution obtained by solving Problem (3.4). The solution to Problem (3.4) is actually a family of feasible solutions[21] that satisfy the constraints given by equations (3.4.1) and (3.4.2). However, the best solution, i.e. $\left(\vec{X}^{best}, \vec{Y}_\delta^{best}, C_\delta^{best}\right)$, is not necessarily the best when the various off-design conditions are taken into account. The vector $\vec{X}^{pf}$, appearing in equation (3.5.3), indicates that the T-1 off-design optimization problems have to be solved for each one of the promising feasible solutions obtained from Problem (3.4), i.e. $\left(\vec{X}^{pf}, \vec{Y}_\delta^{pf}, C_\delta^{pf}\right)$. The first term in equation (3.5) is used to evaluate each of the off-design time segments of the load/environmental profile, while the second term in equation (3.5) accounts for the maintenance costs which vary from one time segment to the next. The solution to Problem (3.5) effectively results in a set of optimal control or operational variable values $\vec{Y}_t$ for each time segment and an optimal total cost C_T for each promising solution from which the final synthesis/design for the system is chosen, i.e.

$$C_T^* = C_\delta^* + C_T^{operational^*} \tag{3.6}$$

[21] This family consists of the global minimum solution C_δ^{best} with corresponding decision variable vectors $\vec{X}^{best}$ and $\vec{Y}_\delta^{best}$, plus a set of near global minimum solutions C_δ^{pf} with corresponding vectors $\vec{X}^{pf}$ and $\vec{Y}_\delta^{pf}$.

$$\text{where, } C_\delta^{\,*} = \left[\left(\sum_{r=1}^{R} c_r \dot{R}_r^{\,*} + \sum_{i=1}^{M} C_i^{operational\,*} \right) \cdot \tau \right]_\delta + \sum_{i=1}^{M} C_i^{*} \qquad (3.6.1)$$

and equation (3.8) is valid for each promising solution.

As mentioned earlier, conceptual decomposition transforms the overall time-dependent problem of synthesis/design into two separate but linked problems (Problems (3.4) and (3.5). In particular, it decomposes a problem with *d*+*ot* variables (*d* design variables, *o* operational variables, and *t* time segments) into two smaller problems of *d*+o and *o(t-1)* variables, respectively. However, as a trade-off for reducing the number of variables which must be handled by any one problem, the expense of possibly having to carry out the optimization represented by Problem (3.5) for several possible promising solutions, i.e. those chosen in the synthesis/design optimization (Problem (3.4)), arises. In addition, even with conceptual decomposition, further decomposition for a very complex problem of synthesis/design optimization may be needed. Thus, both time and physical decomposition may still be needed.

3.3 Time Decomposition

Time decomposition transforms the operational optimization problem into a quasi-stationary problem consisting of a series of stationary sub-problems each of which correspond to a given time interval. Transient (unsteady) behavior within a given time interval is handled by breaking the interval into a series of smaller time segments and then numerically or analytically integrating over all the segments in order to capture the unsteady behavior of a component or sub-system. Each time interval is optimized individually with respect to a set of unique operational/control variables and the results summed over all intervals. This form of decomposition complements conceptual as well as physical decomposition. The form in which equation (3.5) above is written already assumes that time decomposition has been applied since if this were not the case, equation (3.5) would have been written with integrals and not summations

3.4 Physical Decomposition

Most energy systems can be decomposed into a set of units (sub-systems and/or components), each of which must have a clearly defined set of feedback or coupling functions with the other units of the system. Such a physical decomposition reduces

the overall system optimization problem of synthesis/design into a number of unit optimization sub-problems. Two main approaches to physical (unit) decomposition are presented in the following sections. The first is a Local-Global Optimization (LGO) approach characteristic of all other such approaches in the literature and the second is an original development by Muñoz and von Spakovsky (2000a,b,c,d; 2001a,b) called the Iterative Local-Global Optimization (ILGO) approach.

Unit (physical) decomposition, as opposed to time decomposition, tries to isolate the influence that each of the units that form a system has in terms of the overall (system-level) objective function. The unit's impact may be multi-disciplinary as shown below. To illustrate the fundamental differences between the leading decomposition methods (LGO and ILGO) for energy system synthesis/design, the simple two-unit system of Figure 3.1 will be considered where $\vec{Z}_1$ and $\vec{Z}_2$ are the decision variables, each unit is subject to a set of constraints which describe the physical processes present, and u_{12} and u_{21} are functions (in the general case, vectors of functions) that couple the two units. The typical objective function, C, is written as the sum of contributions of each of the units, i.e. $C_1 + C_2$. In turn, the contribution of each unit is composed of two terms as, for example, indicated below for unit 1:

$$C_1 = k_1 R_1 + C_{capital_1} \tag{3.7}$$

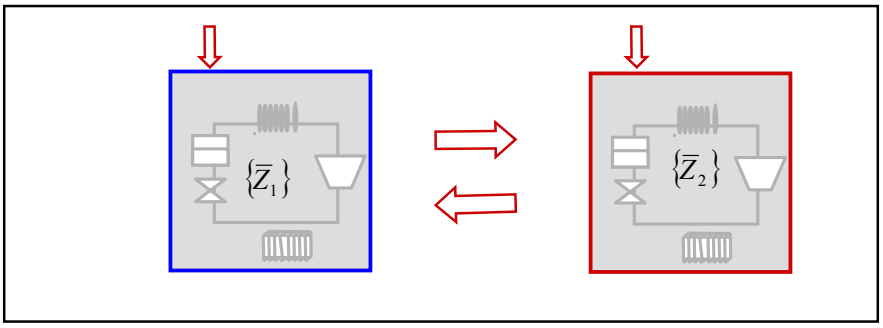

Figure 3.1 Physical decomposition of a 2-unit system.

In equation (3.7), R_1 is some external resource used by unit 1 (typically fuel) and $C_{capital_1}$ is a function related to the size of the unit (weight/volume, or cost) while k_1 is a conversion factor. In a thermoeconomic problem, $C_{capital_1}$ is the capital cost. In a thermodynamic problem $C_{capital_1}$ is either ignored, as may be the case for a stationary

system, or translated into physical terms such as weight, as would be the case for a transportation system.

Before proceeding with a comparison of LGO and ILGO as applied to the system of Figure 3.1, a few words are in order about the origins of the various methods for physical decomposition which come from the field of thermoeconomics. The first to devise a scheme for physical decomposition where Evans and El-Sayed (1970), which has come to be known as the Evans–El-Sayed Formalism. Without a doubt, this is the single most influential work in thermoeconomics, which also applies decomposition. Many of the leading cost assignment and optimization methods such as Engineering Functional Analysis - EFA (von Spakovsky and Evans, 1993; Evans and von Spakovsky, 1993), Thermoeconomic Functional Analysis - TFA (Frangopoulos, 1994), Structural Analysis (Valero et al., 1994) and others (e.g., Tsatsaronis and Pisa, 1994) are to a certain extent variations of the original Evans–El-Sayed method. This method was based on the Lagrange multiplier theorem of optimization and made possible, under certain very specific conditions, the decomposition of a system into units (for a brief discussion of the essential features of the original Evans–El-Sayed method, the reader is referred to Muñoz and von Spakovsky, 2002).

Based on the thermoeconomic approaches developed by Evans, Frangopoulos, and von Spakovsky (i.e. TFA and EFA), the concept of "thermoeconomic isolation (TI)" was introduced (Evans et al., 1980; Frangopoulos, 1983; Frangopoulos and Evans, 1984; von Spakovsky and Evans, 1984). As mentioned in the previous chapter, TI is defined as the ability to optimize independently each unit of a system and yet still arrive at the optimum for the system as a whole. TI is, in fact, a stronger condition than mere *decomposition*. In the latter, the complete set of decision variables for the system and its components can only partially be distributed to the units into which the system is decomposed, i.e. although each unit has its own local set of decision variables independent of those of the other units, there is still a subset of decision variables at the system level which cannot be uniquely assigned to any given unit. Thus, not all of the decision variables can be said to be disjoint, i.e. assignable to one and only one unit. TI, on the other hand, assumes that under certain conditions complete disjointness is possible so that simply optimizing at the unit level is sufficient for ensuring a system level optimum. The conditions required for TI in

these early methods (e.g., von Spakovsky and Evans, 1991) included an adequate functional breakdown of the system (i.e. a breakdown into units as described by the functional diagram of EFA or TFA), system and component cost functions and constraints based on second law quantities, and system and component cost functions linearized with respect to each corresponding function's (unit's) product.[22]

However, the practicality of linearazing in very complex systems as well as the negative associated with a possible loss of information makes the use of EFA and TFA in particular and the Evans / El-Sayed formalism in general questionable for achieving TI. In addition, TI has only been successfully achieved or closely approached using this formalism for very simple systems. Furthermore, none of these methods was developed for units coupled to non-energy systems as is the case in aircraft; and, thus, the conditions for closely approaching TI were never studied for those cases. Finally, the Evans / El-Sayed formalism indirectly assumes that a single group of analysts has access to and the expertise to work with all of the disciplines and the different technologies (units) that compose the system. This may, in fact, not be the case.

To overcome the difficulties mentioned above and eliminate the conditions required by these earlier methods for achieving or closely approaching TI, ILGO was developed. In order to compare the characteristics of LGO[23] with ILGO, a description of the LGO approach is given next.

3.4.1 The Local-Global Optimization (LGO) Approach

In the LGO approach, two levels of optimization instead of one are used. At the local or unit level, an optimization for each unit and each set of values of the coupling functions between units is carried out. These optimum results are then used at a global or system level at which the system synthesis/design is optimized[24] with

[22] Note that in ILGO which is described later, these conditions are completely eliminated and TI is achieved by embedding system-level information (i.e. that due to the decision variables which are not disjoint and, thus, exist at the system-level) explicitly at the unit level through the use of coupling functions and their associated shadow prices (see the discussions on LGO and ILGO below). Achieving or closely approaching TI in effect requires that the system-level optimum response surface (again, see the discussions below on LGO and ILGO) is either a hyperplane or a convex hypersurface.

[23] By definition, LGO is unable to achieve TI unless by happenstance all decision variables can be distributed into disjoint sets, each of which can be assigned to one and only one unit.

[24] Again, the reader is referred to footnotes 2 and 14 in order to emphasize that "optimized" need not be taken here in a strictly mathematical sense of guaranteeing that a Kuhn-Tucker point at the system-level is found. What is guaranteed and what is of importantance here is that with such decomposition approaches an "improved" synthesis/design is found.

respect to the coupling function values. In order to get a better understanding of the LGO approach, let us consider the following optimization problem applied to a system decomposed into two units as shown in Figure 3.1.

Minimize

$$C = k_1 R_1\left(\vec{Z}_1, u_{12}(\vec{Z}_1, \vec{Z}_2), u_{21}(\vec{Z}_1, \vec{Z}_2)\right) + k_2 R_2\left(\vec{Z}_2, u_{12}(\vec{Z}_1, \vec{Z}_2), u_{21}(\vec{Z}_1, \vec{Z}_2)\right) \tag{3.8}$$

w.r.t. $\vec{Z}_1, \vec{Z}_2$

subject to the primary constraints

$$\vec{H} = \begin{bmatrix} \vec{h}_1 \\ \vec{h}_2 \end{bmatrix} = \vec{0} \tag{3.8.1}$$

$$\vec{G} = \begin{bmatrix} \vec{g}_1 \\ \vec{g}_2 \end{bmatrix} \leq \vec{0} \tag{3.8.2}$$

and to the additional (secondary) constraints

$$u_{12}(\vec{Z}_1, \vec{Z}_2) - \xi = 0 \tag{3.8.3}$$

$$u_{21}(\vec{Z}_1, \vec{Z}_2) - \psi = 0 \tag{3.8.4}$$

where R_1 and R_2 are the resources used by units 1 and 2, respectively, k_1 and k_2 their respective unit costs, and $\vec{Z}_1$ and $\vec{Z}_2$ the set of independent variables for each unit used in the optimization of the system. Constraints (3.8.3) and (3.8.4) require that the coupling functions take on values of ξ and ψ such that

$$u_{12\,max} \leq \xi \leq u_{12\,min} \tag{3.8.5}$$

$$u_{21\,max} \leq \psi \leq u_{21\,min} \tag{3.8.6}$$

The cost of operating each unit is clearly identified in Problem (3.8). The contribution of each unit to the overall objective C is a function of the variables of each unit and the values ξ and ψ of the coupling functions. Therefore, for a given set of values ξ and ψ of the coupling functions, Problem (3.8) can easily be decomposed into two sub-problems, one for each of the units, i.e.

Sub-problem 1:

Minimize $C_1 = k_1 R_1\left(\vec{Z}_1, \xi, \psi\right)$ (3.9)

w.r.t. $\vec{Z}_1$

subject to $\vec{h}_1 = \vec{0}$ (3.9.1)

$\vec{g}_1 \le \vec{0}$ (3.9.2)

Sub-problem 2:

Minimize $C_2 = k_2 R_2\left(\vec{Z}_2, \xi, \psi\right)$ (3.10)

w.r.t. $\vec{Z}_2$

subject to $\vec{h}_2 = \vec{0}$ (3.10.1)

$\vec{g}_2 \le \vec{0}$ (3.10.2)

where for purposes of simplification it has been assumed that the capital costs are zero. Thus, Problem (3.8) is effectively reduced to two smaller problems (Problems (3.9) and (3.10)) by physical decomposition. Problems (3.9) and (3.10) have to be solved several times for different values of ξ and ψ of the coupling functions u_{12} and u_{21}. The values selected for the coupling functions must be included within the limits expressed by equations (3.8.5) and (3.8.6). It is assumed in using LGO that it is possible to find different sets of values for the independent variable vectors $\vec{Z}_1$ and $\vec{Z}_2$ which correspond to particular values ξ and ψ of u_{12} and u_{21}.

The results for sub-problems 1 and 2 are a set of optimum values for each objective as a function of the coupling functions such that

$$C_1^* = min\left(k_1 R_1\left(\vec{Z}_1, \xi, \psi\right)\right) \tag{3.11}$$

$$C_2^* = min\left(k_2 R_2\left(\vec{Z}_2, \xi, \psi\right)\right) \tag{3.12}$$

Equations (3.11) and (3.12) imply that there exists a set of unit optimum independent variable vectors $\vec{Z}_1^*$ and $\vec{Z}_2^*$ that satisfy

$$C_1^* = k_1 R_1\left(\vec{Z}_1^*, \xi, \psi\right) \tag{3.13}$$

and $\quad C_2^* = k_2 R_2\left(\vec{Z}_2^*, \xi, \psi\right)$ (3.14)

for each set of values ξ and ψ of the coupling functions u_{12} and u_{21}. Graphically this is shown in Figure 3.2 where each local or unit optimum of the local objectives C_1 and C_2 are plotted as a function of the coupling functions u_{12} and u_{21}. A vector of optimum values for the system-level objective function results from combinations of the sum of the optimum solutions found by solving the local sub-problems, Problems (3.9) and (3.10), i.e. $C^* = C_1^* + C_2^*$.

In fact, every point of C^*_1 and C^*_2 versus u_{12} and u_{21} represents a local or unit optimum. When these two surfaces called unit-level Optimum Response Surfaces (ORSs) are combined, they form what is called the system-level ORS[25] for the system as a whole (see Figure 3.2). The system-level ORS defines the global or system-level problem given by

Minimize $C^* = k_1 R_1(\xi, \psi) + k_2 R_2(\xi, \psi)$ (3.15)

w.r.t. ξ, ψ

subject to

$$\vec{G} = \begin{bmatrix} \xi - u_{12\,\max} \\ -\xi + u_{12\min} \\ \psi - u_{21\,\max} \\ -\psi + u_{21\min} \end{bmatrix} \leq \vec{0} \qquad (3.15.1)$$

This system-level optimization problem consists of finding the optimum values of the coupling functions that minimize the global or system-level objective. At the system-level, the independent variable vectors $\vec{Z}_1$ and $\vec{Z}_2$ of each unit do not appear. This is because of the assumption made earlier that there are a unique set of local or unit optimum values $\vec{Z}_1^*$ and $\vec{Z}_2^*$ for every combination of ξ and ψ.

[25] For a system with more than two coupling functions, the ORS is in fact a hyper-surface.

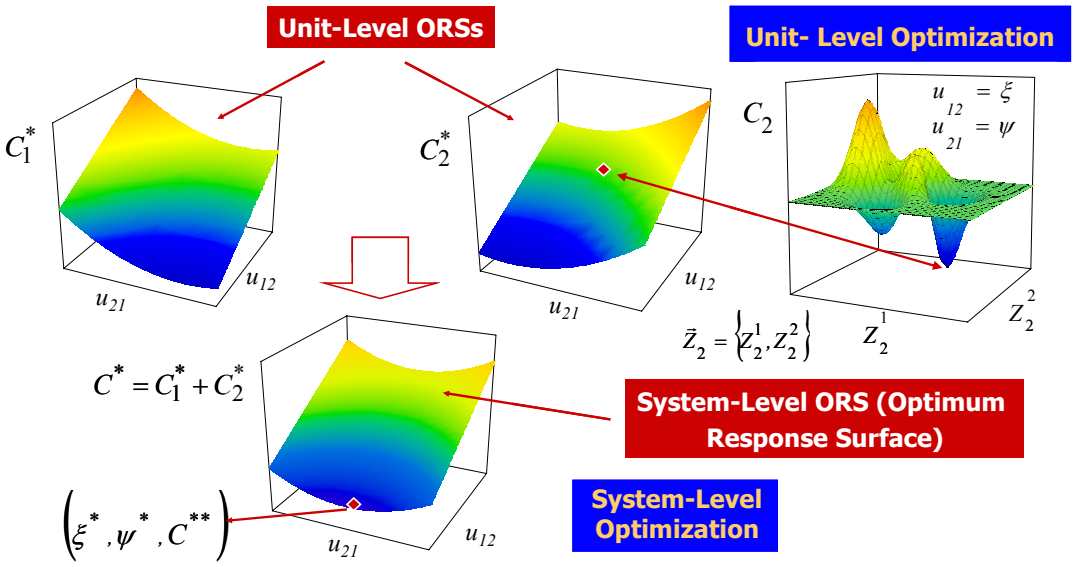

Figure 3.2. Local (unit) and global (system) optimizations.

The LGO technique has the advantage of breaking a large problem into smaller sub-problems that can be solved simultaneously. The drawback is the computational burden that this approach has for large, complex systems since each sub-problem must be solved independently many times in order to generate the system-level ORS. This is further compounded by the need for heuristic algorithms to deal with a mix of real and integer variables in the optimization and by the use of computationally expensive (unit) analyzers. To circumvent these drawbacks Muñoz and von Spakovsky (2000a,b,c,d; 2001a,b) developed the Iterative Local-Global Optimization (ILGO) approach. There are two complementary versions of this approach: ILGO-A and ILGO-B. Both are presented in the following sections. However, before proceeding, the algorithm for LGO is summarized as follows:

- Identify the independent variable vectors ($\vec{Z}_1$ and $\vec{Z}_2$) and the coupling functions (u_{12} and u_{21}).
- Define and solve the unit-level optimization problems (Problems (3.9) and (3.10)) for different values of ξ and ψ of the coupling functions u_{12} and u_{21} and find a set of local or unit optimum values $\vec{Z}_1^*$ and $\vec{Z}_2^*$ for every combination of ξ and ψ.
- Define and solve the system-level optimization problem (Problem (3.15)).

3.4.2 Iterative Local-Global Optimization (ILGO) Approach.

In addition to not having the drawbacks outlined in the previous section for LGO, the ILGO decomposition strategy makes possible the decentralized, integrated synthesis/design optimization of systems by allowing multiple platforms and software tools as well as geographically dispersed and discipline diverse teams of engineers to effectively interact both at the unit (local) and the system (global) levels. This decomposition approach is an advance over other decomposition approaches in the literature (i.e. LGO) in that it

- eliminates the nested optimizations (whether implicit or explicit) required in standard local-global decomposition approaches;
- uses an intelligent search based on shadow prices to effectively search the system-level Optimum Response Surface(s) - ORS(s) without having to actually generate the ORS(s);
- assures consistency between all local objectives and the system-level objective;
- introduces no constraint inconsistencies from one sub-problem to another;
- is conducive to the parallelization of the various sub-problem optimizations.

In the following sections, two versions of the ILGO approach (ILGO-A and ILGO-B) are presented. Even though the presentation is only given for a two unit system (as was done with the LGO approach), both approaches are completely general and applicable to any multiple unit system. In addition, they are applicable whether or not a system is hierarchical[26] or non-hierarchical.

3.4.2.1 Iterative Local-Global Optimization Approach A (ILGO- A).

The Iterative Local-Global Optimization (ILGO) approach eliminates the need for implicitly or explicitly (Muñoz and von Spakovsky, 2000a,b,c,d; 2001a,b) creating the ORSs by using a first order Taylor series expansion to approximate the local behavior of the system-level ORS. A formal presentation of Approach A of this method (i.e. ILGO-A) is given below. Consider a modified version of Problems (3.9)

[26] In a hierarchical system, all the components flow from a principal component.

and (3.10), where the two sub-problems are now solved for particular values ξ_o and ψ_o of the coupling functions u_{12} and u_{21}, i.e.

Sub-problem 1:

Minimize $C_1 = k_1 R_1\left(\vec{Z}_1, \xi_o, \psi_o\right)$ (3.16)

w.r.t. $\vec{Z}_1$

subject to $\vec{h}_1 = \vec{0}$ (3.16.1)

$\vec{g}_1 \le \vec{0}$ (3.16.2)

Sub-problem 2:

Minimize $C_2 = k_2 R_2\left(\vec{Z}_2, \xi_o, \psi_o\right)$ (3.17)

w.r.t. $\vec{Z}_2$

subject to $\vec{h}_2 = \vec{0}$ (3.17.1)

$\vec{g}_2 \le \vec{0}$ (3.17.2)

The resulting values for the optimum solutions are $(C_1^*)_o$ and $(C_2^*)_o$ with corresponding independent variable vectors $(\vec{Z}_1^*)_o$ and $(\vec{Z}_2^*)_o$. The subscript o that accompanies the optimum solutions serves as a reminder that they are calculated at the initial or reference point. At this point, a Taylor series expansion of the unit-level objective functions is performed about the ORS reference point and the linear terms are taken so that

$$C_1^* = \left(C_1^*\right)_o + \left(\frac{\partial C_1^*}{\partial u_{12}}\right)_o \Delta u_{12} + \left(\frac{\partial C_1^*}{\partial u_{21}}\right)_o \Delta u_{21} \tag{3.18}$$

$$C_2^* = \left(C_2^*\right)_o + \left(\frac{\partial C_2^*}{\partial u_{12}}\right)_o \Delta u_{12} + \left(\frac{\partial C_2^*}{\partial u_{21}}\right)_o \Delta u_{21} \tag{3.19}$$

The partial derivatives in equation (3.18), which are in fact "shadow prices"[27] (von Spakovsky and Evans, 1993), are evaluated at the optimum value C_1^* of the objective for sub-problem 1 based on the choice of ξ_o and ψ_o for u_{12} and u_{21}, respectively. In fact geometrically, these partial derivatives or shadow prices are the slopes of the unit-level ORS at each local (unit) optimum point in the u_{12} and u_{21} directions. The shadow prices indicate the relative importance of the coupling functions in terms of the overall system-level objective. Similarly, for sub-problem 2, a set of shadow prices, i.e. slopes, of the surface for unit 2 at ξ_o and ψ_o can be found. Using a more compact notation, equations (3.18) and (3.19) can be written as follows:

$$C_1^* = \left(C_1^*\right)_o + \lambda_{12}^1 \Delta u_{12} + \lambda_{21}^1 \Delta u_{21} \tag{3.20}$$

$$C_2^* = \left(C_2^*\right)_o + \lambda_{12}^2 \Delta u_{12} + \lambda_{21}^2 \Delta u_{21} \tag{3.21}$$

Depending on the sign and absolute value of the partial derivatives or shadow prices for units 1 and 2, an improved restricted optimum value of the system-level objective given by

$$C^* = \left(C_1^*\right)_o + \left(C_2^*\right)_o + \left(\frac{\partial C_2^*}{\partial u_{12}} + \frac{\partial C_1^*}{\partial u_{12}}\right)_o \Delta u_{12} + \left(\frac{\partial C_2^*}{\partial u_{21}} + \frac{\partial C_1^*}{\partial u_{21}}\right)_o \Delta u_{21} \tag{3.22}$$

can be obtained by changing the values of the coupling functions in the directions and with the magnitudes indicated by the shadow prices. Equation (3.22) is obviously a construction of the restricted optimum local objectives, equations (3.18) and (3.19), and furthermore represents the restricted system-level optimum point which appears on the ORS for the system-level optimization given in Figure 3.3. Thus, an iterative procedure called ILGO-A is established where by starting with random values of the coupling functions, new values (ξ and ψ) for these functions are selected based on the slopes. ILGO-A, therefore, moves intelligently using the shadow prices towards the global (system-level) optimum[28] without having to actually create the ORS in Figure 3.4 or any of the local surfaces shown in Figure 3.3. This and the fact that no

[27] A "shadow price" is a type of "marginal cost" since it represents the marginal cost associated with marginal changes in a unit or local objective's optimum value with respect to marginal changes in the value of an associated coupling function.

[28] See footnotes 2, 14, and 22 for a discussion of what is meant here in regards to the use of the term "optimum".

nested optimizations of local (unit-level) within global (system-level) are required prove to be major advantages of ILGO-A over LGO.

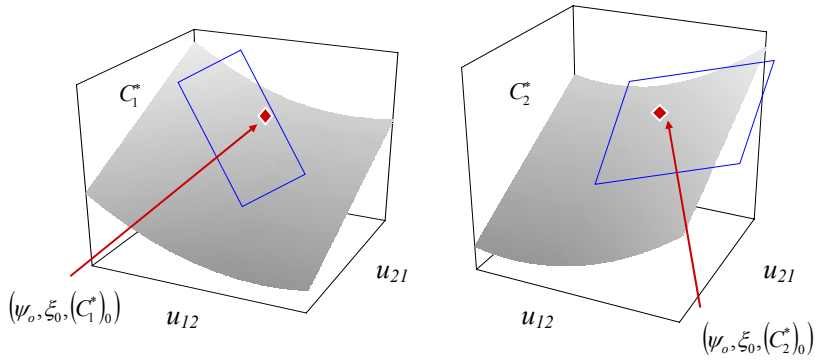

Figure 3.3 Initial restricted unit or local optimum points.

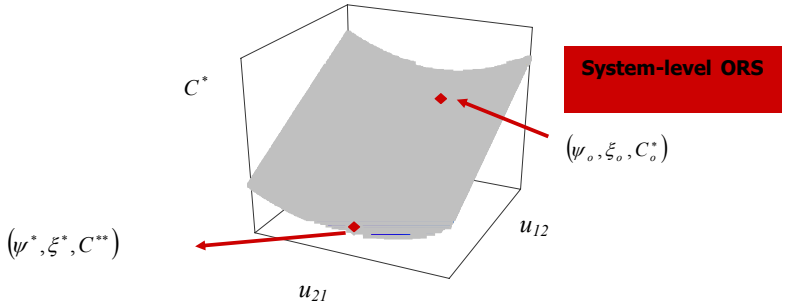

Figure 3.4 The restricted system-level optimum point on the system-level ORS for the initial values ξ_o and ψ_o.

3.4.2.2 Iterative Local-Global Optimization Approach B (ILGO-B).

The feasibility of the ILGO-A approach presented in the previous section is based on the existence of a set of vectors $\vec{Z}_1^*$ and $\vec{Z}_2^*$ for each set of values ξ and ψ that minimizes equations (3.16) and (3.17) and satisfies the unit constraints. However, this assumption, that every combination of ξ and ψ leads to a feasible solution, may not be warranted for some systems. In fact, it is possible that the ILGO-A approach may point towards simultaneous increases in u_{12} and u_{21}, which due to the characteristics of the units is not physically possible. For such cases, Muñoz and von Spakovsky (2000a,b,c,d; 2001a,b) propose an alternative version of ILGO-A called

ILGO-B. The latter redefines the local or unit objectives so that each sub-problem is formulated as follows:

Sub-problem 1 [29]:

$$\text{Minimize } C_1' = C_1 + \left(C_2^*\right)_o + \left(\frac{\partial C_2^*}{\partial u_{12}}\right)_o \Delta u_{12}^{(1)} + \left(\frac{\partial C_2^*}{\partial u_{21}}\right)_o \Delta u_{21}^{(1)} \tag{3.23}$$

w.r.t. $\vec{Z}_1$ and subject to the same constraints as in Problem (3.16)

Sub-problem 2:

$$\text{Minimize } C_2' = C_2 + \left(C_1^*\right)_o + \left(\frac{\partial C_1^*}{\partial u_{12}}\right)_o \Delta u_{12}^{(2)} + \left(\frac{\partial C_1^*}{\partial u_{21}}\right)_o \Delta u_{21}^{(2)} \tag{3.24}$$

w.r.t. $\vec{Z}_2$ and subject to the same constraints as in Problem (3.17).

The above sub-problems have the advantage that only values of the independent variables close to $\left(\vec{Z}_1^*\right)_o$ and $\left(\vec{Z}_2^*\right)_o$, which lead to feasible solutions, are allowed to participate in the optimization, thus, circumventing the physically infeasible solutions which the ILGO-A approach could produce in its search for the global optimum.[30] The expressions for the objective functions C_1' and C_2', i.e. equations (3.23) and (3.24), take into account the fact that variations in the independent (decision) variables of the unit being optimized has an impact on the local (unit) objective function of both units. For example, variations in the decision variables of unit 1, namely, $\vec{Z}_1$, cause changes $\Delta u_{12}^{(1)}$ and $\Delta u_{21}^{(1)}$ in the coupling functions u_{12} and u_{21}, respectively, according to the following relationships:

$$\Delta u_{12}^{(1)} = \frac{\partial u_{12}}{\partial \vec{Z}_1} \Delta \vec{Z}_1 \tag{3.25}$$

and $$\Delta u_{21}^{(1)} = \frac{\partial u_{21}}{\partial \vec{Z}_1} \Delta \vec{Z}_1 \tag{3.26}$$

[29] Note that this problem is the minimization of cost in unit 1 plus the projected change in cost in the rest of the system (in this case, unit 2) as a consequence of the variation of the local independent variables.

[30] See footnotes 2, 14, and 22 for a discussion of what is meant here in regards to the use of the term "global optimum".

where the superscript (1) indicates that the changes in the coupling functions are due to a variation in $\vec{Z}_1$ only[31]. These changes translate into a variation in the optimum value of the local objective function of unit 1 *and* unit 2. The impact on the local objective function of unit 2 (when solving Problem 3.23) is taken into consideration through the shadow prices (the λ's), i.e.

$$\lambda_{12}^2 = \left(\frac{\partial C_2^*}{\partial u_{12}} \right)_o \tag{3.27}$$

and $$\lambda_{21}^2 = \left(\frac{\partial C_2^*}{\partial u_{21}} \right)_o \tag{3.28}$$

Therefore, Problems (3.23) and (3.24) are not strictly speaking local sub-problems. In the work of Muñoz and von Spakovsky (2000a,b,c,d; 2001a,b) such problems are called *unit-based, system-level optimization problems* since in effect system-level information has now been embedded directly into each local or unit-level objective. It is this embedding that leads to the more general nature of ILGO-B over ILGO-A and to the very desirable feature for ILGO-B of eliminating the nested optimizations from which LGO suffers.

The algorithm for versions A and B of the ILGO approach as given in Muñoz and von Spakovsky (2000a,b,c,d; 2001a,b) is as follows:

1- Obtain an initial point of the optimum response surface with u_{12} and u_{21} equal to ξ_o and ψ_o by solving the optimization sub-problems (ILGO-A and -B).
2- Calculate the partial derivatives (shadow prices) of the restricted optimum values of the local objective functions C_1^* and C_2^* with respect to ξ and ψ (ILGO-A and -B).
3- For ILGO-A , update the values of ξ and ψ based on

$$(\xi_o)_{new} = (\xi_o)_{old} - \alpha \left(\frac{\partial C_i^*}{\partial \xi} \right)_o \tag{3.29}$$

[31] In the same fashion, superscript (2) indicates that the changes in the coupling functions are due to a variation in $\vec{Z}_2$ only.

$$(\psi_o)_{new} = (\psi_o)_{old} - \alpha\left(\frac{\partial C_i^*}{\partial \psi}\right)_o \tag{3.30}$$

where the partial derivatives of the equations (3.29) and (3.30) are selected in order to decrease the total system-level objective (equation (3.22)).

For ILGO-B, estimate the maximum allowable values of Δu_{12} and Δu_{21}[32]. If no information is available, assume that the partial derivatives are constant over most of the optimum response surface.

4- For ILGO-A, once the value of the coupling functions have been updated, steps 1 through 3 are repeated until no improvement in the unit optimizations is achieved or until the coupling functions have reached the minimum allowable values.

   For ILGO-B, the unit-based system-level optimization Problems (3.23) and (3.24) are defined and solved subject to the additional constraint that the values of the increment have to be constrained by a maximum (see Georgopoulos, 2002).

5- Finally, for ILGO-B, the solutions from the previous step are used to update $\left(\vec{Z}_1^*\right)_o$, $\left(\vec{Z}_2^*\right)_o$ and ξ_o and ψ_o. Repeat the procedure until no improvement is achieved or until the coupling functions have reached the minimum allowable values.

[32] Note that the values of the coupling function could be limited by physical constraints within the system.

Chapter 4

Total System Description and Synthesis/Design Problem Definition

4.1 Problem Definition

The synthesis/design task at hand is to perform the integrated optimization of five sub-systems, which are part of an advanced military aircraft. The problem is to carry out the preliminary design optimization of a low-bypass turbofan engine with afterburning (Propulsion Sub-system - PS), the preliminary synthesis/design optimization of an air-cycle Environmental Control Sub-system (ECS), a Thermal Management Sub-system (TMS), and an Airframe Sub-system (AFS). Note that the TMS is actually comprised of two sub-systems: a vapor compression/PAO sub-system (VC/PAOS) and a fuel loop sub-system (FLS).

The PS provides the necessary thrust, while the AFS provides the necessary lift for the vehicle to carry out the desired mission. The mission[33] is the set of conditions under which the aircraft must be synthesized/designed. Here, the mission defined by the Request for Proposal for an Air-to-Air Fighter (AAF) given by Mattingly et al. (1987) is used. The mission has 14 different segments (phases or legs). A general description of the mission is given in Figure 4.1. and Tables 4.1 and 4.2. In addition to providing the required rates of climb and acceleration and overcoming the aircraft's drag, the PS must provide the power required to operate all the remaining sub-systems.

[33] The mission is equivalent to the load profile and set of environmental conditions in a stationary application.

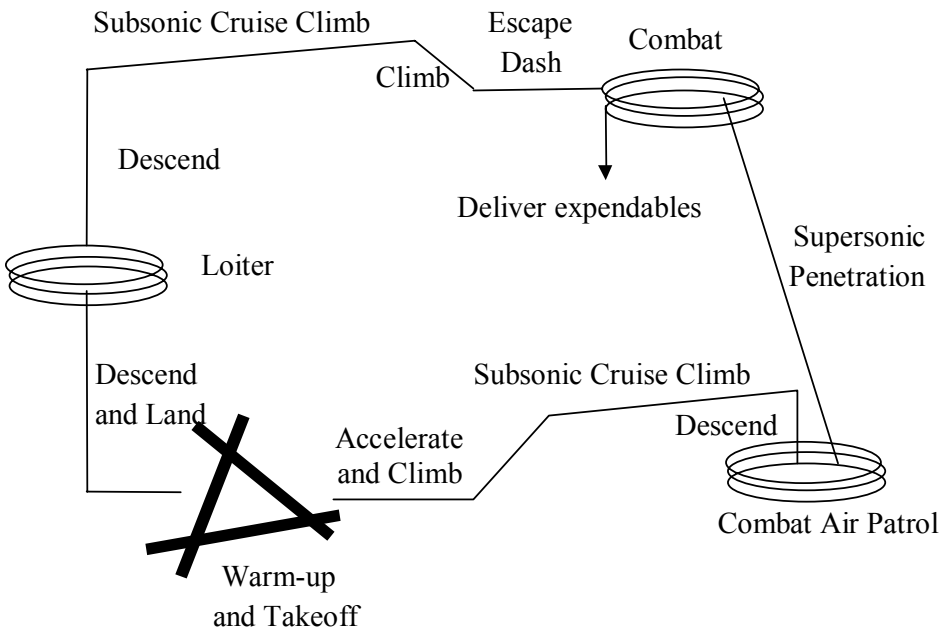

Figure 4.1. Mission profile by phase or leg (Mattingly et. al., 1987).

Table 4.1 Performance requirement/constraints.

Item	Requirement / Constraints
Payload	• 2 AMRAAM missiles (148 kg each) • 2 AIM-9L missiles (87 kg each) • 500 rounds of 25 mm ammo (522 fixed weight (cannon, ammo casings, etc), 125 kg spent ammunition)
Max. Mach Number	2.0 @ 12,200 m
Acceleration	$0.8 \rightarrow 1.6$ M/9150 m $t \leq 5$ s
Sustained g level	$n \geq 5$ at 0.9 M/9150 m, $n \geq 5$ at 1.6 M/9150 m
Crew	One (90 kg pilot plus equipment)
Fuel	JP-4
Cooling	Requirements as per cooling, temperature and pressure schedules given by Muñoz and von Spakovsky (1999)
Jet Engines	One or two engines. Bleed air flow rate and bleed port depend on ECS synthesis/design.

Table 4.2 Mission Specifications.

Phase	Description
1	Warm-up and take-off, field is at 600 m pressure altitude with T=310 K. Fuel allowance is 5 min at idle power for taxi and 1 min at military power for warm-up. Take-off roll plus rotation must be $\leq$ 450 m on the surface with a friction coefficient = 0.05. $V_{TO} = 1.2V_{STALL}$
2	Accelerate to climb speed and perform a minimum time climb in military power to best cruise mach number and best cruise altitude conditions (BCM/BCA)
3	Subsonic cruise climb at BCM/BCA until total range for climb and cruise climb is 280 km
4	Descend to 9150 m
5	Perform combat air patrol loiter for 20 min at 9150 m and a Mach number for best endurance.
6	Supersonic penetration at 9150 m and M=1.5. Range=185 km
7	Combat is modeled by the following: • Fire 2 AMRAAM missiles • Perform one 360 deg., 5g sustained turn at 9150 m, M=0.9 • Accelerate from M=0.8 to M=1.6 at 9150 m at max. power • Fire 2 AIM-9Ls and ½ ammo. Conditions at end of combat are M=1.5 at 9150 m
8	Escape dash, at M=1.5 and 9150 m for 46 km.
9	Using military power, do a minimum time climb to BCM/BCA
10	Subsonic cruise climb to BCM/BCA
11	Subsonic cruise climb at BCA/BCM until total range from the end of combat equals 278 km
12	Descend to 3000 m
13	Loiter 20 min at 3000 m and a Mach number for best endurance
14	Descend and land, field is at 600 m pressure altitude with T=310 K. A 2 s free roll plus breaking distance must be $\leq$ 450 m. Runway has a friction coefficient = 0.18. $V_{TD} = 1.15V_{STALL}$

The ECS and TMS provide the cooling necessary for dissipating the heat generated in the aircraft. A set of cooling requirements has been added to the mission according to the synthesis/design specifications given by Muñoz and von Spakovsky (1999). These requirements are shown in Table 4.2. Overall aircraft performance is

significantly affected by the thermodynamic performance of on board sub-systems. The major factor affecting the thermodynamic performance of these sub-systems is heat sources. These heat sources can be separated in two categories, internal and external. Internal sources are comprised of avionics, hydraulics, generators, fuel pumps, people, engine, gearbox; etc. External sources include kinetic (friction) and solar.

The most commonly used cooling methods are the ECS and the TMS. Modern aircraft cooling sub-systems face a number of challenges that are produced by higher speed flight conditions and increasing internal heat loads such as those due to avionics and those coming from the propulsion sub-system. Heat is transferred from heat sources to heat sinks outside or within the aircraft. The available heat sinks are ambient air, bleed air, and fuel.

Table 4.3 AAF critical mission segments.

Mission segments		
No.	**Name**	
1	wup	Warm-up
2	tka	Take-off acceleration
3	tkr	Take-off rotation
4	clac	Climb/accelerate
5	scc	Subsonic cruise climb
6	cap	Combat air patrol
7	acc	Acceleration
8	pen	Penetration
9	ct1	Combat turn 1
10	ct2	Combat turn 2
11	cac	Combat acceleration
12	esc	Escape dash
13	scc_2	Subsonic cruise climb 2
14	loi	Loiter
15	mmn	Maximum Mach number

Now, in order to complete the definition of the optimization problem for a given objective function, it is necessary to subdivide the mission of Figure 4.1 and Table 4.1 into segments (phases or legs). A preliminary analysis reveals that the mission

segments and phases of Table 4.3 above are the most critical ones, either because their fuel consumption is significant or the operating conditions are very stringent for the five sub-systems being synthesized/designed.

4.2 Air Frame Sub-system Description and Modeling

The fact that the airframe problem as stated below in equation (4.24) can be solved in terms of the drag polar relation and the ratio of thrust at sea level to the gross take off weight opens the possibility for using ILGO to solve the airframe unit-level optimization problem (non-energy sub-system) along with those for the PS, TMS, and ECS (energy sub-systems). Moreover, the drag and the drag due to the lift depend not only on the flight conditions and requirements (e.g., Mach number) but also on the airframe subsystem geometry and weight. In describing the model for the AFS in the following sections, the influence the airframe sub-system geometry (i.e. the aerodynamics) has on the system-level optimization problem will become evident.

4.2.1 Aerodynamics

The Airframe[34] Sub-system in this work is defined as the empty aircraft, which includes all subsystems such as the fuselage, wings tail, gear, etc. but excludes the fuel weight, the payload, and the equipment group[35]. Since the PS, the TMS and the ECS have been defined as independent sub-systems, they are also excluded from the AFS. Designers can take advantage of the fact that the AFS can be separated into sub-components (e.g., fuselage, wings, tail, gear, etc.) to introduce new subsystems into the system level optimization problem.

The AFS has two characteristics especially interesting from an optimization point of view, which are weight and geometry. These characteristics rely on each other (e.g., variation of weight produces changes in the optimum geometry and changes in the geometry affect the final gross take-off weight). This interdependence leads to the fact that improvements (reduction) in weight generated by the usage of new technologies like composite materials lead to an improvement in geometry (e.g., reduction of the wing surface area), which in turn means a reduction in wing weight.

[34] The AFS consists of the wings, tails, fuselage, landing gear, engine mounts, fire walls, engine section (but not the inner workings of the engine, i.e. the PS), and air induction sub-systems.
[35] The equipment group includes: flight controls, instruments, hydraulics, electrical sub-systems, avionics, furnishings, and miscellaneous empty weight.

This synergetic behavior can be effectively exploited using the optimization strategy proposed in this work

Airframe weight and geometry are not only the base for solving the unit-level optimization problem but are also the link between the AFS and the other sub-systems. For instance, equations (4.1) to (4.24) below show the effect of weight and geometry (i.e. aerodynamics, drag and lift) on thrust for each mission segment, which in turn determines the performance requirements and constraints for the PS, which in turn yields the engine weight to be used in the AFS optimization problem.

The relationship between the different sub-systems that make up an aircraft is very complex. Before attempting to understand all of the factors involved in the problem, consider an aircraft system such as the one shown in Figure 4.2. An energy balance on the aircraft leads to the following expression:

$$\{T-(D+R)\}V = W\frac{dh}{dt} + W\frac{d}{dt}\left\{\frac{V^2}{2g}\right\} \tag{4.1}$$

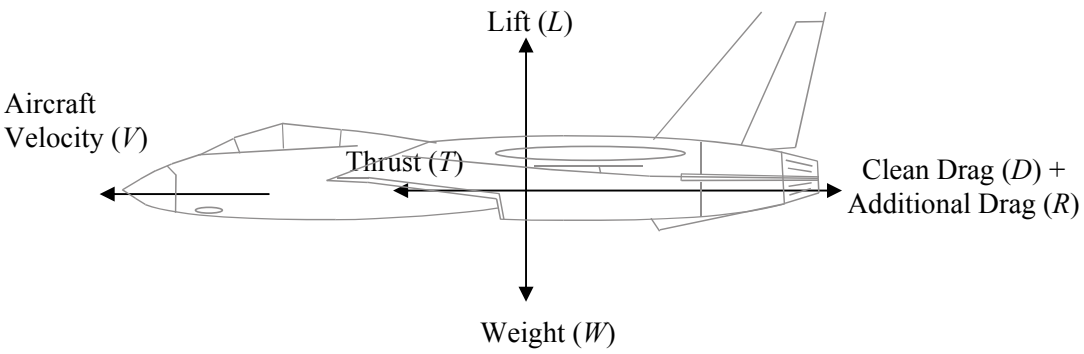

Figure 4.2 Force balance on an aircraft.

The term on the left-hand-side of equation (4.1) is the net rate of mechanical energy input. The first and second terms on the right-hand-side represent the storage of potential and kinetic energy, respectively. Note that the total resistance (D + R) is the sum of the drag of the "clean" aircraft (D) and any additional drag (R) associate with protuberances. Here, R represents the drag due to the TMS and ECS. If the installed thrust is defined as $T_i \equiv \alpha T_{SL}$ where α is the installed full throttle thrust lapse, i.e. the fraction of the sea level take-off thrust, which depends on altitude and

speed, and if the instantaneous weight is given by $W \equiv \beta_i W_{TO}$ here β_i is the fraction of the take-off weight at segment *i*, which depends on how much fuel has been consumed, then equation (4.1) becomes

$$\frac{T_{SL}}{W_{TO}} = \frac{\beta}{\alpha}\left[\frac{D + R}{W_{TO}\beta}\right] + \frac{1}{V_i}\frac{d}{dt}\left(h_i + \frac{V_i^2}{2g}\right) \tag{4.2}$$

The lift and drag analysis begins with the well known aircraft relationships

$$L = nW = qC_L S \tag{4.3}$$

and $$D = qC_D S \tag{4.4}$$

where n is the load factor, which is equal to the number of g's perpendicular to the direction of the velocity.

Aerodynamic Coefficients

A lift-drag polar relationship of the form found in Mattingly, Heiser, and Daley (1987) and Raymer (2000) is assumed such that

Un-cambered: $$C_D = K_1 C_L{}^2 + C_{D_0} \tag{4.5}$$

Cambered: $$C_D = K_1 (C_L - C_{L\,min\_drag}) + C_{D_{min}} \tag{4.6}$$

where

$$C_{D_0} = C_{D\,min} + K'' C_{L\,min\_drag}^2 \tag{4.7}$$

C_{D_0} is the drag coefficient at zero lift. Also, for modern high-performance un-cambered aircraft, $C_{L\,min\_drag} \approx 0$. This leads to a following expression for the drag coefficient at zero lift:

Subsonic: $$C_{D_0} = C_{D_{\min}} = C_{fe}\frac{S_{wet}}{S_{ref}} \tag{4.8}$$

Supersonic: $$C_{D_0} = C_{fe}\frac{S_{wet}}{S_{ref}} + C_{D_{wave}} \tag{4.9}$$

According to the Oswald Span Efficiency Method (Raymer, 2000).

Subsonic: $$K_1 = \frac{1}{ARe\pi} \tag{4.10}$$

Supersonic: $$K_1 = \frac{AR(M^2 - 1)}{4AR\sqrt{M^2 - 1}} - 2\cos\Lambda_{LE} \tag{4.11}$$

where C_{fe} is the skin friction factor, $C_{D_{wave}}$ is the drag coefficient due to wave shocks, AR is the aspect ratio, M is the mach number, Λ_{LE} is the quarter chord sweep angle, and *e* is the span efficiency factor. Different expressions for C_{fe}, $C_{D_{wave}}$, and *e* can be found in the literature. These expressions can be rather general formulations which can be used during the preliminary synthesis/design stage or fairly elaborate statistical regressions which can be used during the detailed design stage. However, they all are a function of aerodynamic parameters such as aspect ratio, sweep angle, wing area, etc.

Subsonic Lift Slope

From the lift and drag model just presented, one can conclude that there is a strong dependence of the drag coefficient on AFS geometry (i.e. aerodynamics). This dependence can be exploited to find the optimum value for the drag coefficient in the context of all the aircraft sub-systems. The dependence of the subsonic lift coefficient on the same geometric parameters can be concluded from

$$C_L = C_{L\alpha}\alpha \tag{4.12}$$

where C_L is the wing lift coefficient, $C_{L\alpha}$ is the wing lift curve slope, and α is the angle of attack. A further analysis yields that

$$C_{L\alpha_{Subsonic}} = \frac{2AR\pi}{2 + \sqrt{4 + \frac{AR^2\beta^2}{\eta^2}\left(1 + \frac{\tan^2\Lambda_{\max t}}{\beta^2}\right)}}\left(\frac{S_{exposed}}{S_{ref}}\right)(F) \tag{4.13}$$

$$\beta^2 = 1 - M^2 \tag{4.14}$$

$$\eta = \frac{C_{\ell\alpha}}{2\pi/\beta} \tag{4.15}$$

$$F = 1.07(1 + d/b)^2 \tag{4.16}$$

In these equations, $\Lambda_{\max t}$ is the sweep of the wing at the chord location where the airfoil is thickest, $C_{\ell\alpha}$ is the airfoil lift curve slope, $S_{exposed}$ is the exposed wing platform, F is the fuselage lift factor, which accounts for the fact that the fuselage creates some lift due to the "spill over" of lift from the wing, d is the fuselage maximum equivalent diameter, and b is the wing span. As before, AR is the wing geometric aspect ratio of the complete reference platform. However the effective aspect ratio could be increased by using wing endplates or winglets, i.e.

$$AR_{effective} = AR(1 + 1.9\,h/b) \tag{4.17}$$

where h is the endplate height.

Supersonic Lift Slope

For a purely supersonic wing, the lift curve slope is given by

$$C_{L\alpha_{Supersonic}} = 4/\beta \tag{4.18}$$

when $M > 1/Cos\Lambda_{LE}$ (4.19)

For a mix flow wing (i.e. supersonic and subsonic are present), which is generally the case for high Mach number sweep wings, it is difficult to predict the lift curve slope. However, it can be done using sophisticated and accurate databases. To use this databases, geometric parameters are again required, i.e. aspect ratio, taper ratio, and leading edge sweep angle. If required, these databases can be added into the optimization code or specialized software to compute the lift curve slope along with state-of-the-art parsing programs, which allow data exchange in real-time between two or more codes built on different platforms (e.g., PERL; Larry Wall, 1995).

The wing is considered to be a purely supersonic flight when the wing leading edge is supersonic, i.e. the Mach cone angle is greater than the leading-edge sweep (see equation (4.19)). The actual lift curve for a wing in supersonic flight is difficult to predict as well without the use of sophisticated software or reliable databases. In this work, normal-force slope curves were used to compute the slope of the lift curve (Raymer, 2000; Hoak-Ellison, et al., 1982). For this research work, a vast number of fitted equations were developed from the normal-force-slope curves. These charts estimate the slope of the normal force coefficient, $C_{N\alpha}$, i.e. the lift curve slope in a

direction perpendicular to the wing. For low angles of attacks, which are usually the case for supersonic flight, this is approximately equals the lift curve slope $C_{L\alpha}$. Figure 4.3 shows a sample of the normal-force slope curves for a taper ratio of 0.25.

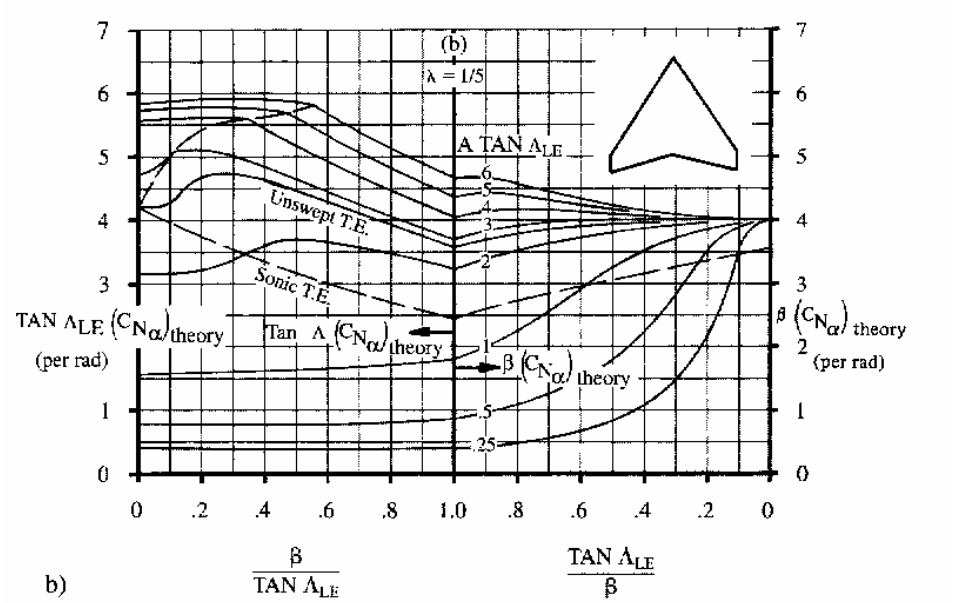

Figure 4.3 Characteristic wing supersonic normal force slope curve (Reprinted from Aircraft Design: A Conceptual Approach, copyright 1999 D. Raymer, All Rights Reserved, Used with author's permission.).

Maximum Lift Clean

The maximum clean lift, $C_{L\,max}$, usually determines the wing area. This in turn has a great influence upon the cruise drag, which strongly affects the aircraft takeoff weight. Therefore, the maximum lift coefficient is critical in determining aircraft weight. The maximum lift coefficient is determined by the wing geometry, e.g., if a wing has a low aspect ratio or has substantial sweep and a relatively sharp leading edge, the maximum lift is increased due to the formation of leading edge vortices. This vortex formation is strongly affected by the shape of the upper surface of the leading edge. A leading edge sharpness parameter (Δy) is defined as the vertical separation between the points of a wing's upper surface, which are 0.15% and 0.6% of the airfoil chord back from the leading edge. The airfoil selected for the advance tactical aircraft to be optimized was the NACA 64-006. The leading edge parameter for the NACA 64 series as a function of thickness ratio is given by

$$\Delta y = 21.3\,{}^{t}\!/_{c} \tag{4.20}$$

The leading edge sharpness parameter has been used to developed methods for the construction of the lift curve up to the stall for low or high aspect ratio wings. For high aspect ratios, equation (4.21) is used along with Figures (4.4a) and (4.4b). The

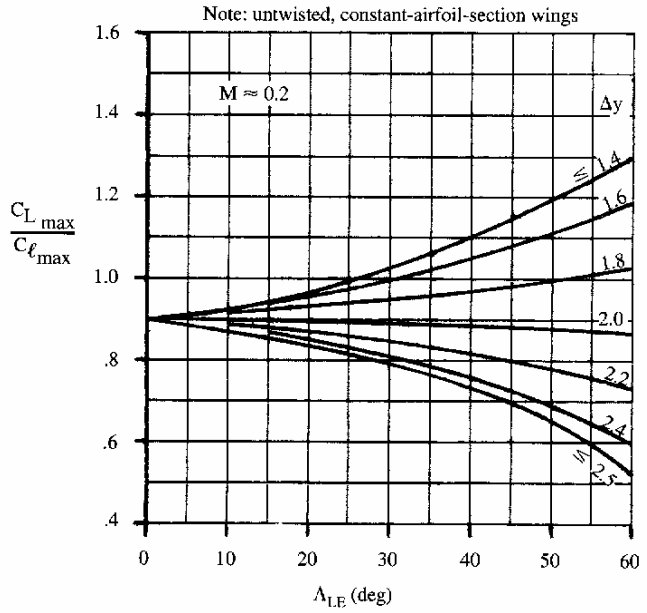

Figure 4.4a Subsonic maximum lift for a high aspect ratio wing (Reprinted from Aircraft Design: A Conceptual Approach, copyright 1999 D. Raymer, All Rights Reserved, Used with author's permission.).

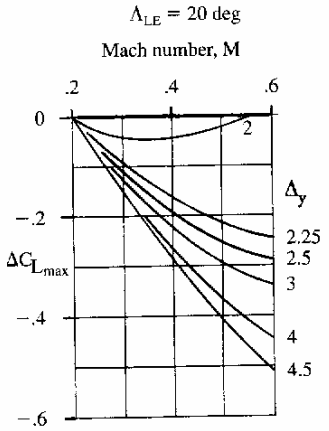

Figure 4.4b Mach number correction for the subsonic maximum lift of a high aspect ratio wing (Reprinted from Aircraft Design: A Conceptual Approach, copyright 1999 D. Raymer, All Rights Reserved, Used with author's permission.).

first term in equation (4.21) represents the maximum lift at a Mach of 0.2 found from Figure 4.4a, while the second term is the correction to a higher Mach number found from Figure 4.4b. This latter figure shows $\Delta C_{L\,max}$ as a function of Mach number and Δy for a leading edge angle of 20 degrees. Thus, a family of curves is necessary for

different sweep angles to compute the Mach number correction for the subsonic maximum lift of a high aspect ratio wing, i.e.

$$C_{L\,max} = C_{l\,max}\left(\frac{C_{L\,max}}{C_{l\,max}}\right) + \Delta C_{L\,max} \tag{4.21}$$

where $C_{l\,max}$ is the airfoil maximum lift coefficient at Mach 0.2. The angle of attack for maximum lift is defined by

$$\alpha_{C\,Lmax} = \frac{C_{Lmax}}{C_{L\alpha}} + \alpha_{0L} + \Delta\alpha_{C_{Lmax}} \tag{4.22}$$

The first term represents the angle of attack as if the lift curve slope were linear all the way up to stall. The second term may be approximated as the airfoil zero lift angle. The third term is the correction for the non-linear effects of vortex flow, which is usually given by charts as a function of sweep angle, Mach number and Δy.

A different set of charts is used for low aspect ratio wings, where vortex flow dominates the aerodynamics. A low aspect ratio is defined by equation (4.23) where C_1 is a function of taper ratio. Thus,

$$A \le \frac{3}{(C_1 + 1)(\cos \Lambda_{LE})} \tag{4.23}$$

The maximum lift and the angle of attack for maximum lift for a low aspect ratio wing are defined by equation (4.24) and (4.25), respectively, such that

$$C_{L\,max} = \left(C_{l\,max}\right)_{base} + \Delta C_{L\,max} \tag{4.24}$$

$$\alpha_{C\,L\,max} = \left(\alpha_{C\,L\,max}\right)_{base} + \Delta\alpha_{C_{L\,max}} \tag{4.25}$$

were $\left(C_{l\,max}\right)_{base}$ and $\Delta C_{L\,max}$ are determined from Figures 4.5a and 4.5b correspondingly. The terms $\left(\alpha_{C\,L\,max}\right)_{base}$ and $\Delta\alpha_{C_{L\,max}}$ are also graphically represented and can be found in Raymer (2000). At transonic and supersonic speeds the maximum lift a wing can achieve is usually limited by structural considerations rather than aerodynamics. Unless the aircraft is flying at very high altitude, the available maximum lift at Mach 1 is usually enough to tear the wing off.

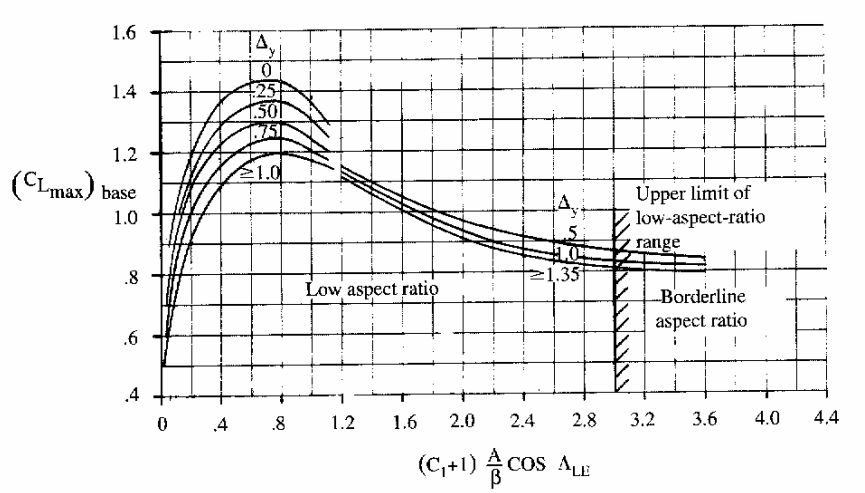

Figure 4.5a Subsonic maximum lift of a low aspect ratio wing (Reprinted from Aircraft Design: A Conceptual Approach, copyright 1999 D. Raymer, All Rights Reserved, Used with author's permission.).

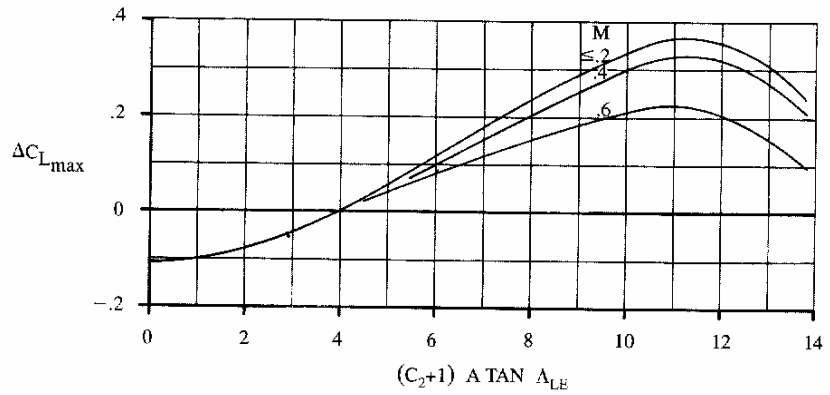

Figure 4.5b Mach number correction for the subsonic maximum lift of a low aspect ratio wing (Reprinted from Aircraft Design: A Conceptual Approach, copyright 1999 D. Raymer, All Rights Reserved, Used with author's permission.).

Maximum Lift with High-Lift Devices

There is always a basic incompatibility in aircraft wing synthesis/design. For cruise, a wing should have little camber and should operate at a high wing-loading. For takeoff and landing, a wing should provide lots of lift, which means lots of camber and low wing-loading. High-lift devices increase lift by increasing camber. There are many complex methods for estimating the effects of high-lift devices some of which are explained by Hoak-Ellison, et al., 1982. For the preliminary synthesis/design stage, equations (4.26) and (4.27) provide a reasonable estimate for the change in maximum lift and the change in zero-lift angle of attack for various types of flaps and leading edged devices, i.e.

$$C_{L\,max} = \Delta C_{l\,max}\left(\frac{S_{flapped}}{S_{ref}}\right)cos\,\Lambda_{H.L.} \tag{4.26}$$

$$\Delta\alpha_{OL} = \left(\Delta\alpha_{OL}\right)_{airfoil}\left(\frac{S_{flapped}}{S_{ref}}\right)\cos\Lambda_{H.L.} \tag{4.27}$$

where $\Delta C_{l\,max}$ is a function of the type of high-lift device and the flap chord and airfoil chord ratio. The subscript $_{H.L.}$ refers to the hinge line of the high-lift surface. The flapped area , $S_{flapped}$, is the projection of the high-lift device over the wing in the wing chord direction.

The Component Buildup Method for Parasitic (Zero-Lift) Drag

The component buildup method (Raymer, 2000) estimates the subsonic parasitic drag of each component of the aircraft using a calculated flat-plate skin-friction drag coefficient (C_f) and a component form factor (*FF*) which accounts for the pressure drag due to viscous separation. The interference effects on the component drag are calculated as the factor *Q*. The subsonic parasitic drag is given by

$$\left(C_{D_O}\right)_{subsonic} = \frac{\sum_{1}^{c}\left(C_{f_c}FF_cQ_cS_{wet_c}\right)}{S_{ref}} + C_{D_{MISC}} + C_{D_{L\&P}} \tag{4.28}$$

where $C_{D_{MISC}}$ is the miscellaneous drag coefficient, which accounts for special features such as flaps, upsweep aft fuselage, base area, etc. $C_{D_{L\&P}}$ is the contribution for leakage and protuberances. The subscript *c* indicates that those parameters are different for each component.

The flat-plate skin friction coefficient, C_f , depends on Reynolds number, Mach number, and skin roughness. The most important factor affecting skin-friction drag is whether or not the flow is laminar or turbulent. Equations (4.29) and (4.30) express the flat-plate skin friction coefficient for laminar and turbulent flow, respectively, i.e.

$$C_f = \frac{1.328}{\sqrt{\mathrm{Re}}} \tag{4.29}$$

$$C_f = \frac{0.455}{\left(\log_{10} \mathrm{Re}\right)^{2.58}\left(1 + 0.144M^2\right)^{0.65}} \tag{4.30}$$

$$\mathrm{Re} = \rho Vl \Big/ \mu \tag{4.31}$$

where l is the characteristic length. If the surface is relatively rough, the friction coefficient may be higher than indicated in equations (4.29) and (4.30). This is handled by using the "cut-off Reynolds number" given by equations (4.32) and (4.33), where k is the skin roughness value, which is 1.015×10^{-5} meters for smooth paint, i.e.

Subsonic: $$\mathrm{Re}_{cutoff} = 38.21\left(l \Big/ k\right)^{1.053} \tag{4.32}$$

Transonic or Supersonic: $$\mathrm{Re}_{cutoff} = 44.62\left(l \Big/ k\right)^{1.053} M^{1.16} \tag{4.33}$$

The lower of the actual Reynolds number and the cut-off Reynolds number should be used in equations (4.29) and (4.30).

Form factors for subsonic drag estimation are given by equations (4.34) to (4.36). These expressions are valid up to the drag divergent Mach number (0.8-0.9). Thus, for

Wing, Tail, Strut, and Pylon:

$$FF = \left[1 + \frac{0.6}{(x/c)_m}\left(\frac{t}{c}\right) + 100\left(\frac{t}{c}\right)^4\right]\left[1.34M^{0.018}\left(\cos\Lambda_m\right)^{0.28}\right] \tag{4.34}$$

Fuselage and Smooth Canopy:

$$FF = \left[1 + \frac{0.6}{f^3} + \frac{f}{400}\right] \tag{4.35}$$

Nacelle and smooth External Store

$$FF = 1 + \left(0.35 \Big/ f\right) \tag{4.36}$$

where $(x/c)_m$ is the chord-wise location at the airfoil maximum thickness point. Λ_m is the sweep angle at the maximum thickness line, and f is given by

$$f = \frac{l}{d} = \frac{l}{\sqrt{(4/\pi)A_{\max}}} \tag{4.37}$$

Parasite drag is increased due to the mutual interference between components. This is taken into account by the component interference factor Q. Estimates of this factor for each component are given by Raymer (2000) and Hoerner (1958). The drag of miscellaneous items can be determined separately using a variety of empirical graphs and equations and then the results added to the parasite drags calculated above. Leaks and protuberances add drag and are difficult to predict by any method. Leakage drag is due to the tendency of an aircraft to "inhale" through holes and gaps in high pressure zones and "exhale" in low pressure zones. Protuberances include antennas, lights, fuel vents, actuators, etc. Typically these drag increments are estimated as a percent of the total parasitic drag. For current fighter designs, leakage and protuberances drag is about 10-15% of the total parasitic drag.

Supersonic Parasitic Drag

The supersonic parasitic drag is calculated in a similar manner to the subsonic parasitic drag. However, there are two differences. First, the supersonic skin friction drag is not adjusted for form factor or interferences effects. Second a new term, the wave drag is added. It accounts for the pressure drag due to shock formation. The buildup for supersonic parasitic drag is given by

$$\left(C_{D_O}\right)_{subsonic} = \frac{\sum_{1}^{c}\left(C_{f_c} S_{wet_c}\right)}{S_{ref}} + C_{D_{MISC}} + C_{D_{L\&P}} + C_{D_{WAVE}} \tag{4.38}$$

where C_{f_c} is compute using equations (4.30) and (4.33). The drag of miscellaneous items can again be determined by empirical graphs and equations, and then the results added to the parasite drags calculated above. Many of the items that produce miscellaneous drag do not appear in supersonic aircraft, i.e. floats, open cockpits, etc. Leaks and protuberances drag for supersonic flight follows approximately the same percentage rule presented for subsonic flight but applied only to the skin friction drag.

Wave drag in supersonic flight is most times greater than all the others put together. Wave drag is pressure drag due to shocks and is a direct result of the way in which the aircraft's volume is distributed. An ideal volume distribution is produced by the Sears-Haack body (Sears, 1947), which follows the supersonic area rule (Nicolai, 1975). This volume distribution is defined by equation (4.39), and its wave

drag is given by Equation (4.40,) which is the minimum possible wave drag for any closed-body with the same length and volume. Thus,

$$\frac{r}{r_{max}} = \left[1 - \left(\frac{x}{l/2}\right)^2\right]^{0.75} \tag{4.39}$$

and $$\left(\frac{D}{q}\right)_{wave} = \frac{9\pi}{2}\left(\frac{A_{max}}{l}\right)^2 \tag{4.40}$$

where l is the longitudinal dimension, which is a function of the takeoff gross weight, r is the cross section radius, and A_{max} is the maximum cross section area. A_{max} and r are functions of the fitness ratio, which is turn is a designer's choice, depending upon drag generation considerations and other practical considerations such as the amount of inboard equipment.

Wave drag is reduced when the volume distribution resembles the Sears-Haack's model, which has a minimal amount of longitudinal curvature. Wave drag at Mach 1.0 is directly proportional to the second derivative of the longitudinal volume distribution. To minimize wave drag, the configuration should provide a smooth and bell-shaped volume distribution. For a typical aircraft, the wing tends to put a "bump" in the volume distribution. This bump can be reduced by pinching in the fuselage at the wing location, creating the characteristic "coke-bottle' area-rule fuselage.

No realistic aircraft will have a volume distribution identical to that of the Sears-Haack body. Nevertheless, a well synthesized/designed supersonic aircraft will have a theoretical wave drag at Mach 1.0 that is about twice the Sears-Haack value. A well-known method to predict the wave drag is the Mach-plane cut-volume distribution. However, it demands lots of computational time and is, thus, used primarily at the end of the preliminary synthesis/design stage or early in the detailed design stage. At high Mach number, it is very difficult to minimize the total wave drag by using area ruling without the Mach-plane cut-volume distribution. Therefore, it is recommended that one smooth the whole configuration through wing-body blending.

For a preliminary wave drag analysis at Mach numbers higher than 1.2, a correlation to the Sears-Haack body wave drag is represented by

$$\left(\frac{D}{q}\right)_{wave} = E_{WD}\left[1 - 0.386(M-1.2)^{0.57}\left(1 - \frac{\pi\Lambda_{LE-\deg}^{0.77}}{100}\right)\right](D/q)_{Sears-Haack} \tag{4.41}$$

where E_{WD} is an empirical wave drag efficiency factor and is the ratio between the actual wave drag and the Sears-Haack value. For supersonic fighters, E_{WD} is about 1.8-2.2. Note that this efficiency factor is less important for drag determination than the fitness ratio as represented by A_{max}/l. This term is squared, which explains why area ruling that actually reduces A_{max} provides a greater reduction in drag than does merely smoothing the volume distribution without lowering A_{max}. A complete parasitic-drag buildup analysis generates the curves seen in Figure 4.6 for a fixed altitude

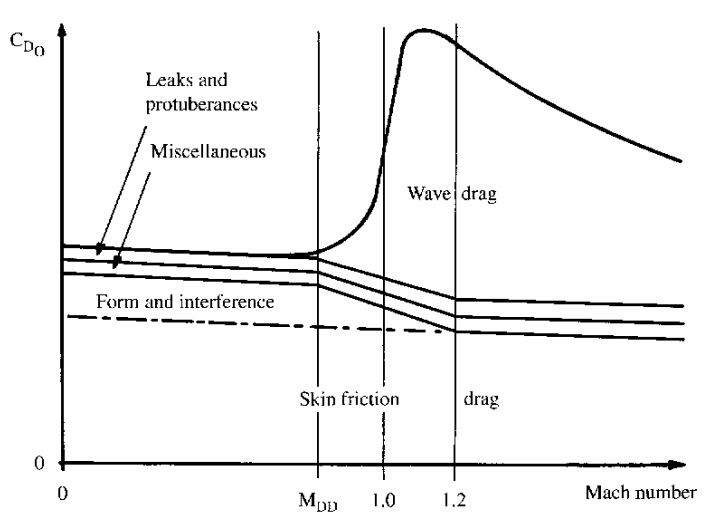

Figure 4.6 Complete parasite drag vs Mach numbre (Reprinted from Aircraft Design: A Conceptual Approach, copyright 1999 D. Raymer, All Rights Reserved, Used with author's permission.).

Drag Due to the Lift (Induced Drag)

The induced drag at moderate angles of attack is proportional to the square of the lift coefficient with a proportionality factor called the drag due to the lift factor or K_1. The literature presents several methods to compute this term. For this research work, the *leading edge suction method* was applied. This method has several advantages. First, for high speed design a better estimation of K_1 is achieved. Second, the effect of the change on viscous separation as the lift coefficient changes is included. Finally, this method reflects the choice of the wing design lift coefficient of the drag due to lift for different lift coefficients.

Drag for a given angle of attack is strongly affected by viscous separation. At high lift coefficient, the drag polar breaks away from the parabolic shape represented by the fixed value of K_1. Most methods neglect the change of K_1 with lift coefficient.

For a wing with a round leading edge, this is acceptable. However, for most supersonic aircraft, it gives a poor approximation. The leading edge suction method takes this into account. Figure 4.7 shows the leading edge suction concept. The thick airfoil on the left is at an angle of attack below that at which substantial separation occurs. The flow stream line curves rapidly to follow the leading edge radius over the top of the wing.

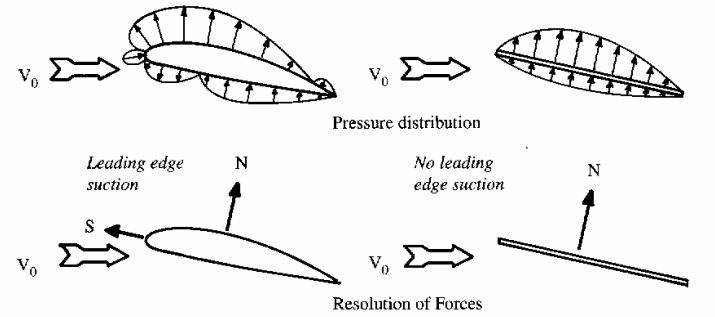

Figure 4.7 Leading edge suction definition (Reprinted from Aircraft Design: A Conceptual Approach, copyright 1999 D. Raymer, All Rights Reserved, Used with author's permission.).

This rapid curvature creates a pressure drop on the upper part of the leading edge. The reduced pressure exerts a suction force on the leading edge in the forward direction. This leading edge suction force *S* is shown at the bottom of the figure in a direction perpendicular to the normal force *N*. If there is no viscous separation or induced downwash, the leading edge suction force exactly balances the rearward component of the normal force and the wing experiences no drag. This is the ideal 2-D case called "100% leading edge suction". On the right side of Figure 4.7, there is a zero thickness flat-plane airfoil. Even without the leading edge separation, this airfoil has a higher drag because there is no forward facing area for the leading edge pressure force to act against. All pressure forces for a zero-thickness flat plate must act in a direction perpendicular to the plate shown as *N*. There is a zero leading-edge suction and the lift and induced drag are simply *N* times the cosine or sine of the angle of attack. Therefore,

$$L = N \cos\alpha \tag{4.42}$$

$$D_i = N \sin\alpha = L \tan\alpha \tag{4.43}$$

$$C_{D_i} = C_L \tan\alpha \tag{4.44}$$

and for small α,

$$C_{D_i} = KC_L{}^2 \cong \alpha C_L \tag{4.45}$$

$$K_1 = \frac{\alpha C_L}{C_L{}^2} = \frac{\alpha}{C_L} = \frac{1}{C_{L\alpha}} \tag{4.46}$$

Thus, in the worst case of zero leading-edge suction, the drag due to lift factor K_1 is simply the inverse of the slope of the lift curve (in radians) as previously determined. All real wings operate between 100% and 0% leading edge suction. The percentage of leading edge suction a wing attains is called *SS*. The method for calculating K_1 for high speed aircraft is based upon an empirical estimation of the actual percentage of leading-edge suction attained by a wing, which is then applied to the actual K_1 values for 100% and 0% leading-edge suction values. The actual K_1 is given by

$$K_1 = SSK_{100} + (1+S)K_0 \tag{4.47}$$

The 0% K_1 value is the inverse of the slope of the lift curve. The 100% K_1 value in subsonic flight is the inverse of the aspect ratio times π. At transonic speed, the shock formation interferes with the leading-edge suction. When the leading edge becomes supersonic, the suction becomes zero and the K_1 value equals the 0% K_1 value (see Figure 4.8). Figure 4.9 shows *SS* as a function of the design lift coefficient and the actual lift coefficient.

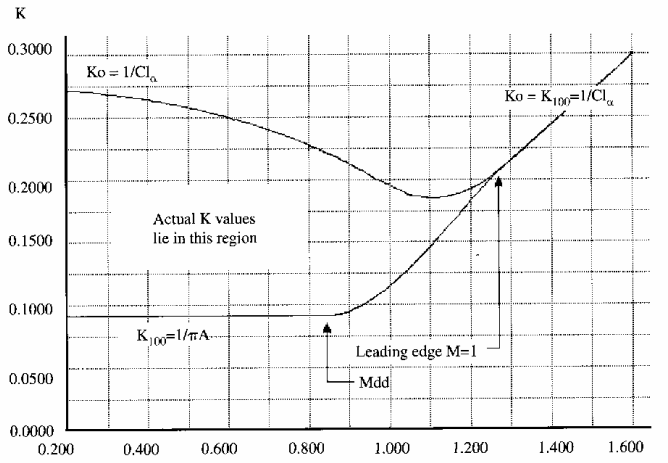

Figure 4.8 0% and 100% K_1 vs Mach number (Reprinted from Aircraft Design: A Conceptual Approach, copyright 1999 D. Raymer, All Rights Reserved, Used with author's permission.).

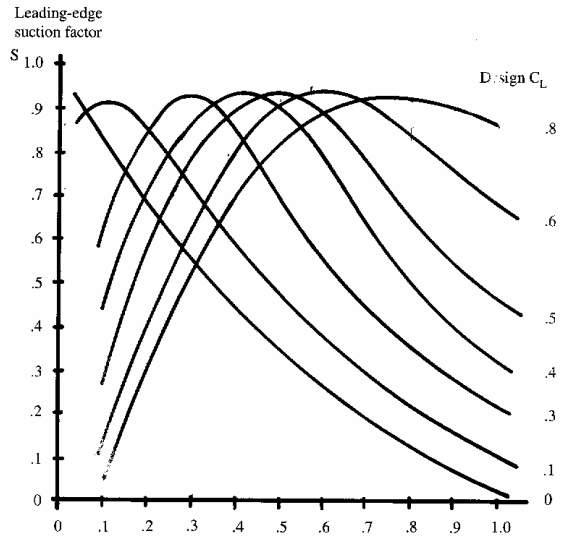

Figure 4.9 Leading-edge suction vs C_L (Reprinted from Aircraft Design: A Conceptual Approach, copyright 1999 D. Raymer, All Rights Reserved, Used with author's permission.).

Since $T_i \equiv \alpha T_{SL}$ and $W \equiv \beta_i W_{TO}$, combining equations (4.2) through (4.5) produces the thrust equation for the i_{th} mission leg, namely,

$$\frac{T_i}{W_i} = \frac{q_i S}{W_i}\left[K_1\left(\frac{n_i}{q_i}\frac{W_i}{S}\right)^2 + C_{D_0} + \frac{D_{ECS_i} + D_{TMS_i}}{q_i S}\right] + \frac{1}{V_i}\frac{d}{dt}\left(h_i + \frac{V_i^2}{2g}\right) \tag{4.48}$$

where the only additional drag, R, considered is the momentum drag created by the ECS and the TMS (i.e. $R = D_{ECS} + D_{TMS}$). In equation (4.48), the velocity V and the rates of climb dh/dt and acceleration dV/dt are directly or indirectly given by the mission specifications. The drag created by the ECS and TMS are also leg-dependent as is discussed below.

An alternative version of equation (4.48) can be given as a function of the sea level take-off thrust (T_{SL}) and the gross take-off weight (W_{TO}), i.e.

$$T_i = \alpha T_{SL} = q_i S\left[K_1\left(\frac{n_i}{q_i}\frac{\beta_i W_{TO}}{S}\right)^2 + C_{D_0} + \frac{D_{ECS_i} + D_{TMS_i}}{q_i S}\right]$$

$$+ \frac{\beta_i W_{TO}}{V_i}\frac{d}{dt}\left(h_i + \frac{V_i^2}{2g}\right) \tag{4.49}$$

Equation (4.49) represents the required thrust for each mission leg as a function of the gross take off weight, the mission weight fraction, additional drag, performance

requirements, and aerodynamic parameters. This equation incorporates the most important set of constraints to be used in the PS optimization problem in determining the optimum weight of the PS. The fact that the engine weight is part of the gross take-off weight allows the designer to use this term as a coupling function into the AFS optimization problem.

Equations (4.2) through (4.47) hint at the tight integration issues associated with the synthesis/design of an aircraft. The synthesis/design and operation of any given sub-system is highly influenced by and in turn influences the synthesis/design and operation of all the others. Take the case of the TMS, for example. The TMS's weight and energy and extra thrust requirements affect the required total thrust which leads to higher fuel consumption and higher take-off gross weight. Equation (4.49) clearly shows that an increase in W_{TO} is associated with higher thrust, which in turns affects the size of the PS. The weight of the AFS is also affected as indicated by table 4.8.

The characteristics and aerodynamics described above define a highly dynamic system where "everything affects everything else". Therefore, it is worthwhile including the AFS in the system-level optimization problem. Moreover, the ILGO-B approach can be used despite of the non-energy basis (i.e. its products are not electricity or heat) of the AFS. In order to set up the AFS unit-level optimization problem, a suitable set of feasible decision variables must be defined. Table 4.4. provides a set of viable variables which could be used. The designer, of course, must decide which of these variables should be introduced into the optimization problem and which should be assigned a value based on the information available. This decision should be made taking into account several factors such as information accuracy and availability, the design phase considerations, deadlines, etc.

Table 4.4 Set of possible AFS decision variables.

AIRFRAME SUB-SYSTEM			**REQUIREMENTS**	**SENSITIVITY STUDIES**
Aerodynamics (design)	**Configuration (synthesis)**	**Advance technologies**		
AR, Λ, t/c, λ	Variable sweep	Composite materials	Range/payload/crew	Dead weight
Fuselage fineness ratio	High-lift devices		Loiter time	C_{Do} and K^*C_{Dwave}
T/W and *W/S*	Tail type		Speed	C_{lmax}
Airfoil camber	Airfoil shape		Runway length	SFC
			Time to climb	Fuel price

Finally, even optimizing with respect to all the decisions variables given in Table 4.4 requires further analysis in the form of a sensitivity study to determine the effect of any number of other parameters on the synthesis/design of the AFS and in turn on the aircraft system as a whole. Such a sensitivity study could be used to determine how much the aircraft weight is impacted if various parameters such as drag or specific fuel consumption are increased. Furthermore, changes in external factors such as fuel price could also be analyzed. To know the expected impact of carrying more dead weight (e.g., two more internal missiles or avionics) might be desirable as well. In such a case, the internal density (i.e. takeoff weight divided by the internal volume) would be kept constant.

4.2.2 Constraint Analysis

Equation (4.49) can be manipulated to yield equation (4.50), which is a "master equation" for the flight performance of aircraft in terms of take-off thrust loading (T_{SL}/W_{TO}) and wing loading (W_{TO}/S). This equation is based on energy considerations and for each mission leg will provide relationships between (T_{SL}/W_{TO}) and (W_{TO}/S) which represents in fact the boundaries of the optimization problem. The derivation and study of these boundaries is known as constraint analysis.

$$\frac{T_{SL}}{W_{TO}} = \frac{\beta}{\alpha}\left\{\frac{q_i S}{W_{TO}}\left[K_1\left(\frac{n\beta}{q}\frac{W_{TO}}{S}\right)^2 + C_{D_0} + \frac{D_{ECS_i} + D_{TMS_i}}{qS}\right] + \frac{1}{V_i}\frac{d}{dt}\left(h_i + \frac{{V_i}^2}{2g}\right)\right\} \quad (4.50)$$

In equation (4.50), β is unknown; consequently, an initial numerical value for this weight fraction (see *section 4.2.3*) for each mission leg is required. This initial value is based on experience (i.e. regression of data from recent aircraft and new technology considerations). The actual values are found in the weight fraction analysis, which in turn needs *TSFC* information from the PS unit-level optimization problem. The actual values are used to update the constraint analysis. This shows the iterative nature of the aircraft synthesis/design optimization process. The fraction of the sea-level take-off thrust, α, is also based on experience and depends on the Mach number and whether or not there is afterburning. Once more the actual values will be produced by the PS unit-level optimization problem.

The constraint analysis is performed on the most stringent mission legs, generally 4 or 5. To show how it works, only the supersonic penetration and escape

dash leg curve are developed here. A complete constraints analysis for the aircraft optimized in this work is shown in Figure 4.10. This constraint analysis yields feasible values for the take-off thrust loading (T_{SL}/W_{TO}) and wing loading (W_{TO}/S) ratios.

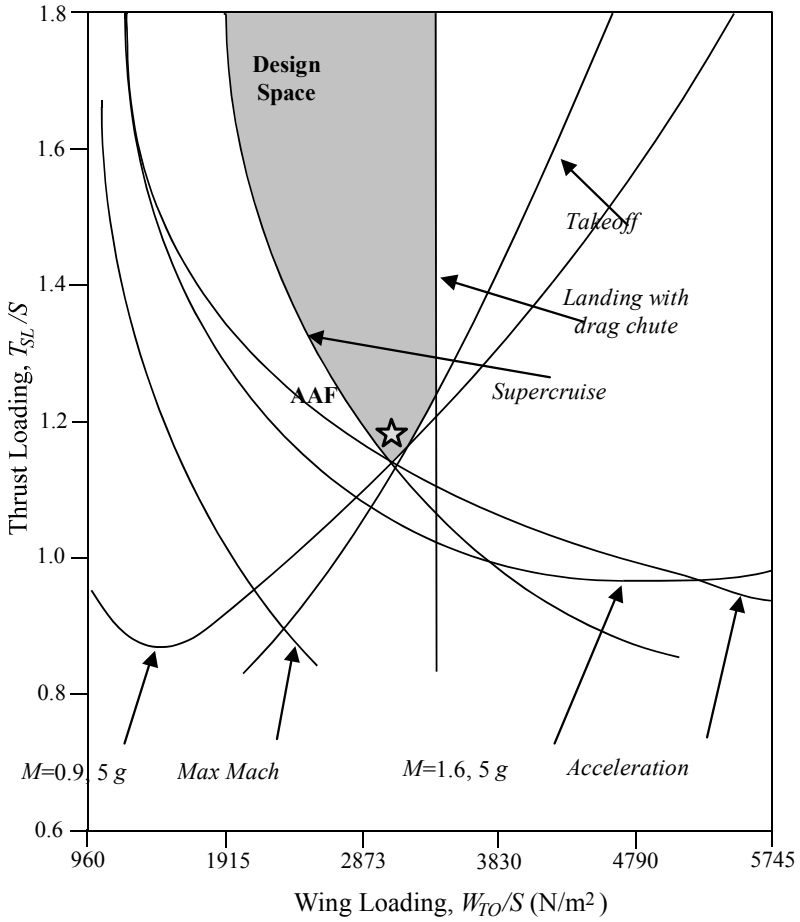

Figure 4.10 Complete Air-to-Air Fighter (AAF) Constraint Diagram Air-to-Air Fighter (Mattingly, Heiser, and Daley, 1987).

For the supersonic penetration and escape dash legs (mission legs 6 and 7), there are no changes in velocity or altitude. During the first stage of the synthesis/design optimization, the initial drag is neglected. However, once this first stage is performed, the computed W_{TO} and S are used to bring into consideration the additional drag ($D_{ECS_i} + D_{TMS_i}$), which work as coupling functions, coming from two of the energy sub-systems (the TMS and the ECS) to the non-energy sub-system (the AFS). Equation (4.50), thus, yields for these two legs

$$\frac{T_{SL}}{W_{TO}} = \frac{\beta}{\alpha}\left\{ K_1 \frac{\beta}{q_i}\left(\frac{W_{TO}}{S}\right) + \frac{C_{D_0}}{\frac{\beta}{q_i}\left(\frac{W_{TO}}{S}\right)} \right\} \tag{4.51}$$

For a given set of aerodynamic variables (i.e. aspect ratio, sweep angle, angle of attack, taper ratio, etc.) and with the inputs from others sub-systems (e.g., pertinent coupling functions), all the terms other than T_{SL}/W_{TO} and W_{TO}/S are known in equation (4.51). Therefore, data for T_{SL}/W_{TO} vs. W_{TO}/S can be tabulated. A numerical example for the mission leg been analyzed is given in Table 4.5.

Table 4.5 Supersonic penetration and escape dash constraints analysis data.

T_{SL}/W_{TO}	2.35	1.77	1.2	0.913	0.746
W_{TO}/S (lb/ft^2)	20	40	60	80	100

The data generated by the execution of the constraint analysis over the most stringent legs is plotted on a graph of T_{SL}/W_{TO} vs. W_{TO}/S. As indicated above, Figure 4.10 is a real representation of the constraint analysis realized in this project for given values of the aerodynamic variables. This figure represents the constraints given by the request for proposal (RFP) given in table 4.1 and 4.2, which specifies the problem constraints and requirements. Figure 4.10 shows the functional relationship between the take-off thrust loading T_{SL}/W_{TO} and wing loading W_{TO}/S. This diagram shows all the possible thrust and wing loading values that will lead to syntheses/designs that comply with the requirements of the RFP.

Table 4.6 Suitable values for T_{SL}/W_{TO} and W_{TO}/S for the optimization problem

T_{SL}/W_{TO}	1.2	1.3	1.4	1.5
W_{TO}/S (N/m^2)	3065	2800	3100	1950

The shaded area indicated in Figure 4.10 represents the synthesis/design optimization space for a given set of aerodynamic variables. Notice that any point in this area meets the RFP constraints. However, this area will change for different values of the aerodynamic variables. This allows the take-off thrust loading T_{SL}/W_{TO}

and wing loading W_{TO}/S to be treated as decision variables in the AFS unit-level optimization problem. Table 4.6 shows some suitable ratios for the AAF, which will be used in the weight fraction analysis in order to determine the total gross take-off weight.

4.2.3 Mission Analysis, Weight Fractions and Sizing

Mission Analysis

With suitable values of the take-off thrust loading (T_{SL}/W_{TO}) and wing loading (W_{TO}/S), the next step is to establish the scale of the aircraft (i.e. wing area, fuselage length, empty weight, fuel weight) via the computation of the gross take-off weight W_{TO}. This is accomplished by flying the aircraft through the entire mission on paper. The fuel weight is calculated based on engine performance and mission requirements and depends on the system synthesis/design and mission requirements. The weight of the ECS, the TMS, and the PS result from the sub-system (unit-level) optimization problems. The weight of the AFS depends on a number of synthesis/design considerations: materials, aerodynamic performance, durability, strength and stability among many others. The gross take-off weight is given by

$$W_{TO} = W_{AFS} + W_{EGS} + W_{PS} + W_{ECS} + W_{TMS} + W_{FUEL} + W_{PPAY} + W_{EPAY} \quad (4.52)$$

where W_{AFS} is the weight of the AFS, which refers to all sub-systems present in the aircraft (wing, fuselage, hydraulics, power distribution, etc.) with the exception of the ECS, TMS, weapons, permanent payload (e.g., crew and accessories) and the PS. W_{PS} is the weight of the engine (PS), W_{ECS} the weight of the ECS, W_{TMS} the weight of the TMS, W_{FUEL} the weight of fuel necessary to carry out the mission, W_{PPAY} is the weight of the permanent payload (crew, equipment), W_{EPAY} is the expendable payload (ammo and missiles), and W_{EGS} is the weight of the equipment group (EGS).

Previously it was considered that the weight of the AFS corresponded to values in agreement with existing design practices. To this end, the data given in Muñoz and von Spakovsky (1999) were used. This data shows the empty weight (in this case, the AFS plus PS plus ECS plus TMS plus EGS[36]) as a function of the gross take-off

[36] Of course, this is not consistent with the definition for "empty weight" given above and, therefore, needs to be adjusted as indicated in the paragraph following equation (4.54).

weight for a number of high performance jet aircraft. However, analytical expressions of the empty weight and the engine weight as a function of the gross take-off weight are also available. These expressions are based on sophisticated state-of-the-art statistical regressions. An expression for the ratio of the empty weight to the total gross take-off weight is given by

$$\frac{W_E}{W_{TO}} = 2.34 W_{TO}^{-0.13} \tag{4.53}$$

where $W_E = W_{AFS} + W_{EGS} + W_{PS} + W_{ECS} + W_{TMS}$ (4.54)

From equation (4.53), it is possible to obtain the weight of the AFS for a given value of the take-off weight. Thus, the weight of the AFS is the empty weight minus the PS weight multiplied by the factors k_{ecs} and k_{tms} to reflect the fact that the empty weight also includes the weight of the ECS and TMS. It will be shown that once an initial estimation for W_{TO} is obtained, the empty weight can be more accurately computed as a function of not only the gross take-off weight but also of the aerodynamic and airframe synthesis/design decision variables. The new empty weight is used to find the final gross take-off weight.

Weight Fraction

Most of the subsequent analysis is dedicated to the development of the weight fraction (π) equations needed for the different mission legs. The fuel consumption analysis is based on calculations which require relatively little information. In addition, it shows the best way of flying certain legs for minimum fuel usage. The fuel expended in each mission segment is expressed as a fraction of the weight at the beginning of the segment.

As to the fuel weight in equation (4.52), it is a complex function of the thermodynamic performance of the PS, the mission requirements, the technology used, and some stability considerations. In general, it is given by

$$W_{FUEL} = g \sum_{mission} \dot{m}_i \Delta t_i = g \sum_{mission} TSFC \cdot T \cdot \Delta t_i \tag{4.54.1}$$

or $$W_{FUEL} = w_{fuel}(W_{TO}, \vec{X}_{PS}, \vec{Y}_{PS}, mission) \tag{4.54.2}$$

where the rate of fuel consumption has been written in terms of the thrust specific fuel consumption *TSFC*. Equation (4.54), however, is fairly inconvenient due to the fact

that the specifications of each of the mission legs are given in terms of different parameters. As seen in Table 4.1, some of the legs have specified range, others specified duration, while still others have specific maneuvers to be carried out. In addition, the duration of some of the legs changes as the decision variables are varied. Therefore, it is useful to employ a transformation, which puts all mission segments under a unified measure. Fuel consumed in each leg written in terms of the weight ratio is such a measure. The ratio of the final to the initial weight for leg *i* is defined as

$$\pi_i = W_f / W_i \tag{4.55}$$

In order to proceed with the calculation of the weight ratios, consider the rate at which aircraft weight diminishes due to the consumption of fuel, namely,

$$\frac{dW}{dt} = -TSFC \cdot T \tag{4.56}$$

or $$\frac{dW}{W} = -TSFC\frac{T}{W}dt = -TSFC\frac{T}{W}\frac{dt}{ds}ds = -TSFC\frac{T}{W}\frac{ds}{V} \tag{4.57}$$

Equation (4.57) represents the weight-time and weight-velocity transformation that is used to unify the different requirements of the mission. The integration of equation (4.57) is done by breaking each mission segment into several (typically 5) intervals. The flight and operating conditions for each sub-segment are assumed to be constant at some representative value so that the integration can be accomplished explicitly (numerically). It was found that in most cases, five intervals are sufficient to ensure excellent accuracy. Proper integration of equation (4.57) requires knowledge of the behavior of the specific fuel consumption and the instantaneous thrust loading as a function of time along the flight path. The integration can be carried out according to the weight specific excess power (Ps). This approach yields equation (4.58.1) for Ps > 0 and equation (4.58.2) for Ps = 0. The derivation of these equations is not presented, since it is not necessary for understanding the problem of optimization in this work.

$$\frac{W_f}{W_i} = exp\left\{-\frac{TSFC}{V\left(1-\frac{D+R}{T}\right)}\Delta\left(h+\frac{V^2}{2g_o}\right)\right\} \qquad \text{(for Ps > 0)} \tag{4.58.1}$$

or $$\frac{W_f}{W_i} = exp\left\{-TSFC\left(\frac{D+R}{W}\right)\Delta t\right\} \qquad \text{(for Ps = 0)} \tag{4.58.2}$$

where Δt is the total mission leg flight time.

The engine installed thrust specific fuel consumption is a complex function of altitude, speed, and throttle setting. This is especially true if the engine has the option of afterburning. Since for the first iteration of the ILGO problem, there is no information from the PS unit-level optimization, it is necessary to find an adequate starting point for the *TSFC* estimation. A satisfactory solution is found by assuming that

$$TSFC = C\sqrt{\theta} \tag{4.59}$$

where C is a constant which is estimated in advance and θ represents the usual thermodynamic cycle improvement due to a lower ambient temperature at higher altitude. Note that once the PS unit-level optimization problem is solved, the actual specific fuel consumption can be used in the AFS unit-level optimization problem to perform the weight fraction analysis. Table 4.7 shows the weight ratio for three different types of mission legs. However, there is a special case, which deviates from the above calculations and corresponds to the mission segment when the expendable

Table 4.7 Weight ratio calculations for different mission legs[37].

Case	$\pi = W_{final} / W_{initial}$
Constant speed climb	$exp\left\{\frac{-TSFC}{V}\left[\frac{\Delta h}{1-\frac{D+D_{ECS}}{T}}\right]\right\}$
Horizontal acceleration	$exp\left\{\frac{-TSFC}{V}\left[\frac{\Delta\left(V^2/2g\right)}{1-\frac{D+D_{ECS}}{T}}\right]\right\}$
Climb and acceleration	$exp\left\{\frac{-TSFC}{V}\left[\frac{\Delta\left(h+V^2/2g\right)}{1-\frac{D+D_{ECS}}{T}}\right]\right\}$

[37] For the weight calculation for all mission segments see Mattingly, Heiser, and Daley (1987).

payload is delivered. If it is assumed that the delivery is done at some point *j* in the mission, then

$$\frac{W_j - W_{EPAY}}{W_j} = 1 - \frac{W_{EPAY}}{W_j} \tag{4.60}$$

With equation (4.60) and the weight ratios and after some manipulation, the fuel consumption can be written as

$$W_{FUEL} = W_{TO}(1 - \prod_{i=1}^{n} \pi_i) - W_{EPAY}(1 - \prod_{i=j}^{n} \pi_i) \tag{4.61}$$

where *n* is the number of legs being considered. The weight fractions depend on the design of the PS and other sub-systems, the required thrust, the afterburner setting, the power requirements of the other sub-systems, ambient conditions, and a number of other factors. However, it should be noted that the weight fraction depends also on the aerodynamics, e.g., the geometric decision variables. These complex set of factors are addressed by means of solving Equation (4.50) for each mission segment.

Algebraic manipulation of equations (4.55), (4.60) and (4.61) yields the following expression for the gross takeoff weight:

$$W_{TO} = \frac{W_{PP} + W_{PE} \prod_{j\_n}}{\prod_{1\_n} - \frac{W_E}{W_{TO}}} \tag{4.62}$$

$$\text{where } \frac{W_E}{W_{TO}} = 2.34 W_{TO}^{-0.13} \tag{4.63}$$

Equation (4.62) not only allows a straightforward calculation of the gross take-off weight but also reveals its dependence on the critical parameters of the mission represented by W_{PP}, W_{PE}, the $\Pi's$, W_E/W_{TO}, and, of course, the aerodynamics. An initial estimation of W_{TO} must be made during this part of the process to solve equation (4.62). Note that the weight fractions have already been computed at this point. If the initial estimation is far from the value given by equation (4.62), then an iterative solution is required. The iteration process should, however, converge rapidly.

Now with the value the gross take-off weight, the values of sea-level thrust, wing area, weight of the fuel, and size of the fuselage can be determined from

equations (4.53), (4.52) and from the definitions of the take-off thrust loading T_{SL}/W_{TO} and wing loading W_{TO}/S. Also, equation (4.50) can be solved to generate the value of the thrust for each mission segment, which in turn is a coupling function to be used in the PS unit-level optimization problem.

Finally, during construction of the constraint analysis graph (figure 4.10), it was necessary to make some assumptions about the weight ratios for several mission segments. These assumptions must be verified before proceeding any further. This is done in the next section.

Sizing

The gross take-off weight calculation will be improved by usage of a refined sizing method. This method gathers the different subcomponents of the AFS in groups, expressing their weights as a function of the gross take-off weight and AFS decision variables and parameters. This is done by applying statistical equations based

Table 4.8 Fighter group weights[38].

Group Weight	Expression
Wing	$= 0.0103 K_{dw} K_{vs} \left(W_{dg} N_z\right)^{0.5} S_w^{0.622} AR^{0.785} \left(t/c\right)_{root}^{-0.4} \cdot \left(1+\lambda\right)^{0.005} \left(\cos\Lambda\right)^{-1} S_{csw}^{0.04}$
Horizontal tail	$= 3.316 \left(1 + \frac{F_w}{B_h}\right) \left(\frac{W_{dg} N_z}{1000}\right)^{0.260} S_{ht}^{0.806}$
Landing gear	$= K_{cb} K_{tpg} \left(W_t N_t\right)^{0.25} L_m^{0.973}$
Fuselage	$= 0.499 K_{dwf} W_{dg}^{0.35} N_z^{0.25} L^{0.5} D^{0.849} W^{0.685}$

on sophisticated regression analysis. When the component weights are estimated using this method they are tabulated and summed to determine the actual empty weight. If the empty weight is different from the one estimated initially, this must be corrected by resizing the aircraft. The new empty weight is replaced in equation (4.62) and the new gross take-off weight is computed by iteration. This new gross take-off weight in turn is used to find a new empty weight by using the group weight technique. The process continues until convergence is reached. Table 4.8 shows some group weight equations for fighter aircraft taken from Raymer, 2000.

[38] For all group weight calculations see Raymer (2000).

4.3 Environmental Control Sub-system (ECS) Description and Modeling

The air cycle of the ECS dissipates heat by transforming it into work. Two types of air cycles are possible:

- Open Cycles: Those in which the air is taken from outside the aircraft and rejected after being used in the cycle.
- Closed Cycles: Those in which air is re-circulated continuously through the cycle.

A survey of the many possible different configurations is given in the SAE Aerospace Applied Thermodynamics Manual (1969). Of these, the bootstrap system is by far the most widely used due to its higher efficiency when compared to a simple air cycle. In the bootstrap system, performance is improved by using the air turbine work output for increased compression of the air upstream of the turbine. Thus, a higher compression ratio is achieved with a correspondingly higher temperature drop across the turbine.

The conventional bootstrap system shown in Figure 4.11 below is similar to the one used by the F-16 fighter. It provides conditioned air to the cockpit and avionics. Airflow to the ECS is from pre-conditioned bleed air. Flow into the ECS is varied by a pressure-modulating valve at the ECS inlet. This valve also limits maximum inlet pressure to the ECS's primary heat exchanger and bootstrap compressor. Air is compressed and cooled in the bootstrap ECS. After compression, the air is cooled in a counter-flow, secondary heat exchanger using ram air from ram-air scoop inlets. Air from the secondary heat exchanger is then cooled in the regenerative heat exchanger, before it is cooled further by expansion in the bootstrap turbine. Most of the water condensed during cooling of the air in the air turbine is removed in a low-pressure water separator. Of course, ECS performance is closely coupled with the PS and aircraft flight conditions. Changes in engine power settings cause changes in bleed air pressures and temperatures, which in turn affect the performance of the ECS.

The mass flow rate and pressure of the bleed air will in general depend on the pressure and temperature at which the cold air must be delivered to the cockpit and avionics and the synthesis/design of the ECS. Quite obviously, the energy or exergy of the air that can then be had from the main engine compressor of the PS is not a continuous function but rather is limited by the fact that it can only be extracted from the discrete stages of the compressor. Typically, modern ECSs have a bleed port at a

low and one at a high-pressure stage. Once the amount of bleed air needed (usually a unique value calculated from the allowed inlet and outlet temperatures of the load (cabin and avionics) and the cooling load itself) and the stage at which air is bled are fixed, the energy of the bleed air can be calculated. It is then possible to estimate the amount of fuel required to produce the compressed air by means of, for example, an engine simulator.

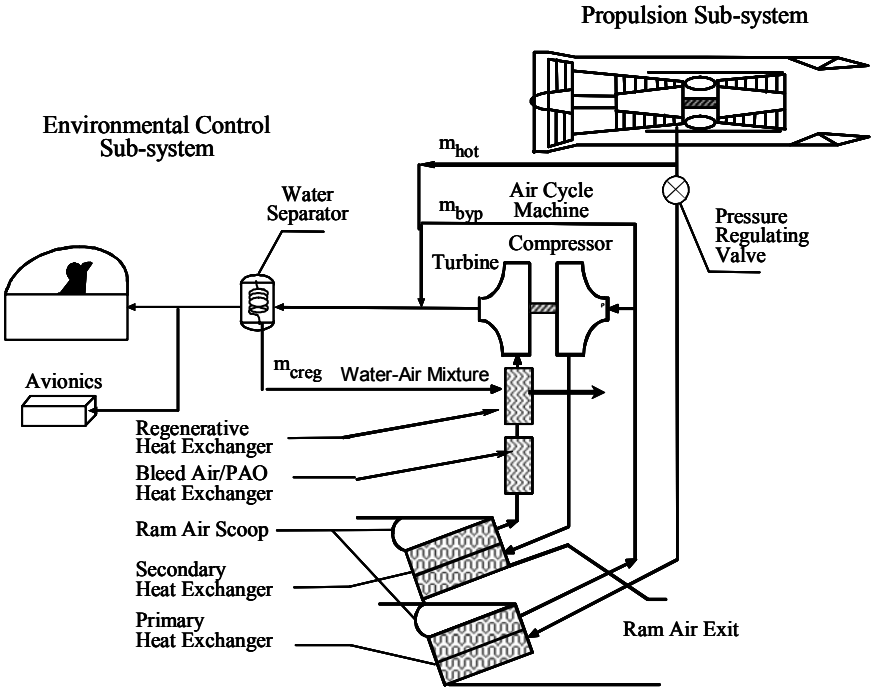

Figure 4.11 Schematic of an ECS bootstrap air-cycle (Muñoz, 2000).

As to the ram-air inlet, it creates a penalty in the system, which is proportional to the drag force created by it. The basic principle is to decelerate the cooling air flow, pass it through the heat exchanger at low speed, and then accelerate it back to ambient pressure. Quantitatively, the drag force created by the inlet-heat-exchanger-exit assembly is defined as the cooling air flow's rate of momentum change. The greater the pressure drop in the heat exchanger and ducts, the higher the associated momentum drag will be. Increasing the heat transfer rate in the heat exchanger has the opposite effect. In addition, there is a profile drag of the inlet and exit and perhaps some 'interference' drag due to unfavorable interactions.

Now, as to the mass of the ECS, the amount of fuel required to carry this mass and the fuel itself is a function of a number of factors including the flight conditions

(altitude, Mach number, angle of attack, etc.) and the relative location of the ECS with respect to the center of gravity of the aircraft. Therefore, the fuel penalty due to weight is highly dependent on the aircraft being analyzed. This weight is affected by the independent variable set which minimizes the ECS objective and includes among others the pressure setting in the regulating valve, the mass flow rate of cooling air in the regenerative heat exchanger, and the mass flow rate of bypass warm air necessary to obtain the pressure, temperature and mass flow rate schedules in the cabin and avionics. The available bleed air pressure is dependent on the altitude and Mach number of the aircraft. It is assumed that the bleed air is extracted from a fixed bleed port (i.e. low-pressure or high-pressure compressor stage. The energy (or exergy) of the bleed air is calculated along with the drag created by the ram air. The weight model, physical model, and thermodynamic model for each component are given in Muñoz and von Spakovsky (1999). Thus, the ECS as will be the case with the TMS introduces the following additional fuel requirements:

- To provide the additional thrust needed for carrying the mass of the ECS;
- To supply power to the ECS; this can be expressed as the amount of fuel required to meet ECS requirements while maintaining constant net thrust; the energy extracted can be in the form of compressed (bleed) air or shaft power;
- To overcome any additional drag, which may result from installing a sub-system in the aircraft due to increases in profile and momentum drag caused by ram-air induction for cooling purposes;
- Carry the quantity of fuel required for the previous items.

4.3.1 ECS Thermodynamic and Heat Transfer Model

A complete description of the ECS thermodynamic and heat transfer models is presented in this section. A complete description of the physical model (i.e. weight and dimensions) for each component is presented in the AFORS Phase I final report of Muñoz and von Spakovsky (1999).

Heat Exchangers

Compact heat exchangers offer the lightweight, economical, and space-saving features required in aircraft and spacecraft applications. Compact heat exchangers are characterized by extended surfaces and the most common configurations are either plate-fin or tube-fin. Tube-fin exchangers are mostly used in liquid-gas applications

and plate-fin in gas-to-gas applications. Here we will focus on plate-fin heat exchangers. The fluid mechanics and heat transfer behavior in and between channels is very complex and as a consequence few predictive models are available. Instead, actual data is used, the monograph by Kays and London (1998) being the most comprehensive source. Other sources of data are Shah and Webb (1982) and Shah (1981).

Among the available enhanced-fin geometries, offset-strip fins appear to be some of the most widely used in aircraft applications. An example is the heat exchangers of the F-16 fighter. Offset-strip fins have a high degree of compactness and offer substantial heat transfer enhancements. This enhancement is obtained as a result of periodic starting and the development of laminar boundary layers over uninterrupted channels formed by the fins and their dissipation in the fin wakes (Manglik and Bergles, 1990). Although offset-strip fins are used in the calculations, the formulation given here is quite general and can be applied to any type of compact heat exchanger. The synthesis/design procedure used is largely based on the formulation given by Kays and London (1998). The basic fin geometry is shown in Figure 4.12 while Tables 4.9a and 4.9b present the geometric and thermodynamic/heat transfer models for the compact heat exchangers.

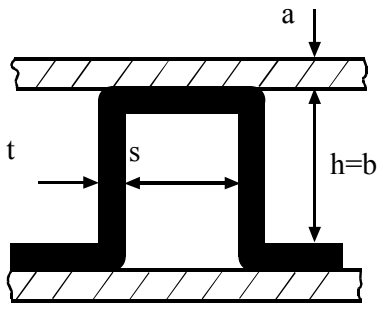

Figure 4.12 Main geometric parameters of the offset-strip fin (Muñoz and von Spakovsky, 1999).

Table 4.9a Geometric and heat transfer models of a compact exchanger.

Variable Description		Model Equation
L_h	Hot-side length	Assigned value
L_c	Cold-side length	Assigned value
D_h	Hydraulic diameter	$D_h = \frac{2shl}{(sl + hl + th)}$
A_{fr}	Frontal area	$A_{fr} = L\, L_n$
σ	Ratio of minimum free flow area to frontal area	$\sigma = \frac{A_O}{A_{fr}}$
β	Heat transfer area / volume between plates	$\beta = \frac{4\sigma}{D_h}$
$\frac{A_f}{A_t}$	Fin area / total area	$\frac{A_f}{A_t} \cong \frac{s+h}{2s+h}$
N_p	Number of plates	$N_p = n_p = \frac{L_n - h_b - 2a}{h_b + h_r + 2a}$
Vp_b Vp_r	Volume between plates, bleed and ram air side	$Vp_b = L_b L_r (N_p + 1) h_b$ $Vp_r = L_b L_r N_p h_b$
A	Heat transfer area	$A = \beta Vp$
A_O	Minimum free flow area	$A_O = \frac{D_h A}{4L}$
G	Mass velocities	$G = \frac{\dot{m}}{A_O}$
R_e	Reynolds number	$R_e = \frac{G\, D_h}{\mu}$
f j	Friction and Colburn coefficients (Manglik and Bergles, 1990).	For $R_e \le R_e^*$ (laminar flow) $f = 9.6243 R_e^{-0.7422} \alpha^{-0.1856} \delta^{0.3053} \gamma^{-0.2659}$ $j = 0.6522 R_e^{-0.5403} \alpha^{-0.1541} \delta^{0.1499} \gamma^{-0.0678}$
f j	Friction and Colburn coefficients (Manglik and Bergles, 1990).	For $R_e \ge (R_e^* + 1000)$ (turbulent flow): $f = 1.8699 R_e^{-0.2993} \alpha^{-0.0936} \delta^{0.6820} \gamma^{0.2423}$ $j = 0.2435 R_e^{-0.4063} \alpha^{-0.1037} \delta^{0.1955} \gamma^{-0.1733}$

Table 4.9b Geometric and heat transfer models of a compact exchanger.

Variable Description		Model Equation
A_w	Wall conduction area	$A_w = L_b L_r 2(N_p + 1)$
R_w	Wall thermal resistance	$R_w = \dfrac{a}{k_w A_w}$
l	Fin length	$l \cong \dfrac{b}{2} - t$
H	Height	$H = b_h + 2a + n_{plates}\left(b_h + b_c + 2a\right)$
A_f	Finned area	$m \cong \left(\dfrac{2h}{kt}\right)^{\frac{1}{2}},\ A_{fr} = L\ H$ $\eta_f = \dfrac{\tanh(ml)}{ml},\ \eta_O = 1 - \left(1 - \eta_f\right)\dfrac{A_f}{A}$
A_{fr}	Frontal area	
η_f	Fin efficiency	
η_o	Outside overall surface efficiency	
$\dot{n}$	Mixture molar flow rate	$G = \dfrac{\dot{m}}{A_O},\ Pr = \dfrac{\mu C_p}{k}$ $h = \dfrac{jGc_p}{P_r^{2/3}}$
j	Colburn factor	
G	Maximum mass velocity	
Pr	Prandtl number	
h	Heat transfer coefficient	
U	Overall heat transfer coefficient	$C_{min} = \min\left(\dot{n}_c C_p^c, \dot{n}_h C_p^h\right),\ C_{max} = \max\left(\dot{n}_c C_p^c, \dot{n}_h C_p^h\right)$ $\dfrac{1}{UA} = \dfrac{1}{\left(\eta_O hA\right)_b} + R_w + \dfrac{1}{\left(\eta_O hA\right)_r},\ C_r = C_{min} / C_{max},$ $NTU = \dfrac{UA}{C_{min}}$
C_{min}	Minimum heat capacity	
C_{max}	Maximum heat capacity	
C_r	Heat capacity ratio	
NTU	Number of transfer units	
ε	Effectiveness	$\varepsilon = 1 - \exp\left[\left(\dfrac{1}{C_r}\right) NTU^{0.22}\left\{\exp\left[-C_r NTU^{0.78}\right] - 1\right\}\right]$
ΔP	The core pressure drop	$\dfrac{\Delta P}{P} = \dfrac{G^2}{2}\dfrac{1}{\rho_i P}\left[\begin{array}{l}\left(K_c + 1 + \sigma^2\right) + 2\left(\dfrac{\rho_i}{\rho_e} - 1\right) \\ + f\dfrac{A}{A_o}\dfrac{\rho_i}{\rho_m} - \left(1 - \sigma^2 - K_e\right)\dfrac{\rho_i}{\rho_e}\end{array}\right]$

The viscosity in the above table is a function of temperature. For the predictive equations given by Manglik and Bergles (1990), $\alpha = s/h$, $\delta = t/l$, and $\gamma = t/s$. In the transition regime, an average of values is calculated using the formulas corresponding to the turbulent and laminar regions. As mentioned earlier, the model was developed for offset-strip fins. However, predictive equations for other types of fins exist as indicated in Table 4.10.

Table 4.10 Some Colburn and friction factor correlations available in the literature

Geometry	Source
Louvered fins	Davenport (1983)
Convex Louvered fins	Hatada and Senshu (1984)
Wavy fins	Gray and Webb (1986), Beecher and Fagan (1987), and Jakob (1938)
Slit fins	Mori and Nakayama (1980)
Spine fins	Eckels and Rabas (1985)

As to the pressure drop expression in Table 4.10, ρ is the average density determined from the inlet and outlet densities, ρ_i and ρ_e, respectively; σ is the ratio of free flow area to frontal area; f is the core friction factor, and K_e and K_c the expansion and contraction pressure drop factors, respectively.

As to the entropy generation, it can be calculated

$$\dot{S}_{gen} = \dot{m}_{ram} c_p \ln\left[\frac{T_e}{T_i}\right]_{ram} + \dot{m}_{bleed} c_p \ln\left[\frac{T_e}{T_i}\right]_{bleed} - \dot{m}_{ram} R \ln\left[1 - \frac{\Delta P}{P_i}\right]_{ram} - \dot{m}_{bleed} R \ln\left[1 - \frac{\Delta P}{P_i}\right]_{bleed} \tag{4.63}$$

and in general terms as

$$\dot{S}_{gen} = \dot{S}^{\Delta T}_{gen\,ram} + \dot{S}^{\Delta T}_{gen\,bleed} + \dot{S}^{\Delta P}_{gen\,ram} + \dot{S}^{\Delta P}_{gen\,bleed} \tag{4.64}$$

Finally, for advanced geometries currently under investigation, a combination of data obtained from experiments and computational fluid dynamics (CFD) can be used to obtain a set of data that combined with a multiple linear or nonlinear regression

lead to predictive equations such as those shown above. These equations can be used in optimization studies in order to obtain optimum values for a particular application.

Air Cycle Machine

The graphs found in Figures 4.12 and 4.13 were used as the basis of performance for the bootstrap compressor and turbine. The velocity factor which appears on the horizontal axis of the turbine map is defined as

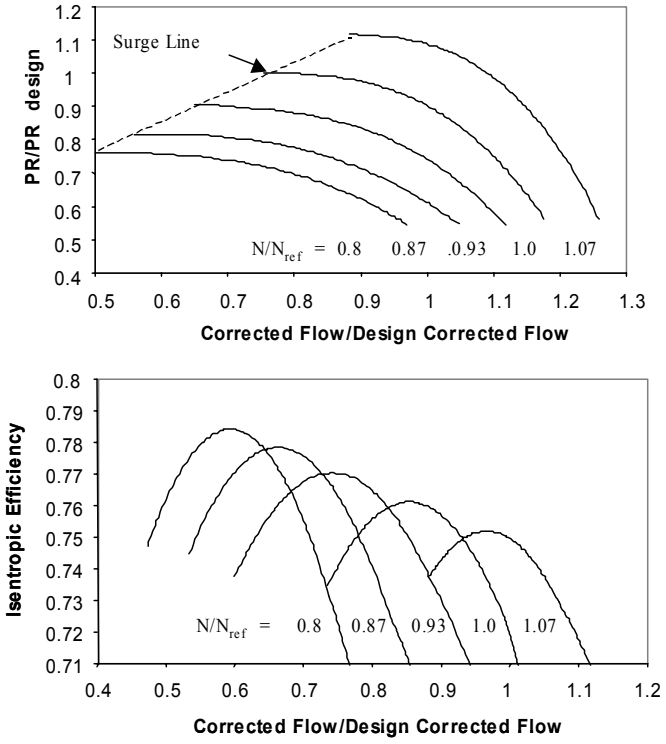

Figure 4.13 Compressor performance maps (Muñoz and von Spakovsky, 1999).

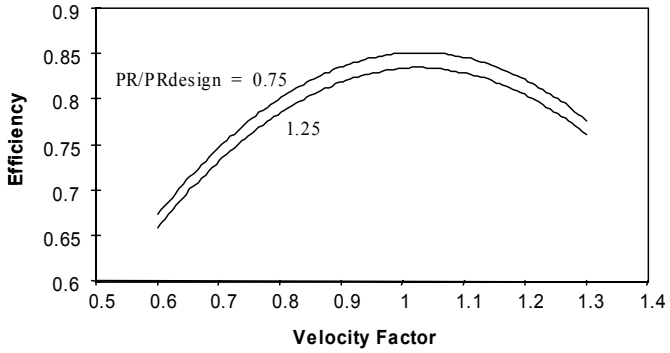

Figure 4.14 Turbine performance map (Muñoz and von Spakovsky, 1999).

$$Fv = \frac{N}{4028\sqrt{T_{in}\left(\frac{Y}{Y+1}\right)}} \tag{4.65}$$

where $$Y = \left[PR^{\frac{\gamma-1}{\gamma}} - 1 \right] \tag{4.66}$$

Low Pressure Water Separator

The water separation process is assumed to occur adiabatically. The performance equations are

$$\eta_{ws} = a + b\left(m_r + m_r^2\right) \tag{4.67}$$

where η_{ws} is the efficiency of the water separator, $a = 0.35 + 2.0\,W_i$, $b = 0.78$, and m_r is the ratio between the mass flow rate and mass flow rate at maximum efficiency. The efficiency is defined as

$$\eta_{ws} = \frac{W_i - W_e}{W_i - W_{sat}} \tag{4.68}$$

where the humidity ratio corresponding to saturation conditions is expressed as

$$W_{sat} = 0.62198\frac{P_{ws} - P_i}{P_i} \tag{4.69}$$

In this equation, the saturation pressure of water vapor, P_{ws}, in the absence of air at the given inlet temperature is given by expressions found in ASHRAE Fundamentals (1996, pag. 6.7) for the temperature range of -100^{o}C to 200^{o}C. Pressure drop, $P_{ws} - P_i$, is given by

$$\frac{\Delta P}{P_{std}} = c\, m_r^d \tag{4.70}$$

where $c = 0.2 - 4.6W_i$, $d = 0.1 + 1.2W_i$, W_i refers to the humidity ratio of the air entering the water separator, and P_{std} is the pressure at standard conditions.

Supersonic Inlet

There are different types of inlets: scoop inlets, flush inlets, and inlets located on engine ducts. Figures 4.15a and 4.15b show typical pressure recovery maps for scoop

inlets at subsonic and supersonic conditions. From these figures it can be inferred that the design inlet area is

$$A = \frac{\dot{m}}{k\rho_\infty V_\infty} \tag{4.71}$$

for a desired mass flow rate. The constant k depends on whether the flow is subsonic or supersonic. The maps can be used to determine the inlet off-design performance. A typical pressure recovery factor r_f has the form

$$r_f = aM^b \tag{4.72}$$

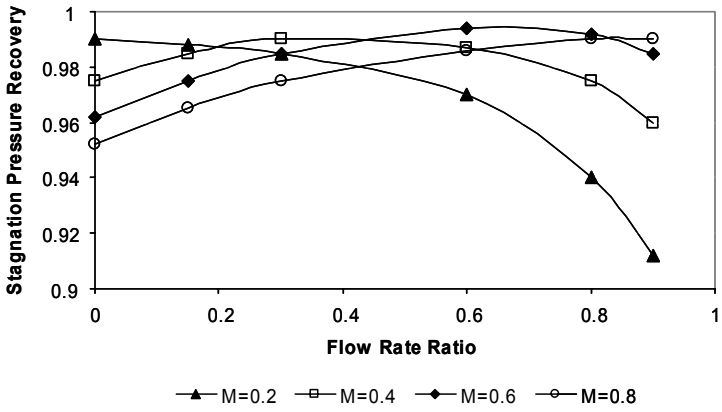

Figure 4.15a Subsonic inlet stagnation pressure recovery map (Muñoz and von Spakovsky, 1999).

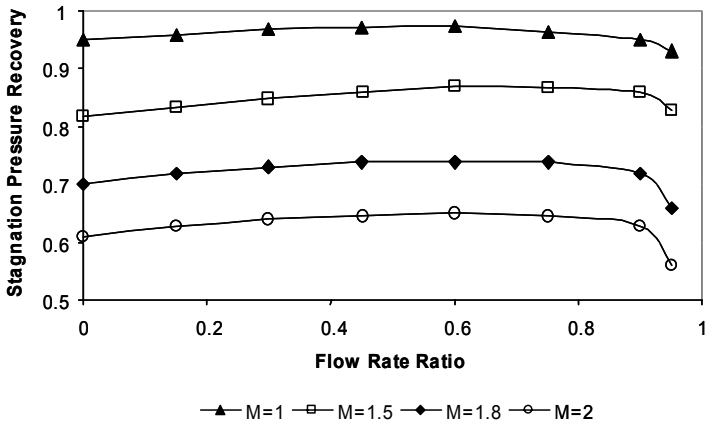

Figure 4.15b Supersonic inlet stagnation pressure recovery map (Muñoz and von Spakovsky, 1999).

ECS Thermodynamic Model

The thermodynamic model presented is based on a perfect gas model. With reference to Figure 4.16,

$$T_9 = T_{load} \tag{4.73}$$

$$P_9 = P_{load} \tag{4.74}$$

where the required load temperature and pressure are given in Muñoz and von Spakovsky (1999).

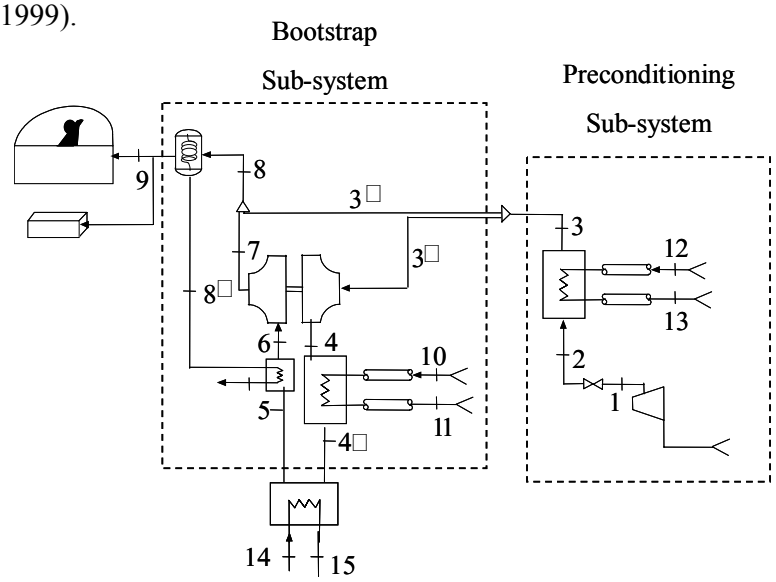

Figure 4.16 Sub-system definition for the ECS of Figure 4.11.

Water separator:

$$T_8 \cong T_9 \tag{4.75}$$

$$P_8 = P_9 + \Delta P_{ws} \tag{4.76}$$

With the pressure drop for the water separator (Muñoz and von Spakovsky, 1999) along with the humidity ratio of the air exiting the water separator, the amount of water extracted can readily be calculated.

Turbine:

$$\frac{T_7}{T_6} = \left\{1 - \eta_{tb}\left[1 - \left(\frac{P_7}{P_6}\right)^{\frac{\gamma-1}{\gamma}}\right]\right\} \tag{4.77}$$

The efficiency of the turbine is a function of the pressure ratio and the velocity factor as indicated in Figure 4.14.

Regenerative heat exchanger

$$T_6 = T_5 - \varepsilon_{rhx}\left(T_5 - T_8{}'\right)\frac{C_{min}}{C_5} \tag{4.78}$$

$$P_6 = \left(1 - \frac{\Delta P}{P_5}\right)P_5 \tag{4.79}$$

where C_{min} is the smallest of the heat capacities C_5 and $C_{8'}$. The heat exchanger effectiveness is estimated iteratively using the equations given above. A pressure drop correlation is also used.

Bleed air / hot PAOS heat exchanger

$$T_5 = T_{4'} - \varepsilon_{bleed/pao\_rhx}\left(T_{4'} - T_{14}\right)\frac{C_{\min}}{C_{4'}} \tag{4.80}$$

$$P_5 = \left(1 - \frac{\Delta P}{P_{4'}}\right)P_{4'} \tag{4.81}$$

where C_{min} is the smallest of the heat capacities $C_{4'}$ and C_{14}. Note, of course, that the heat capacity C_i of a stream i is the product of its mass flow rate and specific heat.

Secondary heat exchanger

$$T_{4'} = T_4 - \varepsilon_{second\_hx}\left(T_4 - T_{o_\infty}\right)\frac{C_{min}}{C_4} \tag{4.82}$$

$$P_{4'} = \left(1 - \frac{\Delta P}{P_4}\right)P_4 \tag{4.83}$$

where C_{min} is the smallest of the heat capacities C_4 and C_{10}.

Compressor

$$\frac{T_4}{T_3} = 1 + \frac{1}{\eta_{cp}}\left[\left(\frac{P_4}{P_3}\right)^{\frac{\gamma-1}{\gamma}} - 1\right] \tag{4.84}$$

The efficiency of the compressor is a function of the pressure drop and the shaft speed and is found from Figure 4.13. The shaft work of the compressor and turbine must be matched using the relationships given in Figures 4.13 and 4.14, i.e.

$$h_4 - h_3 = h_6 - h_7 \tag{4.85}$$

Primary heat exchanger:

$$T_3 = T_2 - \varepsilon_{pri\_hx}\left(T_2 - T_{o_\infty}\right)\frac{C_{\min}}{C_2} \tag{4.86}$$

where C_{min} is the smallest of the heat capacities C_2 and C_{12}

$$P_5 = \left(1 - \frac{\Delta P}{P_4}\right)P_4 \tag{4.87}$$

The flow between the scoop inlet and the heat exchanger is modeled as a constant area, one-dimensional, adiabatic flow with a constant friction coefficient of 0.01. The inlet thermodynamic conditions are calculated using the pressure recovery factor and the mass flow ratio such that

$$\rho_i V_i = k\rho_\infty V_\infty \tag{4.88}$$

and $$P_{o_i} = r_f \; P_{o_\infty} \tag{4.89}$$

The Mach number in the inlet is readily calculated from these last two equations. The constant k is obtained from Figure 4.15. The pressure recovery factor is given by equation (4.72). The calculations are expedited by using sonic flow reference conditions, where the flow properties at sonic conditions are denoted by P^*, T^*, and P_o^*. The necessary equations are given below (Anderson, 1982) and can be used to calculate the thermodynamic properties of states 10' and 12'.

$$\frac{T_i}{T_i^*} = \frac{\gamma + 1}{2 + (\gamma - 1)M_i^{\,2}} \tag{4.90}$$

$$\frac{P_i}{P_i^*} = \frac{1}{M_i}\left[\frac{\gamma + 1}{2 + (\gamma - 1)M_i^{\,2}}\right]^{\frac{1}{2}} \tag{4.91}$$

$$\frac{P_{io}}{P_{o_i}^*} = \frac{1}{M_i}\left[\frac{2 + (\gamma - 1)M_i^{\,2}}{\gamma + 1}\right]^{\frac{\gamma=1}{2(\gamma-1)}} \tag{4.92}$$

$$\frac{4fL^*}{D} = \frac{1 - M_i{}^2}{\gamma M_i{}^2} + \frac{\gamma + 1}{2\gamma} ln\left[\frac{(\gamma + 1)M_i{}^2}{2 + (\gamma - 1)M_i{}^2}\right] \tag{4.93}$$

Once the inlet conditions are known, the factor $4fL/D$ (where L and D are the duct length and diameter, respectively) is subtracted from $(4fL/D)_i$. This value is then used to calculate the properties at the heat exchanger inlet.

The pressure immediately after the heat exchanger is given by

$$P_{13'} = \left(1 - \frac{\Delta P}{P_{12'}}\right) P_{12'} \tag{4.94}$$

A similar procedure is used to calculate the thermodynamic properties of the air just ahead of the ram exit (states 11 and 13). The drag due to the presence of the ram air inlet and exit is approximated as the momentum exchange

$$D = \dot{m}(u - u_e) \tag{4.95}$$

where u_e is the velocity at the ram air exit. This velocity is calculated once the ram air exit Mach number is known. In the above expression, pressure drag has been ignored. In scoop inlets, pressure drag appears to be important at low flow rate values. These low flow rates occur at low speeds when the pressure drag is low compared to the momentum drag.

4.4 Thermal Management System (TMS) Description and Modeling

The TMS considered here uses a basic vapor compressor cycle and interacts with a bootstrap ECS. This combination represents a highly complex cooling system similar to the ones used by advanced fighter aircrafts and uninhabited combat air vehicles (UCAVs), which have two avionics boxes. The TMS has a number of sub-systems including two Polyalphaolefin (PAO) loops, a vapor compressor cycle and a fuel loop. In contrast to the ECS which supplies conditioned air for the cockpit and the low-heat generation avionics, the TMS provides conditioned air for the high-heat generation avionics. The TMS removes heat from the high-heat generation avionics via the cold PAO[39] loop. The pump power required to drive the coolant through the

[39] The cold Polyalphaolefin (PAO) loop is that used as a heat source for the vapor compressor cycle.

loop is calculated from the pressured drops in the liquid line as well as the avionics box and evaporator.

The vapor compression (VC) cycle transfers heat from the cold PAO loop to one at a higher temperature (the hot PAO[40] loop). The VC cycle chosen for this study has a single compression stage. Evaporation of the liquid refrigerant in the evaporator absorbs energy from the heat source fluid, the cold PAO fluid, which in turn takes energy from the avionics. The refrigerant is compressed to a higher pressure and temperature and then cooled in a condenser where the acquired heat is rejected to a heat sink, the hot PAO fluid. The refrigerant liquid leaving the condenser flows again to the evaporator through a throttling (expansion) valve, closing the loop.

Variants on this basic VC cycle which are not considered here are the multiple evaporator operation cycle and the subcooler-superheater cycle in which more than two heat exchangers are allocated to handle separate cooling loads or to improve the COP (coefficient of performance). A detailed analysis of different configurations is presented in SAE Aerothermodynamic System Engineering and Design (1990). In general, since the open air cycles used in ECSs are limited by a relatively small temperature difference between heat sources and sinks, a closed VC cycle may be combined with the air cycle in order to increase the effective temperature range of the cooling system. With moderate temperature differences, one VC cycle may suffice. With larger temperature differences, a cascade VC cycle may be required.

The hot PAO loop is highly coupled to other sub-systems, i.e. the ECS, the fuel loop sub-system and the VC cycle. This PAO loop receives heat from the VC cycle through the condenser. Flow on the PAO side of the condenser is controlled through a valve. Following the condenser, the PAO is pumped toward a bleed air-PAO heat exchanger where it receives heat from the bleed air, which comes from the ECS secondary heat exchanger. The PAO, at high temperature, is then cooled using ram air at the same scoop inlet as that used for the ECS. Before the PAO returns to the condenser, it is cooled using the aircraft fuel as a heat sink. The fuel in the fuel loop also receives heat from the oil sub-system and the PS. The cooling loads from these sub-systems depend on the specific fuel consumption, which is constant for a specific mission segment. After the fuel required by the PS is taken from the fuel stream, the remaining fuel is cooled in a counter-flow heat exchanger using ram air from a

[40] The hot Polyalphaolefin (PAO) loop is that used as the intermediate heat sink between the vapor compression cycle and the fuel loop.

separate ram-air scoop inlet. Although the fuel returning to the main fuel tank is cooled, the inlet temperature is higher than the outlet one, resulting in thermal storage within the tank. Thus, the fuel loop must be solved as a transient problem.

The TMS, in general is highly affected by aircraft flight conditions, since it is highly coupled to the PS whose heat load depends on engine setting, producing a change of conditions in the fuel loop. Moreover, TMS performance depends on the bleed air temperature which depends on the engine setting and on the Mach number which determines the ram air inlet pressure and temperature. In addition, the TMS pumps and compressor and the drag produced by the ram air inlets impose a power load on the PS.

Thus, in summary, the TMS introduces the following additional fuel requirements:

- To provide the additional thrust needed for carrying the mass of the TMS;
- To supply power to the TMS; this can be expressed as the amount of power required to meet the TMS requirements, while maintaining constant net thrust;
- To overcome any additional drag, resulting from the installation of an additional sub-system;
- To compensate for an increased drag profile due to the installation of ram-air scoop inlets for cooling purposes;
- To carry the amount of fuel required for the previous tasks.

4.4.1 Vapor Compression Refrigeration/PAO Loop Sub-system (VC/PAOS)

It is common to choose a single operating point (the one with the most stringent requirements) as the synthesis/design point. The system's sub-systems are then optimized with respect to this point using a suitable criterion (gross tak-eoff weight, fuel consumption, total cost, etc.) for the specified conditions and tested for performance throughout the whole mission profile. The synthesis/design of the VC/PAOS (its heat exchangers, compressor, pumps, and the ram air inlet, exit and ducts) is carried out for the second subsonic cruise climbing mission segment in the context of the overall aircraft system (i.e. PS, ECS, TMS and AFS) using ILGO. What follows is a more in-depth look into the modeling and optimization of the TMS itself.

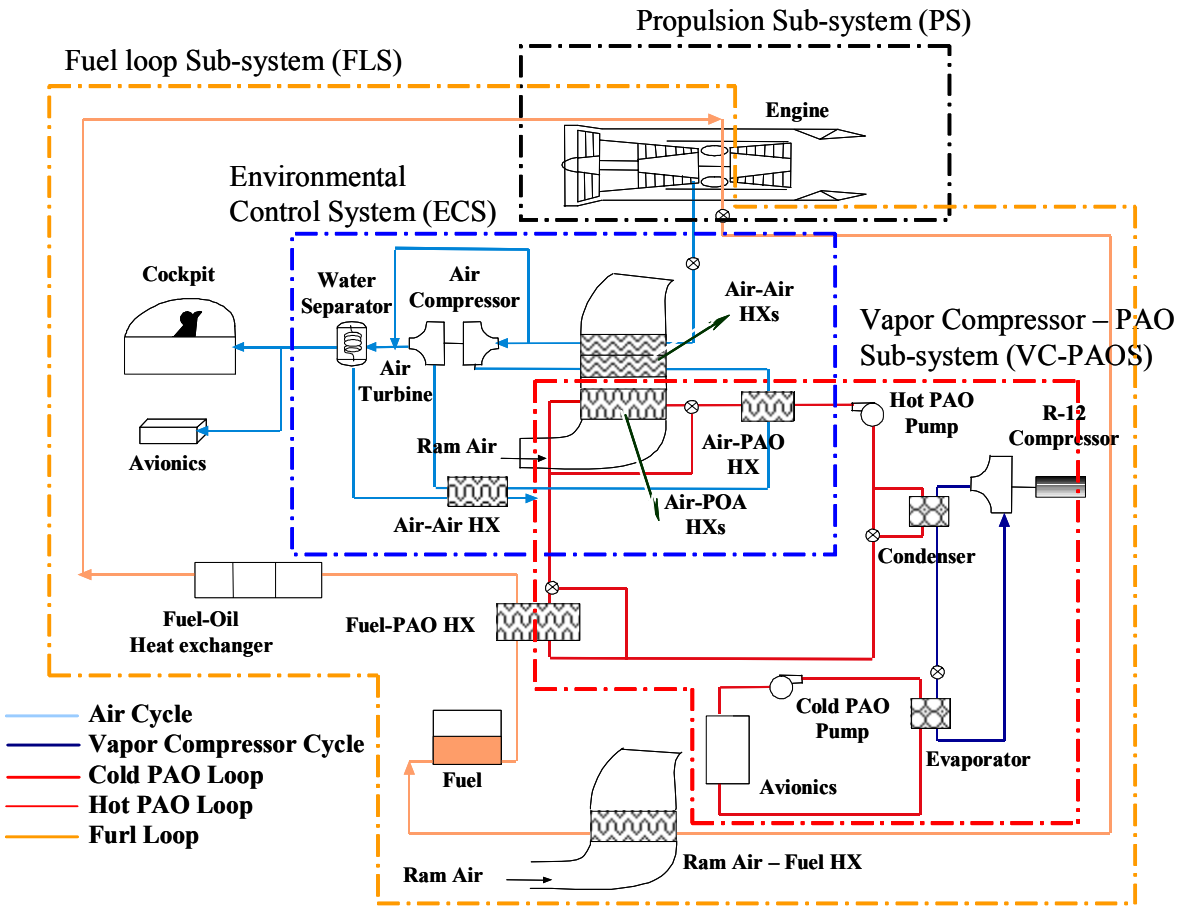

Figure 4.17 Thermal Management Sub-system (TMS) and associated sub-systems of an advanced military aircraft.

In order to approach the highly transient behavior exhibited by the TMS, it was decomposed into two sub-systems, the Vapor Compression Refrigeration / PAO Loops Sub-system (VC / PAOS) and the Fuel Loop Sub-system (FLS). In this way, the transient sub-system is isolated, allowing the design of specific code to simplify the optimization process. Figure 4.17 shows the VC / PAOS in the context of all of the other sub-systems while Figure 4.18 shows it and the connecting streams to the other sub-systems in greater detail. The energy (exergy) of Q_{fuel}, which connects this sub-system with the FLS, provides the necessary thermodynamic and cost link between the two sub-systems. Q_{Bleed} provides the thermodynamic and cost links between the VC / PAOS and the ECS, while stream (13) provides the energy (exergy)

and cost links between the VC/PAOS and the PS. Figure 4.18 also shows the physical boundaries between sub-systems and their associated coupling functions.

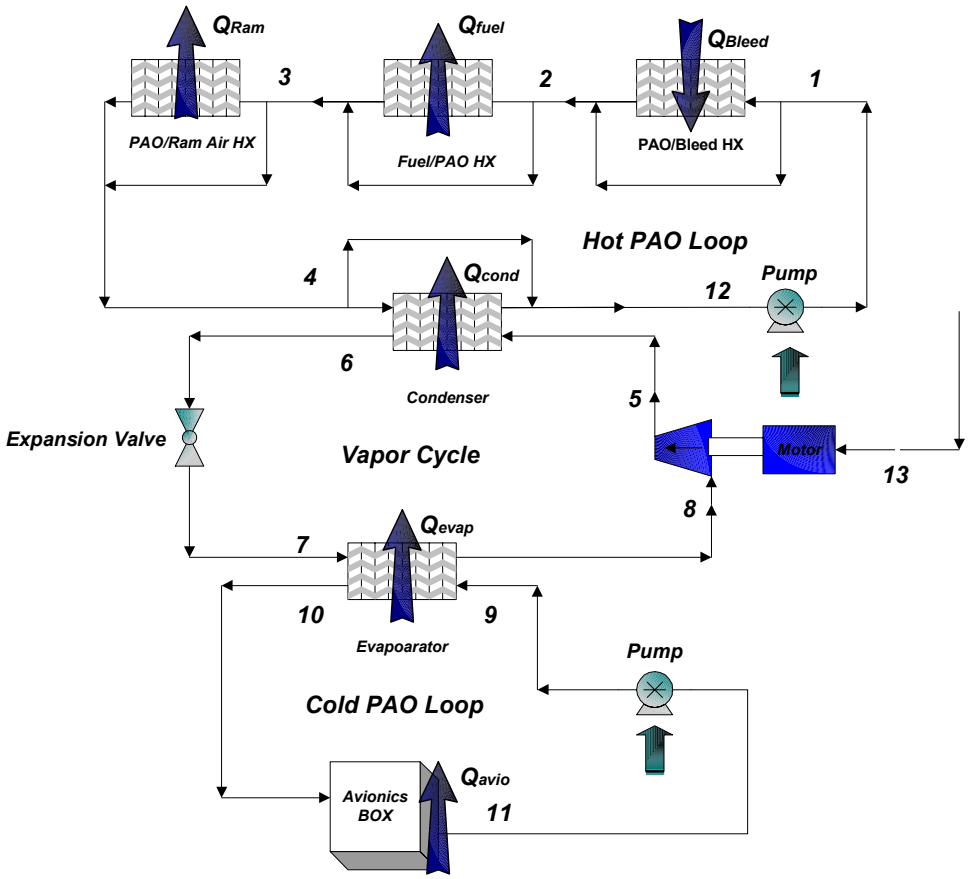

Figure 4.18 Schematic of the VC/PAOS of the TMS.

The VC/PAOS includes three loops and the ducts that connect them as follow: the cold PAO loop, the vapor cycle, and the hot PAO loop. The cold PAO loop includes an avionics box, a pump, and a heat exchanger (evaporator) which is shared with the vapor compression cycle. The vapor cycle includes, in addition to the evaporator, a centrifugal compressor, an expansion valve, and a heat exchanger (condenser) which is shared with the hot PAO loop. The hot PAO loop includes, in addition to the condenser, a pump, a ram-air heat exchanger, a bleed air / PAO heat exchanger, which interconnects the ECS and the TMS, and a fuel / PAO heat exchanger which links the VC/PAOS with the FLS.

The only PS product being used directly by the VC/PAOS is the power required to drive the vapor compressor and PAO loops pumps. This power and the VC/PAOS drag penalty also represent feedbacks (couplings) to the PS as do the VC/PAOS

weight. Each translates into excess thrust. The FLS cooling capacity is used as resource by the VC/PAOS. Finally, an additional feedback is the energy transferred from the ECS to the VC / PAOS through the bleed / PAO heat exchanger. All of these products and feedbacks form the basis for the coupling functions connecting the VC/PAOS with the other sub-systems.

4.4.2 VC/PAOS Thermodynamic and Heat Transfer Model

As with the ECS and for all the same reasons, the types of heat exchangers considered for the VC/PAOS and FLS are compact heat exchangers. There is a wide range of available geometries and types of fins that can be used. In general, once the particular type and geometry of the fin are selected, the only remaining degrees of freedom are the height, width and length of the heat exchanger core, and the number of fins per inch. It is assumed here that the synthesis/design of the manifolds and other accessories has no effect on heat transfer performance. A model for estimating the core weight is given in Muñoz and von Spakovsky (1999). This model correlates extremely well with observed mass values. A linear least squares equation that relates core mass to total mass (i.e. core plus manifolds and insulation) was used to estimate the total heat exchanger weight. As with the ECS, the heat transfer and pressure drop models used are based on the work of Shah (1981) and Kays and London (1998). Both sides of the heat exchangers have one pass unless stated otherwise.

Decision variables and inequality constraints other than those for the heat exchangers are also considered in the synthesis/design optimization, i.e. those for the ram-air intake. For this component, it was assumed that the VC/PAOS and the FLS use scoop-type ram-air inlets. The mass flow rate of air entering the inlet, the performance of the inlets at subsonic and supersonic conditions, and the duct models are the same as to those used for the ECS. The ECS turbomachinery model applies to the same components for the VC/PAOS.

Since all the heat exchangers are modeled as compact heat exchanger as is done with the ECS, the same physical and thermodynamic models apply. The heat transfer model for the condenser and evaporator are taken from Liu and Kakac (2000). The effectiveness-NTU method is applied in order to relate the geometric models of the heat exchangers to the thermodynamic ones. The expression for the heat exchanger effectiveness is obtained from Incropera and DeWitt (1990) and is valid for single-pass, cross-flow arrangements with both fluids unmixed.

As to correlations for the thermodynamic properties for all the fluids involved, these are taken form Lefebvre (1983). In particular, the specific heat and enthalpy for JP-4 fuel is determined as a function of temperature, the fuel's thermal conductivity as a function of temperature and relative density, and the fuel's vaporization point and percentage of vapor as a function of temperature. The Polyalphaolefin (PAO) properties such as viscosity, thermal conductivity, specific heat, Prandtl number, and enthalpy are based on data from the CRC Handbook (1973); Zabrasnky et. al. (1999); the Litron On-line Catalogue (2001); the Schaeffer Catalogue (2001); and the JANAF Thermochemical Tables (1997). The refrigerant (R12)[41] properties such as viscosity, specific heat, Prandtl number, and enthalpy for both the liquid and gas phases were based on data from the CRC Handbook (1973); Zabrasnky et. al. (1999); the JANAF Thermochemical Tables (1997); Wark (1991); and the ASHRAE Fundamentals Handbook (1993).

VC/PAOS Thermodynamic Model

The thermodynamic model presented is based on a perfect gas model. With reference to Figure 4.18, the required load temperature is given in Figliola et. al. (1997). The initial condition is

$$T_{10} = T_{load} \tag{4.96}$$

Cold PAO Loop Pump:

$$T_{11} = T_{10} + \frac{\dot{Q}_{Avio}}{\dot{m}_{PAO} C_{p\,PAO}} \tag{4.97}$$

The process is considered as adiabatic. The efficiency is assumed to be 85%. The physical model is given by Greene (1992). The efficiency, power, and pressure rise are given by

$$\eta_p = \frac{h_{09_s} - h_{011}}{h_{09} - h_{011}} = \frac{T_{09_s} - T_{011}}{T_{09} - T_{011}} \tag{4.98}$$

$$\dot{W}_p = c\left(T_{09} - T_{011}\right) + v\left(P_{09} - P_{011}\right) \tag{4.99}$$

[41] Refrigerant R-134a is also used nowadays. However, the information available in the open literature refers to refrigerant R-12.

$$\eta_p = \frac{v(P_{09} - P_{011})}{c(T_{09} - T_{011}) + v(P_{09} - P_{011})} \tag{4.100}$$

$$\Delta P_p = P_{09} - P_{011} = \Delta P_{Evap} + \Delta P_{Avio\_box} + \Delta P_{pipe} \tag{4.101}$$

Evaporator:

The heat transfer rates, the enthalpy and pressure at state 8, and the temperature and pressure at state 10 are given by

$$\dot{Q}_{load} = \dot{m}_{vap}(h_{10} - h_9) \tag{4.102}$$

$$\dot{Q}_{Evap} = \dot{m}_{vap}(h_8 - h_7) = \dot{m}_{pao}(h_{10} - h_9) = -\dot{m}_{vap}\left[(h_{11} - h_{10}) + (h_9 - h_{11})\right] \tag{4.103}$$

$$h_8 = h_7 + \varepsilon_{Evap}(T_9 - T_7)\frac{C_{min}}{\dot{m}_{Vap}} = h_7 - \frac{\dot{Q}_{Evap}\varepsilon_{Evap}}{\dot{m}_{Vap}} \tag{4.104}$$

$$T_{10} = T_9 - \varepsilon_{evap}(T_9 - T_{10})\frac{C_{min}}{C_9} \tag{4.105}$$

where C_{min} is the smallest of the heat capacities C_9 and C_7. Also,

$$P_{10} = \left(1 - \frac{\Delta P_{9-10}}{P_9}\right)P_9 \tag{4.106}$$

$$P_8 = \left(1 - \frac{\Delta P_{7-8}}{P_7}\right)P_7 \tag{4.107}$$

Compressor:

$$\frac{T_5}{T_8} = 1 + \frac{1}{\eta_{cp}}\left[\left(\frac{P_5}{P_8}\right)^{\frac{\gamma-1}{\gamma}} - 1\right] \tag{4.108}$$

The efficiency of the compressor is a function of the pressure rise and the shaft speed. It is found using Figure 4.13. The rate of work on the fluid and the COP are given by

$$\dot{W} = \dot{m}(h_5 - h_8) \tag{4.109}$$

$$COP = \frac{\dot{Q}_{load}}{\dot{W}_{neto}} \tag{4.110}$$

Condenser:

The heat transfer rates, the enthalpy and pressure at state 6, and the temperature and pressure at state 12 are given by

$$\dot{Q}_{Cond} = \dot{Q}_{Evap} + \dot{Q}_{Comp} \tag{4.111}$$

$$\dot{Q}_{Cond} = \dot{m}_{vap}(h_5 - h_6) = \dot{m}_{pao}(h_{12} - h_4) = \dot{m}_{vap}\left[(h_8 - h_7) + (h_5 - h_8)\right] \tag{4.112}$$

$$h_6 = h_5 - \varepsilon_{Evap}(T_5 - T_4)\frac{C_{min}}{\dot{m}_{Vap}} = h_5 - \frac{\dot{Q}_{Cond}\,\varepsilon_{Cond}}{\dot{m}_{Vap}} \tag{4.113}$$

$$T_{12} = T_4 + \varepsilon_{evap}(T_5 - T_4)\frac{C_{min}}{C_4} \tag{4.114}$$

where C_{min} is the smallest of the heat capacities C_5 and C_4. Also,

$$P_6 = \left(1 - \frac{\Delta P_{6-5}}{P_5}\right)P_5 \tag{4.115}$$

$$P_{12} = \left(1 - \frac{\Delta P_{12-4}}{P_4}\right)P_4 \tag{4.116}$$

Expansion Valve:

For an isenthalpic process,

$$h_{06} = h_{07} \tag{4.117}$$

$$c_v(T_7 - T_6) + v(P_7 - P_6) = 0 \tag{4.118}$$

$$Pr_{val} = Pr_{com} - \Delta P_{Evap} - \Delta P_{Cond} \tag{4.119}$$

Hot PAO Loop Pump:

The process is considered as adiabatic. The efficiency is assumed to be 85%. The physical model is given by Greene (1992). The efficiency, power, and pressure rise are given by

$$\eta_p = \frac{h_{01_s} - h_{012}}{h_{01} - h_{012}} = \frac{T_{01_s} - T_{012}}{T_{01} - T_{012}} \tag{4.120}$$

$$\dot{W}_p = c(T_{01} - T_{012}) + v(P_{01} - P_{012}) \tag{4.121}$$

$$\eta_p = \frac{v(P_{01} - P_{012})}{c(T_{01} - T_{012}) + v(P_{01} - P_{012})} \tag{4.122}$$

$$\Delta P_p = P_{01} - P_{012} = \Delta P_{Cond} + \Delta P_{fuel\_hx} + \Delta P_{bleed\_hx} + \Delta P_{ram\_hx} + \Delta P_{pipe} \tag{4.123}$$

Bleed Air / Hot PAO Heat Exchanger:

The temperature and pressure at state 2 are given by

$$T_2 = T_1 + \varepsilon_{bleed/pao\_rhx}(T_1 - T_{bleed\_in})\frac{C_{min}}{C_1} \tag{4.124}$$

$$P_2 = \left(1 - \frac{\Delta P}{P_1}\right)P_1 \tag{4.125}$$

where C_{min} is the smallest of the heat capacities C_4 and C_{bleed_in}.

Fuel / Hot PAO Heat Exchanger:

The temperature and pressure at state 3 are given by

$$T_3 = T_2 - \varepsilon_{fuel/pao\_rhx}(T_2 - T_{fuel\_in})\frac{C_{min}}{C_2} \tag{4.126}$$

$$P_3 = \left(1 - \frac{\Delta P}{P_2}\right)P_2 \tag{4.127}$$

where C_{min} is the smallest of the heat capacities C_2 and C_{fuel_in}. This component works under dynamic conditions. Its transient model is explained in *section 4.4.2*.

Ram Air / PAO Heat Exchanger

The temperature and pressure at state 4 are given by

$$T_4 = T_3 - \varepsilon_{ram/pao\_rhx}(T_3 - T_{ram\_in})\frac{C_{min}}{C_3} \tag{4.128}$$

$$P_4 = \left(1 - \frac{\Delta P}{P_3}\right)P_3 \tag{4.129}$$

where C_{min} is the smallest of the heat capacities C_3 and C_{ram_in}. The flow between the scoop inlet and the heat exchanger is modeled as a constant area, one-dimensional, adiabatic flow with a constant friction coefficient of 0.01. The thermodynamic model is the same as for the ECS ram-air inlet.

4.4.3 Fuel Loop Sub-system (FLS)

The FLS is composed of a fuel tank, which serves as a sink for the heat taken from the VC/PAOS, a fuel/hot PAO heat exchanger, a fuel / oil heat exchanger, a fuel / hydraulic heat exchanger, a fuel/ram heat exchanger, a pump, and ducts to connect the different components. This sub-system is used to extract heat from different sub-systems (i.e. the VC/PAOS, the PS, and the hydraulic sub-systems). In order to do this, the FLS consumes resources from the PS. The different sub-systems linked to the FLS use its cooling capacity as a resource, which must be taken into account in their respective synthesis/design optimization problems. In this work, the FLS is assumed to take resources only from the PS. The feedbacks from the VC/PAOS, the PS, and the hydraulic sub-systems are the loads imposed on the FLS, which change with the different mission segments.

In contrast to the VC/PAOS, the unit-level synthesis/design optimization problem for the FLS is not solved based on one mission segment, but instead on all mission segments at once subject to heat load constraints as well as a maximum fuel tank temperature. Thus, no time decomposition is applied to the operational optimization problem. This was accomplished using a state-of-the-art transient optimization numerical solver. The operational decision variables used by the optimization are the fuel mass flow, which is time dependent, as well as the hydraulic mass flow and the oil mass flow. The initial fuel tank temperature range is based on data from Hudson (1975).

The thermodynamic and physical models for the heat exchangers, the pump, and the ram-air inlet are the same as the ones for the VC/PAOS. Table 6.2 of Chapter 6 lists the operational and synthesis/design decision variables, the fixed parameters, which are input from the VC/PAOS, the derived variables, and the inequality constraints.

The only PS product being used directly by the FLS is the power extracted to drive the fuel pump. This power and the FLS drag penalty both represent feedbacks (couplings) to the PS as do the FLS weight. Each translates into excess thrust. The VC/PAOS heat load represents an additional feedback. The two sub-systems being optimized, the FLS and VC/PAOS, make use of the same source for extracted power (i.e. the PS), and, thus, the shadow price for extracted power $\lambda_{\dot{E}vc/paos-ps}$ appearing in the unit-level optimization problem definitions is the same for both sub-systems.

Moreover, the penalties produced by the drag and weight due to the FLS and VC/PAOS are of the same nature as those produced by the ECS. Therefore, the ECS shadow prices λ_D and λ_W due to drag and weight can be used for the FLS unit-level synthesis/design optimization as well.

The FLS is shown in detail in Figure 4.19. The purpose of the FLS is to take advantage of the fuel heat capacity using it as a heat sink. The operation of the FLS is dependent on the temperature of the thermal storage tank (i.e. fuel tank) and the heat loads from the PS, hydraulic and VC/PAOS sub-systems. The temperature of the fuel tank should be kept within a certain range in such a way that the difference between the fuel inlet temperature and the hot PAO inlet temperature to the fuel/PAO heat exchanger allows the effectiveness to reach reasonable values and the fuel-side to operate within a certain acceptable flow range.

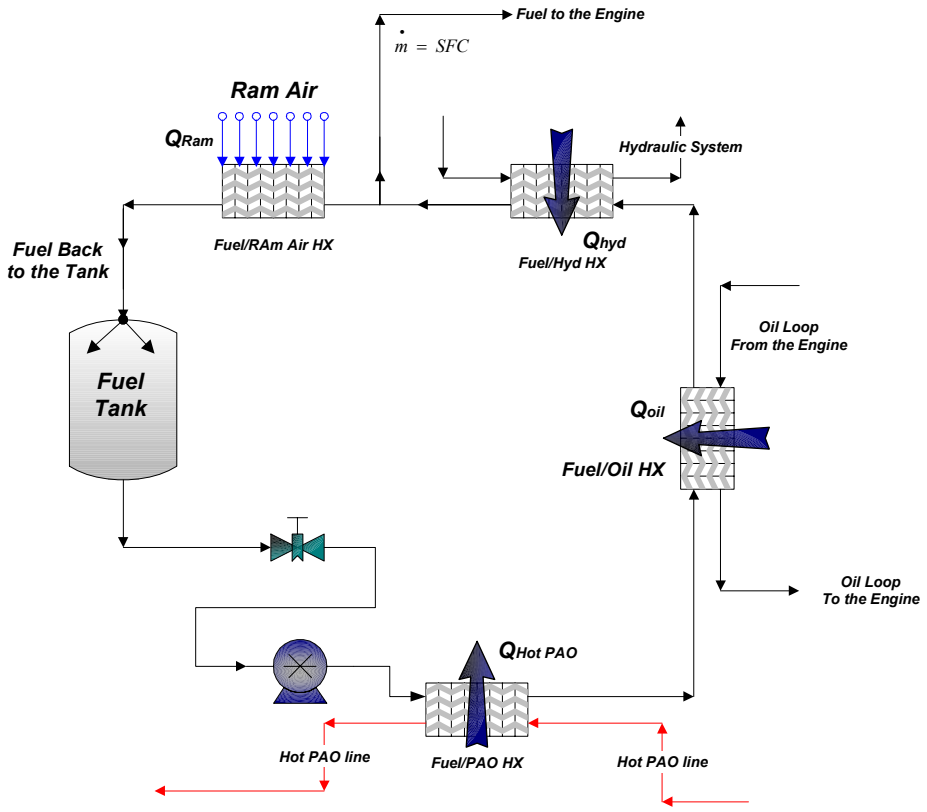

Figure 4.19 Schematic of the fuel loop sub-system (FLS).

The ram air heat exchanger has to be sized in such a way that the temperature of the fuel remaining into the thank is kept within the proper range at nay time. The fuel flow through the system is controlled to assure that the fuel required by the engine is

provided while proper fuel heat capacity is maintained through all heat exchangers. Segments with low fuel consumption are also the ones for which the cooling requirements are lower, which allows to keep proper rations between the fuel leaving the tank and the fuel consumption. The main constraints for the FLS, which are indeed extremely stringent, are to keep constant the flow conditions on the hot PAO side and the amount of heat going from the hot PAO loop to the FLS. In order to do this, the temperature of the tank, which is in turn the inlet fuel temperature to the fuel/PAO heat exchanger and is varying in time, must be taken into account. Therefore, the fuel mass flow must be change and one can, thus, define the FLS problem in terms of the mass of fuel required at any time, subject to the fuel tank temperature increment and the VC/PAOS heat load.

The inlet and outlet conditions of the hot PAO loop in the fuel/PAO heat exchanger are kept constant during the FLS unit-level synthesis/design optimization problem. However, it should be remembered that this conditions is different for each mission segment. This fact allows one to keep the energy transfer through the fuel/PAO heat exchanger constant during each mission segment.

The fuel tank temperature T_{Tank} is a function of time and is determined by the flight conditions, the amount of ram air, the heat loads from the engine and hydraulics (which are constant for each mission segment), and the heat loads from the VC/PAOS. Data from Hudson et. al. (1975) is used to define the initial condition required to solve this highly dynamic problem.

The effectiveness of the fuel / hot PAO heat exchanger is given by

$$\varepsilon_{fuel/pao} = \frac{Q_{actual}}{Q_{max}} = \frac{(\dot{m} * Cp)_{pao} * (T_{pao\_in} - T_{pao\_out})}{(\dot{m} * Cp)_{min} * (T_{pao\_in} - T_{fuel\_in})}$$

$$= \frac{(\dot{m} * Cp)_{fuel} * (T_{fuel\_out} - T_{fuel\_in})}{(\dot{m} * Cp)_{min} * (T_{pao\_in} - T_{fuel\_in})} \tag{4.130}$$

where T_{pao_in} and T_{pao_out} are the inlet and outlet PAO-side temperatures and T_{fuel_in} is equal to the fuel tank temperature. As can be seen, since T_{Tank} is changing with time, the fuel/PAO heat exchanger effectiveness is also changing with time. In general, $(\dot{m} * Cp)_{min}$ is equal to $(\dot{m} * Cp)_{pao}$. If it is not, the effectiveness has to be expressed in terms of fuel flow, which is also changing with time. This, in fact, must be verified by the optimization model.

The effectiveness of the fuel/oil and fuel/hydraulics heat exchanger is given by the equations (4.131) and (4.132), respectively. In the presence of a variable fuel mass flow and temperature, the constant heat rate through this heat exchanger is controlled by varying the oil and hydraulics mass flows. This sub-problem is part of the optimization. In order to set the constraint required to solve the FLS model, the temperature of the fuel leaving the fuel/PAO heat exchanger has to be set to a fixed value for each mission leg. This temperature is, in fact, an operational decision variable in the unit-level optimization problem.

$$\varepsilon_{fuel/oil} = \frac{(\dot{m} * Cp)_{oil} * (T_{oil\_in} - T_{oil\_out})}{(\dot{m} * Cp)_{min} * (T_{oil\_in} - T_{fuel\_in})} \tag{4.131}$$

$$\varepsilon_{fuel/hyd} = \frac{(\dot{m} * Cp)_{hyd} * (T_{hyd\_in} - T_{hyd\_out})}{(\dot{m} * Cp)_{min} * (T_{hyd\_in} - T_{fuel\_in})} \tag{4.132}$$

The effectiveness of the fuel/ram-air heat exchanger is given by

$$\varepsilon_{fuel/ram} = \frac{Q_{actual}}{Q_{max}} = \frac{(\dot{m} * Cp)_{ram} * (T_{ram\_out} - T_{ram\_in})}{(\dot{m} * Cp)_{min} * (T_{fuel\_in} - T_{ram\_in})}$$

$$= \frac{(\dot{m} * Cp)_{fuel} * (T_{fuel\_in} - T_{fuel\_out})}{(\dot{m} * Cp)_{min} * (T_{fuel\_in} - T_{ram\_in})} \tag{4.133}$$

From Equation (4.130) and considering that the ram air mass flow is constant for each leg and the fuel mass flow and temperature are changing with time, it can be deduced that both the effectiveness and the energy transferred through the fuel/ram-air heat exchanger are also changing with time.

Taking into account all the heat sources and the change in mass of the tank fuel, an energy balance on the storage tank gives

$$\frac{\partial E}{\partial t} = M * Cp * \frac{\partial T_{Tank}}{\partial t} + \frac{\partial M}{\partial t} * Cp * T_{Tank}$$

$$= \dot{m} * Cp * T_{fuel\_out} - \dot{m} * Cp * T_{fuel\_in} \tag{4.134}$$

where the work interaction and heat interaction of the tank through its walls are neglected. M is the fuel mass in the tank at any time, which is expressed as

$$M(t) = M_o - SFC * t \tag{4.135}$$

In equation (4.135), M_o is the initial fuel mass in the tank at the beginning of the leg. *SFC* is the specific fuel consumption, which is given by the PS and is fixed for each leg. The derivative of equation (4.135) with respect to time is

$$\frac{\partial M}{\partial t} = -SFC \tag{4.136}$$

The variable T_{fuel_out} in equation (4.134) is equal to T_{Tank}, since no losses are considered between the output of the tank and the inlet of the fuel/PAO heat exchanger. The expression for the fuel mass flow exiting the tank is determined from the heat transfer analysis of the fuel/PAO heat exchanger, where the hot PAO-side conditions are constant. Thus,

$$\dot{Q}_{fuel/PAO\_HX} = \dot{m}_{fuel} * Cp * (T_{fuel\_out} - T_{fuel\_in}) \tag{4.137}$$

Combining equations (4.130) and (4.137), gives the following output fuel mass flow expression:

$$\dot{m}_{fuel\_out} = \frac{(\dot{m} * Cp)_{pao} * (T_{pao\_in} - T_{pao\_out})}{Cp_{fuel} * \left[T_{fuel\_out} + \left(\frac{(T_{pao\_in} - T_{pao\_out})}{\varepsilon_{fuel/pao}} - T_{pao\_in} \right) \right]} \tag{4.138}$$

where all the terms do not change with time other than the effectiveness of the fuel/PAO heat exchanger and the fuel mass flow. A mass balance yields the following expression for the inlet fuel mass flow:

$$\dot{m}_{fuel\_in} = \dot{m}_{fuel\_out} - SFC \tag{4.139}$$

The only term left to be found from equation (4.134) is the inlet fuel temperature (Tf_{Fuel_in}). From equation (4.130), this temperature is equal to

$$T_{fuel\_in} = T_{fuel\_to\_engine} - \frac{(\varepsilon_{fuel/ram} * (\dot{m} * Cp)_{min} * (T_{fuel\_to\_engine} - T_{ram\_in})}{Cp_{fuel} * \dot{m}_{fuel\_in}} \tag{4.140}$$

where the inlet fuel temperature to the fuel/ram-air heat exchanger is equal to the temperature of the fuel going to the engine ($T_{fuel\_to\_engine}$), which is known since the heat load from the engine and hydraulics are constant for a given mission leg.

Combining equations (4.130) to (4.140) and after algebraic manipulation, equation (4.134) yields a new expression for the energy balance, namely,

$$\frac{\partial T_{tank}}{\partial t} = \frac{(\alpha \ + \beta \ ) * T(t)_{tank} + \lambda}{\mu \ - t * \alpha} \tag{4.141}$$

where $\alpha \ = Cp_{fuel} * SFC$ (4.142.1)

$$\beta \ = \frac{\varepsilon_{fuel/pao} * (Cp * \dot{m})_{pao} * (T_{pao\_in} - T_{pao\_out})}{Cp_{fuel} * (T_{pao\_out} - T_{pao\_in} + \varepsilon_{fuel/pao} * (T_{fuel\_out} - T_{pao\_in})} \tag{4.142.2}$$

$$\lambda \ = \varepsilon_{fuel/ram} * (Cp * \dot{m})_{ram} * (T_{fuel\_to\_engine} - T_{ram\_in}) - T_{fuel\_to\_engine} \tag{4.142.3}$$

$$\mu \ = Cp_{fuel} * M_0 \tag{4.142.4}$$

Equation (4.142) shows that the fuel tank temperature is a function of, among others, the effectivenesses of the fuel/PAO and fuel/ram heat exchangers. These effectivenesses are not constant with time, since the fuel mass flow and fuel temperature are changing with time. To introduce them into equation (4.142) as a function of time, fuel mass flow, and fuel temperature yields a differential equation with no analytical solution. The transient optimization problem was solved using gPROMS®, which is a state-of-the-art dynamic modeling, simulation and optimization software by PS Enterprise Ltd.

A quasi-static approach can also be used to solve this unit-level optimization problem in which each mission segment is divided in n sub-intervals, and in each sub-interval the effectiveness can be treated as constant. This approach yields the following analytical expression for the fuel tank temperature at any instance of time:

$$T_{tank} = \frac{\frac{-\lambda}{\lambda + \beta} + (t \ * \alpha - \mu)^{\frac{-\alpha-\beta}{\alpha}} * \left[T_{0\_tank} \ + \frac{\lambda}{\lambda + \beta} \right]}{\left[\mu^{\frac{-\alpha-\beta}{\alpha}} \right]} \tag{4.143}$$

where T_{0_tank} is the fuel tank's initial temperature. Knowing the temperature of the tank at any time allows one to compute the fuel mass flow through the fuel/PAO heat exchanger in order to keep the energy transfer rate constant. At the same time, the fuel tank temperature is kept below certain limits.

4.5 Propulsion Sub-system Description and Modeling

The PS has eighteen components as indicated in Figure 4.20. The sub-system is a low-bypass turbofan engine with afterburning. The on- and off-design behavior of the engine is simulated using a modern performance code (FAST by Honeywell) developed by an engine manufacturer for modeling any type of aircraft engine system. The model of the engine uses typical component maps (e.g., compressor, fan hub, fan tip, turbine, burner, and compressor maps) and functional relationships and numerical constants that modify the maps to make the simulation as realistic as possible. The component maps are chosen from several alternatives depending on the design pressure ratio. The computer program has its own set of solvers to carry out the mass, momentum, energy, and shaft speed balances. Results from the simulation are the thermodynamic properties at each of the engine stations (pressure, temperature, Mach number, etc.), the inlet air flow rate, nozzle areas, and the fuel consumed in the combustor and afterburner adjusted to provide the thrust required by the mission during the different segments of the mission. No major detail on the thermodynamic model is presented due to propriety reasons. However, the reader can find a full thermodynamic and physical model in Mattingly, Heiser, and Daley (1987).

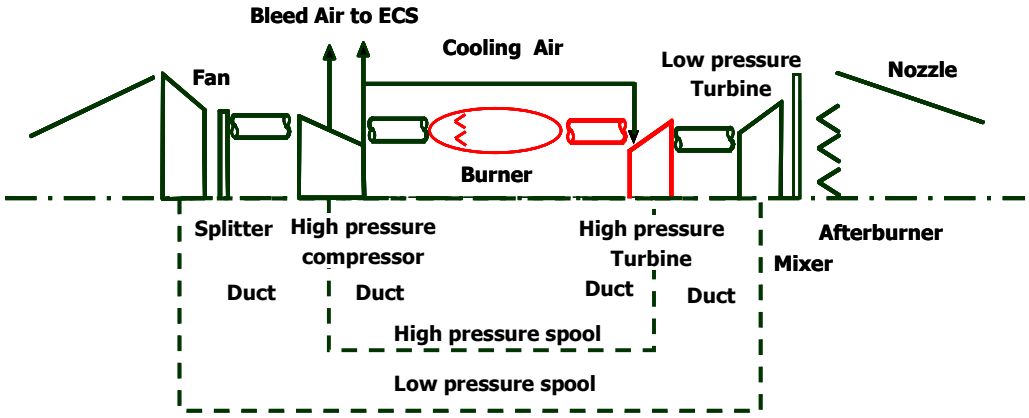

Figure 4.20 Turbofan engine components of the propulsion sub-system (PS).

Inlet and Nozzle Drag Models

The thrust provided by the engine simulator does not account for the drag created by the installation of the engine. This "uninstalled" thrust (F) must be adjusted for the drag created by the engine inlet and nozzle. Thus,

$$T = F - \phi_{inlet} F - \phi_{nozzle} F \tag{4.144}$$

The drag created by the inlet ($\phi_{inlet} F$) at subsonic conditions is approximated as the momentum drag created by the isentropic, one-dimensional flow of a perfect gas. Assuming massive separation and no recovery of the additional drag (i.e. the worst case scenario), the conservation of mass and perfect gas relationships lead to Equation (4.145). For the supersonic case, a compressible model that uses a normal shock approximation and neglects internal friction and the disturbed pressure field on the cowl yields Equation (4.146).

$$\phi_{inlet} = \frac{\frac{M_0}{M_1}\sqrt{\frac{T_1}{T_0}}\left(1+\gamma M_1^2\right)-\left(\frac{A_1}{A_0}+\gamma M_0^2\right)}{\left(\frac{F}{m_0}\right)\left(\frac{\gamma M_0}{a_0}\right)} \tag{4.145}$$

$$\phi_{inlet} = \frac{\left(\frac{A_1}{A_0}-1\right)\left\{M_0-\left(\frac{2}{\gamma+1}+\frac{\gamma-1}{\gamma+1}M_0^2\right)^{1/2}\right\}}{\frac{F}{m_0 a_0}} \tag{4.146}$$

The computer program that simulates the PS cycle also provides the inlet and exit areas of the nozzle at various segments of the mission. The installation penalty due to the nozzle is given by

$$\phi_{nozzle} = \frac{M_0 \frac{C_{D_{nozzle}}}{2}\left(\frac{A_{exit}-A_{in}}{A_0}\right)}{\frac{F}{m_0 a_0}} \tag{4.147}$$

where the drag coefficient is a function of the Mach number as presented in Mattingly, Heiser, and Daley (1987).

Physical Model

The weight and dimensions of the PS are calculated using the computer code Weight Analysis of Turbine Engines - WATE (WATE User's Guide, 2000). WATE was originally developed by the Boeing Military Aircraft Company in 1979 and improved by NASA and the McDonnell Douglas Corporation. The original weight and dimensions were derived using a semi-empirical method obtained from analyzing

a database of 29 engines. The improved code (used in this research) is based on analytical and dimensional calculations (the primary method is to calculate material volume and then multiply by density). The new code also accounts for more of the individual parts that make up an engine component than the original empirical method.

Chapter 5

Optimization Strategy and Coupling Function Definitions for the Proposed Advanced Tactical Fighter Aircraft System

This chapter presents in detail the procedure followed for the synthesis/design optimization of the proposed advance tactical aircraft. Both *time* and *physical decomposition* are used for this purpose. In the case of physical decomposition, five different sub-systems, namely the AFS, PS, ECS, VC/PAOS and FLS, are taken into account and their coupling functions are described. The decomposed optimization problems for the five units considered are defined and the ILGO approach presented in the previous chapter is applied.

5.1. System-Level Optimization Problem Definitions

As explained above, the interdependence between the five units being synthesized/designed (the PS, VC/PAOS, FLS, ECS and AFS) is quite tight. Although the other units, namely the payload sub-systems and equipment group (EG, EPAYS and PPAYS), are not synthesized/designed, i.e. they do not have decision variables which are optimized, their role is not strictly passive. Thus, for example, the AFS's optimal design is affected by the optimal synthesis/design decisions made in the PS, ECS, FLS and VC/PAOS as well as by the mission requirements dictated for the EG, EPAYS, and PPAYS. The result is that the advance tactical aircraft system at hand constitutes the typical case of a system in which "everything influences everything else".

Thus, determining the optimal synthesis/design of the aircraft system requires that the optimal synthesis/design of each of the aircraft sub-systems (e.g., the PS, VC/PAOS, FLS, ECS, and AFS[42]) be carried out in an integrated fashion. Individually

[42] Of course these sub-systems do not comprise all of the aircraft sub-systems but do nonetheless represent a large number of its principal ones.

optimizing each without consideration for their integration as a system does not lead to the optimum for the system as a whole. The decomposition approach (LGO and ILGO) described in *Chapter 3* are two means by which each sub-system can be individually optimized consistent with their integration into the overall system.

The latter of these two approaches (i.e. ILGO) is applied to the synthesis/design optimization problem at hand. How ILGO is applied is discussed in this chapter. However, the next section begins with a description of the overall system synthesis/design optimization problem and is followed in the remaining section of *Chapter 5* with a description of each of the sub-system optimization problems. What follows is the overall system problem definition in terms of three different objective functions. However in this thesis work the gross take-off weigh problem is solved.

5.1.1 Gross Take-Off Weight System-Level Optimization Problem Definition[43]

The first system-level optimization problem formulated for the military advanced fighter aircraft and mission given in *section 4.1* uses gross take-off weight as the figure of merit. Thus, the problem statement is as follows:

$$\text{Minimize} \quad W_{TO} = W_{AFS} + W_{PS} + W_{ECS} + W_{TMS} + W_{FUEL} + W_{EG} + W_{PPAY} + W_{EPAY} \tag{5.1}$$

$$\text{w.r.t.} \quad \left\{\vec{X}_{PS}, \vec{Y}_{PS}\right\}, \quad \left\{\vec{X}_{ECS}, \vec{Y}_{ECS}\right\}, \quad \left\{\vec{X}_{TMS}, \vec{Y}_{TMS}\right\}, \quad \left\{\vec{X}_{AFS}, \vec{Y}_{AFS}\right\}$$

subject to

$$\vec{H}_{PS} = \vec{0}, \quad \vec{G}_{PS} \le \vec{0} \tag{5.2}$$

$$\vec{H}_{ECS} = \vec{0}, \quad \vec{G}_{ECS} \le \vec{0} \tag{5.3}$$

$$\vec{H}_{TMS} = \vec{0}, \quad \vec{G}_{TMS} \le \vec{0} \tag{5.4}$$

$$\text{and} \quad \vec{H}_{AFS} = \vec{0}, \quad \vec{G}_{AFS} \le \vec{0} \tag{5.5}$$

where the vectors of equally constraints $\vec{H}$ represent the thermodynamic and physical models for each of the sub-systems. The vectors of inequality constraints $\vec{G}$ represent the physical limits placed on independent and dependent variables or other physical

[43] W_{TO} is a figure of merit commonly used by the aircraft/aerospace community.

quantities. W_{EG} is the weight of the equipment group, which is made up of the flight controls, instruments, hydraulics, electrical equipment, avionics, and miscellaneous empty weight. W_{EG} is not being optimized due to the fact that it is a function of the AFS and PS unit-level optimization problems results, along with fix parameter given by the RFP. Also note that the weights W_{PPAY} and W_{EPAY} are fixed for the mission and, thus, are not minimized along with the remaining terms in the objective, which consist of the weight of each of the sub-systems plus the weight of the fuel.

It is important to observe that although the minimization of weight is not a thermoeconomic problem, it shares many of its characteristics. For example, the synthesis/design and operation of any given sub-system forces the sub-systems with which it interacts to change their size. In the present problem, that change is reflected in different weights and in a thermoeconomic problem in different capital costs.

5.1.2 Fuel Consumption System-Level Optimization Problem Definition

The minimization of total fuel consumption is also a problem of great interest. This system-level optimization is defined as

$$\text{Minimize } W_{FUEL} = W_{FUEL}\left(W_{TO}, \vec{X}_{PS}, \vec{Y}_{PS,}, \vec{X}_{TMS}, \vec{Y}_{TMS,}, \vec{X}_{ECS}, \vec{Y}_{ECS,}, \vec{X}_{AFS}, \vec{Y}_{AFS,}, mission\ \right) \tag{5.6}$$

$$\text{w.r.t. } \left\{\vec{X}_{PS}, \vec{Y}_{PS}\right\} \ , \ \left\{\vec{X}_{ECS}, \vec{Y}_{ECS}\right\} \ , \ \left\{\vec{X}_{TMS}, \vec{Y}_{TMS}\right\} \ , \ \left\{\vec{X}_{AFS}, \vec{Y}_{AFS}\right\}$$

subject to

$$\vec{H}_{PS} = \vec{0}, \quad \vec{G}_{PS} \le \vec{0} \tag{5.7}$$

$$\vec{H}_{ECS} = \vec{0}, \quad \vec{G}_{ECS} \le \vec{0} \tag{5.8}$$

$$\vec{H}_{TMS} = \vec{0}, \quad \vec{G}_{TMS} \le \vec{0} \tag{5.9}$$

$$\text{and } \vec{H}_{AFS} = \vec{0}, \quad \vec{G}_{AFS} \le \vec{0} \tag{5.10}$$

5.1.3 Total Cost System-Level Optimization Problem Definition

Future air vehicles present a unique set of requirements not previously addressed. For example, future Uninhabited Air Vehicles (UAVs) must be

substantially more affordable than comparable manned systems both in terms of acquisition and operational costs. Future UAVs will likely be high Mach, high performance vehicles. To permit an integrated approach to their and other aerospace vehicles' optimal synthesis/design, it will be necessary to combine into a single comprehensive model thermodynamic as well as cost functions so that a large number of independent variables related to how different technologies optimally accommodate limited payload spaces can be investigated (Brown, 1999).Thus the system-level optimization problem would be that of minimizing the total cost. It is formulated as follows:

$$\text{Minimize} \quad C_T = C_{SS} + C_{PS} + C_{ECS} + C_{TMS} + C_{FUEL} + C_{EG} + C_{PPAYS} + C_{EPAYS} \tag{5.11}$$

$$\text{w.r.t.} \ \left\{\vec{X}_{PS}, \vec{Y}_{PS}\right\} \ , \ \left\{\vec{X}_{ECS}, \vec{Y}_{ECS}\right\} \ , \ \left\{\vec{X}_{TMS}, \vec{Y}_{TMS}\right\} \ , \ \left\{\vec{X}_{AFS}, \vec{Y}_{AFS}\right\}$$

subject to

$$\vec{H}_{PS} = \vec{0}, \quad \vec{G}_{PS} \le \vec{0} \tag{5.12}$$

$$\vec{H}_{ECS} = \vec{0}, \quad \vec{G}_{ECS} \le \vec{0} \tag{5.13}$$

$$\vec{H}_{TMS} = \vec{0}, \quad \vec{G}_{TMS} \le \vec{0} \tag{5.14}$$

$$\text{and} \ \ \vec{H}_{AFS} = \vec{0}, \quad \vec{G}_{AFS} \le \vec{0} \tag{5.15}$$

Note that C_{EG}, C_{PPAYS}, and C_{EPAYS} are fixed costs and are, thus, not minimized along with the rest of the objective, which consists of the total cost of each sub-system and its associated fuel cost penalties. From Munoz (2000), the total cost for the advance tactical aircraft system is linearly dependent on W_{TO}. Thus, the sub-system optimization problems are expressed in terms of W_{TO} and W_{fuel} only since the analog cost optimization problem follows straight from the former.

5.2 Decomposition and Coupling Function Definitions: Applying ILGO to the Proposed Advanced Tactical Fighter Aircraft System Synthesis/Design Optimization Problem

In order to solve the system-level optimization problems (i.e. equations (5.1) to (5.15)) one can use the local-global optimization (LGO) decomposition technique

presented in Muñoz and von Spakovsky (2000b). In order to do this, the design of the PS would need to be carried out for multiple bleed air flow rates, ECS drags and ECS weights, bleed port selections, and TMS drag, weight, and power extractions. This would mean that a number of unit-level optimization runs with respect to the PS design and operational variables would have to be solved for innumerable combinations of values of the constraints related to the quantities listed in the previous sentence. A similar number of unit-level optimizations would have to be done for the ECS, VC/PAOS, FLS, and AFS. The results would then be used to generate the optimum response surface (ORS) for the system, which in this case would be in the W_{TO} versus ECS drag, bleed, and weight; VC/PAOS and FLS drag, weight, and power demanded; and AFS drag and weight. If the off-line version of the method (OL-LGO; see Muñoz and von Spakovsky (2000b)) were used, the results would have to be stored for later use by the system-level optimization problem for the PS, ECS, VC/PAOS, FLS, and AFS combined. The latter problem involves finding the combination of bleed air; ECS drag and weight; VC/PAOS and FLS drag, weight, and power; and AFS drag and weight that minimize the system-level objective function.

From a practical standpoint, the principal difficulty associated with the implementation of the OL-LGO technique (or for that matter RT-LGO, i.e. real-time LGO) in its general form for this case is the computational burden which it entails. For example, for the PS, the calculation of the take-off gross weight involves "flying" the engine on paper over the entire mission to obtain the fuel consumption. The process is repeated a number of times until convergence on the take-off weight is achieved. The resulting W_{TO} value can then be sent to the optimizer for analysis. The process just described requires different computer codes. First, there is a computer program that calculates the necessary thrust for each of the mission legs by solving the differential equation (4.50) (flight dynamics code). The thermodynamic engine simulation follows. This step is particularly slow due to the fact that the engine performance code in use is not 'persistent', i.e. it is necessary to launch the program every time the engine is 'flown' over the mission. The thrust obtained from the engine simulator is adjusted by a different computer code to account for inlet and nozzle losses, i.e. equations (4.145) to (4.147). Some of the outputs of the thermodynamic simulation added to aerodynamic, materials, and other synthesis/design variables are used by WATE (NASA's engine weight code) to calculate the weight of the engine.

The final step before going to the optimizer is the post-processing of all of the codes' results. This entire process makes the simulation of the PS very expensive computationally. For reference, the calculation of a single value of the gross takeoff weight takes on average about 75 seconds on a current dual processor PC workstation, a duration which can be prohibitive for large-scale optimization, especially since this duration accounts for only one of the five sub-systems being optimized here as part of the aircraft system.

Thus, another decomposition approach is needed which significantly lessens this prohibitive computational burden, i.e. ILGO, as discussed in *Chapter 3*[44]. Of the two versions of ILGO, version A requires that the PS, ECS, TMS, and AFS be synthesized /designed for arbitrary values of the coupling functions (i.e. ECS bleed, drag, and weight; TMS drag, weight and power; and AFS drag and weight). Such a constraint is easy to meet in the PS design. However, the ECS and TMS synthesis/design would unnecessarily be constrained by this requirement. In fact, arbitrary combinations of the coupling functions between the PS and ECS and TMS may not necessarily lead to feasible solutions for the ECS and TMS. Therefore, version B of ILGO, which does not have these shortcomings, is used for the ECS, AFS and TMS synthesis/design optimization while version A is retained for the PS. Furthermore, in addition to these four sub-systems, an additional decomposition at the sub-system level of the TMS is performed in order to effectively deal with the highly dynamic behavior of the fuel loop. The two additional sub-systems are the fuel loop subsystem (FLS) and the vapor compression/PAO loops sub-system (VC/PAOS). Details of the model developed for the TMS are given in *Chapter 4*.

In order to apply ILGO to the system-level optimization problem for gross takeoff weight (equations (5.1.) to (5.5.)), one unit-level optimization problem is defined (i.e. ILGO-A applied to the PS) and four system-level, unit based optimization problems are defined (i.e. ILGO-B applied to the ECS, VC/PAOS, FLS, and AFS). The boundaries of each unit (sub-system), their associated local decision variables as well as the coupling functions connecting each unit to the rest are clearly seen in Figure 5.1. The resource used to produce the system-level product (thrust) is fuel. The coupling functions which along with their associated shadow prices[45] are

[44] Note that there are a number of other advantages that ILGO brings to the table (see Muñoz and von Spakovsky, 2001a,b; 2002) including the elimination of nested optimization and the ability to be used across geographically dispersed teams of synthesis/ design specialists.
[45] See discussion in the following sections.

used in ILGO to eliminate the system level optimization problem by incorporating system–level information in the unit-level (ILGO-A) and system-level, unit-based (ILGO-B) problems include the power for the VC/PAOS; the bleed air for the ECS; the ECS, the VC/PAOS, and FLS drag penalties; the VC/PAOS, the FLS, and ECS mass; and the ECS bleed port selection. This figure illustrates the decomposition of the system-level problem for aircraft synthesis/design into five separate but integral sub-problems.

Now, in order to define the optimization sub-problems for each of the five sub-systems, i.e. the PS, ECS, VC/PAOS, FLS and AFS, it is necessary to first subdivide the mission of Figure 4.1. and Table 4.1 into segments (phases or legs), which are shown in Table 4.3. Furthermore, given the relatively high fidelity of the simulations and the number and type of decision variables and constraints (see Tables 5.1 to 5.6), one can clearly see that one is confronted with a very complex, large-scale, mixed integer, non-linear optimization problem. The difficulties associated with solving this problem are exacerbated by the following:

- There is a need to iterate the engine simulation until proper convergence of the take-off weight is achieved.
- The engine simulation tool was not specifically written for optimization purposes. Each time a simulation is run, it is necessary to launch the program and read the necessary software licenses. This difficulty added to the previous item makes the take-off weight calculation (for any given values of the decision variables) very expensive computationally. The ECS, AFS, VC/PAOS, and FLS simulation codes do not have this drawback since they were developed in-house.
- The presence of both binary and discrete variables makes it necessary to use a heuristic approach: either a genetic algorithm or a simulated annealing optimization algorithm. There are no general gradient-based methods able to solve this mixed integer, non-linear programming (MINLP) problem. However, heuristic algorithms impose a significant time penalty in terms of solution time.

What follows in section 5.3. is the formulation of the unit-level and system-level, unit-based optimization problems for the five units considered, namely the PS, ECS, VC/PAOS, FLS, and AFS, along with a detailed description of their independent (decision) variables and a definition of their shadow prices.

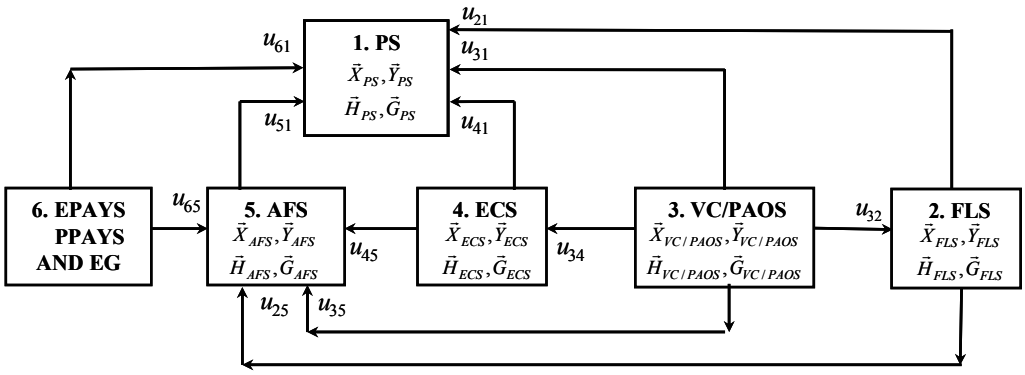

u_{15}	**Weight of the PS**
$\vec{u}_{21}$	**Momentum drag, FLS weight, power**
$\vec{u}_{25}$	**FLS weight**
$\vec{u}_{31}$	**Momentum drag, VC/PAOS weight, power**
$\vec{u}_{32}$	**Heat rejection**
$\vec{u}_{34}$	**Heat rejection**
$\vec{u}_{35}$	**VC/PAOS weight**
$\vec{u}_{41}$	**Momentum drag, ECS weight, bleed air**
$\vec{u}_{45}$	**ECS weight**
$\vec{u}_{51}$	**Drag, weight of the AFS**
$\vec{u}_{61}$	**PPAY, EPAY, EG weight**
$\vec{u}_{65}$	**PPAY, EPAY, EG weight**

Figure 5.1 Sub-systems and sub-system coupling functions.

5.3 ECS System-Level, Unit-Based Synthesis/Design Optimization Problem Definition

The synthesis/design and operational decision variables for the ECS are given in Tables 5.1a and 5.1b. The ranges of the decision variables are based on existing designs and on the work of Muñoz and von Spakovsky (1999, 2000a).

Figure 5.1 shows the coupling functions between the ECS and the PS (the bleed air mass flow, the ECS weight and drag), each of which demands additional thrust from the PS and in turn results in an increment in fuel consumption. This tight dependence shows the effects that the coupling functions have on the total fuel

consumption and, thus, on the system-level objective function. Figure 5.1 also shows the coupling function between the ECS and the VC/PAOS (the rate of heat transferred between the two sub-systems and the physical exergy of the bleed air at the bleed/PAO heat exchanger inlet). This coupling function as well affects the amount of fuel due to the ECS and the system-level objective. A measure of these effects is the shadow prices (equations (3.27) and (3.28) in *Chapter 3*) which shows the relative importance of the coupling functions in terms of the overall system-level objective. In ILGO-B, these shadow prices (λ's) are used to define the system-level, unit-based objective functions. The shadow prices for the coupling functions of the ECS for a given selection of bleed port, mission segment, and optimum fuel weight for the i^{th} segment are given by

$$\lambda_{\dot{m}Bleed_{ECS\,i}} = \frac{\partial W^*_{FUEL_{PS\,i}}}{\partial \dot{m}_{Bleed_{ECS\,i}}} \tag{5.16}$$

$$\lambda_{D_{ECS\,i}} = \frac{\partial W^*_{FUEL_{PS\,i}}}{\partial D_{ECS_i}} \tag{5.17}$$

$$\lambda_{W_{ECS-PS\,i}} = \frac{\partial W^*_{FUEL_{PS\,i}}}{\partial W_{ECS}} \tag{5.18}$$

$$\lambda_{\dot{Q}_{ECS\text{-}VC/PAOS\,i}} = \frac{\partial W^*_{FUEL_{VC/PAOS\,i}}}{\partial \dot{Q}_{ECS-VC/PAOS_i}} \tag{5.19}$$

and

$$\lambda_{W_{ECS-AFS\,i}} = \frac{\partial W^*_{FUEL_{AFS\,i}}}{\partial W_{ECS}} \tag{5.20}$$

where the $*$ indicates and optimal value and the weight of the fuel at the *ith* leg (see *Chapter 3*) is given by

$$W_{FUEL_i} = W_{TO}\left(1-\pi_i\right)\cdot \overset{i-1}{\underset{1}{\pi}} \tag{5.21}$$

and the fuel consumed due to the ECS can then be written as

$$W_{FUEL_{ECS}} = \sum_{i=1}^{n} \begin{pmatrix} \lambda_{\dot{m}\,Bleed_{ECS\,i}} \dot{m}_{Bleed_{ECS\,i}} + \lambda_{\dot{Q}_{ECS\text{-}VC/PAOS\,i}} \partial \dot{Q}_{ECS-VC/PAOS\,i} \\ + \lambda_{D_{ECS\,i}} D_{ECS\,i} + \lambda_{W_{ECS-PS\,i}} W_{ECS} + \lambda_{W_{ECS-AFS\,i}} W_{ECS} \end{pmatrix} \quad (5.22)$$

It has been assumed in equation (5.22) that the shadow prices are constant over the range of bleed mass flow and physical exergy and drag and weight of the ECS. This assumption is later probe in *Chapter 6*. Each term on the right of equation (5.22) can be written with respect to a reference fuel weight W^{o}_{FUEL} such that

Table 5.1a ECS synthesis/design decision variables and inequality constraints $\left(\vec{X}_{ECS}\right)$.

Component	Synthesis/design Decision Variable			Constraints
Primary and secondary heat exchangers	L_c	Cold side length (m)		$0.06<L_c<0.9$
	L_h	Hot side length (m)		$0.5<L_h<0.9$
	L_n	Non flow length (m)		$0.5<L_n<0.9$
Air cycle machine	PR_{cp}	Compressor design pressure ratio		$1.8<PR_{cp}<3.0$
	PR_{tb}	Turbine design pressure ratio		$PR_{tb}<12$
First and second regenerative heat exchangers	L_c	Cold side length (m)		$0.15<L_c<0.3$
	L_h	Hot side length (m)		$0.3<L_h<0.5$
	L_n	Non flow length (m)		$0.3<L_n<0.5$
	Reg_1 Reg_2	Existence-nonexistence of regenerative heat exchanger in configuration		$Reg_1, Reg_2=0,1$
				$Reg_1+Reg_2=1$
Ram air inlet, outlet	A_1, A_2	Areas of inlet, outlet (cm^2)		$120< A_1, A_2<220$
Primary and secondary heat exchanger fin type: hot and cold sides[46, 47]	Fin_{hot} Fin_{cold}	Fin No.	Surface designation[48]	Re_{max}
		1	¼(s)-11.1	8000
		2	1/8-15.2	6000
		3	1/8-13.95	6000
		4	1/8-15.61	6000
		5	1/8-19.86	5000
		6	1/9-22.68	5000
		7	1/9-25.01	4000
		8	1/9-24.12	4000
		9	1/10-27.03	4000
		10	1/10-19.35	4000

[46] Discrete variable.
[47] The plate thickness is 0.254 mm.
[48] See Kays and London (1998).

Table 5.1b ECS operational decision variables and inequality constraints $(\vec{Y}_{ECS})$.

	Operational Decision Variables		
Pressure regulating valve	PR_{vv}	Pressure setting	PR_{vv}<6.0
Low pressure bleed port	BP_{low}	Low pressure bleed port[49]	BP_{low}=0,1
High pressure bleed port	BP_{high}	High pressure bleed port[5]	BP_{high}=0,1
Splitter	m_{byp}	Bypass air flow rate	m_{byp}<0.2 kg/s
Bleed port	m_{hot}	Hot air flow rate	m_{hot}<0.2 kg/s
Regenerative heat exchanger	m_{creg}	Cold air flow rate	m_{creg}<0.2 kg/s
	Dependent variables		
Cold and hot sides heat exchangers	Re_c[50]	Reynolds number, cold air side	$R_{ec/}$ R_{emax} <1
	Re_h[6]	Reynolds number, hot air side	$R_{eh/}$ R_{emax} <1
Cabin and avionics	T_{cold}[6]	Cooling air temperature	$\|T_{cold}-T_{sched}\|$< 3
	P_{cold}[6]	Cooling air pressure	$P_{cold} = P_{sched}$
	m_{cold}[6]	Cooling air flow rate	$m_{cold} = m_{sched}$
ACM	W_{cp}, W_{tb}[6]	Compressor and turbine work	$W_{cp}=W_{tb}$

$$W_{FUEL_{\dot{m}Bleed_{ECS}}} = W^{o}_{FUEL} + \sum_{i=1}^{n}\left(\lambda_{\dot{m}Bleed_{ECS\,i}} \dot{m}_{Bleed_{ECS\,i}}\right) \tag{5.23}$$

$$W_{FUEL_{D_{ECS}}} = W^{o}_{FUEL} + \sum_{i=1}^{n}\left(\lambda_{D_{ECS\,i}} D_{ECS\,i}\right) \tag{5.24}$$

$$W_{FUEL_{\dot{Q}_{ECS-VC/PAOS}}} = W^{o}_{FUEL} + \sum_{i=1}^{n}\left(\lambda_{\dot{Q}_{ECS-VC/PAOS\,i}} \dot{Q}_{ECS-VC/PAOS_i}\right) \tag{5.25}$$

$$W_{FUEL_{W_{ECS-PS}}} = W^{o}_{FUEL} + \sum_{i=1}^{n}\left(\lambda_{W_{ECS-PS\,i}} W_{ECS}\right) \tag{5.26}$$

$$W_{FUEL_{W_{ECS-AFS}}} = W^{o}_{FUEL} + \sum_{i=1}^{n}\left(\lambda_{W_{ECS-AFS\,i}} W_{ECS}\right) \tag{5.27}$$

The reference fuel weight W^{o}_{FUEL} has been set to correspond to the case with no bleed air, ECS drag or weight, no heat rejection to the VC/PAOS, and no weight effects on the AFS.

[49] Binary variable: 0 means no bleed air is taken from the bleed port.
[50] This variable takes different values at different mission segments.

To obtain the impact of these factors on the system-level objective function such as, for example, the gross take-off weight, problem (5.1) is solved (i.e. iterated on W_{TO} until convergence is achieved) with the fuel weight values given by equations (5.23) to (5.27). Thus, the increase in the gross take-off weight due to the ECS coupling functions are given by

$$\Delta W_{TO\dot{m}Bleed_{ECS}} = W_{TO}(W_{FUEL\dot{m}Bleed_{ECS}}) - W_{TO}(W^{o}_{FUEL}) \tag{5.28}$$

$$\Delta W_{TOD_{ECS}} = W_{TO}(W_{FUELDecs}) - W_{TO}(W^{o}_{FUEL}) \tag{5.29}$$

$$\Delta W_{TO\dot{Q}_{ECS-VC/PAOS}} = W_{TO}(W_{FUEL\dot{Q}_{ECS-VC/PAOS}}) - W_{TO}(W^{o}_{FUEL}) \tag{5.30}$$

$$\Delta W_{TOW_{ECS-PS}} = W_{TO}(W_{FUELW_{ECS-PS}}) - W_{TO}(W^{o}_{FUEL}) \tag{5.31}$$

$$\Delta W_{TOW_{ECS-AFS}} = W_{TO}(W_{FUELW_{ECS-AFS}}) - W_{TO}(W^{o}_{FUEL}) \tag{5.32}$$

Note that both the bleed and drag have been represented in the above equations by the bleed air flow rate and drag force. In the case of bleed air, other options are to use instead energy, exergy or other thermodynamic properties. Drag can be represented as a force or a form of energy (i.e. propulsive power loss). The work of Muñoz and von Spakovsky (2000b) indicates that there is a mathematical advantage with the use of properties that make the shadow prices monotonic and, ideally, linear. In a different paper, the same authors (Muñoz and von Spakovsky, 2000a) found a linear relationship between fuel consumption and bleed air flow rate as well as between fuel consumption and drag force. Thus, these findings constitute a good choice for the properties to represent bleed and drag. In addition, there is an intrinsic practical advantage with the use of these two properties. The engine simulator can be easily adjusted to provide variable air flow rates at the high and low bleed ports. It is also easy to increase or decrease the necessary thrust according to the drag penalty created by the ECS.

One problem arising from the use of bleed air flow rate is the need for "matching" the bleed port temperatures and pressures in both sub-systems for all mission legs. The PS is designed with assumed values for the drag, bleed air flow rate, and weight of the ECS. If the overall system is optimized without decomposition, the values used by the PS and obtained from optimizing the ECS are identical. However, the iterative version of the decomposition approach used (ILGO) makes it necessary

in the ECS synthesis/design to use the temperature and pressure of the bleed port obtained from running the PS in the previous iteration. Therefore, it is necessary to check that in addition to flow rate, the bleed thermodynamic conditions are consistent. Although this potentially poses a problem in terms of convergence, the expected low variability of the bleed port conditions after a few iterations should render this problem insignificant.

With the above comments and taking into account that there is no external resource being used by the ECS, the system-level, unit-based synthesis/design optimization problem is set up as follows:

ECS System-Level, Unit-Based Fuel Consumption Problem

Minimize

$$\Delta W_{FUEL\,ECS} = \sum_{i=1}^{n} \left(\begin{array}{c} \lambda_{\dot{m}\,Bleed_{ECS\,i}} \dot{m}_{Bleed_{ECS\,i}} + \lambda_{\dot{Q}_{ECS-VC/PAOS\,i}} \dot{Q}_{ECS-VC/PAOS_i} \\ + \lambda_{D_{ECS\,i}} D_{ECS_i} + \lambda_{W_{ECS-PS\,i}} W_{ECS} + \lambda_{W_{ECS-AFS\,i}} W_{ECS} \end{array} \right) \quad (5.33)$$

w.r.t. $\left\{ \vec{X}_{ECS}, \vec{Y}_{ECS} \right\}$

subject to the inequality constraints given in Table 5.1 as well as

$$[P_{bleed}]_{PS} = [P_{bleed}]_{ECS} \;\; , \;\; [T_{bleed}]_{PS} = [T_{bleed}]_{ECS} \quad (5.34)$$

i.e. the bleed pressures and temperatures must match as well as the heat rejected to the VC/PAOS.

ECS System-Level, Unit-Based Gross Takeoff Weight Problem

Minimize $\Delta W_{TO\,ECS} = \Delta W_{TO\,\dot{m}\,Bleed\,ECS} + \Delta W_{TO\,D_{ECS}} + \Delta W_{TO\,\dot{Q}_{ECS-VC/PAOS}}$

$$+ \Delta W_{TO W_{ECS-PS}} + \Delta W_{TO W_{ECS-AFS}} \quad (5.35)$$

w.r.t. $\left\{ \vec{X}_{ECS}, \vec{Y}_{ECS} \right\}$

subject to the same constraints as problem (5.33).

5.4 VC/PAOS System-Level, Unit-Based Synthesis/Design Optimization Problem Definition

The only PS product being used directly by the VC/PAOS is the power required to drive the vapor compressor and the PAO loop pumps. This power and the VC /PAOS drag penalty also represent feedbacks to the PS as do the VC/PAOS weight. Each translates into excess thrust. The FLS cooling capacity is used as resource by the VC/PAOS. The VC/PAOS weight affects the AFS weight and demands fuel. Finally, an additional feedback is the bleed air physical exergy at the inlet of the bleed/PAO heat exchanger. All of these products and feedbacks form the basis for the coupling functions connecting the VC/PAOS with the other sub-systems.

Let us now define the shadow prices for these feedbacks (power taken from the PS) and products (VC/PAOS weight and drag, and heat rejection from the ECS) for different mission legs. The shadow prices based on the optimum fuel weight for a fixed leg are given by

$$\lambda_{\dot{E}_{VC/PAOS-PS\,i}} = \frac{\partial W^*_{FUEL_i}}{\partial \dot{E}_{VC/PAOS-PS}} \tag{5.36}$$

$$\lambda_{D_{VC/PAOS\,i}} = \frac{\partial W^*_{FUEL_i}}{\partial D_{VC/PAOS}} \tag{5.37}$$

$$\lambda_{W_{VC/PAOS-PS\,i}} = \frac{\partial W^*_{FUEL_i}}{\partial W_{VC/PAOS-PS}} \tag{5.38}$$

$$\lambda_{W_{VC/PAOS-AFS\,i}} = \frac{\partial W^*_{FUEL_i}}{\partial W_{VC/PAOS-AFS}} \tag{5.39}$$

$$\lambda_{\dot{Q}_{ECS-VC/PAOS\,i}} = \frac{\partial W^*_{FUEL_i}}{\partial \dot{Q}_{ECS-VC/PAOS_i}} \tag{5.40}$$

$$\lambda_{\dot{Q}_{FLS-VC/PAOS\,i}} = \frac{\partial W^*_{FUEL_i}}{\partial \dot{Q}_{FLS-VC/PAOS_i}} \tag{5.41}$$

where the weight of the fuel at the *ith* leg is given by equation (5.21) and the fuel consumed due to the VC/PAOS can then be written as

$$W_{FUEL_{vc/paos}} = \sum_{i=1}^{n} \begin{pmatrix} \lambda_{\dot{E}_{VC/PAOS-PS\,i}} \dot{E}_{VC/PAOS-PS\,i} + \lambda_{D_{VC/PAOS\,i}} D_{VC/PAOS\,i} \\ + \lambda_{W_{VC/PAOS-PS\,i}} W_{VC/PAOS} + \lambda_{\dot{Q}_{ECS-VC/PAOS\,i}} \dot{Q}_{ECS-VC/PAOS\,i} \\ + \lambda_{\dot{Q}_{FLS-VC/PAOS\,i}} \dot{Q}_{FLS-VC/PAOS\,i} + \lambda_{W_{VC/PAOS-AFS\,i}} W_{VC/PAOS} \end{pmatrix}$$

(5.42)

It has been assumed in equation (5.42) that the shadow prices are constant over the ranges of power, drag, weight, and rate of energy exchange of the VC / PAOS for a given mission leg. Equation (5.42) can be written, as was for the ECS, with respect to the reference fuel weight W^o_{FUEL}, i.e.

$$W_{FUEL\dot{E}_{VC/PAOS-PS}} = W^o_{FUEL} + \sum_{i=1}^{n} \left(\lambda_{\dot{E}_{VC/PAOS-PS\,i}} \dot{E}_{VC/PAOS-PS\,i} \right) \tag{5.43}$$

$$W_{FUEL D_{VC/PAOS}} = W^o_{FUEL} + \sum_{i=1}^{n} \left(\lambda_{D_{VC/PAOS\,i}} D_{VC/PAOS\,i} \right) \tag{5.44}$$

$$W_{FUEL W_{VC/PAOS-PS}} = W^o_{FUEL} + \sum_{i=1}^{n} \left(\lambda_{W_{VC/PAOS-PS\,i}} W_{VC/PAOS} \right) \tag{5.45}$$

$$W_{FUEL W_{VC/PAOS-AFS}} = W^o_{FUEL} + \sum_{i=1}^{n} \left(\lambda_{W_{VC/PAOS-AFS}} W_{VC/PAOS} \right) \tag{5.46}$$

$$W_{FUEL\dot{Q}_{ECS-VCPAOS}} = W^o_{FUEL} + \sum_{i=1}^{n} \left(\lambda_{\dot{Q}_{ECS-VC/PAOS\,i}} \dot{Q}_{ECS-VC/PAOS\,i} \right) \tag{5.47}$$

$$W_{FUEL\dot{Q}_{FLS-VC/PAOS}} = W^o_{FUEL} + \sum_{i=1}^{n} \left(\lambda_{\dot{Q}_{FLS-VC/PAOS\,i}} \dot{Q}_{FLS-VC/PAOS\,i} \right) \tag{5.48}$$

where the reference fuel weight W^o_{FUEL} has been set to correspond to the case with no power extraction, no VC/PAOS drag or weight, and no energy transfer from or toward any other sub-system.

To obtain the impact of these factors on the system-level objective function such as, for example, the gross take-off weight, problem (5.1) is solved (i.e. iterated on W_{TO} until convergence is achieved) with the fuel weight values given by equations (5.43) to (5.48). Thus, the increase in the gross take-off weight due to the VC/PAOS products and feedback are given by

$$\Delta W_{TO\dot{E}_{VC/PAOS-PS}} = W_{TO}(W_{FUEL\dot{E}_{VC/PAOS-PS}}) - W_{TO}(W^{o}_{FUEL}) \quad (5.49)$$

$$\Delta W_{TOD_{VC/PAOS}} = W_{TO}(W_{FUELD_{VC/PAOS}}) - W_{TO}(W^{o}_{FUEL}) \quad (5.50)$$

$$\Delta W_{TOW_{VC/PAOS-PS}} = W_{TO}(W_{FUELW_{VC/PAOS-PS}}) - W_{TO}(W^{o}_{FUEL}) \quad (5.51)$$

$$\Delta W_{TOW_{VC/PAOS-AFS}} = W_{TO}(W_{FUELW_{VC/PAOS-AFS}}) - W_{TO}(W^{o}_{FUEL}) \quad (5.52)$$

$$\Delta W_{TO\dot{Q}_{FLS-VC/PAOS}} = W_{TO}(W_{FUEL\dot{Q}_{FLS-VC/PAOS}}) - W_{TO}(W^{o}_{FUEL}) \quad (5.53)$$

$$\Delta W_{TO\dot{Q}_{ECS-VC/PAOS}} = W_{TO}(W_{FUEL\dot{Q}_{ECS-PAOS}}) - W_{TO}(W^{o}_{FUEL}) \quad (5.54)$$

With the above comments and taking into account that there are additional feedbacks and products being used by the VC/PAOS, the system-level, unit-based synthesis/design optimization problem is set up as follows:

VC/PAOS System-Level, Unit-Based Fuel Consumption Optimization problem

Minimize

$$\Delta W_{FUEL_{VC/PAOS}} = \sum_{i=1}^{n} \begin{pmatrix} \lambda_{\dot{E}_{VC/PAOS-PS\,i}} \dot{E}_{VC/PAOS-PS\,i} + \lambda_{D_{VC/PAOS\,i}} D_{VC/PAOS\,i} \\ + \lambda_{W_{VC/PAOS-PS\,i}} W_{VC/PAOS} + \lambda_{\dot{Q}_{ECS-VC/PAOS\,i}} \dot{Q}_{ECS-VC/PAOS\,i} \\ + \lambda_{\dot{Q}_{FLS-VC/PAOS\,i}} \dot{Q}_{FLS-VC/PAOS\,i} + \lambda_{W_{VC/PAOS-AFS\,i}} W_{VC/PAOS} \end{pmatrix} \quad (5.55)$$

w.r.t. $\left\{\vec{X}_{VC/PAOS}, \vec{Y}_{VC/PAOS}\right\}$

subject to the inequality constraints given in Table 5.2. below as well as the equality constraints of the VC/PAOS model.

VC/PAOS System-Level, Unit-Based Gross Take-off Weight Optimization Problem

Minimize

$$\Delta W_{TO_{vc/paos}} = \begin{pmatrix} \Delta W_{TO\dot{E}_{VC/PAOS-PS}} + \Delta W_{TOD_{VC/PAOS}} + \Delta W_{TOW_{VC/PAOS-PS}} \\ + \Delta W_{TOW_{VC/PAOS-AFS}} + \Delta W_{TO\dot{Q}_{FLS-VC/PAOS}} + \Delta W_{TO\dot{Q}_{ECS-VC/PAOS}} \end{pmatrix} \quad (5.56)$$

w.r.t. $\left\{\vec{X}_{VC/PAOS}, \vec{Y}_{VC/PAOS}\right\}$, subject to the same constraints as in problem (5.55).

From Muñoz and von Spakovsky (1999), the shadow prices in equation (5.37) and equation (5.38) are correctly considered as constant for a given mission segment, since they are of the same nature as their counterparts in the ECS. However, the assumption that the shadow prices for the power exchange and energy exchange with other sub-systems are constant must be proved. In the same manner, the shadow price for the AFS due to the VC/PAOS weight must be determined.

The proofs are given in *Chapter 6.* To this end, the effect of power extraction and energy exchange variations on total fuel consumption for a turbofan engine were studied. As mentioned before, an engine deck from one of our industrial partners, which dynamically simulates the real performance characteristics of an aircraft engine, was used[51]. The model of an F-109 turbofan engine to perform the calculations was employed. The effect of the VC/PAOS weight on total fuel due to the AFS was determined using the detailed AFS model developed for this project.

The functions that describe the shadow prices of extracted power, energy exchange, and weight are dependent on flight conditions and on the aerodynamic and thermodynamic behavior of the main engine of a particular aircraft. When the shadow prices are calculated on a unit price basis, i.e. in terms of mass flow rates of fuel, they can be seen as the penalties that a given sub-system imposes on the overall aircraft system. The synthesis/design and operational decision variables for the VC/PAOS are given in Table 5.2. The ranges of the decision variables are based on existing designs and on the work of Hudson (1986).

[51] Note that industrial engine decks such as the one we have employed use values from average engines and employ a number of simplifying assumptions and, therefore, fail to capture all the important factors involved.

Table 5.2 VC/PAOS decision variables, fixed parameters, and inequality constraints.

Component	Decision variable			Constraints
	Design Variables $\left(\vec{X}_{VC/PAOS}\right)$			
Bleed air / PAO heat exchanger	L_c	Cold-side length (m)		$0.05<L_c<0.9$
	L_h	Hot-side length (m)		$0.1<L_h<0.9$
	L_n	Non-flow length (m)		$0.1<L_n<0.9$
Condenser	L_c	Cold-side length (m)		$0.05<L_c<0.9$
	L_h	Hot-side length (m)		$0.1<L_h<0.9$
	L_n	Non-flow length (m)		$0.1<L_n<0.9$
Evaporator	L_c	Cold-side length (m)		$0.05<L_c<0.9$
	L_h	Hot-side length (m)		$0.1<L_h<0.9$
	L_n	Non-flow length (m)		$0.1<L_n<0.9$
Ram air / hot PAO heat exchanger	L_c	Cold-side length (m)		$0.05<L_c<0.9$
	L_h	Hot-side length (m)		$0.1<L_h<0.9$
	L_n	Non-flow length (m)		$0.1<L_n<0.9$
Heat exchangers fin type: hot and cold sides[52, 53]	Fin_{hot} Fin_{cold}	Fin No.	Surface designation[54]	R_{emax}
		1	¼(s)-11.1	8000
		2	1/8-15.2	6000
		3	1/8-13.95	6000
		4	1/8-15.61	6000
		5	1/8-19.86	5000
		6	1/9-22.68	5000
		7	1/9-25.01	4000
		8	1/9-24.12	4000
		9	1/10-27.03	4000
		10	1/10-19.35	4000
	Operational Variables $\left(\vec{Y}_{VC/PAOS}\right)$			
Vapor Compressor	$PR_{v\text{-}comp}$	Pressure ratio vapor Compressor		$1<Pr<9$
	m_{vap}	Vapor mass flow(kg/s)		$0.2<m_v<2.2$
Hot PAO cycle	m_{Hpao}	Hot PAO loop mass flow		$0.2<m_{HPAO}<3.5$
	V_5	Fuel / hot PAO heat exchanger bypass valve position		$0<V_5<0.3$
	V_4	Bleed Air / hot PAO heat exchanger bypass valve position		$0<V_4<0.3$
	V_2	Vapor / hot PAO heat exchanger bypass valve position		$0<V_2<0.3$
	Synthesis Variables $\left(\vec{X}_{VC/PAOS}\right)$			
Ram air / hot PAO heat exchanger	*onoff*	Existence or not of the ram air/hot PAO heat exchanger		0 or 1
	Fixed Parameter			
Ram Air Inlet	A_i	Area of inlet, outlet (cm^2)		From the ECS optimization problem
Bleed/hot PAO heat exchanger inlet	$T_{bi,}$	Bleed air inlet temperature (K)		
	m_{bi}	Bleed air inlet mass flow (k/s)		

[52] Discrete variable.
[53] The plate thickness is 0.254 mm.
[54] See Kays and London (1998).

5.5. FLS System-Level, Unit-Based Synthesis/Design Optimization Problem Definition

The only PS product being used directly by the FLS is the power extracted to drive the fuel pump. This power and the FLS drag penalty also represent feedbacks to the PS as do the FLS weight. Each translates into excess thrust. The VC/PAOS heat rejection represents an additional feedback. The two sub-systems being optimized, the FLS and VC/PAOS, make use of the same source for extracted power (i.e. the PS). The shadow price for extracted power ($\lambda_{\dot{E}_{VC/PAOS-PS}}$) appearing in the VC/PAOS optimization problem definition is the same for the FLS. Moreover, the penalties produced by the drag and weight due to the FLS and VC/PAOS are of the same nature as those produced by the ECS. Therefore, the ECS shadow prices due to drag and weight (λ_D *and* λ_W) can be used for the FLS synthesis/design optimization. The effects of the FLS on the AFS are of the same nature as those produced by the ECS and the VC/PAOS. Thus, the corresponding shadow price is used.

Let us now define the shadow prices of the coupling functions (products and feedbacks) for different mission legs. The shadow prices based on the optimum fuel weight for a fixed i^{th} leg are given by

$$\lambda_{\dot{E}_{FLS-PS}i} = \frac{\partial W^*_{FUEL_i}}{\partial \dot{E}_{FLS-PS}} \tag{5.57}$$

$$\lambda_{D_{FLS}i} = \frac{\partial W^*_{FUEL_i}}{\partial D_{FLS}} \tag{5.58}$$

$$\lambda_{W_{FLS-PS}i} = \frac{\partial W^*_{FUEL_i}}{\partial W_{FLS-PS}} \tag{5.59}$$

$$\lambda_{W_{FLS-AFS}i} = \frac{\partial W^*_{FUEL_i}}{\partial W_{FLS-AFS}} \tag{5.60}$$

where as before the weight of the fuel at the i^{th} leg is given by equation (5.21) and the fuel consumed due to the FLS can then be written as

$$W_{FUEL_{FLS}} = \sum_{i=1}^{n}\left(\lambda_{\dot{E}_{FLS\_PS}i}\dot{E}_{FLS-PS_i} + \lambda_{D_{FLS}i}D_{FLS_i} + \lambda_{W_{FLS\_PS}i}W_{FLS} + \lambda_{W_{FLS\_PS}i}W_{FLS}\right) \tag{5.61}$$

As before it is assumed in equation (5.61) that the shadow prices are constant over the ranges of power, drag, weight, and rate of energy exchange of the FLS. As was done for the ECS and VC/PAOS, equation (5.61) can be written with respect to the reference fuel weight W^o_{FUEL}, i.e.

$$W_{FUEL\,\dot{E}_{FLS-PS}} = W^o_{FUEL} + \sum_{i=1}^{n}\left(\lambda_{\dot{E}_{FLS-PS\,i}}\dot{E}_{FLS-PS\,i}\right) \tag{5.62}$$

$$W_{FUEL\,D_{FLS}} = W^o_{FUEL} + \sum_{i=1}^{n}\left(\lambda_{D_{FLS\,i}}D_{FLS\,i}\right) \tag{5.63}$$

$$W_{FUEL\,W_{FLS-PS}} = W^o_{FUEL} + \sum_{i=1}^{n}\left(\lambda_{W_{FLS-PS\,i}}W_{FLS}\right) \tag{5.64}$$

$$W_{FUEL\,W_{FLS-AFS}} = W^o_{FUEL} + \sum_{i=1}^{n}\left(\lambda_{W_{FLS-AFS\,i}}W_{FLS}\right) \tag{5.65}$$

where the reference fuel weight W^o_{FUEL} has been set to correspond to the case with no power extraction, FLS drag or weight and no energy transfer from or toward any other sub-system.

To obtain the impact of these factors on the system-level objective function such as, for example, the gross take-off weight, problem (5.1) is solved (i.e. iterated on W_{TO} until convergence is achieved) with the fuel weight values given by equations (5.62) to (5.65). Thus, the increase in the gross take-off weight due to the FLS products and feedback are given by

$$\Delta W_{TO\,\dot{E}_{FLS-PS}} = W_{TO}(W_{FUEL\,\dot{E}_{FLS-PS}}) - W_{TO}(W^o_{FUEL}) \tag{5.66}$$

$$\Delta W_{TO\,D_{FLS}} = W_{TO}(W_{FUEL\,D_{FLS}}) - W_{TO}(W^o_{FUEL}) \tag{5.67}$$

$$\Delta W_{TO\,W_{FLS-PS}} = W_{TO}(W_{FUEL\,W_{FLS-PS}}) - W_{TO}(W^o_{FUEL}) \tag{5.68}$$

and

$$\Delta W_{TO\,W_{FLS-AFS}} = W_{TO}(W_{FUEL\,W_{FLS-AFS}}) - W_{TO}(W^o_{FUEL}) \tag{5.69}$$

The linear behavior of the power extraction, drag and weight marginal cost has already been proven. With the above comments and taking into account the additional feedback being used by the FLS, the system-level unit-based synthesis/design optimization problem is set up as follows:

Table 5.3 FLS decision variables, fixed parameters, and inequality constraints.

Component	Decision variable			Constraints
	Design Variables $\left(\vec{X}_{FLS}\right)$			
Fuel / Oil heat exchanger	L_c	Cold-side length (m)		$0.05<L_c<0.9$
	L_h	Hot-side length (m)		$0.1<L_h<0.9$
	L_n	Non-flow length (m)		$0.1<L_n<0.9$
Fuel / PAO Heat Exchanger	L_c	Cold-side length (m)		$0.05<L_c<0.9$
	L_h	Hot-side length (m)		$0.1<L_h<0.9$
	L_n	Non-flow length (m)		$0.1<L_n<0.9$
Fuel / Ram air heat exchanger	L_c	Cold-side length (m)		$0.05<L_c<0.9$
	L_h	Hot-side length (m)		$0.1<L_h<0.9$
	L_n	Non-flow length (m)		$0.1<L_n<0.9$
Fuel / hydraulic heat exchanger	L_c	Cold-side length (m)		$0.05<L_c<0.9$
	L_h	Hot-side length (m)		$0.1<L_h<0.9$
	L_n	Non-flow length (m)		$0.1<L_n<0.9$
Ram Air Inlet	A_i	Area of inlet, outlet (cm^2)		$50<A_i<290$
Heat exchangers fin type: hot and cold sides[55, 56]	Fin_{hot} Fin_{cold}	Fin No.	Surface designation[57]	Re_{max}
		1	¼(s)-11.1	8000
		2	1/8-15.2	6000
		3	1/8-13.95	6000
		4	1/8-15.61	6000
		5	1/8-19.86	5000
		6	1/9-22.68	5000
		7	1/9-25.01	4000
		8	1/9-24.12	4000
		9	1/10-27.03	4000
		10	1/10-19.35	4000
	Operational Variables $\left(\vec{Y}_{FLS}\right)$			
Oil/fuel HX	mO	Oil mass flow (kg/s)		0< mf <4
Hyd/fuel HX	mH	Hyd mass flow (kg/s)		0< mf <4
Ram air HX	mf	Fuel mass flow (kg/s)		0< mf <2
	Fixed Parameter			
Fuel Tank Initial Temp.	T_{Ti}	Fuel tank initial temperature (K)		*300*

FLS System-Level, Unit-Based Fuel Consumption Optimization Problem

Minimize

$$\Delta W_{FUEL\,FLS} = \sum_{i=1}^{n}\left(\lambda_{\dot{E}_{FLS-PS\,i}}\dot{E}_{FLS-PS\,i} + \lambda_{D_{FLS\,i}}D_{FLS\,i} + \lambda_{W_{FLS-PS\,i}}W_{FLS} + \lambda_{W_{FLS-AFS\,i}}W_{FLS}\right) \tag{5.70}$$

w.r.t. $\left\{\vec{X}_{FLS}, \vec{Y}_{FLS}\right\}$

subject to the constraints given in Table 5.3 as well as

$$\left[\dot{Q}_{FLS}\right]_{VC/PAOS} = \left[\dot{Q}_{VC/PAOS}\right]_{FLS} \tag{5.71}$$

[55] Discrete variable.
[56] The plate thickness is 0.254 mm.
[57] See Kays and London (1998).

FLS System-Level, Unit-Based Gross Takeoff Weight Optimization Problem

$$\text{Minimize} \quad \Delta W_{TO\,FLS} = \left(\Delta W_{TO\dot{E}_{FLS-PS}} + \Delta W_{TOD_{FLS}} + \Delta W_{TOW_{FLS-PS}} + \Delta W_{TOW_{FLS-AFS}}\right) \tag{5.72}$$

w.r.t. $\left\{\vec{X}_{FLS}, \vec{Y}_{FLS}\right\}$, Subject to the same constraints as problem (5.70).

5.6 AFS System-Level, Unit-Based Synthesis/Design Optimization Problem Definition

The energy balance for the advanced tactical aircraft developed in *Chapter 4* shows how the thrust produced by the PS is used both to overcome the AFS drag and to generate the required lift force. Thus, any change in the AFS drag and weight will produce a change in the required thrust and therefore, a change in mission fuel consumption. The AFS and the PS are mutually dependent, since any change in the mission fuel consumption will produce a change in the take-off gross weight, which in turn will affect the AFS optimal shape and weight. The ECS, the FLS, and the VC/PAOS are not directly (although indirectly they are) affected by any change in the AFS. The penalties produced by changes in the AFS drag and weight are of the same nature as those produce by the ECS. Therefore, the ECS shadow prices due to drag and weight (λ_{D} *and* λ_{W}) can be used for the FLS synthesis/design optimization.

Let us now define the shadow prices for the coupling functions (products and feedbacks) for different mission legs. The shadow prices based on the optimum fuel weight for a fixed i^{th} leg are given by

$$\lambda_{D_{AFS}\,i} = \frac{\partial W^{*}_{FUEL_i}}{\partial D_{AFS_i}} \tag{5.73}$$

$$\lambda_{W_{AFS}\,i} = \frac{\partial W^{*}_{FUEL_i}}{\partial W_{AFS}} \tag{5.74}$$

where as before the weight of the fuel at the i^{th} leg is given by equation (5.21) and the fuel consumed due to the AFS can then be written as

$$W_{FUEL_{AFS}} = W^{o}_{FUEL} + \sum_{i=1}^{n}\left(\lambda_{D_{AFS}\,i}\Delta D_{AFS\,i} + \lambda_{W_{AFS}\,i}\Delta W_{AFS}\right) \tag{5.75}$$

where the reference fuel weight W^{o}_{FUEL} has been set to correspond to a reference value of AFS weight and drag and where

$$\Delta D_{AFS\,i} = D_{AFS\,i} - D^{\circ}{}_{AFS\,i} \tag{5.76.1}$$

$$\Delta W_{AFS} = W_{AFS} - W^{\circ}{}_{AFS} \tag{5.76.2}$$

Here the subscript *o* refers to the optimum coupling function value obtained in the previous optimization iteration.

As before it is assumed in equation (5.75) that the shadow prices are constant over the ranges of the AFS drag and weight. As was done for the ECS and VC/PAOS, equation (5.76) can be written with respect to the reference fuel weight W^{o}_{FUEL}, i.e.

$$W_{FUEL D_{AFS}} = W^{o}_{FUEL} + \sum_{i=1}^{n} \left(\lambda_{\ D_{AFS}\,i} \Delta D_{AFS_i} \right) \tag{5.77}$$

$$W_{FUEL W_{AFS}} = W^{o}_{FUEL} + \sum_{i=1}^{n} \left(\lambda_{\ W_{AFS}\,i} \Delta W_{AFS} \right) \tag{5.78}$$

Table 5.4 AFS decision variables, fixed parameters, and inequality constraints.

Component	Decision variable[58]		Constraints
	Design Variables $\left(\bar{X}_{AFS}\right)$		
Wing	*WT*	Wing Type	Delta/Trap
	AR	Wing aspect ratio	2.1< *AR* <4
	t/c	Wing thickness ratio	0.06< *t/c*<*0.15*
	λ	Wing taper ratio	0<λ<1
	Λ	Wing sweep angle (degrees)	25<Λ<45
	S_f/S_{ref}	Flapped area to reference area ratio	0.2< S_f/S_{ref} <*0.95*
	C_L *design*	Design lift coefficient	0.3< C_L <0.8
Tail	*T_AR*	Tail aspect ratio	3.5<T_ *AR* <6.5
	T_t/c	Tail thickness ratio	0.06<T_ *t/c*<*0.25*
	*T_*λ	Tail taper ratio	0<T_λ<1
	Fixed Parameter		
AFS	*l/d*	Fuselage fineness ratio	7
	E_{wd}	Supersonic wave drag empirical factor	2
	δ	Flaps hinge line angles	10 and 39
	S_f/S_{ref}	Exposed area to reference area ratio	0.75
	Derived variables		
Air Frame	W_{to}/S_{ref}	Gross take-off weight to reference surface ratio	
	T_{sl}/S_{ref}	sea-level thrust to reference surface ratio	

[58] No Operational decision variables $\left(\bar{Y}_{FLS}\right)$ are defined for the AFS.

To obtain the impact of these factors on the system-level objective function, for example, the gross take-off weight, problem (5.1) is solved (i.e. iterated on W_{TO} until convergence is achieved) with the fuel weight values given by equations (5.77) to (5.78). Thus, the increase in the gross take-off weight due to the AFS products and feedback are given by

$$\Delta W_{TO\,\Delta D_{AFS}} = W_{TO}(W_{FUEL\,D_{AFS}}) - W_{TO}(W^{o}_{FUEL}) \tag{5.79}$$

and

$$\Delta W_{TO\Delta W_{AFS}} = W_{TO}(W_{FUEL\,W_{AFS}}) - W_{TO}(W^{o}_{FUEL}) \tag{5.80}$$

The linear behavior of the power extraction, drag, and weight shadow prices has already been proven. The only assumption that has been necessary so far is the linearity of the VC/PAOS energy transfer shadow prices, which will be proven in *Chapter 6*. With the above comments and taking into account the additional feedback being used by the FLS, the system-level, unit-based synthesis/design optimization problem is set up as follows:

AFS System-Level, Unit-Based Fuel Consumption Optimization problem

Minimize

$$\Delta W_{FUEL\,AFS} = \sum_{i=1}^{n}\left(\lambda_{\,D_{AFS}\,i}\Delta D_{AFS\,i} + \lambda_{\,W_{AFS}\,i}\Delta W_{AFS}\right) \tag{5.81}$$

w.r.t. $\left\{\vec{X}_{FLS}, \vec{Y}_{FLS}\right\}$

subject to the constraints given in Table 5.4 as well as the equality constraints of the AFS model, which include the flight dynamics equation for the entire aircraft system i.e.

$$T_i = \alpha T_{SL} = q_i S\left[K_1\left(\frac{n_i}{q_i}\frac{\beta_i W_{TO}}{S}\right)^2 + C_{D_0} + \frac{D_{ECS_i} + D_{TMS_i}}{q_i S}\right] + \frac{\beta_i W_{TO}}{V_i}\frac{d}{dt}\left(h_i + \frac{V_i^2}{2g}\right) \tag{5.82}$$

AFS System-Level, Unit-Based Gross Take-off Weight Optimization Problem

$$\text{Minimize} \quad \Delta W_{TO\,FLS} = \left(\Delta W_{TO\,\Delta D_{AFS}} + \Delta W_{TO\Delta W_{AFS}}\right) \tag{5.83}$$

w.r.t. $\left\{\vec{X}_{FLS}, \vec{\mathrm{Y}}_{FLS}\right\}$

subject to the same constraints as problem (5.81).

5.7 PS Unit-Level Design Optimization Problem Definition

The following types were selected for several of the PS components:

- Inlet: 2D external compression
- Nozzle: 2D convergent-divergent
- Combustor: single-dome
- Mixer: Forced mechanical mixer

The fan and high-pressure compressor are designed with constant tip radius. Both of these components have inlet guide vanes (variable in the case of the high pressure compressor (HPC)). The high-pressure turbine (HPT) and the low-pressure turbine (LPT) have constant mean and tip radii, respectively. They use metallic blades. In addition, some important geometric, thermodynamic and aerodynamic decision variables held fixed during the optimization for the rotating turbo-machinery are given in Table 5.5. The decision variables and inequality constraints are given in Table 5.6.

Table 5.5 Some important thermodynamic, geometric, and aerodynamic parameter values for the PS optimization.

Parameter	fan	HPC	Parameter	HPT	LPT
$Mach_{in}$	0.50	0.45	$Mach_{in}$	0.20	0.17
$Mach_{exit}$	0.50	0.45	$Mach_{exit}$	0.30	0.32
Max. 1st stage PR	1.80	1.40	Ratio of exit to entrance radius	1.20	1.00
Hub to tip ratio	0.40	0.46	Blade solidity	0.71	1.22
Blade solidity	1.10	0.84	Blade thickness ratio	0.20	0.20
Blade thickness ratio	0.10	0.08	1st stage aspect ratio	1.20	1.20
1st stage aspect ratio	2.00	1.00	Last stage aspect ratio	1.80	1.80
Last stage aspect ratio	1.50	1.00	Blade taper ratio	1.00	1.00
Blade taper ratio	0.556	0.83	Stator solidity	0.92	1.11
Stator solidity	0.80	0.75	Isentropic efficiency	0.90	0.90
Polytrophic efficiency Hub Tip	 0.89 0.88	0.88	Turbine loading parameter	0.35	0.30

The number of stages for the fan and HPC are calculated by the engine sizing code (WATE) based on the design pressure ratio. The HPT and LPT have one stage

each. As to the coupling functions between the PS and ECS and the PS and TMS, have already been described in the previous section. Thus, the definition of the PS unit-level design optimization problem[59] is as follows:

Table 5.6 PS decision variables and inequality constraints.

Component	Design Decision Variables $(\vec{X}_{PS})$		Constraints
Fan	α	Fan bypass ratio	$0.3 \le \alpha \le 0.6$
	PR_{fan}	Fan design pressure ratio (tip and hub)	$3.0 \le PR_{fan} \le 5.0$
Compressor	PR_{hpc}	High pressure compressor design pressure ratio	$4.0 \le PR_{hpc} \le 8.0$
Turbine	PR_{hpt}	High pressure turbine design pressure ratio	$1.8 \le PR_{hpt} \le 3.0$
	PR_{lpt}	Low pressure turbine design pressure ratio	$1.8 \le PR_{lpt} \le 3.0$
	Operational Decision Variables $(\vec{Y}_{PS})$		
Compressor	BP_{low}	Low pressure bleed port[60]	$BP_{low}=0,1$
	BP_{high}	High pressure bleed port	$BP_{high}=0,1$
Turbine	T_{it}	Turbine inlet temperature	$T_{it} \le 1778$ K
	Dependent Variables		
Afterburner	T_{aft}	Afterburner temperature[61]	$T_{aft} \le 2000$ K
Fan	φ_{hub}	Fan (hub) % stall margin[8]	$\varphi_{hub} > 10$
	φ_{tip}	Fan (tip) % stall margin[8]	$\varphi_{tip} > 10$
Fan and compressor	PR_{cp}	Overall pressure ratio	$17.0 \le PR_{cp} \le 32.0$
Compressor	φ_{hpc}	Compressor % stall margin[8]	$\varphi_{hpc} > 10$
	N/A	Bleed port selection[8]	$BP_{low}+BP_{high}=1$

PS Unit-Level Gross Takeoff Weight Problem

Minimize

$$W_{TO} = w_{AFS}(W_{TO}) + W_{EGS} + W_{PS} + W_{ECS} + W_{TMS} + W_{FUEL} + W_{PPAY} + W_{EPAY} \tag{5.84}$$

w.r.t. $\{\vec{X}_{PS}, \vec{Y}_{PS}\}$

[59] Note that a unit-level as opposed to a system-level, unit-based optimization problem is defined here since ILGO-A instead of ILGO-B is applied to the PS.
[60] Binary variable: 0 means no bleed air is taken from the bleed port.
[61] This variable takes different values at different mission segments.

subject to the inequality constraints of Table 5.6. and the equality constraints of the PS and AFS models the latter of which include the flight dynamics equation for the entire aircraft system, i.e.

$$T_i = \alpha T_{SL} = q_i S\left[K_1\left(\frac{n_i}{q_i}\frac{\beta_i W_{TO}}{S}\right)^2 + C_{D_0} + \frac{D_{ECS_i} + D_{TMS_i}}{q_i S}\right] + \frac{\beta_i W_{TO}}{V_i}\frac{d}{dt}\left(h_i + \frac{V_i^2}{2g}\right) \tag{5.85}$$

Furthermore, note that for this unit-level optimization problem (as opposed to the system-level optimization, problem (5.1)), W_{ECS}, W_{TMS} and W_{AFS} are held constant, i.e.

$$W_{ECS} - W_{ECS}^o = 0 \tag{5.86a}$$

$$W_{AFS} - W_{AFS}^o = 0 \tag{5.86b}$$

$$W_{VC/PAO} - W_{VC/PAOS}^o = 0 \tag{5.86c}$$

$$W_{FLS} - W_{FLS}^o = 0 \tag{5.86d}$$

In addition, the following constraints are also imposed:

$$\dot{m}_{bleed\,i} - \dot{m}_{bleed\,i}^o = 0 \tag{5.86e}$$

$$Port_{Bleed\,low_i} - Port^o{}_{Bleed\,low_i} = 0 \tag{5.86f}$$

$$Port_{Bleed\,high_i} - Port^o{}_{Bleed\,high_i} = 0 \tag{5.86g}$$

$$\dot{E}_{FLS-PS_i} - \dot{E}^o{}_{FLS-PS_i} = 0 \tag{5.86h}$$

$$\dot{E}_{VC/PAOS-PS_i} - \dot{E}^o{}_{VC/PAOS-PS_i} = 0 \tag{5.86i}$$

$$D_{AFS} - D_{AFS}^o = 0 \tag{5.86j}$$

$$D_{FLS} - D_{FLS}^o = 0 \tag{5.86k}$$

$$D_{VC/PAOS} - D_{VC/PAOS}^o = 0 \tag{5.86l}$$

$$D_{ECS} - D_{ECS}^o = 0 \tag{5.86m}$$

Constraints (5.86a) through (5.86b) indicate that the weight and drag of the ECS and TMS, the bleed air flow rate, the bleed port from which it is taken, the pressure and temperature of the bleed, the power extracted by the TMS, and the drag of the AFS are set equal to the values indicated with the superscript $_0$. These values are set externally. In addition, the necessary initial estimates of the weight fractions β_i in equation (5.86) are given by Nicolai (1975) or Mattingly, Heiser, and Daley (1987).

PS Unit-Level Fuel Optimization Problem

$$\text{Minimize} \qquad W_{FUEL} = w_{fuel}(W_{TO}, \vec{X}_{PS}, \vec{Y}_{PS,} mission) \tag{5.87}$$

w.r.t. $\left\{\vec{X}_{PS}, \vec{Y}_{PS}\right\}$

subject to the same constraints as in problem (5.85)

5.8 Solution Approach Using ILGO

The implementation of ILGO-A for the PS and ILGO-B for the ECS, AFS, VC/PAOS, and FLS requires the following steps:

1. The first step is to optimally design the PS at the unit-level (i.e. perform problem (5.85)) for an initial estimate of the necessary amount of bleed air, ECS drag and weight, power extraction, FLS and VC/PAOS drag and weight, and AFS drag and weight. Since no information about the ECS and TMS exists at this stage of the synthesis design process, estimates are used based on Muñoz and von Spakovsky (2000a) and Figliola (1997). Initial values of the amount of bleed air, power extraction, FLS, VC/PAOS and ECS drag and weight are estimated from theses references. Initial values for the AFS weight and are taken from Mattingly, Heiser, and Daley (1987) and Raymer (2000).
2. After completing the PS unit-level optimal design, the bleed port thermodynamic conditions are calculated at all operating conditions (mission segments). The fuel-based shadow prices for each of the mission legs are calculated as well in this step. The entire modeling/optimization process for the PS design optimization is depicted in Figure 5.2.
3. The bleed air temperature and pressure values for each of the mission legs along with the shadow prices are used to carry out the system-level, unit-based synthesis/design optimization of the ECS (Problem (5.35)). Based on the previous work of Muñoz and von Spakovsky (2000a) and what was presented in *Chapter 3*,

the shadow prices are assumed constant over the synthesis/design space, which allows the coupling function take arbitrarily large or small values. To begin the solution of problem (5.1), the bleed pressure and temperature maps presented by Muñoz and von Spakovsky (1999) are used. The initial coupling functions from the VC/PAOS required for the ECS to be optimally synthesized/designed are estimated based on Hudson (1975) and Figliola (1997). The total number of decision variables is 109. Given the large number of variables for the ECS problem and the fact that four of them are integer for the ECS problem, time decomposition is used in the manner described in Muñoz and von Spakovsky

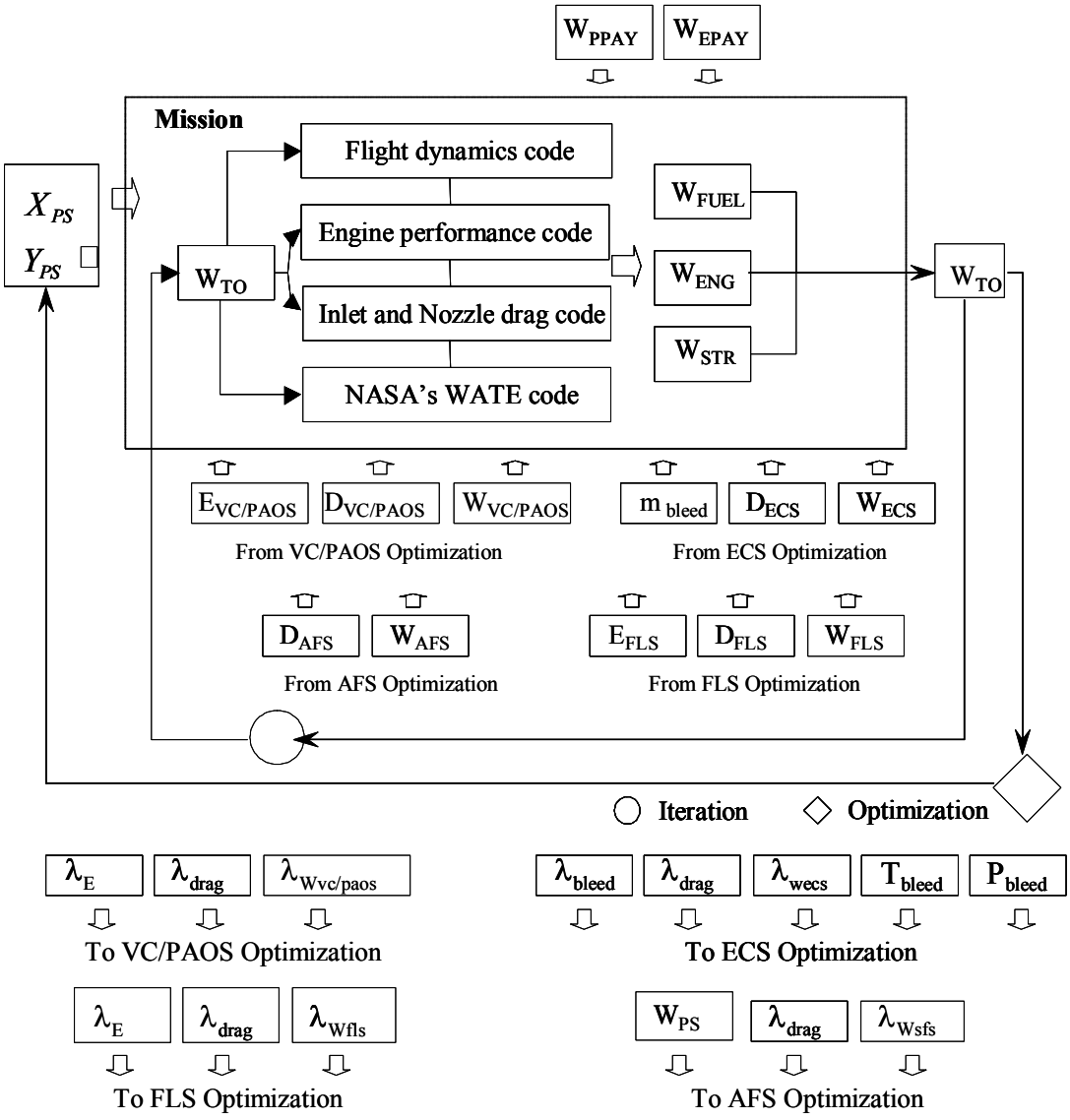

Figure 5.2 The PS unit-level modeling and optimization procedure.

(2000b) and in *Chapter 3*. The work of Muñoz and von Spakovsky (1999) shows that the most demanding operating condition for the ECS corresponds to the mission segment with high altitude and subsonic speed. This point is critical because of the combination of relatively low bleed pressures, high cooling temperatures, and low ram-air availability. Thus, the selected synthesis/design or reference condition corresponds to the second subsonic cruise climb leg (scc_2) of Table 4.2.

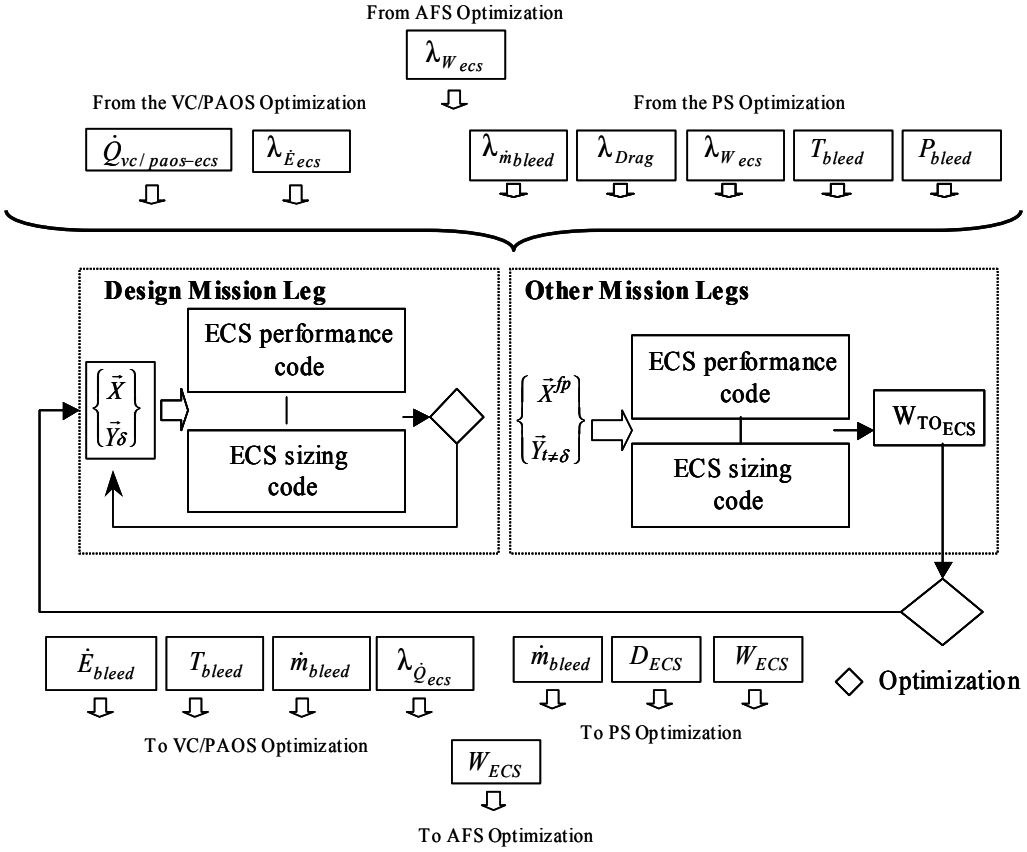

Figure 5.3 ECS system-level, unit-based modeling and optimization procedure.

4. The second subsonic cruise climb leg is used to obtain a set of the most promising solutions. Each of these (typically 5) provides values for the ECS synthesis/design decision variables, which are then used in the off-design optimization. At the operational-level, fourteen problems are resolved each with respect to the operational decision variables for each leg. The optimization procedure for the ECS is shown in Figure 5.3.
5. Once completed, the ECS synthesis/design provides updated values for the coupling functions of the ECS. The fuel-based shadow prices for each of the

mission legs are calculated. The ECS coupling functions (i.e. bleed air mass flow and inlet temperature to the bleed/PAO heat exchanger) along with the corresponding shadow prices are used to carry out the synthesis/design optimization of the VC/PAOS. As in step 3, the shadow prices are held constant for the given iteration. The second subsonic cruise climb leg is used to find a set of the most promising solutions for the VC/PAOS. Afterwards, the operational-level problem is solved. At the operational-level, fourteen problems are resolved each with respect to the operational decision variables for each leg. The procedure is shown in Figure 5.4.

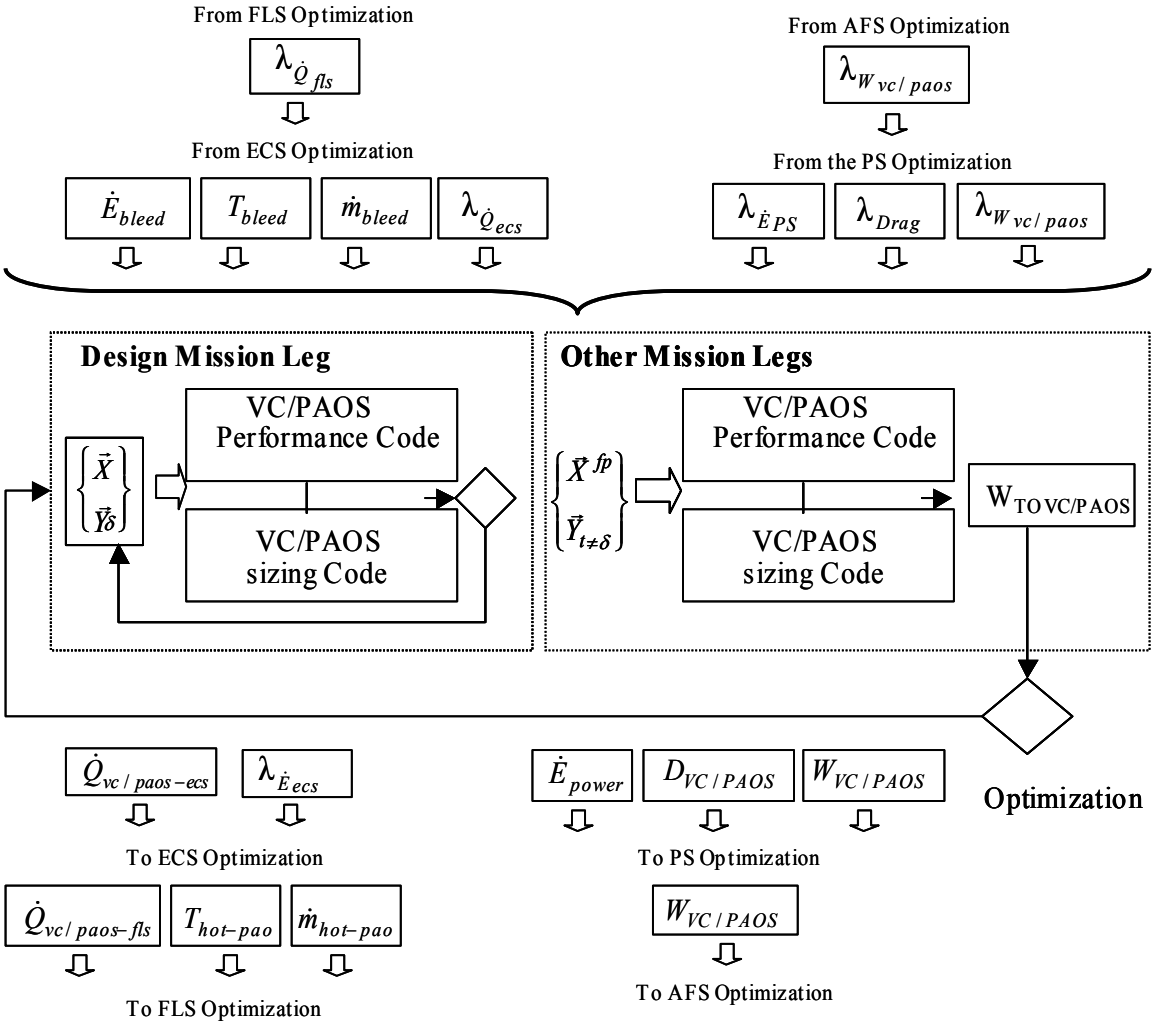

Figure 5.4 VC/PAOS system-level, unit-based modeling and optimization procedure.

6. Once completed, the VC/PAOS synthesis/design provides updated values for the coupling functions of the VC/PAOS. The fuel-based shadow prices for each of the mission legs are calculated. The VC/PAOS coupling functions (i.e. heat

rejected from the ECS through the bleed/PAO heat exchanger and heat rejected to the AFS) along with the corresponding shadow prices are used to carry out the synthesis/design optimization of the FLS. As in step 3, the shadow prices are held constant for the given iteration. No time decomposition is used to solve the FLS transient operational level. Ii is solved along with the synthesis/design problem using gPROMS transient numerical solvers. The procedure is shown in Figure 5.5.

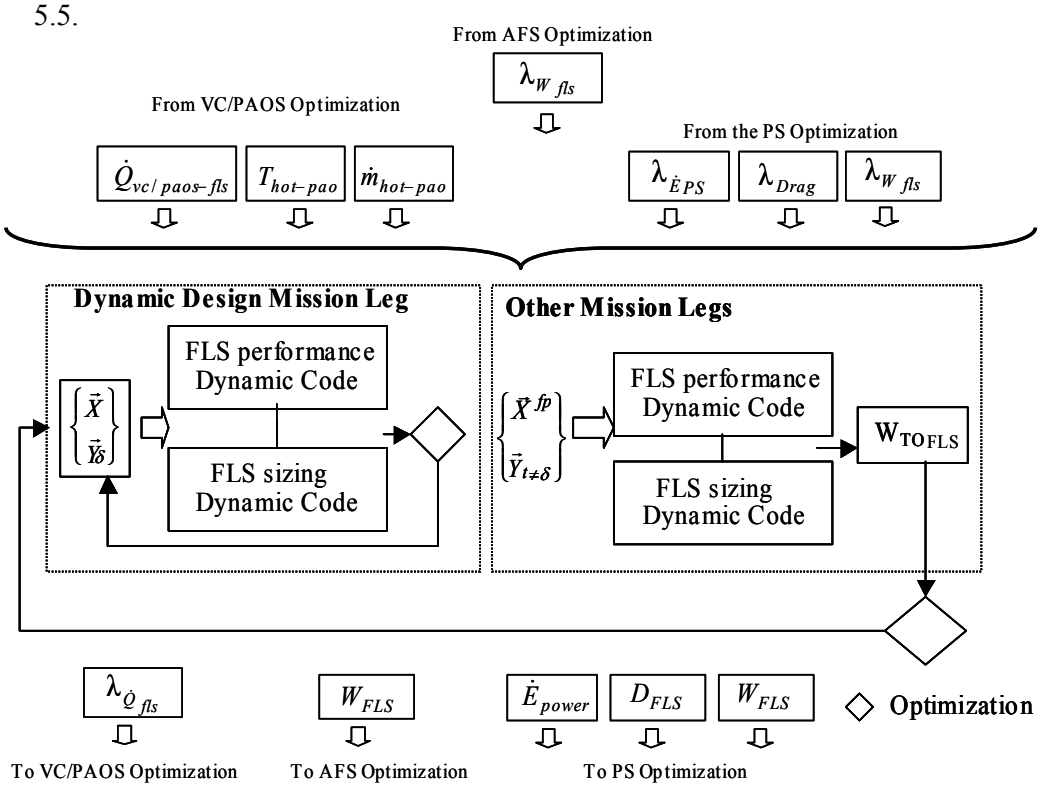

Figure 5.5 FLS system-level, unit-based modeling and optimization procedure.

7. Once completed, the FLS synthesis/design provides updated values for the coupling functions of the FLS. The fuel-based shadow prices for each of the mission legs are calculated. The FLS, ECS, VC/PAOS and PS coupling functions along with the corresponding shadow prices are used to carry out the synthesis/design optimization of the AFS. As in step 3, the shadow prices are held constant for the given iteration. No operational decision variables are considered. At the operational-level, fourteen mission segments are solved and the dependant operational variables for each leg are computed. The procedure is shown in Figure 5.6.

8. Once completed, the ECS, FLS, VC/PAOS, and AFS syntheses/designs provides updated values for the coupling functions of these sub-systems. These values are used in step 1 to optimally redesign the PS. The iterative process continues until no improvement in the system-level objective function is observed.

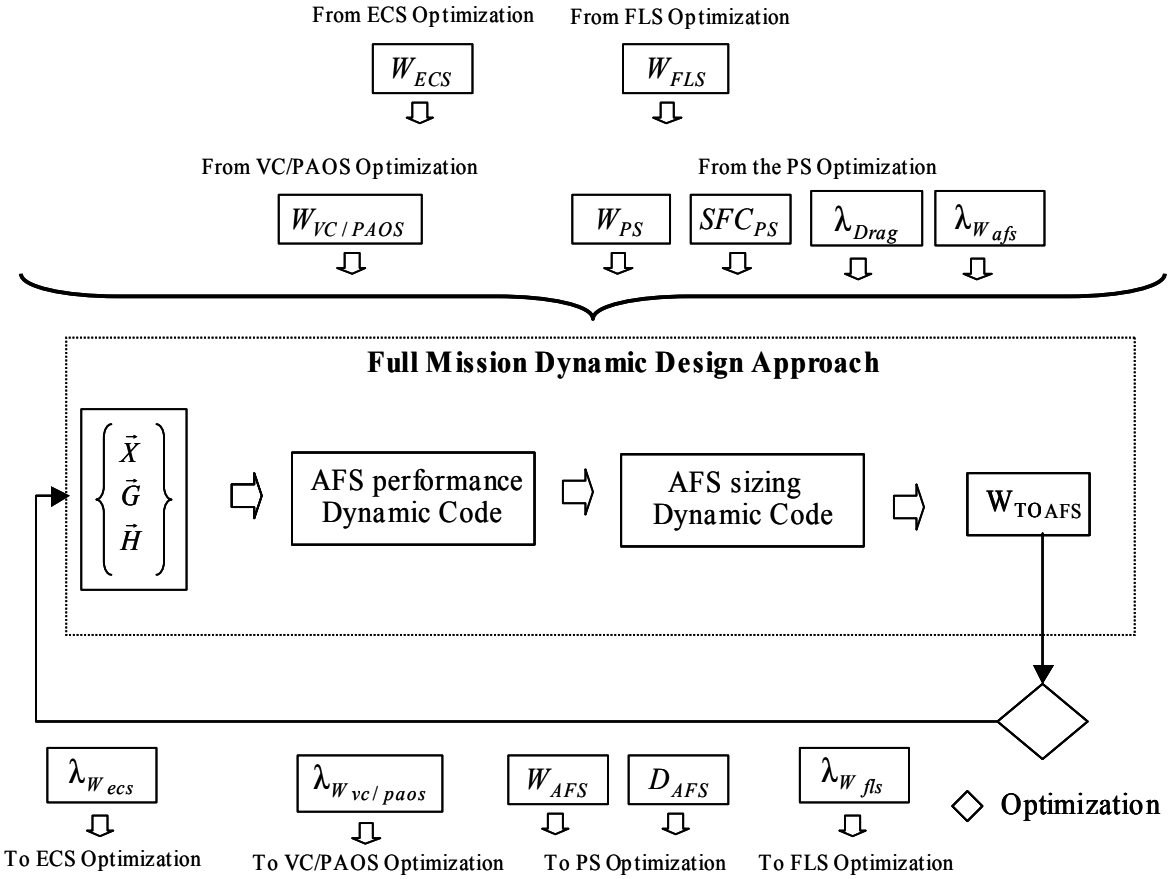

Figure 5.6 AFS system-level, unit-based modeling and optimization procedure.

The procedure described above is the same regardless of whether the objective function is the total take-off gross weight or the fuel consumed to carry out the mission or the total cost. Figure 5.7 shows the coupling function flows between sub-systems and the system optimization scheme.

All of the optimization problems are solved using the commercial optimization package iSIGHT (1999). Each optimization iteration typically consists of two steps. The first uses a Genetic Algorithm (GA) in order to effectively deal with the mixed integer variables and possible local minima problems in each of the sub-system (unit-level for the PS and system-level, unit-based for the ECS, VC/PAOS, FLS, and AFS) optimizations. Each GA optimization run has a minimum population size equal to

three times the number of variables with a minimum of 100. The minimum number of iterations for the GA is set to 300 times the population size for the PS and 1000 times the population size for the VC/PAOS, FLS, AFS, and the ECS optimization problems. In the first step, the convergence criterion for the calculation of the take-off gross weight is set at 0.2 %. This means that the value of W_{TO} sent to the optimization algorithms has an error of approximately ±200 N. The second step uses the top two or three solutions obtained with the GA to narrow down the best solutions using a gradient-based algorithm (Method of Feasible Directions). For the second step, the convergence criterion on the take-off gross weight calculation is set at 0.1 %.

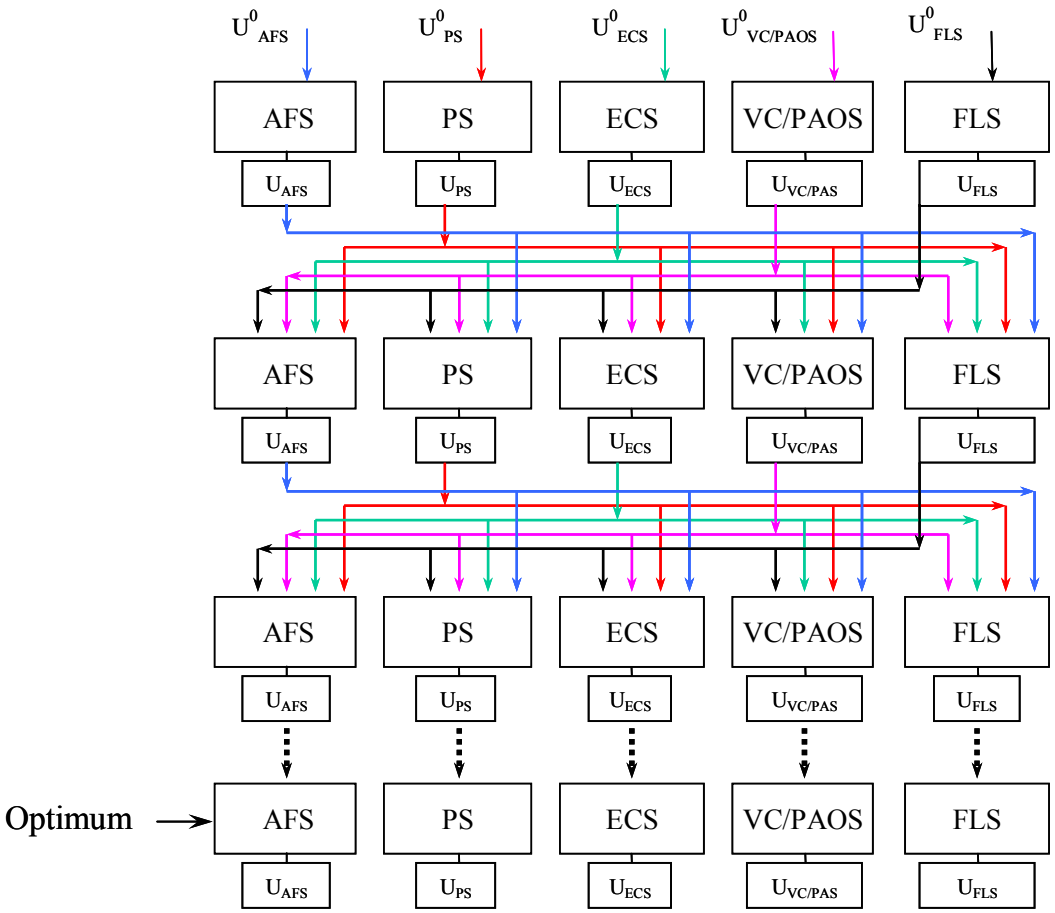

Figure 5.7 Aircraft system ILGO optimization scheme.

Chapter 6

Results and Discussion

The results for the synthesis/design optimization of the proposed advanced tactical fighter aircraft are discussed in this chapter. The thorough presentation of the solution obtained using the ILGO decomposition technique is followed by the presentation of the coupling functions shadow prices for the corresponding sub-system as well as a detailed description of the system-level ORS as well as unit-level ORS's for the AFS, FLS, ECS, VC/PAOS and PS. The most promising sub-system syntheses/designs along with their off-design performance results are presented next, and the system final optimum synthesis/design is identified. Finally, the unique component geometries and the most interesting aerodynamic properties over the entire load/environmental profile for the final optimum ATA (advance tactical aircraft) synthesis/design are presented and discussed in the last section of this chapter.

6.1 Synthesis/Design Optimization Problem Results Using the ILGO Approach

As indicated in Chapter 5, the ILGO physical decomposition technique is used in order to optimize the total advanced tactical aircraft system's synthesis/design for the time segment with the most stringent load/environmental conditions, i.e. the synthesis/design point. The solutions to the PS, AFS, ECS, VC/PAOS, and FLS unit-level and system-level, unit-based optimization problems for each iteration of the ILGO approach as well as the corresponding total gross take-off weight are presented in Table 6.1. A graphical representation of this tabulated data is given in Figure 6.1.

Table 6.1 Optimum values of the aircraft gross take-off weight as well as PS, AFS, ECS, FLS, VC/PAOS weights for each iteration of the ILGO approach.

ILGO Iteration No.	W_{TO} (kg)	W_{PS} (kg)	W_{ECS} (kg)	W_{AFS} (kg)	W_{FLS} (kg)	$W_{VC/PAOS}$ (kg)	Percentage Improvement
1	13100	1520	450	4200	560	410	---
2	11400	1260	360	3600	460	320	-14.91
3	10800	1140	305	3400	390	270	-5.56
4	10450	1110	280	3200	340	250	-3.35
5	10350	1060	270	3140	330	242	-0.97
6	10200	1040	265	3100	322	237	-1.47
7	10180	1032	260	3100	319.5	232	-0.20

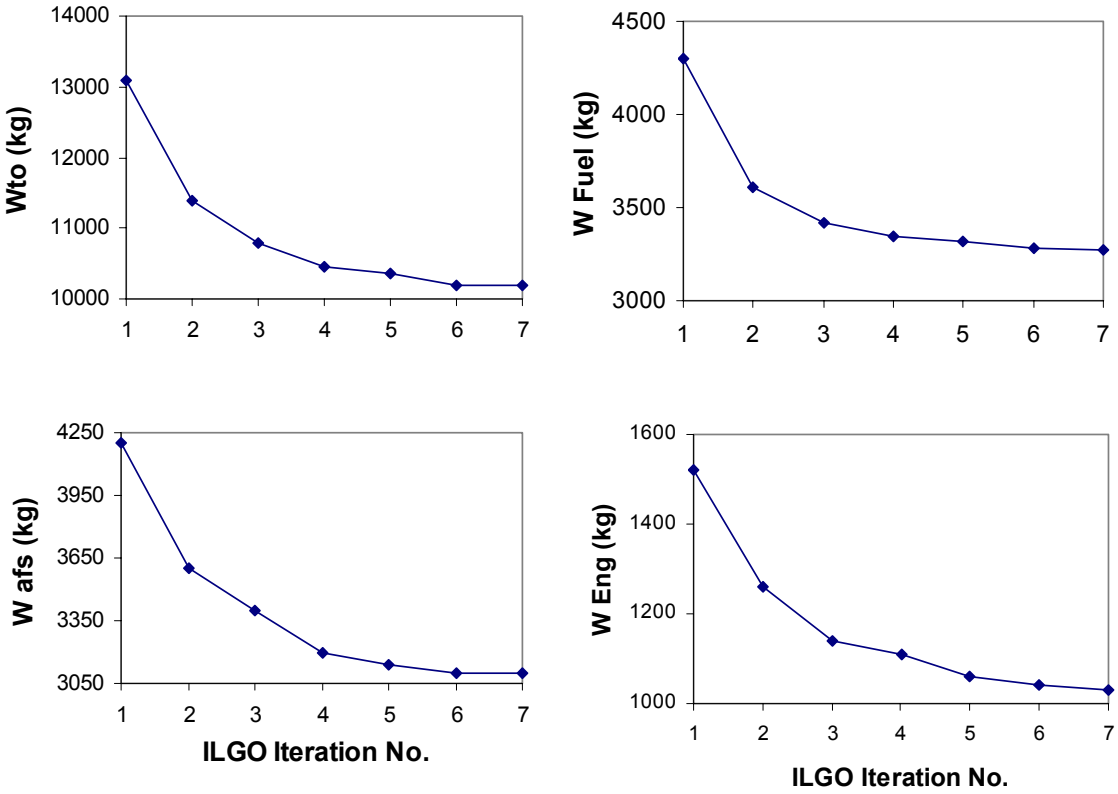

Figure 6.1 Evolution of the take-off gross weight, fuel weight, AFS weight, and PS weight at different points of the iterative local-global optimization (ILGO) approach.

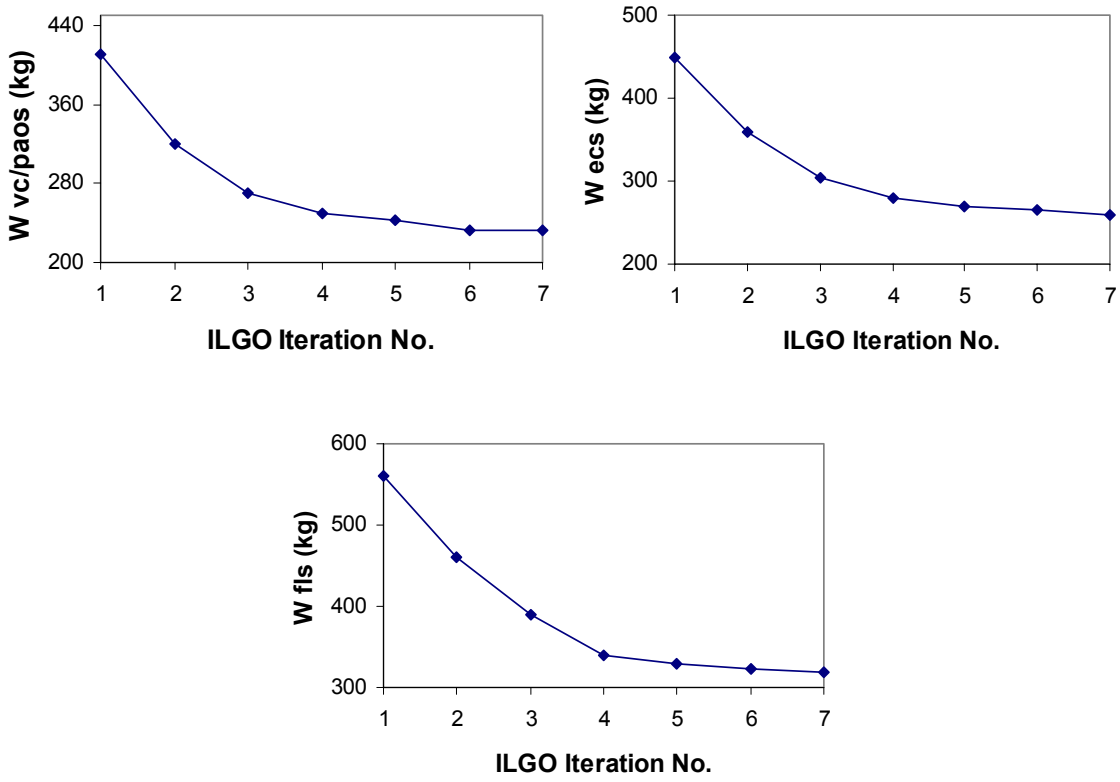

Figure 6.2 Evolution of the VC/PAOS, ECS, and FLS weights at different points of the iterative local-global optimization (ILGO) approach

What is believed to be the global optimum[62] value for the total gross take-off weight of the aircraft system, W_{TO}, is obtained in seven iterations of ILGO. A significant improvement in the value of the system-level objective function is observed upon completion of the second ILGO iteration. In particular, the final gross take-off weight is lower by 2920 kg than that of the first iteration, which translates to a 28.68% decrease.

Figures 6.1 and 6.2 shows the evolution of the gross take-off weight, the weight of fuel, and the weights of the PS, AFS, FLS, VC/PAOS and ECS for the different iterations of the ILGO process. It is clearly evident that in every run some improvement was achieved in the system-level objective function (gross take-off

[62] See footnotes 2, 14, and 22 for a discussion of what is meant here in regards to the use of the term "global optimum".

weight) and the weight of each sub-system. The flat behavior of W_{TO} for the last three iterations indicates that the overall iterative optimization scheme converged, i.e. no improvement is achieved after iteration 7. This observation was verified by running the problem an eighth time with no observable change in the independent variables or the system-level objective function. The purpose of the eighth iteration is to verify that no further significant improvement in the system-level objective function can be achieved and, therefore, gain confidence in the solution as the optimum one.

Optimum results for the PS, ECS, VC/PAOS, and FLS independent operational and synthesis/design variables appear in Tables 6.2 and 6.3, respectively. Optimum objective function values and weights appear in Table 6.4.

The shadow prices (the slopes of the curves) for the intermediate products (coupling functions) going from the PS to the ECS and the feedbacks (coupling functions) coming from the ECS back to the PS at the global (system-level) optimum for select mission legs are given in Figure 6.3. The linear behavior of the shadow prices, for both design and off-design conditions, is clearly evident. This behavior is observed even though no energy or exergy quantities were used. The fact that the marginal costs represented by the slope of the curves in Figure 6.3 are constant helped the relatively fast overall convergence of the ILGO scheme used. In Muñoz and von Spakovsky (2000b), it was theorized that relatively constant shadow prices would lead to the final solution in only one iteration i.e., achieve "thermoeconomic solution". This was not the case in this application, primarily due to the initial mismatch between the coupling functions for the different sub-systems, e.g., bleed conditions used in the ECS optimization, electric power used by the VC/PAOS optimization, and those obtained from running the PS optimization. Nonetheless, a very close approach to "thermoeconomic isolation" was achieved.

The shadow prices are indicative of the relative importance of the intermediate products going from the PS to the ECS and the feedback coming from the ECS back to the PS. A first order approximation using the allowable ranges for the ECS independent variables of Table 5.1 reveal that the variability of heat rejection to the VC/PAOS, the PS bleed air flow rate, and the ECS drag and weight are approximately 30 ± 20 kW, 0.75 ± 0.2 kg/s, 350 ± 200 N and 700 ± 500 kg, respectively. With these values and the shadow prices of Figures 6.3 through 6.5 and Figure 6.7 one can readily conclude that the effect of the ECS weight is significantly higher than that of

heat rejection, bleed air flow rate, and momentum drag. Thus, the optimum ECS solution is expected to have the smallest possible value of weight.

Table 6.2 PS, ECS, VC/PAOS, and FLS optimum values for all mission segment operational[63] decision variables.

Leg	PR_{vv}	m_{creg}	m_{byp}	m_{hot}	BP_{low}[64]	BP_{high}[52]	T_{it}	$PR_{v\text{-}comp}$	m_{vap}	m_{Hpao}
tkr	1.406	0.0174	0.000	0.000	0	1	1778	3.05	1.37	1.23
tka	2.193	0.0349	0.200	0.000	0	1	1778	3.11	1.29	1.24
wup	1.845	0.001	0.063	0.000	0	1	1778	3.01	1.22	1.11
clac	3.440	0.056	0.101	0.000	1	0	1778	3.7	1.31	1.42
scc_1	2.459	0.104	0.002	0.000	1	0	1355	3.35	1.27	1.61
cap	1.380	0.200	0.002	0.000	0	1	1090	3.4	1.31	1.62
acc	4.029	0.101	0.001	0.044	1	0	1778	4.1	1.56	1.7
pen	5.564	0.062	0.001	0.000	1	0	1588	4.31	1.61	1.65
ct1	6.000	0.069	0.016	0.000	1	0	1778	4.13	1.56	1.59
ct2	4.229	0.087	0.032	0.000	1	0	1778	3.9	1.48	1.48
cac	5.885	0.058	0.016	0.000	1	0	1778	3.99	1.51	1.49
esc	5.287	0.086	0.032	0.000	1	0	1574	3.6	1.46	1.71
mmn	4.229	0.137	0.024	0.000	1	0	1636	1.2	1.6	1.69
scc_2	1.463	0.088	0.000	0.000	1	0	1275	3.35	1.07	1.61
loi	2.115	0.015	0.048	0.000	1	0	1113	3..3	1.36	1.73

[63] Synthesis/design variables are fixed during the mission. Operational variables change through the mission according to the mission segment requirements and environment.
[64] This variable is common to the ECS and PS optimization problems.

Table 6.3 PS, FLS, VC/PAOS, AFS, and ECS optimum values for the synthesis/design variables.

Sub-System	*Component Variable*	Value	*Sub-System*	*Component Variable*	Value
ECS	L_h (Prim HX)	0.505	PS	α	0.536
	L_c (Prim HX)	0.060		PR_{fan}	4.829
	L_n (Prim HX)	0.504		PR_{hpc}	5.014
	L_h (Sec. HX)	0.505		PR_{hpt}	3.017
	L_c (Sec. HX)	0.061		PR_{lpt}	1.843
	L_n (Sec. HX)	0.508			
	L_c (Reg. HX)	0.300	VC/PAOS	L_h (Bleed/Pao HX)	0.30
	L_c (Reg. HX)	0.150		L_c (Bleed/Pao HX)	0.15
	L_n (Reg. HX)	0.300		L_n (Bleed/Pao HX)	0.30
	PR_{cp}	2.60		L_h (Cond HX)	0.302
	PR_{tb}	8.56		L_c (Cond HX)	0.16
	A_1	103.0		L_n (Cond HX)	0.306
	A_2	103.0		L_h (Evap HX)	0.35
	Fin_{hot}	14		L_c (Evap HX)	0.17
	Fin_{cold}	14		L_n (Evap HX)	0.34
	Reg_1	0		L_h (Ram HX)	Na
	Reg_2	1		L_c (Ram HX)	Na
				L_n (Ram HX)	Na
FLS	L_h (Fuel/Pao HX)	0.60		*onoff*	0
	L_c (Fuel/Pao HX)	0.11			
	L_n (Fuel/Pao HX)	0.60	AFS	Wing *AR*	3.046072
	L_h (Fuel/Oil HX)	0.500		Wing *t/c*	0.077494
	L_c (Fuel/Oil HX)	0.06		Wing λ	0.240061
	L_n (Fuel/Oil HX)	0.500		Wing Λ	31.05784
	L_h (Fuel/Hyd HX)	0.37		Wing S_f/S_{ref}[65]	0.75
	L_c (Fuel/Hyd HX)	0.15		Wing C_{L_design}	0.6
	L_n (Fuel/Hyd HX)	0.38		Tail *T_AR*	5.004859
	L_h (Fuel/Ram HX)	0.38		Tail *T_t/c*	0.12
	L_c (Fuel/Ram HX)	0.17		Tail T_λ	0.461185
	L_n (Fuel/Ram HX)	0.36		$S_{ref}(ft^2)$	364.2
	A_1	140.2		T_{sl}/W_{to}	1.13
				W_{to}/S_{ref}	61.49

[65] Exposed area to reference area ratio.

Table 6.4 PS, FLS, VC/PAOS, AFS, and ECS optimum objective function values and weights.

W_{TO}/g (kg)	**10180**
W_{FUEL}/g	**3270**
W_{EMPTY}/g	**3855**
$W_{PAYLOAD}$/g	**1209**
$W_{Equipment}$/g[54]	**755**
W_{ECS}/g[66]	**260**
Prim HX	24
Sec. HX	24
Reg. HX	11
ACM	14
Ram Inlets	12
Ram exits	11
Ducting[67]	137
Other[55]	27
ΔW_{TOECS}/g (kg)	800
$\Delta W_{FUELECS}$/g	540
$\Delta W_{FUELbleed}$/g	76
$\Delta W_{FUELdecs}$/g	49
$\Delta W_{FUELwecs}$/g	415
W_{FLS}/g[54]	**319.5**
Ram/fuel HX	20.5
Hydraulics HX	18
Fuel/Oil HX	26
Fuel/PAO HX	36
Ram Inlet	8
Ram exit	6
Pumps	15
Ducting[55]	173
Other[55]	17
ΔW_{TOFLS}/g (kg)	881
$\Delta W_{FUELFLS}$/g	561.5
$\Delta W_{FUELpower}$/g	5
$\Delta W_{FUELdfls}$/g	48
$\Delta W_{FUELwfls}$/g	508.5

W_{AFS}/g	**3100**
Wing	998.4
Tail	193.3
Fuselage	1076.6
Main Landing Gear	432.5
Nose Landing Gear	117.8
Engine Mounts	25.7
Firewall	40.7
Engine Section	14.4
Air Induction	199.4
W_{ENG}/g[54]	**1032**
fan	218
hpc	115
hpt	136
lpt	240
noz	49
other	274
$W_{VC/PAOS}$/g[54]	**232**
Evaporator	16
Condenser	20
Bleed/PAO HX	10.6
Vapor Compressor and electrical motor	17
Pumps	12
Ram Inlets	0
Ram exits	0
Ducting[55]	139
Other[55]	18
$\Delta W_{TOVC/PAOS}$/g (kg)	622.2
$\Delta W_{FUELVC/PAOS}$/g	390.2
$\Delta W_{FUELpower}$/g	32
$\Delta W_{FUELdvc/paos}$/g	0
$\Delta W_{FUELwvc/paos}$/g	358.2

[66] Includes 15% additional mass for packaging and installation. All of the component weights include accessories.
[67] Not participating in the optimization.

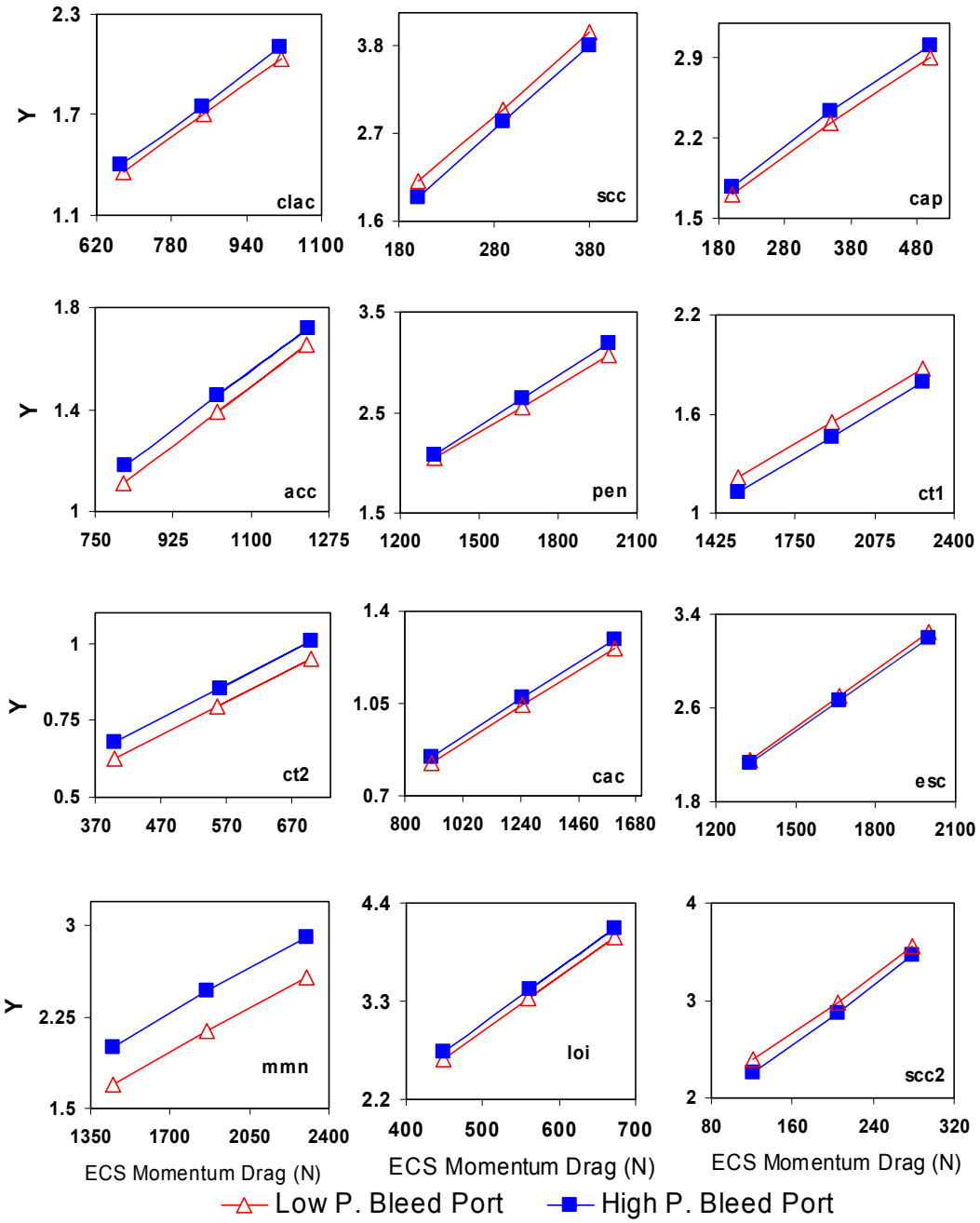

Figure 6.3 Incremental fuel consumption Y due to ECS momentum drag at different mission legs during the final iteration.

The slopes of the curves are the drag shadow prices based on fuel.

$$Y \equiv \frac{W_{FUEL}(bleed, \dot{Q}_{VC/PAOS}, W_{ECS}, D_{ESCS}) - W_{FUEL}(bleed, \dot{Q}_{VC/PAOS}, W_{ECS}, 0)}{W_{FUEL}(bleed, \dot{Q}_{VC/PAOS}, W_{ECS}, 0)} x100$$

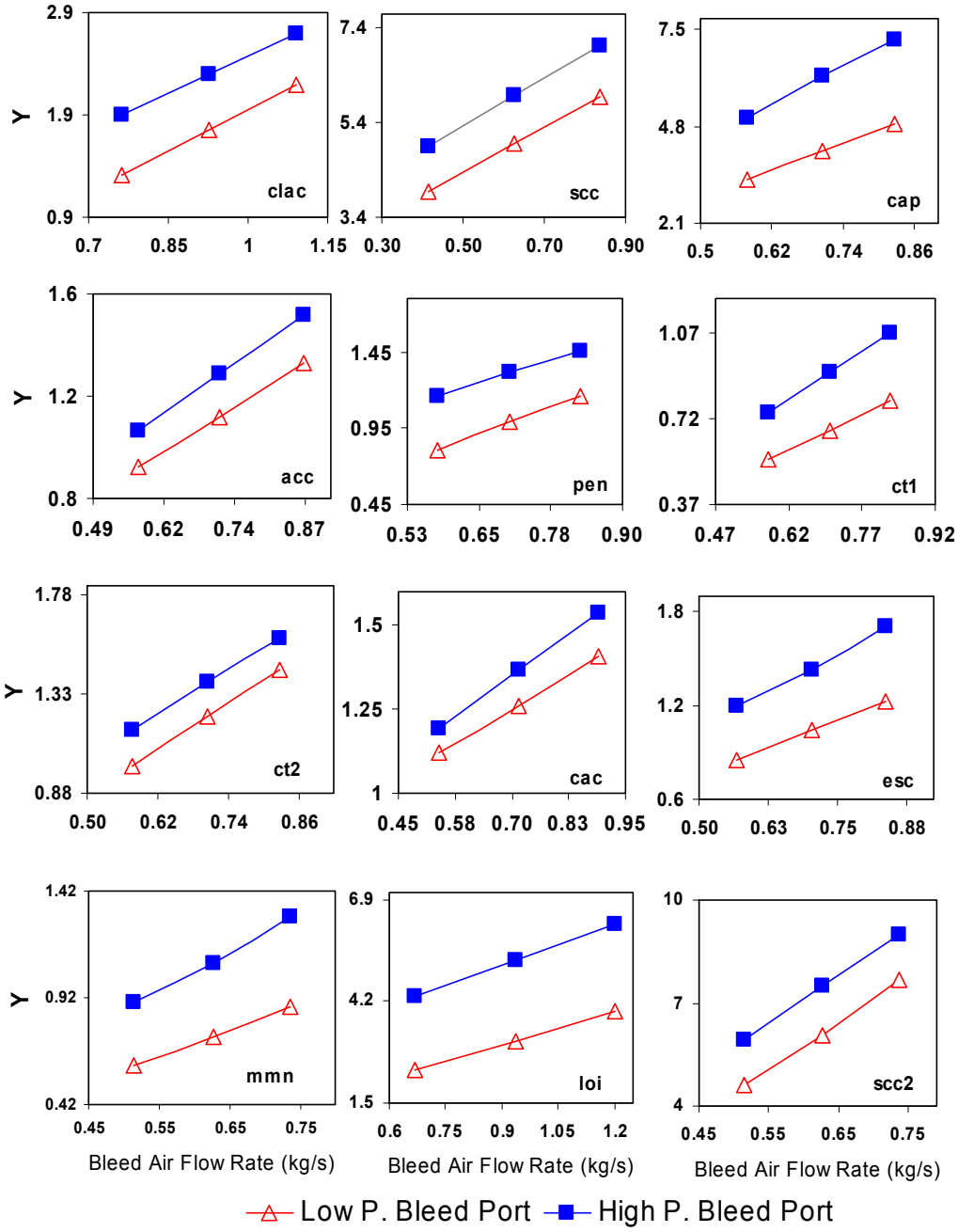

Figure 6.4 Incremental fuel consumption Y due to the ECS bleed air extraction for different mission legs during the final iteration.

The slopes of the curves are the bleed air shadow prices based on fuel.

$$Y \equiv \frac{W_{FUEL}(bleed, D_{ECS}, \dot{Q}_{VC/PAOS}, W_{ECS}) - W_{FUEL}(0, D_{ECS}, \dot{Q}_{VC/PAOS}, W_{ECS})}{W_{FUEL}(0, D_{ECS}, \dot{Q}_{VC/PAOS}, W_{ECS})} x100$$

The fact that the bleed, drag, and weight shadow prices have positive values indicates that a solution with lower bleed and drag will be preferred for a given value of ECS weight. The negative sign for the heat rejection shadow price, Figure 6.7, indicates that at the unit-level, high heat rejection is favorable. However, at the system-level, an increase in the heat rejected from the ECS to the VC/PAOS would not only mean a reduction in the ECS unit-level objective, but also an increase in the VC/PAOS and FLS respective unit-level objectives. This because the bigger the heat rejection to the VC/PASO, the bigger the bleed/PAO and PAO/fuel heat exchanger required and the bigger the cooling demand on the FLS, which is the ultimate heat sink for the VC/PAOS. Thus, it is not evident what level of heat rejection is more convenient at the system-level. This is only determined by solving the system-level, unit-based optimization problem for each unit involved.

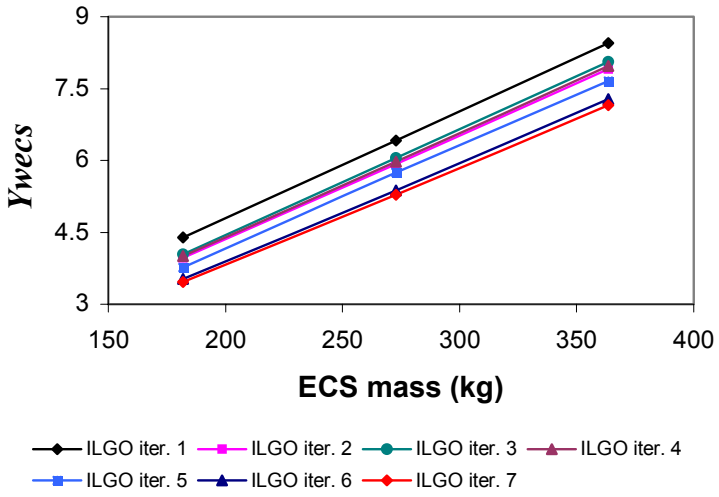

Figure 6.5 ECS mass shadow prices through the mission for different iterations of ILGO.

The shadow prices are the slopes of the curves. The fact that the shadow prices are constant indicates that the ORS is a hyper-plane

$$Y_{wecs} \equiv \frac{W_{FUEL}(bleed, D_{ECS}, W_{ECS}, \dot{Q}_{VC/PAOS}) - W_{FUEL}(bleed, D_{ECS}, 0, \dot{Q}_{VC/PAOS})}{W_{FUEL}(bleed, D_{ECS}, 0, \dot{Q}_{VC/PAOS})} x100$$

The shadow prices presented in Figures 6.6 and 6.8 are indicative of the relative importance of the intermediate products going from the PS to the VC/PAOS and to the FLS and the feedback coming from them to the PS. A first order approximation

using the allowable ranges for the VC/PAOS independent variables of Table 5.2 reveal that the variability of heat rejection from the ECS to the VC/PAOS, the power extraction, and the VC/PAOS drag and weight are approximately 30 ± 30 kW, 50 ± 40 kg/s, 200 ± 200 N and 300 ± 200 kg, respectively. With these values and the marginal costs of Figure 6.6 through 6.8 one can readily conclude that the effect of the VC/PAOS weight is significantly higher than that for power extraction, heat rejection and momentum drag. Thus, as with the ECS, the optimum VC/PAOS solution is expected to have the smallest possible weight value. The fact that all of the shadow prices have positive values indicates that a solution with lower power extraction, heat rejection and drag will be preferred for a given value of VC/PAOS weight.

The shadow prices (the slopes of the curves) for the power extraction going from the PS to the VC/PAOS and FLS at the global (system-level) optimum for select mission legs are given in Figure 6.6. As with the ECS, the linear behavior of the shadow prices for both design and off-design conditions are clearly evident. Once more, the fact that the shadow prices represented by the slope of the curves in Figure 6.6 are constant helped the relatively fast overall convergence of the ILGO scheme used.

The shadow prices for the VC/PAOS and FLS drag and weight are the same as those for the ECS, shown in Figures 6.3 and 6.4. The shadow prices (the slopes of the curves) for the intermediate products going from the ECS to the VC/PAOS and the feedback coming from the VC/PAOS back to the ECS at the global (system-level) optimum for select mission legs are given in Figure 6.7. As before, the linear behaviors of the shadow prices for both design and off-design conditions are clearly evident. The negative slope shown in Figure 6.7 indicates that an increase in the heat rejection from the ECS to the VC/PAOS will produce a reduction in the total fuel due to the ECS, along with a increase in the total fuel due to the VC/PAOS and FLS, because of the necessary increase in the weight of the bleed/PAO heat exchanger, the fuel/PAO heat exchanger, and the fuel/ram-air heat exchanger. The increases in the fuel due to the FLS appear since it is the ultimate heat sink and no ram/PAO heat exchanger is used by the optimum VC/PAOS synthesis.

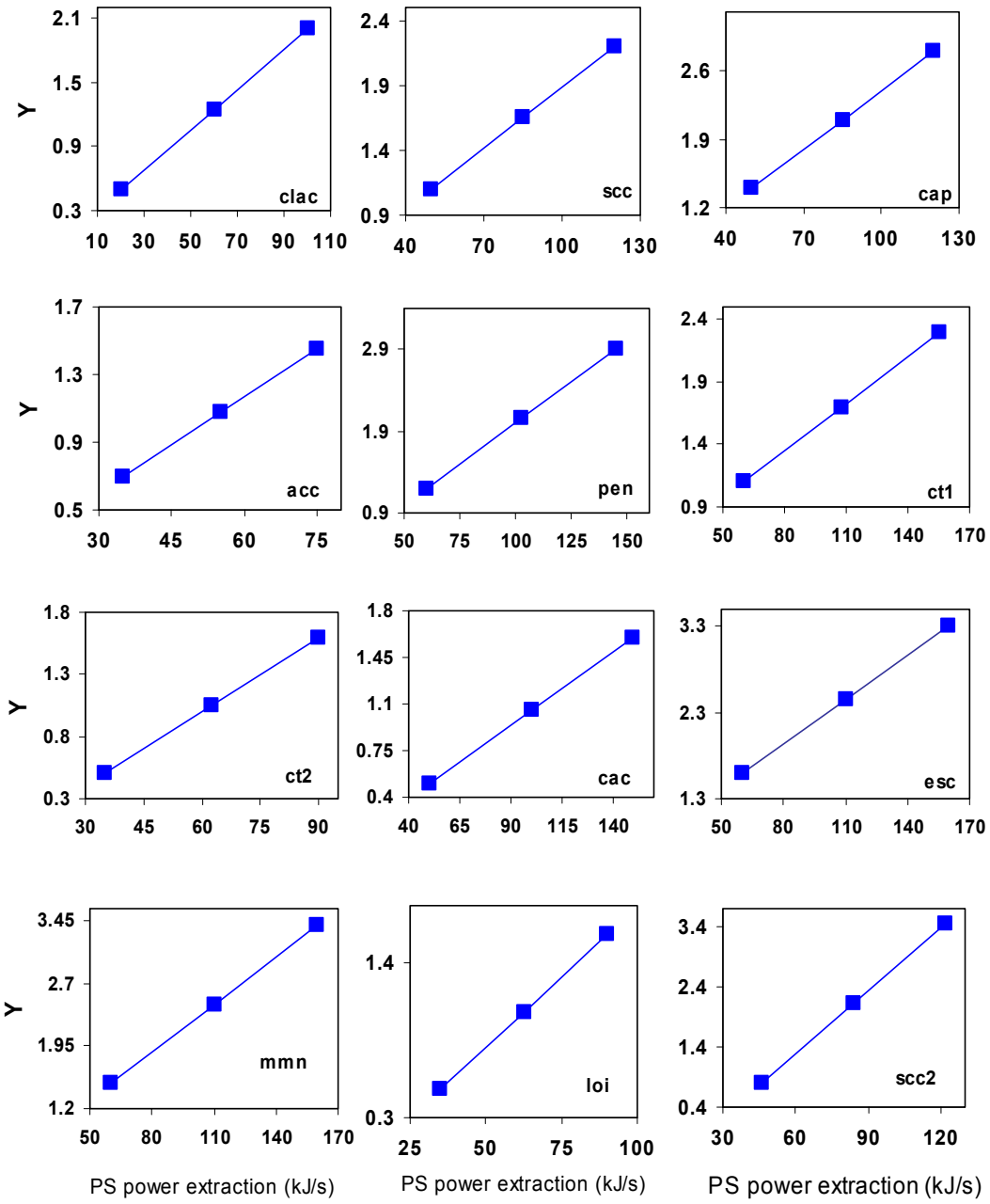

Figure 6.6 Incremental fuel consumption Y due to VC/PAOS and FLS power extraction from the PS for different mission legs during the final iteration. The slopes of the curves are the bleed air shadow prices based on fuel.

$$Y \equiv \frac{W_{FUEL}(W_{VC/PAOS}, D_{VC/PAOS}, \dot{E}) - W_{FUEL}(W_{VC/PAOS}, D_{VC/PAOS}, 0)}{W_{FUEL}(W_{VC/PAOS}, D_{VC/PAOS}, 0)} x100$$

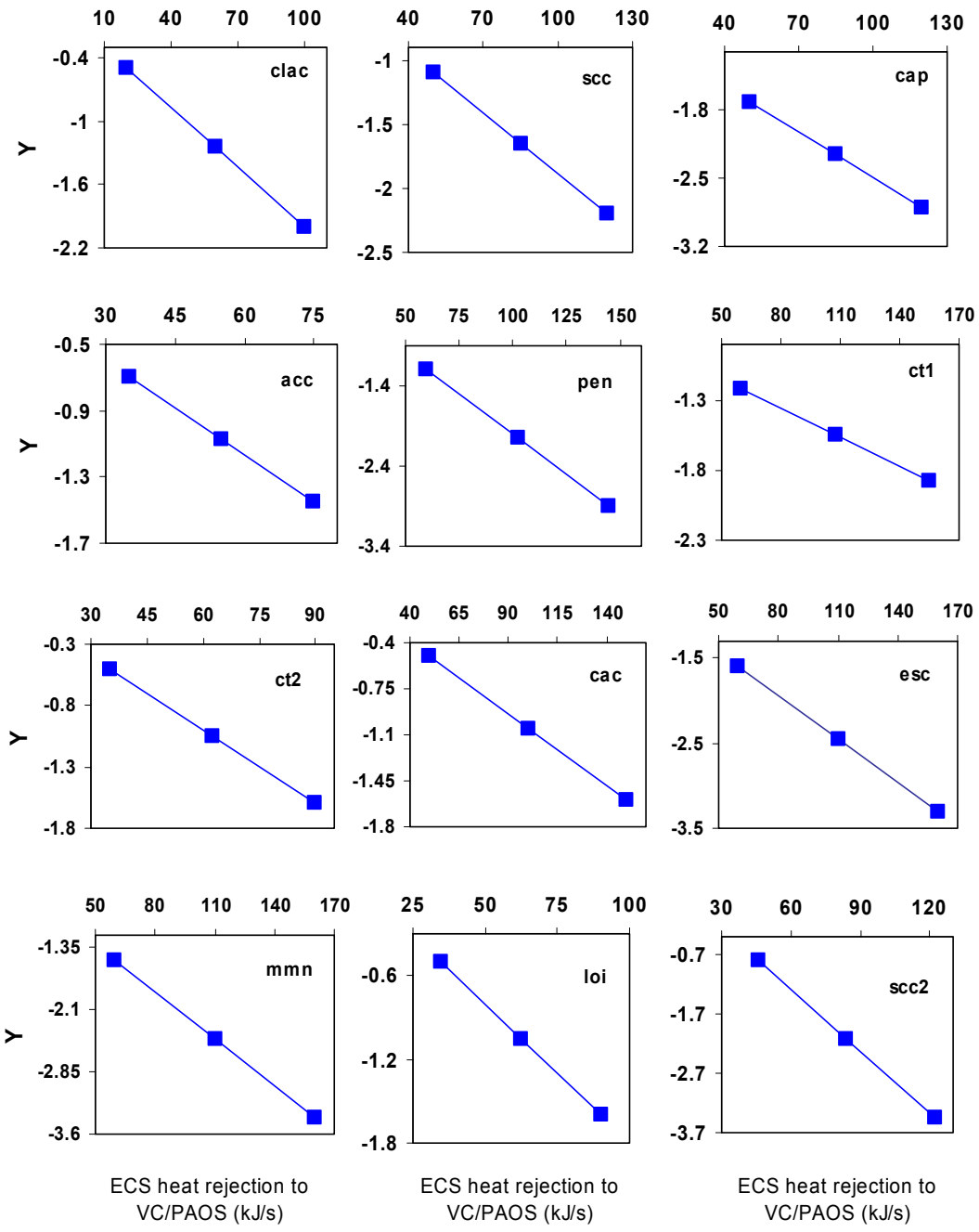

Figure 6.7 Incremental fuel consumption Y for the ECS due to ECS heat rejection to the VC/PAOS for different mission legs during the final iteration. The slopes of the curves are the heat rejection shadow prices based on fuel.

$$Y \equiv \frac{W_{FUEL}(\dot{Q}) - W_{FUEL}(0)}{W_{FUEL}(0)} x100$$

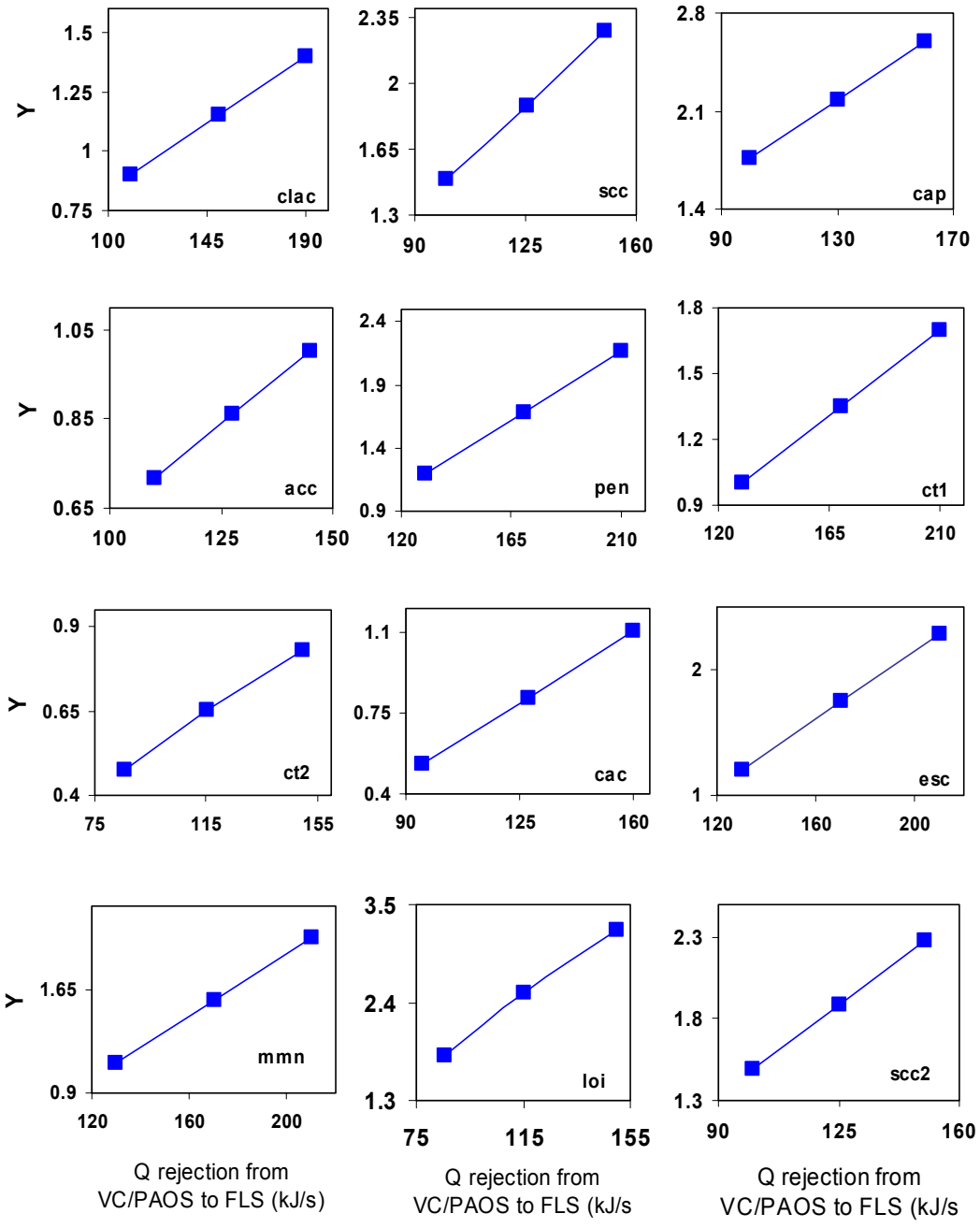

Figure 6.8 Incremental fuel consumption Y for the FLS due to VC/PAOS heat rejection to the FLS for different mission legs during the final iteration. The slopes of the curves are the bleed air shadow prices based on fuel.

$$Y \equiv \frac{W_{FUEL}(\dot{Q}_{VC/PAOS-FLS}) - W_{FUEL}(0)}{W_{FUEL}(0)} x100$$

The fact that the optimum solutions for the gross take-off weight and fuel consumption problems are identical (see Table 6.3 above) can be explained by the near linear relationship between W_{TO} and W_{FUEL} shown in Figure 6.9 from Muñoz (2000). Furthermore, the shadow prices show that weight is the most important of the intermediate products and feedbacks going to and coming from the ECS, FLS, VC/PAOS and AFS. Table 6.4 above indicates that the heat exchangers have the biggest contribution to all sub-system weights among the components participating in the optimization. With these last two observations in mind, it comes as no surprise that the optimum solution found for the ECS, FLS, VC/PAOS corresponds to the synthesis/design with the lowest possible heat exchanger core dimensions. Additionally, since ram air is to augment fuel consumption (and hence on W_{TO}) due to the extra thrust needed (via momentum drag) and mass required (that of the ram-air inlet and exit and the increased PS size), the minimum required ram air inlet areas for the ECS, FLS and VC/PAOS are also what would be expected. Finally, since any electrical power extraction from the PS through the generator produces an increase in fuel consumption, and again in W_{TO}, due to the extra thrust needed and mass required (that of components such as compressors, pumps, etc. and the increased PS size), the minimum electrical power extraction for the VC/PAOS and FLS is expected.

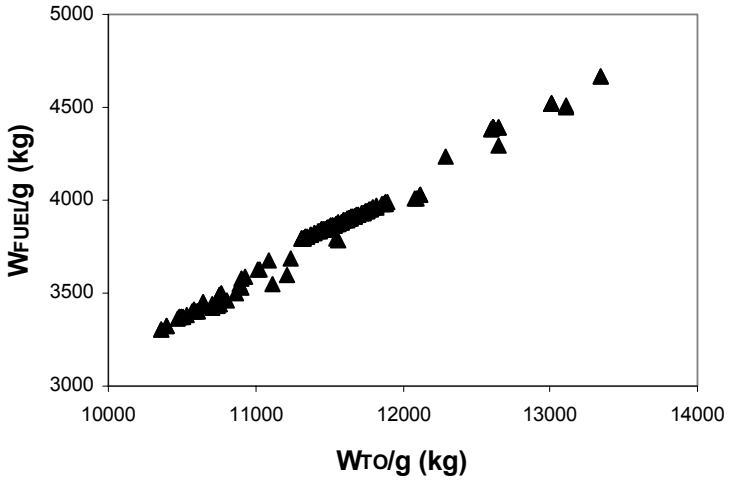

Figure 6.9 Fuel weight versus gross take-off weight corresponding to feasible solutions obtained at different iterations of the overall (system-level) optimization.

Figure 6.10 shows the incremental fuel consumption Y for the AFS due to the weight of the ECS, VC/PAOS, and FLS at the synthesis/design point for different iterations of the ILGO. The shadow prices are the slopes of the curves. With respect to the AFS, the relationship between total drag and weight is even more evident. For a steady level constant-speed mission segment the analysis is as follows: any increase in AFS weight means an increase in the need for lift force, which in turn causes the growth of drag due to lift. Thus, it is clear that there is an augmentation in fuel consumption (and hence in W_{TO}) due to the extra thrust needed. The same is also true for mission segments with changes in altitude and speed. An effective way to reduce the drag due to the lift is by increasing the wing aspect ratio. However, this is limited by the fact that In general increases in wing span also translate into increases in weight due to the need for a stronger structure. Moreover, higher wing spans may produce a counter effect during the supersonic mission segments.

Finally, on the PS side, an optimum solution with the highest possible turbine inlet temperatures is found. Again, this is an expected result due to the fact that it is much more efficient to burn fuel in the combustor than in the afterburner.

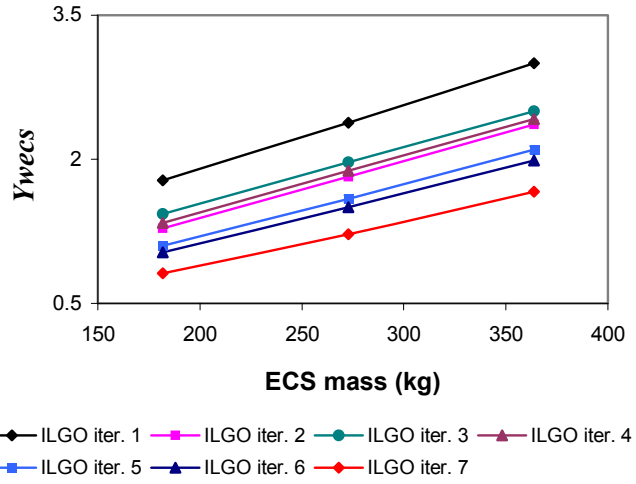

Figure 6.10 ECS mass shadow prices through the mission for the AFS for different iterations of ILGO.
The shadow prices are the slopes of the curves.

$$Y_{wecs} \equiv \frac{W_{FUEL}(bleed, D_{ECS}, W_{ECS}, \dot{Q}_{VC/PAOS}) - W_{FUEL}(bleed, D_{ECS}, 0, \dot{Q}_{VC/PAOS})}{W_{FUEL}(bleed, D_{ECS}, 0, \dot{Q}_{VC/PAOS})} x100$$

The evolution of the most dominant coupling functions (intermediate products and/or feedbacks), at the synthesis/design point, i.e. $\dot{m}_{bleed}$, D_{ECS}, W_{ECS}, $\dot{E}_{VC/PAOS}$, $\dot{Q}_{ECS-VC/PAOS}$, $D_{VC/PAOS}$, $W_{VC/PAOS}$, $\dot{Q}_{VC/PAOS-FLS}$, D_{FLS}, W_{FLS}, D_{FLS}, and W_{AFS}, and D_{AFS} going to or coming from the different sub-systems, is illustrated in Figures 6.11 and 6.1 and 6.2 Their exact values obtained at each iteration of the optimization procedure are given in Tables 6.5a and 6.5b.

Table 6.5a Coupling function values at the synthesis/design point for each iteration of the ILGO approach.

ILGO Iteration No.	D ecs (N)	W ecs (kg)	bleed (kg/s)	D vc/paos (N)	W vc/paos (kg)
1	332	450	0.85	130	410
2	310	360	0.79	150	320
3	306	305	0.65	0	270
4	263	280	0.61	0	250
5	232	270	0.59	0	242
6	222	265	0.57	0	237
7	220	260	0.57	0	232

Table 6.5b Coupling function values at the synthesis/design point for each iteration of the ILGO approach.

ILGO Iteration No.	E vc/paos (kW)	Q ecs-vcpaos (kW)	Q vc/paos-fls (kW)	W fls (kg)	W ps (kg)
1	68	41.3	135	560	1520
2	60	29.8	119	460	1260
3	52	21.1	105	390	1140
4	56	15.6	102	340	1110
5	47	14.2	95	330	1060
6	45	13.4	92	322	1040
7	45	13.3	92	319.5	1032

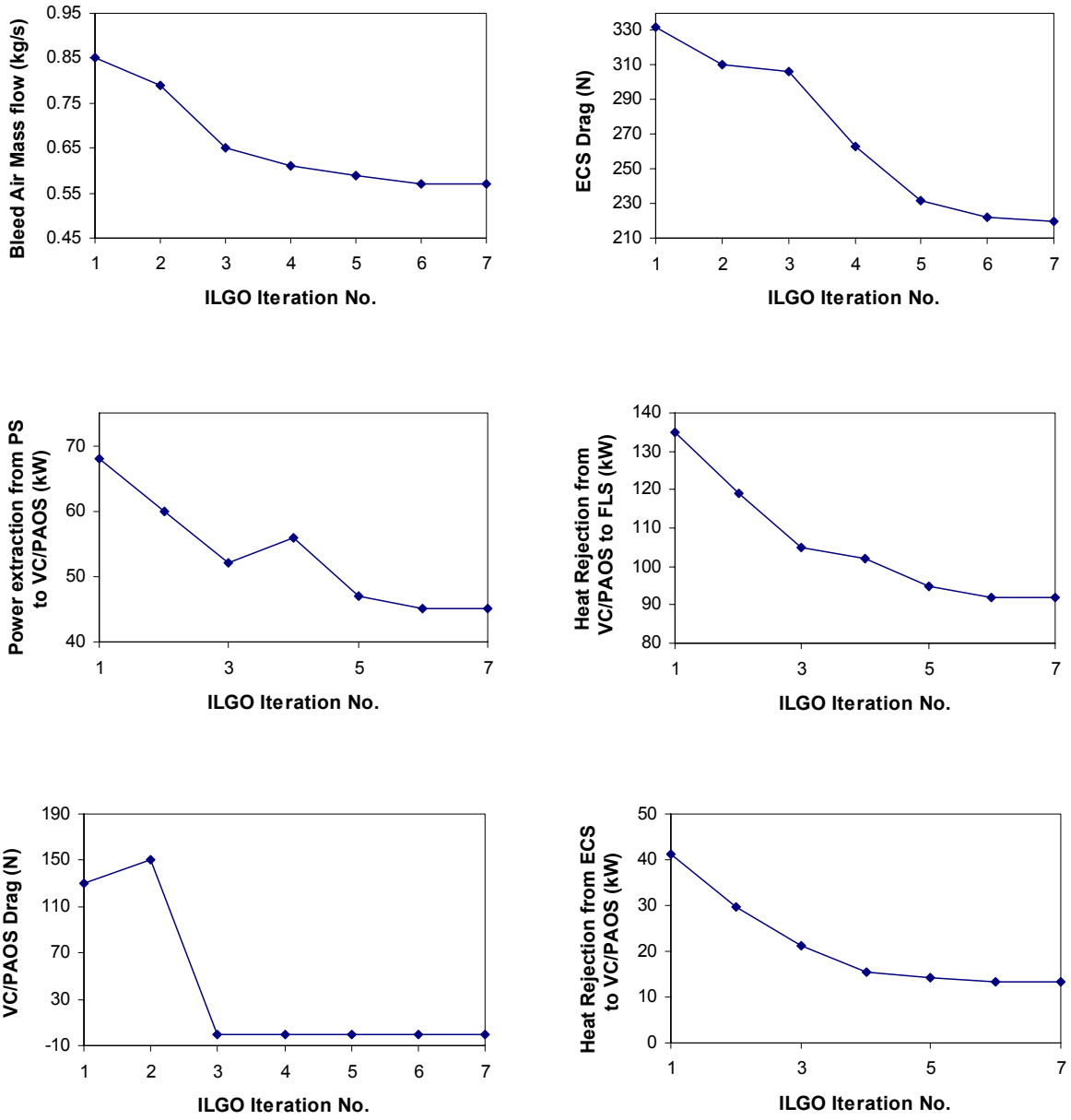

Figure 6.11 Operational coupling function values at the synthesis/design point for each iteration of the ILGO approach.

6.2 Unit-Level and System-Level Optimum Response Surfaces

In order to verify some of the theoretical foundations for the ILGO approach and the reasons for its convergence, both the unit-level and the system-level ORSs were generated. The solutions obtained from the necessary calculations of the shadow prices at each iteration of ILGO made it possible to create the five sub-system unit-level ORSs. In order to generate the advance tactical aircraft system-level ORS, in

addition to the solutions obtained from the necessary calculations of the shadow prices at each iteration of ILGO, each sub-system was optimized for a number of fixed values for their respective coupling functions, these values were keep into reasonable ranges. Each sub-systems optimization results were used in the other sub-system optimization problems so that enough information was generated to make it possible to plot the fourteen-dimensional, system-level ORS.

The complete system-level ORS for the aircraft system consists of thirteen coupling functions (system-level variables) and the objective function (i.e. W_{TO} or W_{fuel}). Such a surface is obviously impossible to depict in one graph. Thus, Figures 6.12 to 6.16 show partial representations of the system-level ORS by plotting three-dimensional graphs of the system-level objective function versus pairs of coupling functions (system-level variables). The System-level ORS shown in Figure 6.16b is the three-dimensional graphical representation of the optimum values of the take-off gross weight and fuel weight versus the coupling function W_{Engine} , which in turn is a PS feedback required by the AFS system-level, unit-based optimization problem. It is obvious that the minimum gross take-off weight and minimum required mission fuel corresponds to the minimum possible PS weight. The flat behavior of the surface is consistent with the fact that the values of the weight related shadow prices remain effectively constant during the optimization process, which agrees perfectly with Muñoz (2000). The system-level ORS shown in Figure 6.12a shows in fact the great impact that sub-system weights have on the gross take-off weight, which increases not only due to an increase in sub-system weights but also due to the additional amount of fuel required to carry the additional weight and the additional fuel itself. Moreover, the increase in weight of any sub-system affects the final weight of at least two of the most important sub-systems, i.e. the PS and AFS, which in turn demands more fuel. The slopes of the system-level ORS in the W_{FLS} and $W_{VC/PAOS}$ directions serve as a confirmation of the sign of their corresponding shadow prices.

The system-level ORS shown in Figure 6.13a is a three-dimensional graphical representation of the optimum values of the gross take-off weight with respect to the FLS weight and the ECS weight. These in turn are feedbacks required by the PS and AFS unit-level and system, level, unit based optimization problems. Based on what was stated above, it comes as no surprise that the global (system-level) optimum corresponds to the minimum FLS and ECS weights. Nevertheless, it is worth noticing that planar behavior of the ORS results from two coupling functions from two

different sub-systems, which do not share any direct product or feedback. The flat behavior of the surface is consistent with the fact that the values of the weight related shadow prices remain effectively constant during the optimization process, which agrees perfectly with Muñoz (2000).

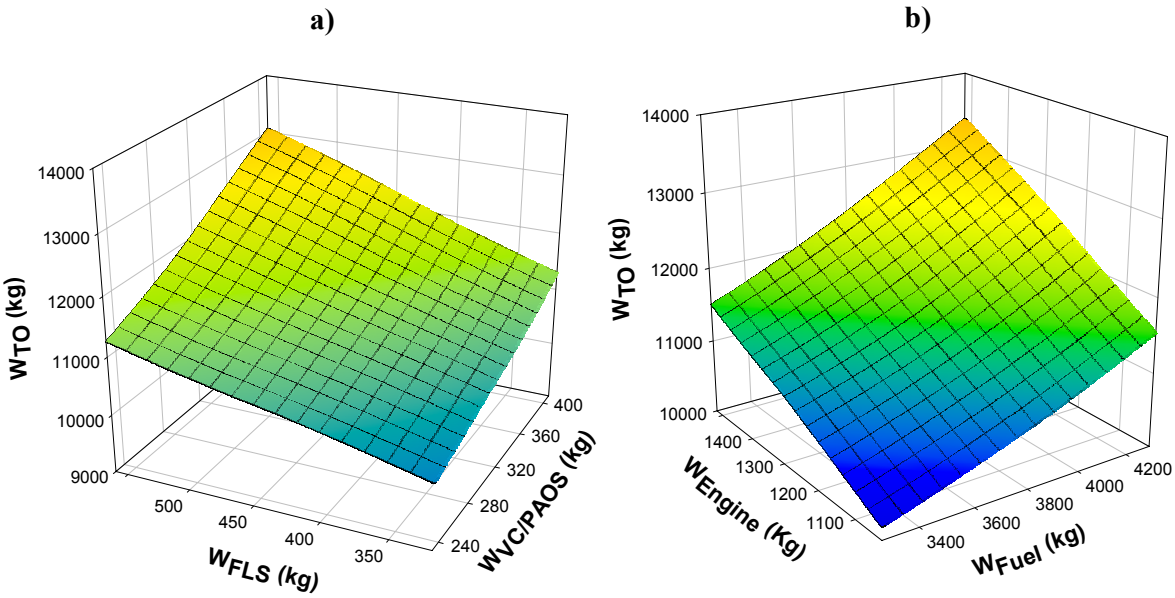

Figure 6.12 **a)** The aircraft system-level ORS in the $W_{VC/PAOS}$ and W_{FLS} dimensions; **b)** Objective function variations in the W_{Engine} dimension.

The system-level ORS shown in Figure 6.13b shows again the impact that sub-system weighs, i.e. VC/PAOS and ECS weights, has on the gross take-off weight, which increases not only are due to the increase in the sub-system weights, but also due to the additional amount of fuel required to carry the additional weights and the additional fuel itself. Moreover, the increase in weight of any sub-system affects the final weight of at least two of the most important sub-systems, i.e. the PS and AFS, which in turn demands more fuel. The slopes of the system-level ORS in the W_{ECS} and $W_{VC/PAOS}$ directions serve as a confirmation of the sign of their corresponding shadow prices.

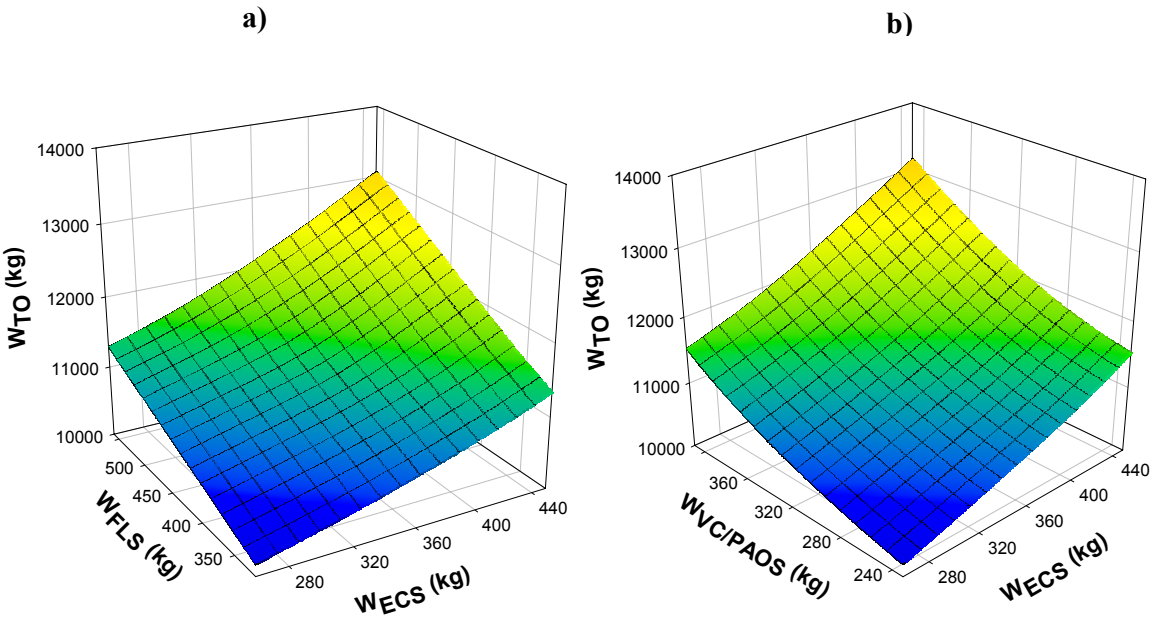

Figure 6.13 **a)** The aircraft system-level ORS in the W_{ECS} and W_{FLS} dimensions; **b)** The aircraft system-level ORS in the $W_{VC/PAOS}$ and W_{ECS} dimensions.

Figure 6.14a shows the system-level objective function, W_{TO}, as a function of the ECS weight and drag. This figure has several interesting features. The first is the fact that the synthesis/design space in the ECS drag and weight dimensions is not only convex but shows flat behavior, typical of a linear system[68]. This is to be expected since the partial derivatives of the objective function (W_{TO}) with respect to the intermediate products and feedbacks (i.e. the shadow prices) are basically constant throughout the entire optimization process. The second important feature is that Figure 6.14a shows that the impact of the ECS weight on the objective function is greater than that of the ECS drag. The best solution is the one with the lowest possible weight. This, again, is to be expected given the large value of the weight marginal shadow prices when compared to that for the bleed and drag. This may explain the relatively minor effect of ECS drag, although there is clearly a tendency to have smaller W_{TO} values with low drag for a given weight. The effect of drag is not completely independent of weight, however, since ECS drag implies the need for a bigger and, therefore, heavier ram-air scoop inlet. Furthermore, a larger ram-air duct

[68] It must be stressed that the objective function is linear with respect to the intermediate products and feedbacks and not with respect to the individual sub-system independent variables.

leads to increased ram air flow and possibly larger heat exchangers. It is important to note that the linearity mentioned above was obtained by representing the intermediate products and feedbacks with properties that were non-exergy or even non-energy-based. The properties used resulted not only in linear behavior but also eased calculation of the shadow prices. This essential feature of a non-energy coupling function propelled the possibility of linking the energy based sub-system syntheses/designs to the non-energy based sub-system syntheses/designs (e.g., to the AFS).

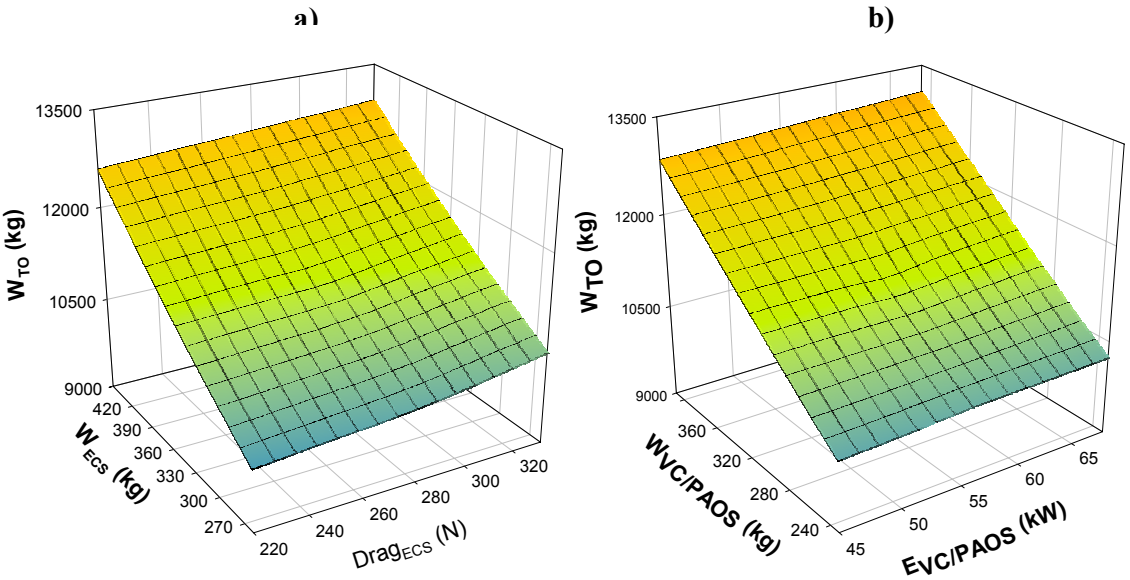

Figure 6.14 **a)** The aircraft system-level ORS in the W_{ECS} and Drag $_{ECS}$ dimensions; **b)** The aircraft system-level ORS in the $W_{VC/PAOS}$ and VC/PAOS Power Extraction ($E_{VC/PAOS}$) dimensions.

Figure 6.14b shows how the synthesis/design space in VC/PAOS power extraction and weight dimensions is not only convex but shows a flat behavior, confirming the linear behavior of the total aircraft system. As before this is expected since the shadow prices showed a linear behavior throughout all the coupling function ranges. Figure 6.14b also shows the much larger effect that VC/PAOS weight has on the system-level objective function compared to that exerted by the electrical power extraction. This means that the optimum VC/PAOS is that with the lowest possible weight, which is confirmed by the sign and magnitude of the weight shadow price. Figure 6.14b presents a planar shape regardless of the different natures of the coupling

function used, one non-exergy or non-energy-based (i.e. sub-system weight) and the other energy-based (electrical power extraction from the PS). All this lends credence to the suitability of incorporating non-energy sub-systems in with energy sub-systems during the ILGO systems optimization process.

As was mentioned in *Chapters 4* and *5*, two synthesis decision variables were introduced into the VC/PAOS system-level, unit-based optimization problem. These were the location and placement of the ram-air heat exchanger. The placement possibilities were three. The first was to allocate it between the bleed/PAO heat exchanger and the fuel/PAO heat exchanger. The second was to allocate it between the fuel/PAO heat exchanger and the condenser. Finally, the third option was not to have a ram-air heat exchanger at all, which means that all the rejected heat goes to the FLS through the fuel/PAO heat exchanger. This has a positive effect on the VC/PAOS by reducing its total weight. However, it raises the total weight of the FLS, since a bigger fuel/PAO heat exchanger is required. The final optimization results show that the global (system-level) optimum is reached for the VC/PAOS with no ram-air heat exchanger. This is explained by the fact that this configuration avoids ram-air ducts and prompts the optimal usage of the fuel as a heat sink.

The purpose of introducing synthesis decision variables into the VC/PAOS system-level, unit-based optimization problem was to prove the capability of successfully using the ILGO approach in discontinuous synthesis/design spaces. Two important characteristics of ILGO which permit this are the capability ILGO has of measuring the effects that changes in any sub-system have on the others sub-systems and on the global objective function, and the fact that ILGO works perfectly with genetic algorithms, which can help to keep the optimization process from falling into local optima. An additional synthesis decision variable used was the wing type (i.e. trapezoidal or delta). The global (system-level) optimum was reach for a trapezoidal-shaped wing (see Figure 6.19 at the end of the chapter) with a relative low aspect ratio (an AR of 3) which perfectly agrees with well-known design practice for a swept wing. A trapezoidal wing with low taper ratio offers the ideal balance between drag generation, both at subsonic and supersonic mission segments, and lift production at low Mach number mission segments. In the case of a trapezoidal wing, the taper ratio, λ, was considered as a decision variable for which the optimum value found was 0.24. For a supersonic fighter, a delta wing, at least at first, may look as a good option. However, considering the mission requirements at hand, a delta wing will reduce the

drag generation at supersonic conditions but at very low Mach number segments, e.g., take-off and landing, this king of wings requires a bigger reference area, which entails an augmentation in the airframe weight, and thus, a higher gross take-off weight. Moreover, a trapezoidal wing provides better maneuverability during dog fights. Thus, one can see how the optimum aerodynamic variable values found perfectly agree high performance aircraft theory and modeling, and how ILGO approach is well suited to handling non-continuous synthesis/design spaces.

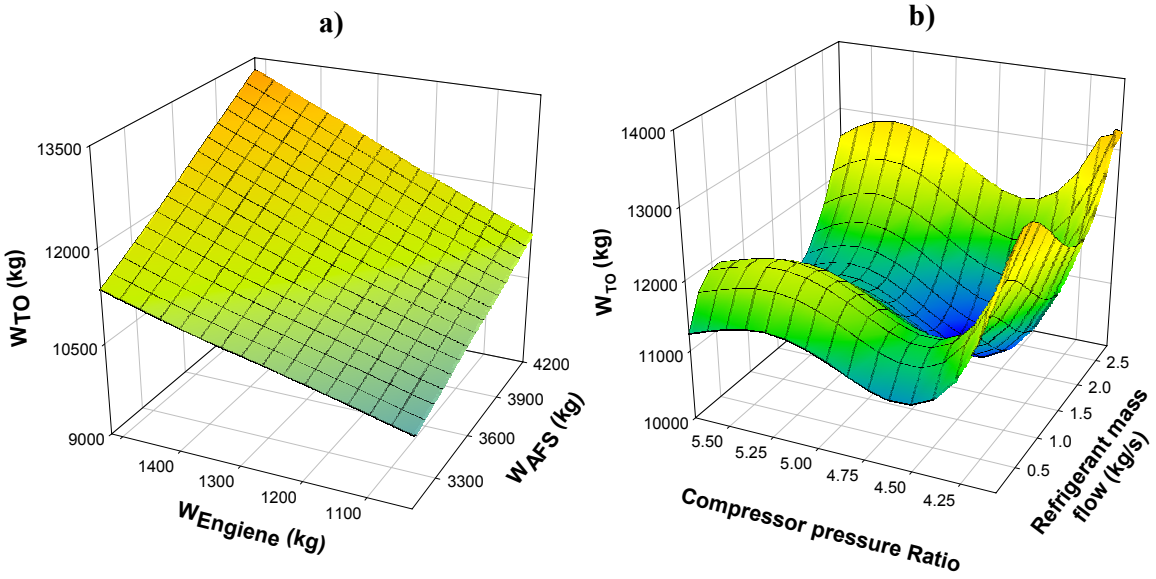

Figure 6.15 **a)** The aircraft system-level ORS in the W_{AFS} and W_{Engine} dimensions; **b)** The gross take-off weight versus design vapor compressor pressure ratio and refrigerant mass flow.

Once more it should be stressed that the convergence of ILGO depends on the convexity of the ORS independently of whether the actual synthesis/design space for each of the units, i.e. the behavior of the objective function with respect to the local decision variables, is convex or not. Figure 6.15a shows the system-level ORS for gross take-off weight versus the AFS and PS weight dimensions. AS already mentioned, the planar shape makes the optimization process converge faster. To better observe this, consider Figure 6.15b, which shows the behavior of the gross take-off weight as a function of the CV/PAOS design vapor compressor pressure ratio and refrigerant mass flow for the optimum VC/PAOS weight, drag and power extraction.

Also consider Figure 6.16b, which depicts the change in gross take-off weight due to the ECS versus ECS primary heat exchanger hot-side length and ECS primary heat exchanger cold-side length. Figure 6.16a shows the behavior of gross take-off weight as a function of the PS high-pressure turbine pressure ratio and the PS low-pressure turbine pressure ratio. It should be noticed, in particular for this figure, the planar characteristic of the surface. These figures were constructed with all of the feasible solutions found during the last iteration of ILGO for the complete problem. These figures, of course, are not a complete representation of the synthesis/design space because it does not contain all of the synthesis/design and operational variables. Obviously, a graphic representation with the same number of dimensions as the number of decision variables is impossible to create. However, despite the planar behavior exhibited in Figure 6.16a, Figures 6.15b and 6.16b hint at the possible non-convexity and non-linearity of the objective function with respect to the synthesis/design variables. The rapid convergence of ILGO was not compromised by the apparent non-convexity and non-linearity of the synthesis/design space.

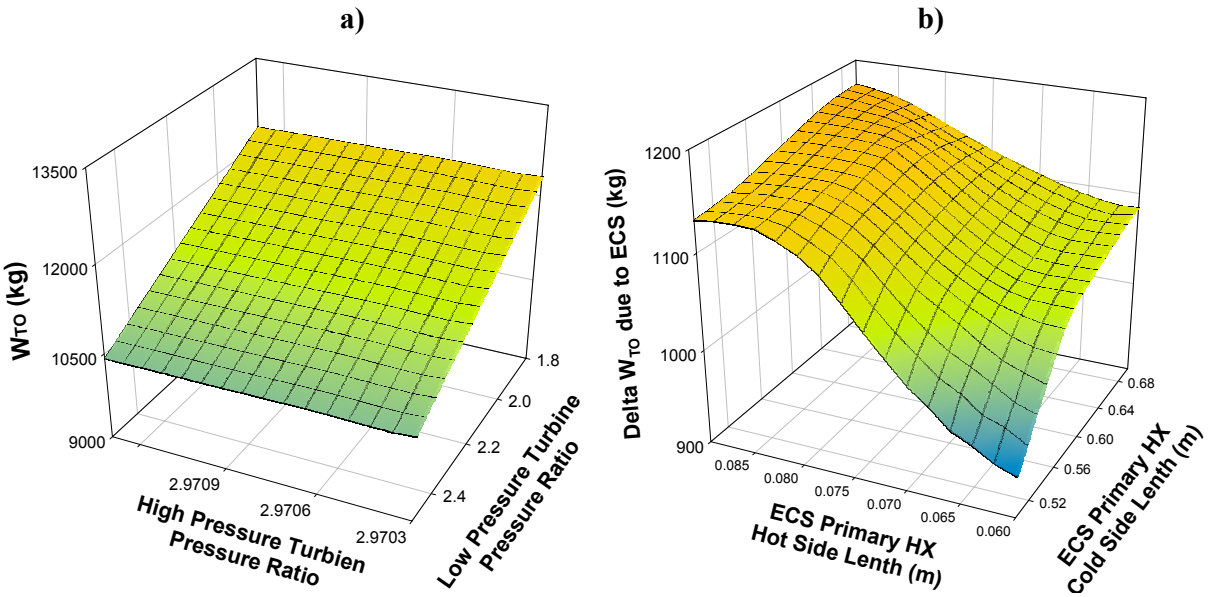

Figure 6.16 **a)** Gross take-off weight versus PS high-pressure turbine pressure ratio and PS low-pressure turbine pressure ratio; **b)** Delta gross take-off weight due to the ECS versus ECS primary heat exchanger hot-side length and ECS primary heat exchanger cold- side length.

The type of behavior above mentioned with respect to the decision variables as opposed to coupling functions underlines the importance of the choice of optimization algorithm(s) used to solve the problem. As indicated in earlier chapters, a genetic algorithm was used in this work followed by a gradient-based algorithm. Genetic algorithms are classified among the so-called global optimization methods[69] because of their ability to escape local minima when properly conditioned (Olsommer, von Spakovsky, Farrat, 1999a). It was found in Muñoz (2000) that using a purely gradient-based method prompts the optimization process to fall into local minima. Additionally, the hypothesis that the synthesis/design space is non-convex is somewhat substantiated by the clear tendency that gradient-based algorithms have of getting trapped in local minima.

6.3 Most Promising Sub-systems Syntheses/Designs and their Off-Design Feasibility

The time decomposition approach presented by Muñoz and von Spakovsky (2000), which is used in this work, has to be implemented in two stages. First, a synthesis/design point is chosen to guarantee that the most demanding conditions are met. In the case of the advanced tactical aircraft, this means the most stringent mission segment for each sub-system. It has to be pointed out that each sub-system may be under its most critical condition at different mission segments, i.e. different synthesis/design points for each sub-system. Notice that in the case of the PS and the FLS no time decomposition was used. Thus, the optimum operational decision variables for the whole mission were determined simultaneously with the synthesis/design decision variables. For the AFS, no time decomposition was used since no operational decision variables were chosen for the system-level, unit-based optimization problem. Thus, the synthesis/design optimization and flight dynamics performance evaluation were executed all at once, and the design and operational dependent variables determined using the flight dynamics software built in-house. The effects of any change in the AFS on other sub-systems operational variables are defined by the AFS coupling functions and shadow prices

For the cases of the ECS and VC/PAOS, an initial synthesis/design optimization for that most stringent point yields a set of feasible solutions which can then be evaluated at all of the other operating conditions (i.e. mission segments). Based on the

[69] See footnote 14.

instantaneous objective function value at the synthesis/design point, a ranking of feasible solutions can be created. This attribute is enhanced by the fact that the sub-system most influential aspect in the definition of the system-level, unit-based optimum is its weight, which is determined during the synthesis/design point optimization process. In general, however, the best solutions at the synthesis/design point do not necessarily lead to the lowest overall objective function value when all of the operating conditions are taken into account (e.g., see Oyarzabal et al., 2002).

The basis of the ILGO approach (A and B) is to find values of the coupling functions that lead to a decrease in the overall objective function - i.e. in a dynamic problem, a time-integrated value for the weight or fuel functions. In the discretized version of the problem, which has been used throughout this work, the latter quantity is the sum of the individual impacts of the coupling function changes (in rate form) in terms of the objective function rate multiplied by the length of time during which that variation takes place. Understanding these ILGO features is important for assessing which of the feasible solutions can be considered "promising" and, therefore, suitable for the time-integrated optimization with respect to the operational variables. Based on these comments, it becomes clear that various considerations as given below need to be taken into account in order to make such a selection. The first aspect to be considered is the length of the time of the synthesis/design versus that of the off-design segments. Naturally, the shorter the operation under the most demanding conditions is, the least likely it is for the best solutions at the synthesis/design point to lead to an optimum synthesis/design when all time segments are taken into account.

Secondly, one must consider the instantaneous impact that changes in the coupling functions have in terms of the overall objective. This impact is in turn the product of two quantities: the shadow prices and the change in the coupling function (intermediate product or feedback). As mentioned above, once the optimization at the synthesis/design point has been carried out and a number of candidate solutions have been identified, it is possible to compute what the intermediate product / feedback (coupling function) changes are at all operating conditions. With this information and the shadow prices, it is then a straightforward matter to rank the feasible solutions based on their time-integrated behavior.

A graphical representation of the impact of the coupling functions (i.e. shadow prices) such as those given in Figures 6.8 through 6.13 becomes very important for identifying promising solutions. These figures show the change in the overall

objective function that can be achieved by varying the intermediate products at various instances of time. Once a potential synthesis/design has been identified (by solving the optimization problem at the synthesis/design point, for example), one can take the intermediate products / feedbacks (ECS weight and drag and bleed air in this case, and VC/PAOS weight and power extraction and drag) and easily evaluate their individual contributions to, say, W_{TO} or W_{FUEL}, in Figure 6.8. In the case of the ECS, once a synthesis/design is given, the weight and drag for each mission segment are known and the only remaining degree of freedom is the amount of bleed air, which is known with a maximum error of 10%. In the case of the VC/PAOS, it is even easier to evaluate the prospects for optimum solutions. This is because the weight and drag shadow prices are the same as those for the ECS,. Thus no additional computation time need to be expended. Regarding the electrical extraction power there are two important characteristics. Its variation with respect to mission segments is between 15% and 20%. Besides, as was determined before, its impact on the global objective function is small. This information is sufficient to evaluate all of the potential solutions very inexpensively, if desired. This is not necessary, however, because of the information inherent in the shadow prices. To begin with, the shadow prices associated with the ECS and VC/PAOS weight is much higher than that of drag and bleed and electrical power extraction. This is true in all time segments. Thus, for the ECS, a candidate solution with high weight would be considered promising only if it had a really low momentum drag and bleed. In the same way, for the VC/PAOS a candidate solution with high weight would be considered promising only if it had a really low momentum drag and electrical power extraction. In turn, the greatest contributor to momentum drag is the inlet area. Based on this analysis, a synthesis/design with a comparatively large weight could potentially lead to the best possible solution only if it had low inlet area. The amount of bleed air and power extraction remains within tight ranges and, therefore, need not be studied.

Tables 6.6 and 6.7 show the top four solutions of the synthesis/design segment (scc2) for the ECS and VC/PAOS for the last ILGO iteration respectively. Tables 6.8 and 6.9 show how these solutions perform when the complete mission (i.e. integrated over the entire mission) is carried out. Notice that for the ECS and VC/PAOS, the ranking remains invariant due to the fact that the best solution at the synthesis/design point has both the lowest possible weight and inlet areas. Tables 6.3 and 6.4 show the optimal geometry and weight values, respectively, for the FLS, PS and AFS. Table

6.10 shows the last ILGO iteration rank for the FLS. Despite the fact that no time decomposition was used, one can see that the system-level, unit-based optimum was reach for the lowest weight and inlet area.

Table 6.6 Top four solutions for the ECS based on the synthesis/design segment (scc_2).

			Solution Ranking			
			1	2	3	4
Primary heat exchangers	L_b	Hot-side length (m)	0.505	0.511	0.508	0.520
	L_r	Cold-side length (m)	0.060	0.063	0.060	0.060
	L_n	Non-flow length (m)	0.504	0.508	0.502	0.502
	Fin_{hot}	Heat exchanger fin number: hot sides	14	16	19	19
	Fin_{cold}	Heat exchanger fin number: cold sides	14	16	16	17
Secondary heat exchangers	L_b	Hot-side length (m)	0.505	0.508	0.512	0.501
	L_r	Cold-side length (m)	0.061	0.066	0.062	0.060
	L_n	Non-flow length (m)	0.508	0.500	0.513	0.503
	Fin_{hot}	Heat exchanger fin number: hot sides	14	14	18	19
	Fin_{cold}	Heat exchanger fin number: cold sides	16	16	18	17
Air cycle machine	PR_{cp}	Compressor design pressure ratio	2.60	2.8	2.7	2.8
	PR_{tb}	Turbine design pressure ratio	8.56	7.9	6.5	6.4
Regenerative heat exchangers	L_b	Hot-side length (m)	0.300	0.300	0.300	0.306
	L_r	Cold-side length (m)	0.150	0.151	0.155	0.179
	L_n	Non-flow length (m)	0.300	0.300	0.303	0.308
	Reg_1	Existence-nonexistence	0	0	0	0
	Reg_2	Existence-nonexistence	1	1	1	1
Ram air inlet, outlet 1	$A_{1,}$	Areas of inlet, outlet (cm^2)	103.0	118	123	135
Ram air inlet, outlet 2	A_2	Areas of inlet, outlet (cm^2)	103.0	125	135	148
W_{ECS}/g		kg	237	249	261	268

Table 6.7 Top four solutions for the VC/PAOS based on the synthesis/design segment.

			Solution Ranking			
			1	2	3	4
Bleed air / PAO heat exchanger	L_b	Bleed-side length (m)	0.30	0.30	0.30	0.30
	L_r	PAO-side length (m)	0.15	0.15	0.15	0.15
	L_n	Non-flow length (m)	0.30	0.30	0.30	0.30
Condenser	L_b	Vapor-side length (m)	0.302	0.304	0.302	0.31
	L_r	PAO-side length (m)	0.16	0.16	0.17	0.16
	L_n	Non-flow length (m)	0.306	0.306	0.308	0.309
	Fin_{hot}	Heat exchanger fin number: hot sides	16	16	16	18
	Fin_{cold}	Heat exchanger fin number: cold sides	14	14	16	19
Evaporator	L_b	PAO-side length (m)	0.35	0.37	0.38	0.39
	L_r	Vapor-side length (m)	0.17	0.17	0.176	0.17
	L_n	Non-flow length (m)	0.34	0.34	0.374	0.382
	Fin_{hot}	Heat exchanger fin number: hot sides	16	16	18	19
	Fin_{cold}	Heat exchanger fin number: cold sides	16	16	16	20
Ram air / hot PAO heat exchanger	L_b	Bleed-side length (m)	0	0	0	0.305
	L_r	ram-side length (m)	0	0	0	0.156
	L_n	Non-flow length (m)	0	0	0	0.304
	Fin_{hot}	Heat exchanger fin number: hot sides	Na	Na	Na	18
	Fin_{cold}	Heat exchanger fin number: cold sides	Na	Na	Na	18
Vapor Compressor	Pr	pressure ratio vapor compressor	3.35	3.38	3.51	3.48
	m_v	vapor mass flow(kg/s)	1.07	1.10	1.13	1.19
Hot PAO cycle	m_{HPAO}	Hot PAO loop mass flow	1.61	1.63	1.56	1.60
	V_5	Fuel / hot PAO heat exchanger bypass valve position	0.024	0.028	0.016	0.017
	V_4	Bleed-air/hot-PAO heat exchanger bypass valve position	0.058	0.048	0.039	0.037
	V_2	Vapor/hot-PAO heat exchanger bypass valve position	0.070	0.060	0.023	0.027
Ram air inlet	A_i	Area of inlet, outlet (cm^2)	0	0	0	120
Ram-air/hot-PAO heat exchanger	*onoff*	Allocate or not ram-air/hot-PAO heat exchanger	0	0	0	1
W_{ECS}/g		Kg	232	238	252	269

Table 6.8 Optimum ECS weight results.

Design point Rank	Mission Rank	ΔW_{TOECS}/g (kg)	$\Delta W_{FUELECS}$/g (kg)	$\Delta W_{FUELbleed}$/g (kg)	$\Delta W_{FUELdecs}$/g (kg)	$\Delta W_{FUELwecs}$/g (kg)	W_{ECS}/g (kg)
1	1	800	563	76	52	435	237
2	2	848	599	80	62	457	249
3	3	885	624	77	68	479	261
4	4	920	652	85	74	493	268

Table 6.9 Optimum VC/PAOS weight results.

Design point Rank	Mission Rank	$\Delta W_{Tovc/PAOS}$/g (kg)	$\Delta W_{FUELVC/PAOS}$/g (kg)	$\Delta W_{FUELpower}$/g (kg)	$\Delta W_{FUELdvc/paos}$/g (kg)	$\Delta W_{FUELwvc/paos}$/g (kg)	$W_{VC/PAOS}$/g (kg)
1	1	622.2	390.2	32	0	358.2	232
2	2	634.5	396.5	34	0	367.5	238
3	3	675.1	423.1	34	0	389.1	252
4	4	745	476	37	24	415	269

6.4 Results for the Final Optimum System Synthesis/Design

6.4.1 FLS Optimal Performance

The challenge on the FLS optimization is that of finding out the sub-system synthesis/design and operational condition, which yield the minimum sub-system weight, drag generation, and power consumption, while meeting the sub-system requirements as energy carrier and heat sink. Figure 6.17 shows the fuel tank temperature versus time. This figure shows the advantage of using the fuel as a heat sink according to the FLS configuration and control strategy used in this work. A number of interesting characteristics should be pointed out. Notice that at the beginning of the mission fuel consumption is higher than the require fuel flow through any of the FLS heat exchangers. Thus, all the fuel heated up going through the sub-system is directed to the PS and burned and no fuel comes back to the tank, avoiding any heating (i.e., no temperature rise). No extra fuel is passed through the ram/fuel heat exchanger because the ram air cooling capacity at low Mach number is extremely low.

Table 6.10 Top four solutions for the FLS based on the synthesis/design segment (scc_2).

			Solution Ranking			
			1	2	3	4
Fuel/oil heat exchanger	L_b	Oil-side length (m)	0.500	0.505	0.51	0.515
	L_r	Fuel-side length (m)	0.06	0.063	0.067	0.072
	L_n	Non-flow length (m)	0.500	0.504	0.505	0.509
	Fin_{hot}	Heat exchanger fin number: hot side	16	16	16	20
	Fin_{cold}	Heat exchanger fin number: cold side	14	14	16	20
Fuel/PAO heat exchanger	L_b	PAO-side length (m)	0.60	0.608	0.612	0.63
	L_r	Fuel-side length (m)	0.11	0.114	0.119	0.121
	L_n	Non-flow length (m)	0.60	0.601	0.60	0.623
	Fin_{hot}	Heat exchanger fin number: hot side	14	15	17	18
	Fin_{cold}	Heat exchanger fin number: cold side	14	14	12	18
Fuel/ram air heat exchanger	L_b	Fuel-side length (m)	0.38	0.382	0.389	0.398
	L_r	Ram-side length (m)	0.17	0.178	0.173	0.187
	L_n	Non-flow length (m)	0.36	0.358	0.367	0.376
	Fin_{hot}	Heat exchanger fin number: hot side	14	14	16	17
	Fin_{cold}	Heat exchanger fin number: cold side	14	14	16	16
Fuel / hydraulic heat exchanger	L_b	Hyd-side length (m)	0.37	0.371	0.369	0.379
	L_r	Fuel-side length (m)	0.15	0.155	0.159	0.176
	L_n	Non-flow length (m)	0.38	0.384	0.380	0.398
	Fin_{hot}	Heat exchanger fin number: hot side	16	15	18	20
	Fin_{cold}	Heat exchanger fin number: cold side	14	15	18	20
Ram air inlet	A_i	Area of inlet (cm^2)	140.2	143	149	163.3
W_{ECS}/g		Kg	319.5	328	341	346

After theses segments, the rate of temperature rise rate is small, since the fuel mass at the fuel tank is still big enough. During the combat segments the fuel consumption is also large enough to deplete out all the fuel used by the FLS, thus, again the fuel tank temperature remains constant. This, obviously has the additional advantage of raising the fuel temperature entering the PS. No extra fuel is passed by the ram/fuel heat exchanger during the supersonic mission segments since at these conditions the ram air cooling capabilities are particularly small.

After the combat segments, which have elevated fuel consumption, the amount of fuel in the tank is greatly diminished. Thus its heat sink capabilities are greatly reduced. Therefore, the fuel tank temperature increment rate is particularly high. However, this coincides with the mission segments during which the ram-air cooling capabilities are sufficient. No fuel tank temperature decrease occurs at any mission segment, showing in this way that indeed the ram/fuel heat exchanger sizing is optimum, i.e. no unnecessary incoming ram-air. Additionally, the fuel tank usage as a heat sink is maximized, since the final fuel temperature is the highest possible, without exceeding the vapor formation temperature.

6.4.2 AFS Optimal Geometry and Constraint Analysis Space

Figure 6.18 shows the constraint space for both the optimum AFS geometry and the baseline AFS geometry (i.e. the so-called optimum AFS geometry at the first ILGO iteration). One can see the evolution of the thrust load (T_{SL}/W_{TO}) and wing load (W_{TO}/S_{ref}). The optimum AFS geometry entails a reduction of these two factors (see Table 6.11). In both cases, the three most stringent mission segments are the supersonic penetration, combat turn 2, and take-off. The landing segment sets up the right limit for the synthesis/design space. In general, the aerodynamic variables have multiples effects on the global objective function. These effects are well known for the total system at hand. However, the magnitudes of these effects are not simple to establish. Thus, variations in a given aerodynamic variable may yield a reduction in the component weight, but at the same time an augmentation of the generated drag, which entails an increase in the PS size and fuel or even an unfeasible aircraft. Therefore, the usage of an inclusive aero-thermodynamic software like the one developed in-house is absolutely necessary to be able to evaluate the effects that aerodynamic variables changes have on flight performance, take-off gross weight, fuel weight, component weight, etc. The optimum AFS geometry is depicted in Figure 6.19. As explained above (see section 6.2), a trapezoidal-shaped wing led to the optimum.

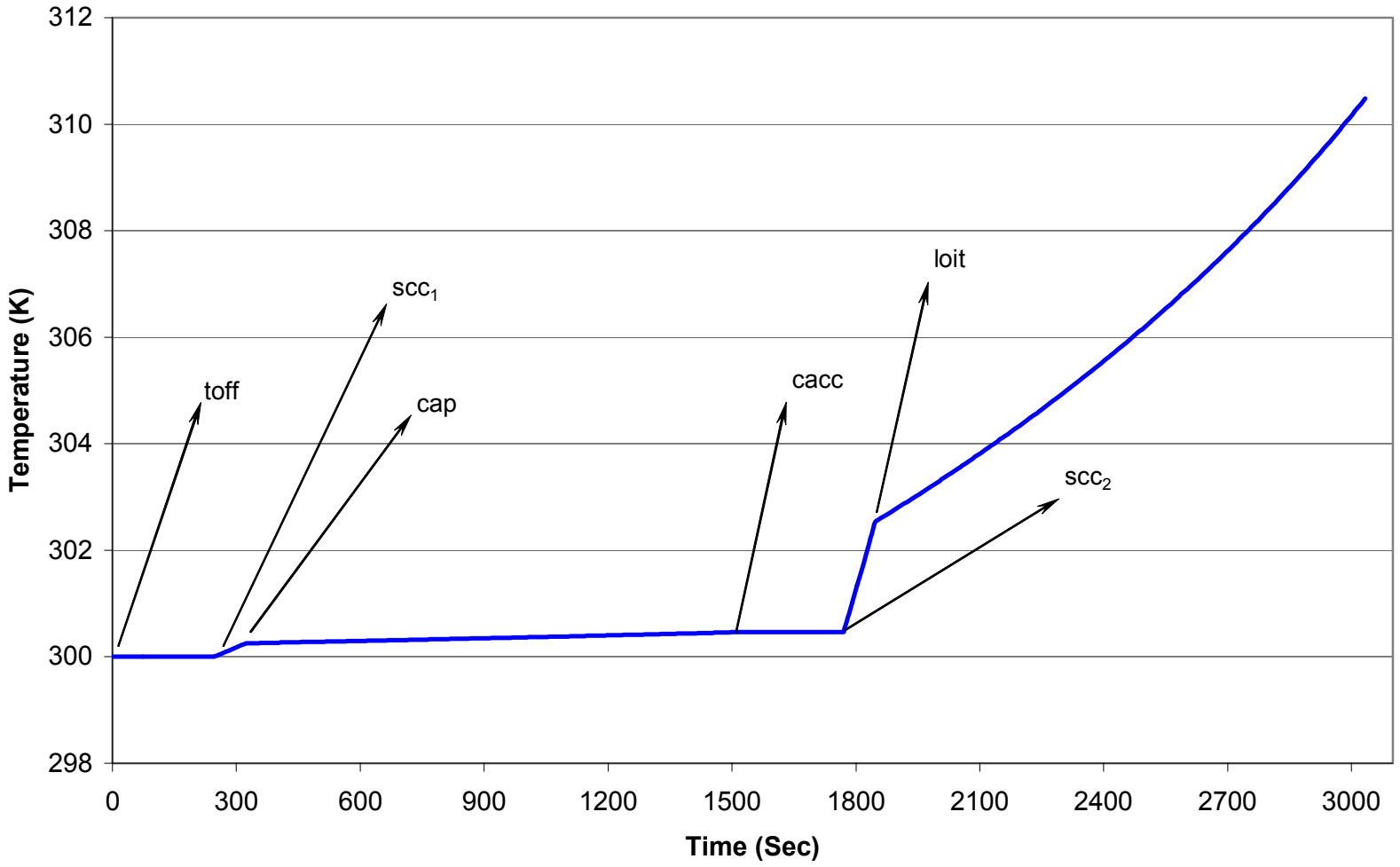

Figure 6.17 Fuel tank temperatures versus time.

Table 6.11 AFS "so-called optimum" geometry for the first ILGO iteration and the optimum geometry found in the last ILGO iteration.

	Optimum	**Baseline**
W_{TO}/S_{ref} (lb/ft^2)	61.49	64.3
T_{SL}/W_{TO}	1.13	1.27
W_{TO}, kg (lb)	10180 (22396)	13100 (28820)
S_{ref} (ft^2)	364.2	448
T_{SL}, kg (lb)	11503 (25306)	16637 (36600)
W_{fuel} (kg)	3270	4300
W_{AFS} (kg)	3100	4200
Wing AR	3.046072	2.506
Wing t/c	0.077494	0.11
Wing λ	0.240061	0.3
Wing Λ	31.05784	39.06
Wing S_f/S_{ref}	0.75	0.75
Wing C_{L}_design	0.5	0.6
Tail T_AR	5.004859	5
Tail T_t/c	0.12	0.1
Tail T_λ	0.461185	0.4

For the aspect ratio (AR) any increase entails a reduction in the generated drag due to lift, since the slope of the lift curve increases (see equation 4.16) and the lift coefficient decrease (see equation 4.12). These are positive effects on the system. However, it causes a higher weight to the wing component (see Table 4.8). Therefore, the direction and magnitude of variations in the aspect ration with respect to the baseline, which produces a reduction in the global objective function, is not evident. Solving equation (4.25) and (4.26) for the combat turn 2 and supersonic penetration, one can see that an increase in the aspect ratio will pull the constraint curves down. The same kind of analysis is valid for any other aerodynamic variable.

Figure 6.20 shows the characteristic slope of the lift curve for the actual wing ($C_{L\alpha}$), which is a measure of the capability of the actual wing of producing more lift

without producing more aerodynamic inefficiency. This is not the airfoil lift curve slope ($C_{l\alpha}$), which is a characteristic of the airfoil and is the same for a wing regardless of the aspect ratio, wing sweep, or any other variable. One can see how the baseline wing presents a lower lift coefficient curve for the whole Mach number range. The wing is considered to be in purely supersonic flight when the wing leading edge is supersonic, i.e. the Mach cone angle is greater than the leading-edge sweep (see equation (4.22)). The actual lift curve for a wing in supersonic flight is difficult to predict without the use of sophisticated software or a reliable database. In this work, the normal-force slope curves were used to compute the slope of the lift curve (Raymer, 2000; Hoak-Ellison, 1982). A vast number of fitted equations were developed from the normal-force slope curves. These charts estimate the slope of the normal force coefficient, C_N, i.e. the lift curve slope in a direction perpendicular to the wing. For low angles of attacks, which are usually the case for supersonic flight, this is approximately the lift curve slope.

Figure 6.21 shows the optimum suction factor curve as a function of the design lift coefficient and the actual lift coefficient, for the firs and last ILGO iteration. The lower the gross take-off weight, the lowest the optimum C_L design, which provides a higher suction factor at low lift coefficients, which is in turn the actual range for most mission segments and for most of the mission time. Figure 6.22 depicts the characteristic induced drag factor curve as a function of the Mach number and the lift coefficient for the airframe at the first and last ILGO iteration. K_0 corresponds to the point where the suction factor is a minimum and the lift coefficient is a maximum, which yields the maximum possible induced drag factor for a given airframe geometry. K_{100} corresponds to the point where the suction factor is a maximum and the lift coefficient is a minimum. This yields the minimum induced drag factor. One can see how the optimum geometry generates a lower induced drag factor at all Mach numbers and for all lift coefficients. The induced drag factor at supersonic conditions is not a function of the suction factor. At this condition K_0 equals K_{100} which is inversely proportional to the slope of the lift curve, $C_{L\alpha}$. Thus, Figure 6.19 shows clearly how the slope of the lift curve is lower for the baseline airframe, resulting in, as expected, a higher induced drag factor for this geometry.

The optimum Advanced Tactical Aircraft meets the mission requirements for all segments according to the request for proposal (RFP) presented in Chapter 4, which was taken from Mattingly, Heiser, and Daley, 1987. In their work, the authors present

a final gross take-off weight of 23,800 lb. In this research work, the optimum take-off gross weight was 22,396 lb, i.e. 1404 lb lighter. This result is explained by the fact that in this research work, aerodynamic optimization is performed in conjunction with engine design optimization and, of course, the other aircraft sub-systems. In their work, the authors make some educated decisions about the aerodynamic variables and use very simplified diagrams to compute parameters such as the lift coefficient factor (K_1) and the parasitic drag (C_{D0}). Table 6.12 shows a comparison between the optimum found in this research work and the aircraft proposed by Mattingly, Heiser, and Daley (1987). Table 6.12 shows a significant improvement in the final gross take-off weight and total fuel weight. At the same time, this comparison validates the results presented in this thesis.

Table 6.12. Comparison between the optimum ATA and the aircraft proposed by Mattingly, Heiser, and Daley (1987).

	Optimum	**Mattingly, Heiser, and Dalley (1987)**
W_{TO}, (lb)	22,396	23,800
$W_{Fuel,}$ (lb)	7,194	7,707
W_{TO}/S_{ref} (lb/ft^2)	61.49	64
T_{SL}/W_{TO}	1.13	1.27
S_{ref} (ft^2)	364.2	371.87
T_{SL} ,kg (lb)	25306	30226
W_{AFS} (kg)	3100	4200

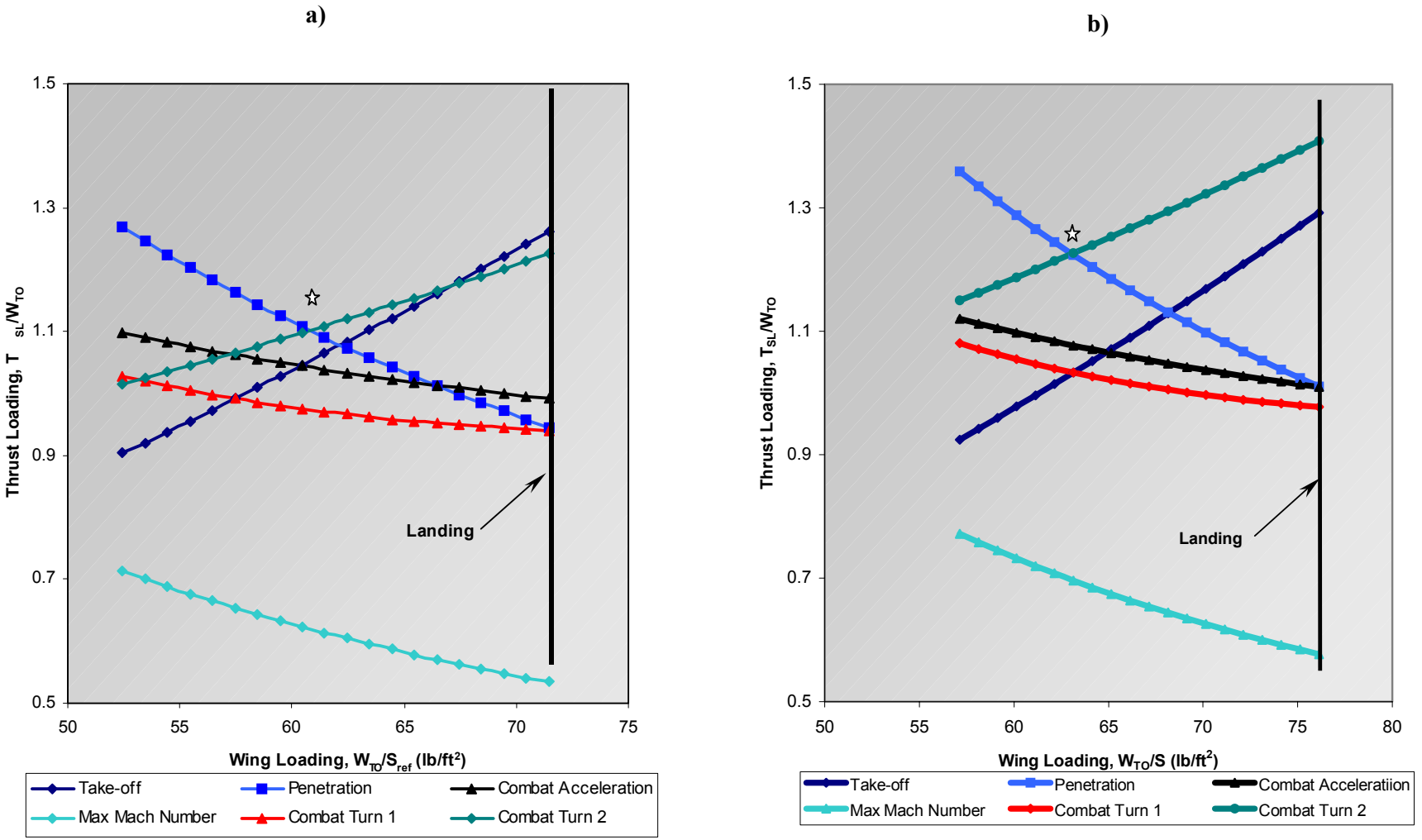

Figure 6.18 Constraint analysis space: a) global (system-level) optimum; b) baseline.

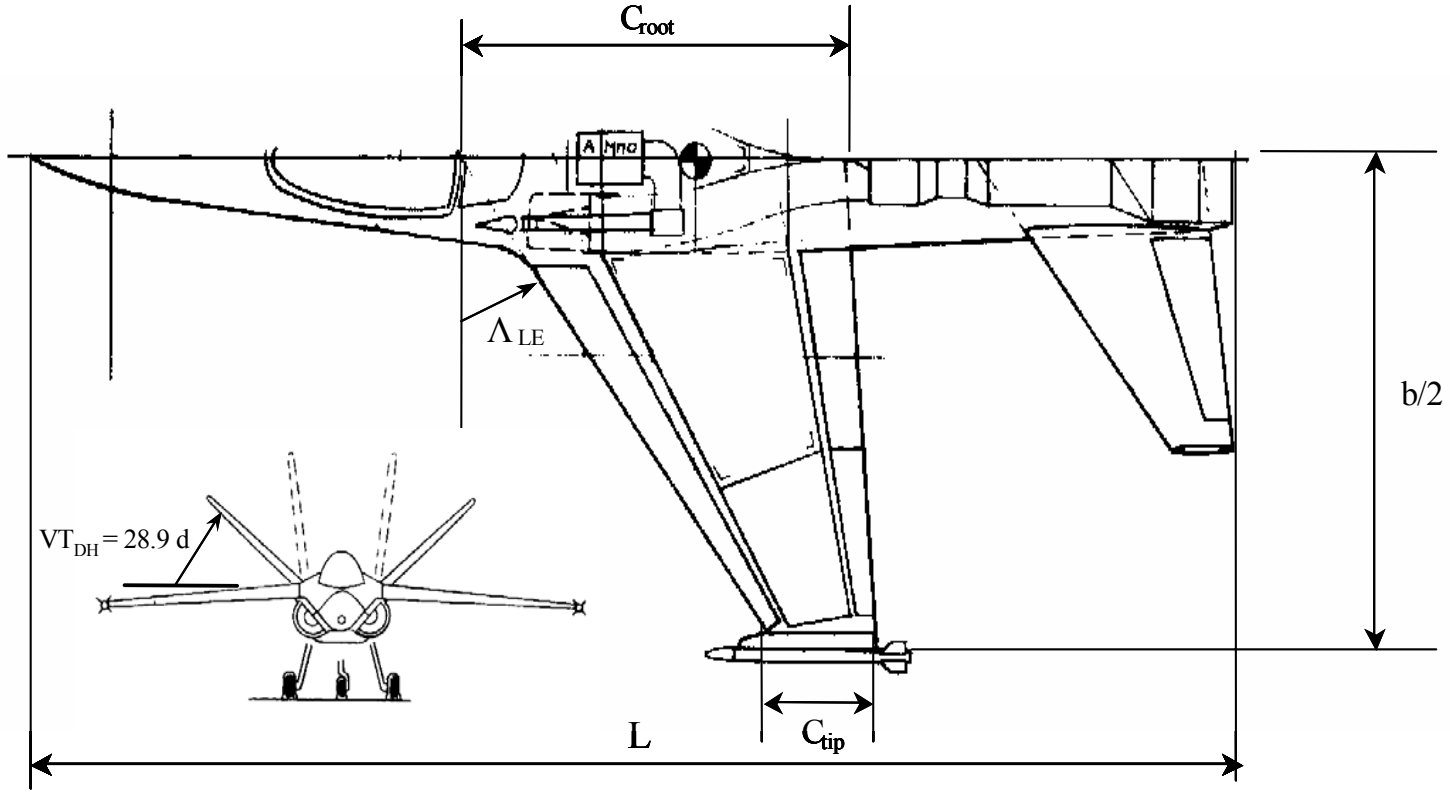

W_{TO}/S_{ref} (lb/ft²)	61.49	**Fuselage L (ft)**	56.1	**Wing AR**	3.046072	**Tail T_AR**	5.004859
T_{SL}/W_{TO}	1.13	**Wing Span, b, (ft)**	34.569	**Wing t/c**	0.077494	**Tail T_t/c**	0.12
W_{TO} (kg)	10180	**Wing C root, (ft)**	18.0767	**Wing λ**	0.240061	**Tail T_**	0.461185
S_{ref} (ft²)	364.2	**Wing C root, (ft)**	4.59148	**Wing Λ_{LE}**	31.05784		

Figure 6.19 Optimum aircraft dimensions

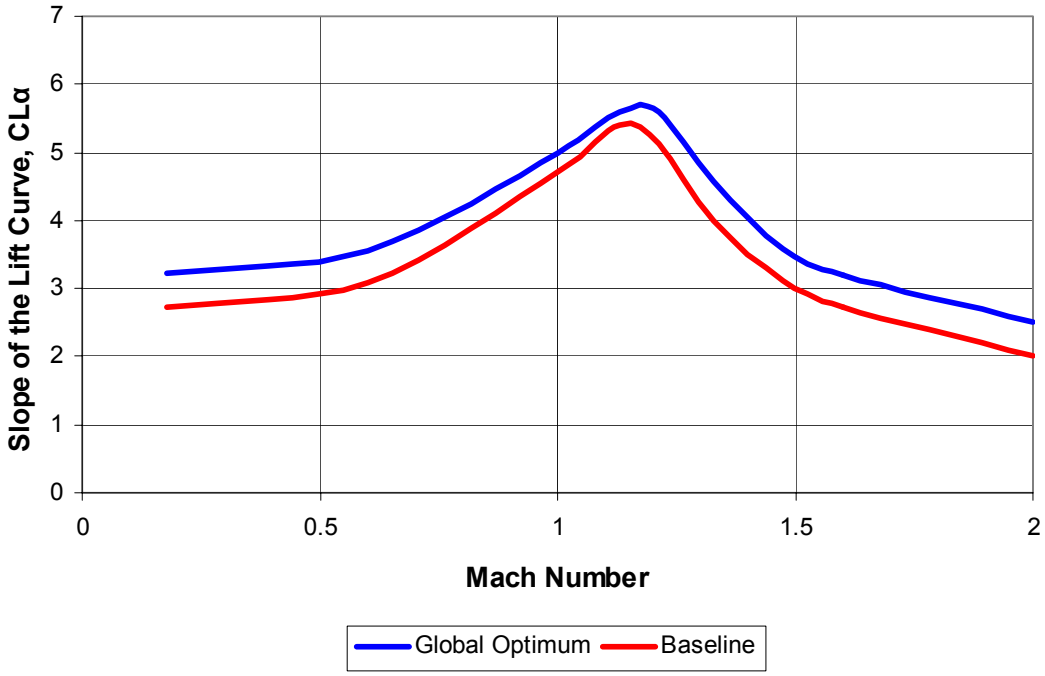

Figure 6.20 Slope of the lift curve.

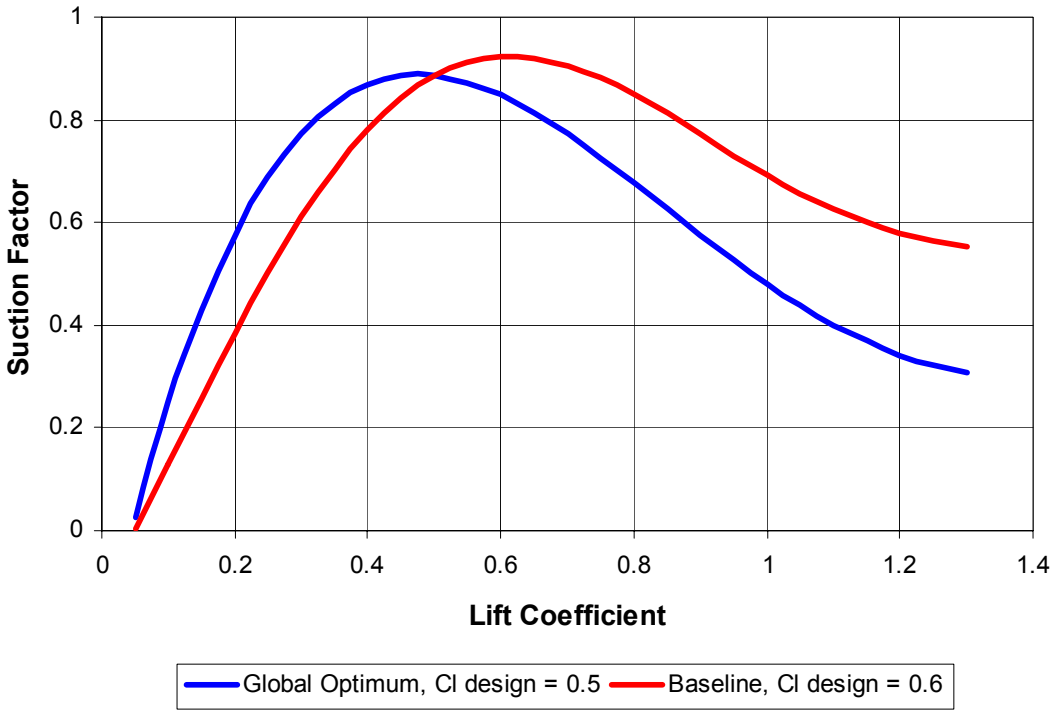

Figure 6.21 Suction factor curve.

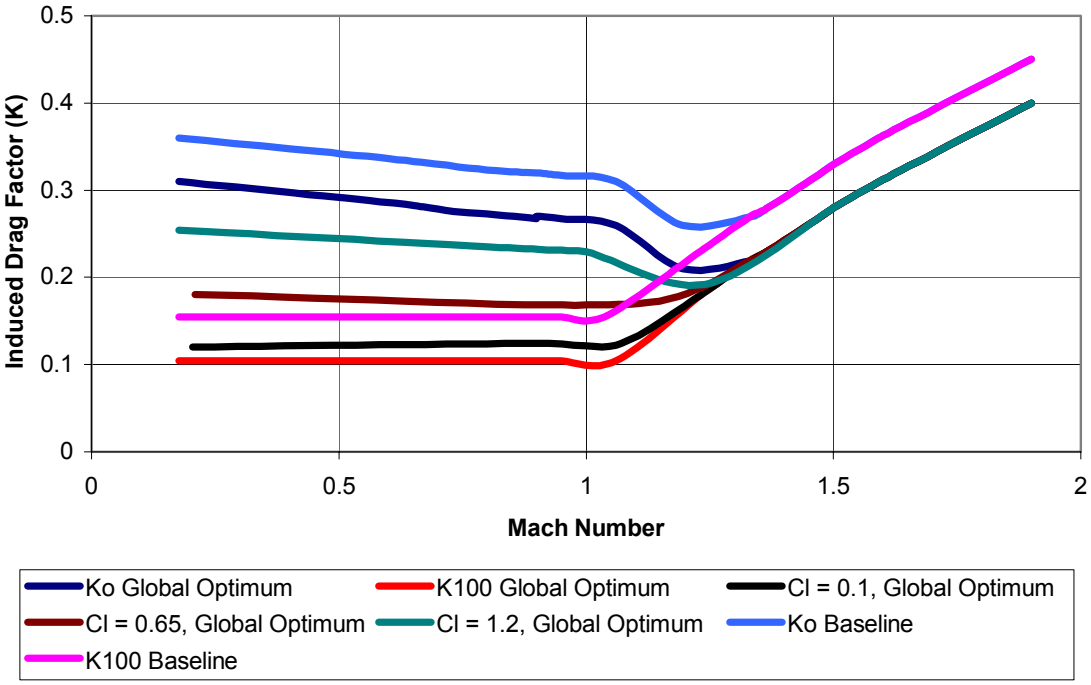

Figure 6.22 Induced drag factor.

Chapter 7

Conclusion

A number of conclusions on the effectiveness of the optimization and decomposition techniques used in this research work for the synthesis/design optimization of an advance tactical aircraft as well as the main conclusions derived from the results of this research are summarized as follow:

1. ILGO has shown its ability to handle large-scale MINLP problems for energy system and energy sub-systems (e.g., Muñoz, 2000; Georgopoulos, 2002). In the afore mentioned works, the energy systems were decompose into two principal sub-systems. In this research work, a non-energy sub-system (i.e. AFS) was included in the optimization problem along with four energy sub-systems. This opens the possibility of successfully applying ILGO and the other types of decomposition used in this research work to a broad number of applications, involving diverse disciplines and objective functions. ILGO effectively handles the information transfer problem between energy and non-energy sub-systems in such a way as to be able to ensure that the decomposed unit optimizations result in an overall system-level optimum. Furthermore, the number of sub-systems, both energy and non-energy based, which ILGO can handle, shows no limits other than those due to some practical considerations .

2. The linear (planar) and relatively smooth behavior of both the unit-level and system-level ORS's shows that the appropriate selection of the coupling functions for the units has been made. The properties that Muñoz and von Spakovsky (2000a,b,c,d; 2001a,b) used to represent the intermediate products and/or feedbacks (coupling functions) when optimizing a completely different set of energy sub-systems, namely, the PS and the ECS of an advanced military aircraft, led to a highly linear behavior of the system-level ORS. In the same manner, the introduction of new coupling functions, not used in this

previous ILGO application (i.e. heat transfer rate through a heat exchanger and electrical power rate), have been shown to be appropriate, yielding constant shadow prices.

3. The mixed integer non-linear programming (MINLP) problem for the Advanced Tactical Aircraft was solved and the global convergence of the ILGO method was verified. From the generation of the system-level ORS, a very important conclusion is drawn. The linearity of the system-level ORS is a significant contributing factor to the relatively fast convergence of the ILGO approach. Therefore, an additional constraint imposed on the coupling functions for convergence of the ILGO algorithm (see Georgopoulos, 2002; in this reference the ORS is indeed non-planar and convex but with the additional constraint converges nonetheless) is not necessary. This additional constraint can be applied if necessary but requires some knowledge of the solution space and on observation of the optimization algorithm's behavior.

4. The selection of the energy transfer rate (i.e. heat transfer rate) for the FLS and VC/PAOS are shown to be an adequate choice, since the linearity of the ORSs remains. The energy transfer rate between the VC/PAOS and the PS (i.e. the vapor compressor power requirement) is also shown to be an appropriate choice for coupling function. Therefore, in this work and previous work, it has been demonstrated that ILGO (physical decomposition) works for a broad range of coupling function types.

5. This original ILGO decomposition strategy is the first to successfully closely approach the theoretical condition of "thermoeconomic isolation" when applied to highly complex, highly dynamic, non-linear systems. This contrasts with past attempts to approach this condition, all of which were applied to very simple systems under very special and restricted conditions such as those requiring linearity in the models and strictly local decision variables

6. By dividing the total energy system into sub-systems, the technique of physical decomposition (ILGO in particular) has the advantage of breaking the overall optimization problem into a set of much smaller, unit sub-problems, which simplifies a highly complex, non-linear problem of synthesis/design optimization and allows one to take into account a larger number of decision

variables (degrees of freedom) than would otherwise be possible. Therefore, this physical decomposition strategy makes it possible to simultaneously optimize not only at a system level, i.e. with respect to the system's performance and configuration, but also at a detailed component/sub-system level, i.e. with respect to the detailed geometry of the components themselves.

7. Unit-based decomposition also allows the different sub-systems to be modeled using the most appropriated software. As a matter of fact, different sub-systems are designed by different groups and even different companies, which in turn are most probably in different geographical locations. Therefore, diverse modeling platforms are almost assuredly unavoidable.

8. The technique of time decomposition facilitates the solution of the complex problem of synthesis/design optimization for the proposed Advanced Tactical Aircraft by dividing the time period of the entire mission profile into fourteen time segments, each one representing a mission segment, which corresponds to a particular set of performance requirements, loads and corresponding environmental conditions (e.g., ambient temperature and pressure). In addition to simplifying the complexity of such a problem, time decomposition greatly decreases the time required for the overall optimization procedure by allowing the various off-design optimization problems to be solved simultaneously once the most promising sub-system syntheses/designs have been identified. Moreover, this particular decomposition strategy gives one an opportunity to better investigate the total energy system's off-design behavior and, therefore, evaluate the significance of key synthesis/design decision variables on the operational performance of the system.

9. The geometry of the final optimum Advanced Tactical Aircraft configuration is unique since geometric as opposed to thermodynamic variables were used as the independent variables of the synthesis/design optimization problem. In this research work, the optimum AFS geometry for the given mission was determined. This was possible using a highly detailed aerodynamic model built at Virginia Tech in the course of this research. The optimum geometry corresponds to a trapezoidal wing, which yields the minimum gross take-off weight and the minimum fuel consumption. In general, during the optimization, the trapezoidal geometry showed better characteristics than the

delta geometry throughout the whole mission. This was expected since for this mission supersonic flight time is much less than that for subsonic flight. Therefore, the gain in drag reduction for supersonic and transonic flight achieved by a delta wing is not large enough to compensate for the extra weight due to the fact that for a given required maximum lift, a delta wing needs a bigger reference area than a trapezoidal wing. Furthermore, a trapezoidal wing provides better maneuverability, which is required for specific mission segments (e.g., dog fights).

10. The optimum configuration for the VC/PAOS was the one without a ram-air heat exchanger. Therefore, the ultimate heat sink for this sub-system is the FLS. Thus, the fuel's heat sink capacity was indeed optimized. As a result, it can be seen that this research work yielded an optimum configuration for the VC/PAOS. The optimum Advanced Tactical Aircraft meets the mission requirements for all segments according to the request for proposal (RFP) presented in Chapter 4, which was taken from Mattingly, Heiser, and Daley, 1987. In their work, the authors present a final gross take-off weight of 23,800 lb. In this research work, the optimum take-off gross weight was 22,396 lb., i.e. 1404 lb lighter. This result is explained by the fact that in this research work aerodynamic optimization was performed in conjunction with engine design optimization and, of course, the other aircraft sub-systems.

11. The FLS was successfully optimized in such a way that the fuel never reached the vaporization temperature, while satisfying the VC/PAOS cooling requirements. The fact that these geometric variables become fixed parameters at the simulation level coupled with the transient nature of the FLS problem are some of the reasons why the final system of equations requires the implementation of non-linear differential equation solvers that are both robust and relatively fast. For that reason, the gPROMS (2000) environment, a very powerful general-purpose process modeling and simulation development environment, was used to implement both the thermodynamic and physical model. Noteworthy is the fact that the FLS was solved "all at once". This means that no time decomposition was used. This was achievable thanks to the powerful nature of gPROMS as a transient model solver and to the development of the appropriate control strategy.

References

Anderson, J.D. Jr., 1999, Aircraft Performance and Design, WCB/McGraw-Hill

ASHRAE, 1993, Hand Book Fundamentals. ASHRAE, Inc.

Balling R.J.and Sobieszczanski-Sobieski, J, 1996, Optimization of Coupled Systems: A Critical Overview of Approaches, AIAA Journal, Vol. 34, No. 1, January

Bejan, A., 1995, Entropy Generation Minimization, CRC Press, Boca Raton, Florida.

Bejan, A., R., A Role for Exergy Analysis and Optimization in Aircraft Energy-System Design, AIAA Paper No. 2000-4855, 8th AIAA/USAF/NASA/ISSMO Symposium on Multidisciplinary Analysis and Optimization, Long Beach, California, September 6-8, 2000.

Bejan, A., Tsatsaronis, G., et al., 1996, Thermal Design and Optimization, John Wiley and Sons, New York.

Bertin J. Aerodynamics for Engineers, Prentice-Hall Inc. New Jersey.

Boland, D. and Linnhoff, B., 1979, The Preliminary Design of Networks for Heat Exchange by Systematic Methods, Chemical Engineer, pp 222-228.

Brown, D.A., Integrated Energy Management System for Uninhabited Combat Air Vehicles (UCAVs), IECEC 1999, Paper No.249. Vancouver, 1999.

Chong, E.K.P., and Zak, S.H., 1996, An Introduction to Optimization, Wiley-Interscience, New York, New York.

Covert E.E., 1985, Progress in Astronautics. Thrust and Drag Its Prediction and Verification. AIAA New York.

CRC, 1976, Handbook of Tables for Applied Engineering Science. CRC Press.

Curti, V., von Spakovsky, M.R., Favrat, D., 2000, An Environomic Approach for the Modeling and Optimization of a District Heating Network Based on Centralized and Decentralized Heat Pumps, Cogeneration and/or Gas Furnace (Part I: Methodology), International Journal of Thermal Sciences, vol. 39, no. 6, June, Elsevier, France.

Curti, V., von Spakovsky, M.R., Favrat, D., 2000, An Environomic Approach for the Modeling and Optimization of a District Heating Network Based on Centralized and Decentralized Heat Pumps, Cogeneration and/or Gas Furnace (Part II: Application), International Journal of Thermal Sciences, vol. 39, no. 6, June, Elsevier, France.

Dieckmann, R.R, Watson, A.C. and Glover, S.F., 1972, Development of Integrated Environmental Control Systems for Aircraft, Report No. AFFDL-TR-72-9, Air Force Flight Dynamics Laboratory, WPAFB, OH.

El-Sayed Y., 1989, A Decomposition Strategy for Thermoeconomic Optimization, ASME Journal of Energy Resources Technology, vol. 111, pp 1-15

El-Sayed Y., 1996, A Second-Law-Based Optimization: Part I Methodology & Part 2, ASME Application, Journal of Energy Resources Technology, Vol. 118, pp. 693-703.

El-Sayed, Y.M. and Evans, R.B., 1970, Thermoeconomics and the Design of Heat Systems, Journal of Engineering for Power, ASME Transactions, Vol. 92, 27, Jan.

El-Sayed, Y.M., 1996, A Second-Law-Based Optimization: Parts 1 and 2, Journal of Engineering for Gas Turbines and Power, ASME Transactions, vol. 118, October, N.Y.

Evans, R.B. and Tribus, M., 1962, A Contribution to the Theory of Thermoeconomics, UCLA Dept. of Engineering: Report No. 62-63, Los Angeles, CA, August.

Evans, R.B. and von Spakovsky, M.R., 1993, Engineering Functional Analysis (Parts II), Journal of Energy Resources Technology, ASME transactions, Vol. 115, No. 2, N.Y., N.Y., June.

Evans, R.B. and von Spakovsky, M.R., 1993, Engineering Functional Analysis (Parts II), Journal of Energy Resources Technology, ASME transactions, Vol. 115, No. 2, N.Y., N.Y., June.

Evans, R.B., 1980, Thermoeconomic Isolation and Exergy Analysis, Energy: The International Journal, Vol. 5, Nos. 8-9, 805-821.

Evans, R.B., and von Spakovsky, M.R., 1993, Engineering Functional Analysis (Part II), Journal of Energy Resources Technology, ASME Transactions, Vol. 115, No. 2, N.Y., June.

Figliola R. S., et al.,1997. Thermal Optimization of the ECS on an Aircraft with an Emphasis on System Efficiency and Design Methodology. Society of Automotive Engineers, Inc. 971241 pp 137-143.

Frangopoulos, C. A., 1994, Application of the Thermoeconomic Functional Approach to the CGAM Problem, Energy-The International Journal, Vol. 19, No. 3, pp. 323-342.

Frangopoulos, C.A., 1983, Thermoeconomic Functional Analysis: A Method for Optimal Dsign or Improvement of Complex Thermal Systems, School of Mechanical Engineering, Georgia Institute of Technology, Ph.D. Dissertation.

Frangopoulos, C.A., 1984, Thermoeconomic Functional Analysis: An Innovative Approach to Optimal Design of Thermal Systems, Second Law Aspects of Thermal Design. HTD Vol. 33, ASME, N.Y., N.Y., August.

Frangopoulos, C.A., 1989, Optimal Synthesis and Operation of Thermal Systems by the Thermoeconomic Functional Approach, ASME Winter Annual Meeting, AES 10-3, 49.

Frangopoulos, C.A., 1994, Application of Thermoeconomic Optimization Methods to the CGAM Problem, Energy: The International Journal, special edition, Vol. 19, No. 3, pp. 323-342, Pergamon Press, Great Britain.

Frangopoulos, C.A., and von Spakovsky, M.R., 1993, The Environomic Analysis and Optimization of Energy Systems (Part I), Proceedings of the International Conference on Energy Systems and Ecology: ENSEC'93, Vol. I, pp. 123-132, ASME, Cracow, Poland, July.

Frangopoulos, C.A., Evans R.B., 1984, Thermoeconomic Isolation and Optimization of Thermal System Components, Second Law Aspects of Thermal Design. HTD Vol. 33, ASME, N.Y., N.Y., August.

Gaggioli R. and El-Sayed Y., 1989, A Critical Review of Second Law Costing Methods, Journal of Energy Resources Technology, ASME Transactions, vol. 111, pp 1-15.

Gaggioli, R., Sama, D.A., Qian, S., and El-Sayed, Y. M., 1991, Integration of a New Process into an Existing Site: A Case Study in the Application of Exergy Analysis, Journal for Engineering for Gas Turbines and Power, ASME Transactions, vol. 113, no. 2.

Georgopoulos, N., 2002, *Application of a Decomposition Strategy to the Optimal Synthesis/Design and Operation of a Fuel Cell Based Total Energy System*, M.S. thesis, Department of Mechanical Engineering, Virginia Polytechnic Institute and State University, Blacksburg, VA.

Goldberg, D. E., 1989, Genetic Algorithms in Search, Optimization and Machine Learning, Addison Wesley, Reading, MA.

Greene R., 1992, Compressors, Selection, Usage, and Maintenance. Mc Graw Hill Inc, USA.

Hajela P., 1999, Nongradient Methods in Multidisciplinary Design Optimization-Status and Potential, Journal of Aircraft, Vol. 36, No.1, Jan-Feb.

Hill P. and Peterson C., 1992, Mechanics and Thermodynamics of Propulsion. Addison-Wesley Publishing Company, Inc.

Hoak-Ellison, et al., 1982; "USAF DATCOM", Air force Flight Dynamic Lab, Wright-Patterson AFB, OH.

Hodgkinson J., 1999, Aircraft Handling Qualities, AIAA Educational Series.

Hoerner S. and Borst H., 1975, Fluid-Dynamic Lift. Mrs. Liselotte A. Hoener.

Hudson W. A. and Levin M. L., 1986. Integrate Aircraft Fuel Thermal Management. Rockwell International Corp. El Segundo, CA. Intersociety Conference on Environmental Systems (16th : 1986 : San Diego, Calif.). Aerospace environmental systems : proceedings of the Sixteenth ICES conference. Pp 11-25.

Incropera F. and DeWitt D., 1990, Fundamental of Heat and Mass Transfer. John Wiley and Sons, Inc.

iSIGHT version 5 User's Guide, 1999, Engineous Software Inc., Morrisville, N.C.

Jane's All the World's Aircraft 1999-2000, 1999, Jane's Information Group, Couldson, UK

Kakac S. and Liu H., 2002, Heat Exchangers Selection, Rating, and Thermal Design. CRS press.

Kays, W.M. and London, A.L., 1998, Compact Heat Exchangers, Krieger Publishing Company, Malabar, FL.

Kotas T.J., 1985, The Exergy Method of Thermal Plant Analysis, Krieger Publishing Company, Malabar, Florida.

Lazzaretto, A. and Andreatta, R., 1995, Algebraic Formulation of a Process-Based Exergo-economic Method, Thermodynamics and the Design, Analysis and Improvement of Energy Systems, AES-Vol. 35.

Le Claire, R., 1975, Evaluation of the Overall Fuel Mass Penalty of an Aircraft System, Aeronautical Journal, May, pp 225-228.

Lefebvre A., 1983, Gas Turbine Combustion, McGraw Hill Inc. USA.

Letton, Jr, G., 1976, Avionics Cooling on USAF Aircraft, AGARD Conference Proceedings on Avionic Cooling and Power Supplies for Advanced Aircraft, The Hague, Netherlands, June.

Lykins, R et al., 1998, Preliminary Thermodynamic Analysis of Power System Impact on Tactical Aircraft Performance, Proceedings of the Aerospace Power Systems Conference, SAE 981288.

Manglik, R.M. and Bergles, A.E., 1990, The Thermal-Hydraulic Design of the Rectangular Offset-Strip-Fin Compact Heat Exchanger in Compact Heat Exchangers, R.K. Shah, A.D. Kraus, and D. Metzger editors, Hemipshere Publishing Corporation, pp 123-149.

Mattingly, J.D., Heiser,W.H. and Daley, D.H., 1987, Aircraft Engine Design, AIAA Education Series, New York, New York.

Muñoz J. R., von Spakovsky M.R., 1999, A Second Law Based Integrated Thermoeconomic Modeling and Optimization Strategy for Aircraft / Aerospace Energy System Synthesis and Design (Phase I - Final Report), final report, Air Force Office of Scientific Research, New Vista Program, December.

Muñoz, J.R. and von Spakovsky, M.R., 2000a, An Integrated Thermoeconomic Modeling and Optimization Strategy for Aircraft / Aerospace Energy System Design, Efficiency, Costs, Optimization, Simulation and Environmental Aspects of Energy Systems (ECOS'00), Twente University, ASME, Netherlands, July 5-7.

Muñoz, J.R. and von Spakovsky, M.R., 2000b, The Use of Decomposition for the Large Scale Synthesis/ Design Optimization of Highly Coupled, Highly Dynamic Energy Systems: Part I - Theory, 2000 ASME International Mechanical Engineering Congress and Exposition, Orlando, FL, Nov 5-10.

Muñoz, J.R. and von Spakovsky, M.R., 2000c, The Use of Decomposition for the Large Scale Synthesis/ Design Optimization of Highly Coupled, Highly Dynamic Energy Systems: Part II - Applications, 2000 ASME International Mechanical Engineering Congress and Exposition, Orlando, FL, Nov 5-10.

Newberry, C.F., Exergy - The Aircraft Design Variable of Choice?, AIAA Paper No. 2000-4851, 8th AIAA/USAF/NASA/ISSMO Symposium on Multidisciplinary Analysis and Optimization, Long Beach, California, September 6-8, 2000.

Nicolai, L., 1975, Fundamentals of Aircraft Design, published by the author.

Paulus, D. and Gaggioli, R., Rational Objective Functions for Vehicles, AIAA Paper No. 2000-4852, 8th AIAA/USAF/NASA/ISSMO Symposium on Multidisciplinary Analysis and Optimization, Long Beach, California, September 6-8, 2000.

Rao, S. S., 1996, Engineering Optimization-Theory and Practice, John Wiley and Sons, N.Y.

Raymer, D., AIRCRAFT DESIGN: A Conceptual Approach, American Institute of Aeronautics and Astronautics, Washington, D.C., Third Edition 1999

Resetar, S.A., Rogers, J.C., and Hess, R.W., Advanced Airframe Structural Materials: A Primer and Cost Estimating Methodology, RAND, R-4016-AF, Jan 1, 1991.

SAE Aerospace Applied Thermodynamics Manual, 1969, Society of Automotive Engineers, New York.

SAE AIR 1168/8, 1989 Aircraft Fuel Weight Penalty Due to Air Conditioning SAE Aerospace Applied Thermodynamics Manual, Warrendale, PA.

Sama D. A., 1995, Differences Between Second Law Analysis and Pinch Technology, Journal of Energy Resources Technology, ASME Transactions. Vol. 117, pp. 186-190

Sciubba, E., 1995, Artificial Intelligence Applications to the Synthesis of Thermal Processes, Second Law Analysis of Energy Systems: Towards the 21st Century, ASME, Univ. di Roma.

Sciubba, E., 1998, Artificial Intelligence in Thermal Systems Design: Concepts and Applications, Nova Science Publishers, Commack, N.Y.

Shah, R.K. and Webb, R.L., 1982, Compact and Enhanced Heat Exchangers, in Heat Exchangers: Theory and Practice, J. Taborek, G.F. Hewitt, and N. Agfan editors, Hemisphere Publishing Corporation, pp 435-468

Shah, R.S., 1981, Compact Heat Exchanger Design Procedure, in Heat Exchangers, Thermal-Hydraulic Fundamentals and Design, S. Kakac, A.E. Bergles and F. Matinger editors, Hemisphere Publishing Corporation, pp 495-536.

Sobieszczanski-Sobieski, J, 1989, Optimization by Decomposition: A step from Hierarchic to Non-hierarchic Systems, NASA CP-3031, Part 1.

Sobieszczanski-Sobieski, J, 1990, Sensitivity of Complex, Internally Coupled Systems, AIAA Journal, Vol. 28, pp.153-161, January.

Sobieszczanski-Sobieski, J. and Haftka, 1997, Multidisciplinary Aerospace Design Optimization: Survey of Recent Developments, Structural Optimization, Vol. 14, No. 1, pp 1-23.

Tsatsaronis, G. and Pisa, J., 1994, Exergoeconomic Evaluation and Optimization of Energy Systems-Application to the CGAM Problem, Energy-The International Journal, Vol. 19, No. 3, pp. 287-321.

Tsatsaronis, G. and Winhold, M., 1984, Thermoeconomic Analysis of Power Plants, EPRI AP-3651 Project 2029-8, Palo Alto, California, Electric Power Research Institute.

Tsatsaronis, G., 1985, Thermoökonomische Analzse von Energieumwandlungs-prozessen, Dr. Habilitatus Thesis, Dept. of Mechanical Engineering, Technical University of Aachen, West Germany.

Tsatsaronis, G., and Pisa, J., 1994, Exergoeconomic Evaluation and Optimization of Energy Sytsems: Application to the CGAM Problem, Energy: The International Journal, Vol. 19, No. 3, pp. 287-321, Pergamon, Great Britain.

Tsatsaronis, G., Pisa, J., et al., 1989, Thermodynamic Analysis and Improvement of Energy Systems, Proceeedings of the International Symposium, Beijing, China, Pergamon Press, pp. 195-200.

Valero, A., Lozano, M., et al., 1994, Application of the Exergetic Cost Theory to the CGAM Problem, Energy-The International Journal, Vol. 19, No. 3, pp. 365-381.

Valero, A., Lozano, M., et al., 1994, CGAM Problem: Definition and Conventional Solution, Energy-The International Journal, Vol. 19, No. 3, pp. 279-286.

Valero, A., Lozano, M.A., and Muñoz, M., 1986, A General Theory of Exergy Savings (Parts I, II, and III), Computer-Aided Engineering of Energy Systems, ASME, AES-Vol. 2-3, pp. 1-21.

Valero, A., Serra, L., Lozano, M.A., 1993, Structural Theory of Thermoeconomics, Thermodynamics and the Design, Analysis and Improvement of Energy Systems, ASME, AES-Vol. 30, N.Y., N.Y..

Valero, A., Serra, L., Lozano, M.A., and Torres, C., 1994, Application of the Exergetic Cost Theory to the CGAM Problem, Energy: The International Journal, Vol. 19, No. 3, pp. 365-381, Pergamon, Great Britain.

von Spakovsky M.R., 1986, A Practical Generalized Analysis Approach for the Optimal Thermoeconomic Design and Improvement of Real-World Thermal Systems,

School of Mechanical Engineering, Georgia Institute of Technology, Ph.D. Dissertation.

von Spakovsky M.R., Evans R.B., 1984, Detailed Second Law Design of Components in Complex Thermal Systems, Second Law Aspects of Thermal Design. HTD Vol. 33, ASME, N.Y., N.Y., August.

von Spakovsky M.R., Evans R.B., 1990, The design and performance Optimization of thermal systems. Journal of Engineering for Gas Turbines and Power. ASME Vol. 112. January 1990.

von Spakovsky M.R., Evans R.B., 1990, Engineering Functional Analysis- Part I and Part II. Journal of Energy Resources Technology. ASME Vol. 115. June 1993.

von Spakovsky M.R., Frangopoulos, C.A., 1994, The Environomic Analysis and Optimization of a Gas Turbine Cycle with Cogeneration, Thermodynamics and the Design, Analysis and Improvement of Energy Systems, ASME, AES-Vol. 33, N.Y., N.Y., November.

von Spakovsky, M., 1994, Application of the Functional Analysis to the Analysis and Optimization of the CGAM Problem, Energy-The International Journal, Vol. 19, No. 3, pp. 343-364.

von Spakovsky, M.R., 1994, Application of Engineering Functional Analysis to the Analysis and Optimization of the CGAM Problem, Energy: The International Journal, Vol. 19, No. 3, pp. 343-364, Pergamon, Great Britain.

von Spakovsky, M.R., and Evans, R.B., 1993, Engineering Functional Analysis (Part I), Journal of Energy Resources Technology, ASME Transactions, Vol. 115, No. 2, N.Y., June.

von Spakovsky, M.R., and Frangopoulos, C.A., 1993, The Environomic Analysis and Optimization of Energy Systems (Part II), Proceedings of the International Conference on Energy Systems and Ecology: ENSEC'93, Vol. I, pp. 123-132, ASME, Cracow, Poland, July.

WATE User's Guide, 1999, NASA Lewis Research Center.

Zimering, B., Burnes, D., Rowe, J., 1999, Gas Turbine Power Generation System Configuration Study and Optimization, 1999 International iSIGHT Users Conference, Chapel Hill, N.C., Oct 4-6.

Vitae

Diego Fernando Rancruel Arce was born in Santiago de Cali, Colombia on April 3, 1972. After graduating with honors from Colegio San Juan Bosco he served as a soldier in the Colombian Army. He then attended Universidad del Valle in Cali, Colombia, and in early 1995 he received his Bachelor of Science degree with honors in Mechanical Engineering. After graduation he worked for Bayer AG. a pharmaceutical and chemical multinational company, where he worked for five years in total, one year as metrology chief engineer, two years as maintenance manager and two years as projects manager, respectively. He was a steam generator instructor for the insurance company Seguros Bolivar. He attended graduate school in Universidad del Valle in Cali, Colombia; in 1997 he received an engineering degree as Specialist in Engineering Materials. He attended graduate business school in Universidad ICESI in Cali, Colombia; in 1999 he received a business degree as Specialist in Administration. Upon completion of his Master of Science in Mechanical Engineering he will pursue his Ph.D. at Virginia Tech.